frontiers | Research Topics

# Exploration and utilization of marine and freshwater high-value biological resources

**Edited by**
Shuhao Huo, Pengfei Cheng, Wei Liu and Liandong Zhu

**Published in**
Frontiers in Marine Science

ISSN 1664-8714
ISBN 978-2-8325-2826-6
DOI 10.3389/978-2-8325-2826-6

## About Frontiers

Frontiers is more than just an open access publisher of scholarly articles: it is a pioneering approach to the world of academia, radically improving the way scholarly research is managed. The grand vision of Frontiers is a world where all people have an equal opportunity to seek, share and generate knowledge. Frontiers provides immediate and permanent online open access to all its publications, but this alone is not enough to realize our grand goals.

## Frontiers journal series

The Frontiers journal series is a multi-tier and interdisciplinary set of open-access, online journals, promising a paradigm shift from the current review, selection and dissemination processes in academic publishing. All Frontiers journals are driven by researchers for researchers; therefore, they constitute a service to the scholarly community. At the same time, the *Frontiers journal series* operates on a revolutionary invention, the tiered publishing system, initially addressing specific communities of scholars, and gradually climbing up to broader public understanding, thus serving the interests of the lay society, too.

## Dedication to quality

Each Frontiers article is a landmark of the highest quality, thanks to genuinely collaborative interactions between authors and review editors, who include some of the world's best academicians. Research must be certified by peers before entering a stream of knowledge that may eventually reach the public - and shape society; therefore, Frontiers only applies the most rigorous and unbiased reviews. Frontiers revolutionizes research publishing by freely delivering the most outstanding research, evaluated with no bias from both the academic and social point of view. By applying the most advanced information technologies, Frontiers is catapulting scholarly publishing into a new generation.

## What are Frontiers Research Topics?

Frontiers Research Topics are very popular trademarks of the *Frontiers journals series*: they are collections of at least ten articles, all centered on a particular subject. With their unique mix of varied contributions from Original Research to Review Articles, Frontiers Research Topics unify the most influential researchers, the latest key findings and historical advances in a hot research area.

Find out more on how to host your own Frontiers Research Topic or contribute to one as an author by contacting the Frontiers editorial office: frontiersin.org/about/contact

# Exploration and utilization of marine and freshwater high-value biological resources

**Topic editors**

Shuhao Huo — Jiangsu University, China

Pengfei Cheng — Ningbo University, China

Wei Liu — Qilu University of Technology (Shandong Academy of Sciences), China

Liandong Zhu — Wuhan University, China

**Citation**

Huo, S., Cheng, P., Liu, W., Zhu, L., eds. (2023). *Exploration and utilization of marine and freshwater high-value biological resources*. Lausanne: Frontiers Media SA.

doi: 10.3389/978-2-8325-2826-6

# Table of contents

frontiers | Frontiers in Marine Science

TYPE Editorial
PUBLISHED 13 June 2023
DOI 10.3389/fmars.2023.1230069



OPEN ACCESS

EDITED AND REVIEWED BY
Stephen J. Newman,
Department of Primary Industries and Regional Development of Western Australia (DPIRD), Australia

*CORRESPONDENCE
Shuhao Huo
huo@ujs.edu.cn

RECEIVED 28 May 2023
ACCEPTED 05 June 2023
PUBLISHED 13 June 2023

CITATION
Zhu F, Zhu L, Liu W, Cheng P and Huo S (2023) Editorial: Exploration and utilization of marine and freshwater high-value biological resources.
*Front. Mar. Sci.* 10:1230069.
doi: 10.3389/fmars.2023.1230069



# Editorial: Exploration and utilization of marine and freshwater high-value biological resources

Feifei Zhu[1], Liandong Zhu[2], Wei Liu[3], Pengfei Cheng[4] and Shuhao Huo[5]*

[1]School of Life Sciences, Jiangsu University, Zhenjiang, China, [2]School of Resource and Environmental Sciences, Wuhan University, Wuhan, China, [3]Shandong Analysis and Test Center, Qilu University of Technology (Shandong Academy of Sciences), Jinan, China, [4]College of Food and Pharmaceutical Sciences, Ningbo University, Ningbo, China, [5]School of Food and Biological Engineering, Jiangsu University, Zhenjiang, China

KEYWORDS

**biological resources, microalgae, cyanobacteria, high-value utilization, high value-added products, functional active substances**

Editorial on the Research Topic
Exploration and utilization of marine and freshwater high-value biological resources

The efficient, safe, and sustainable utilization and exploitation of high-value resources in marine and freshwater systems are conducive to agriculture, food, and environmental security (a recent research hotspot). Marine microalgae biological resources have great economic, social, and ecological value, and play an important role in maintaining material circulation, energy flow, and water purification in the ocean-living systems. As a major contributor to marine primary productivity, carbon dioxide fixation transforms microalgae into high-value bioactive compounds and releases oxygen. Research and development of microalgae biological resources, including natural pigments such as phycoglobin, phycocyanin, carotenoids, astaxanthin, and fucoxanthin, as well as unsaturated fatty acids such as arachidonic acid and docosahexaenoic acid, along with extracellular polysaccharides and minerals, are one of the most practical and innovative fields in global scientific and technological activities. The research and development of microalgae biological resources provide a primary pathway to solving major social and economic problems such as resource shortages and food safety.

With the help of modern biotechnology, there have been important breakthroughs in the development and high-value utilization of marine biological resources to obtain high-value products such as food, medicine, and functional products. In this Research Topic, Yin et al. established an integrated biological process utilizing Porphyridium cruentum for the production of B-phycoglobin (B-PE) and extracellular polysaccharide (EPS). They extracted the highest content of phycobilin through repeated freeze-thaw treatment and finally obtained 7.99 mg/L B-PE (16500 Da), with a purity index of 0.82. Li et al. showed that the zero N condition and lowlight condition were conducive to the highest astaxanthin concentration in the thin-wall motile cell Haematococcus pluvialis, and it was more economical in terms of electricity usage and other costs. Yang et al. used nitrogen

utilization analysis and showed that urea and arginine had synergistic effects on promoting the biosynthesis of phyxanthin in Phaeodactylum tricornutum, which is a promising and efficient strategy for increasing phyxanthin production in the microalgae. Spirulina is an important species for phycocyanin production. Yao et al. simply added mineral elements and peptides to Spirulina maximus culture to improve the phycocyanin yield. Guo et al. discovered that a high bicarbonate level and low temperature significantly increased biomass production and accumulation of arachidonic acid and docosahexaenoic acid (DHA) in Dunaliella salina. In addition, Shang et al. examined the roles of the interacting proteins of the transcription factor DpAP2, which regulates carotenoid anabolism in Dunaliella parva. DpAP2 can promote carotenoid accumulation by binding to the promoter of target genes. Last but not least, this Research Topic also mentions the dynamic changes in fishing resources such as skipjack in the South China Sea and Antarctic krill in the Bransfield Strait, which are of significant value but lack data in global marine fisheries.

In conclusion, the Research Topicon the *Exploration and Utilization of Marine and Freshwater High-Value Biological Resources* paves the way to realize efficient production processes for biomass and bioactive substances of microalgae and cyanobacteria. It is conducive to the development of marine microalgae and cyanobacteria industries for value-added products worldwide.

## Author contributions

FZ: writing the original draft, editing, and reviewing. LZ: reviewing and editing. WL: funding acquisition and reviewing. PC: reviewing. SH: reviewing and funding acquisition. All authors approved the submitted version.

## Funding

The National Natural Science Foundation of China (21978120), the Innovation Ability Improvement Project of Small and Medium-sized High-tech Companies in Shandong Province (2022TSGC2199), and the Key R&D projects in Jiangsu Province (BE2020405) partially supported the work on this Research Topic.

## Acknowledgments

We would like to express our sincere gratitude to all the authors who proposed their work and all the researchers who reviewed the submissions on this Research Topic.

## Conflict of interest

The authors declare that the research was conducted in the absence of any commercial or financial relationships that could be construed as a potential conflict of interest.

## Publisher's note

frontiers in Marine Science

ORIGINAL RESEARCH
published: 14 January 2022
doi: 10.3389/fmars.2021.830590

# Effect of Nitrogen Concentration on the Alkalophilic Microalga *Nitzschia* sp. NW129-a Promising Feedstock for the Integrated Production of Lipids and Fucoxanthin in Biorefinery

*Zihao Cao[1], Xiaotong Shen[1], Xujing Wang[1], Baohua Zhu[1], Kehou Pan[1,2] and Yun Li[1]**

*[1] The Key Laboratory of Mariculture (Ministry of Education), Ocean University of China, Qingdao, China, [2] Function Laboratory for Marine Fisheries Science and Food Production Processes, Qingdao National Laboratory for Marine Science and Technology, Qingdao, China*

OPEN ACCESS

**Edited by:**
*Shuhao Huo, Jiangsu University, China*

**Reviewed by:**
*Abd El-Fatah Abomohra, Chengdu University, China*
*Xupeng Cao, Dalian Institute of Chemical Physics, Chinese Academy of Sciences (CAS), China*

***Correspondence:**
*Yun Li*
*sxsdlwl@ouc.edu.cn*

**Specialty section:**
*This article was submitted to Marine Fisheries, Aquaculture and Living Resources, a section of the journal Frontiers in Marine Science*

**Received:** *07 December 2021*
**Accepted:** *27 December 2021*
**Published:** *14 January 2022*

**Citation:**
*Cao Z, Shen X, Wang X, Zhu B, Pan K and Li Y (2022) Effect of Nitrogen Concentration on the Alkalophilic Microalga Nitzschia sp. NW129-a Promising Feedstock for the Integrated Production of Lipids and Fucoxanthin in Biorefinery. Front. Mar. Sci. 8:830590. doi: 10.3389/fmars.2021.830590*

Microalgae are considered promising resources for producing a variety of high-value-added products, especially for lipids and pigments. Alkalophilic microalgae have more advantages than other microalgae when cultured outdoors on a large scale. The present study investigated the comprehensive effects of different nitrogen concentrations on fucoxanthin (Fx), lipids accumulation and the fatty acid profile of the alkaliphilic microalgae *Nitzschia* sp. NW129 to evaluate the potential for simultaneous production of Fx and biofuels. Fx and Lipids amassed in a coordinated growth-dependent manner in response to various concentrations, reaching 18.18 mg $g^{-1}$ and 40.67% dry weight (DW), respectively. The biomass of *Nitzschia* sp. NW129 was 0.58 ± 0.02 g $L^{-1}$ in the medium at the concentration of 117.65 mM. The highest productivities of Fx (1.44 mg $L^{-1}$ $d^{-1}$) and lipid (19.95 ± 1.29 mg $L^{-1}$ $d^{-1}$) were obtained concurrently at this concentration. Furthermore, the fatty acid methyl esters revealed excellent biofuel properties with an appropriate value of the degree unsaturation (49.97), cetane number (62.72), and cold filter plugging point (2.37), which met the European standards for biofuel production (EN14214). These results provided a reliable strategy for further industrialization and comprehensive production of biofuel and Fx by using the alkaliphilic microalgal *Nitzschia* sp. NW129.

**Keywords: alkaliphilic microalgae, biodiesel, fucoxanthin, lipids, nitrogen concentration, *Nitzschia* sp., simultaneous production**

## INTRODUCTION

It was reported that microalgae contributed 20% of global primary productivity (Malviya et al., 2016). Microalgae not only play a critical ecological role but also are capable of synthesizing a variety of chemicals with high commercial value, such as pigments, unsaturated fatty acids and microalgal polysaccharides and so on (Wang et al., 2018a). As one of the prospects for the third-generation biofuels, the microalgae have faster growth rates and higher productivity than oil-producing terrestrial plants by directing more energy to growth and propagation processes (Gomez-Loredo et al., 2016). Previous studies also demonstrated that microalgal biofuel was technically feasible

(Zeng et al., 2011; Bondioli et al., 2012). Moreover, microalgae, as potential sources of fucoxanthin (Fx), are capable of replacing macroalgae due to the advantages of high content (2.24–59.20 mg $g^{-1}$) and manual control in the bioreactor (Xia et al., 2013; Mohamadnia et al., 2020). Fx is a carotenoid involved in photosynthesis, accounting for more than 10% of the total carotenoids in nature (Zarekarizi et al., 2019). In recent years, Fx attracted increasing attention due to its nutraceutical effects on human health such as antioxidant, anti-obesity and anti-tumor (Riccioni, 2012; Tanaka et al., 2012; Zeng et al., 2018). It has been proved to be safe for animals, including humans and hence can be used as ingredients in food industry and medical purposes, as well as an animal feed additive (Sathasivam and Ki, 2018; Mohamadnia et al., 2020).

Taking account of the commercial value of biofuel and Fx, it is of great significance to study their integrated production from microalgae. The integrated production of pigments with algal lipids has emerged as an economic strategy worth looking forward to Campenni' et al. (2013), such as simultaneous production of astaxanthin and triacylglycerol by *Chlorella zofingiensis*, docosahexaenoic acid and Fx by *Isochrysis* and so on (Liu et al., 2016; Sun et al., 2019). Previous studies showed that manipulating nitrogen concentrations was an effective way to promote the accumulation of lipid and Fx. Nitrogen stress can induce the increase of lipid content in microalgae, while Fx was the opposite (Gao et al., 2017; Yang et al., 2017; Lai et al., 2019). The response of lipids to adverse growth conditions also inhibited the growth of algal cells, resulting in constant or even reduced productivity, which was not economically feasible (Griffiths et al., 2012; Guo et al., 2021). Furthermore, nitrogen concentration can also markedly affect the fatty acid composition (Sahin et al., 2019). It determines the quality of biofuel such as combustion efficiency, cold-flow properties and viscosity (Cui et al., 2020; Andeden et al., 2021), which is rarely considered in current studies.

However, the industrialization of microalgae culture in large-scale outdoor open-ponds still faces difficulties such as low productivity, contamination by invasive species, continuous supply of inorganic carbon and inefficient harvesting (Wensel et al., 2014). An effective way to reduce the cost of $CO_2$ supply is to culture microalgae in an extremely high pH medium (pH > 10) that is capable of capturing more $CO_2$ for microalgae growth by direct reaction of $CO_2$ with $OH^-$ in the liquid boundary layer around gas bubbles (Santos et al., 2013; Kuo et al., 2017). The $CO_2$ utilization efficiency of *Chlorella* sp. AT1 cultured in pH 11 medium was reported to enhance several times (Kuo et al., 2017). The higher pH culture media would also effectively limit microbial contamination (Peng et al., 2015). Thus, compared with other microalgae, alkalophilic microalgae that have the ability to survive and thrive at extremely high pH (pH > 10) (Qu and Miao, 2021) are more appropriate for outdoor large-scale culture. In commercial production, the successful use of high pH growth conditions for the cultivation of *Spirulina*. also proves the above view (Vadlamani et al., 2017). Previous studies on alkaliphilic microalgae focused on lipid production, and to our best knowledge, there have been no efforts to produce Fx and lipids simultaneously using alkalophilic microalgae. In this study, an alkalophilic microalgae *Nitzschia* sp. NW129, rich in lipid and Fx, was used as material. Its additional characteristic was attributed to rapid settlement, which was conducive to reducing the collection cost. The effects of different nitrogen concentrations on lipid and Fx productivities and fatty acid composition of the alkalophilic microalga *Nitzschia* sp. NW129 were comprehensively analyzed. The favorable performance at appropriate nitrogen concentration suggested its potential as a feedstock for the co-production of Fx and biofuel in biorefinery.

# MATERIALS AND METHODS

## Microalgal Strain and Growth Conditions

An oleaginous and high Fx content alkalophilic microalga isolated from Hamatai Lake (Latitude = 39°06′N and Longitude = 108°02′E) in Mongolia, China, was identified and named *Nitzschia* sp. NW129 (Wang et al., 2019). The strain was preserved in the Laboratory of Applied Microalgae Biology, Ocean University of China. The *Nitzschia* sp. NW129 was precultured in 500 mL Erlenmeyer flasks placed in an Oscillating incubator at 28 ± 1°C and under 100 μmol photons $m^{-2}$ $s^{-1}$, following a 12:12-h light/dark photoperiod. The Zarrouk medium was used, with modifications as follows: $NaHCO_3$, 3.78 g $L^{-1}$; $Na_2CO_3$ 16.43 g $L^{-1}$; $NaNO_3$ 2.5 g $L^{-1}$; $K_2HPO_4$ 0.5 g $L^{-1}$; NaCl 1.0 g $L^{-1}$; $K_2SO_4$ 1.0 g $L^{-1}$; $CaCl_2$ 0.08 g $L^{-1}$; $MgSO_4{\cdot}7H_2O$ 0.2 g $L^{-1}$; $FeSO_4{\cdot}7H_2O$ 0.01 g $L^{-1}$; $Na_2EDTA$ 0.08 g $L^{-1}$; $A_5$ 1.0 ml. $A_5$ consisted of the following salts, in g $L^{-1}$: $H_3BO_3$, 5.72; $MnC1_2{\cdot}4H_2O$, 3.60; $ZnSO_4{\cdot}7H_20$, 0.44, $CuSO_4{\cdot}5H_2O$, 0.16, $(NH_4)6Mo_7O_{24}$ 0.04. The pH of the medium was initially 10.5 and increased with the extension of cultivation time.

Late-logarithmic growth phase cells were collected by centrifuging at 4,500 × g for 8 min. The harvested cells were washed several times with N-free Zarrouk medium to completely remove the N. Then the collected algal cells were re-inoculated into eight nitrogen concentrations set as 0.11, 0.46, 1.84, 7.35, 29.41, 58.82, 117.65, 235.29 mM (that was 1/256, 1/64, 1/16, 1/4, 1, 2, 4, 8-folds of the standard nitrogen concentration of Zarrouk medium, respectively), and used as inoculum at 0.2 of OD750.

## Growth Analysis

5 mL culture samples were taken out and filtered at each sampling time point through a pre-weighed GF/C glass microfiber filter ($W_1$), then washed three times with triple distilled water to remove salts. After the filter was placed at 65°C for more than 6 h, it was transferred to a drying dish and weighed again after cooling ($W_2$). The difference between $W_2$ and $W_1$ was the dry weight (DW) (Zhang et al., 2001). The algal cells cultured for 0, 2, 4, 6, and 7 days were collected by centrifugation to determine the biomass and calculate the specific growth rate. Based on the measured biomass, the specific growth rate was calculated as follows:

$$\mu = (\ln N_2 - \ln N_1)/(t_2 - t_1) \quad (1)$$

where $N_2$ and $N_1$ are the biomass at time $t_2$ and $t_1$, respectively.

## Determination of Photosynthetic Performance

The maximum photochemical quantum yield (*Fv/Fm*) and the non-photochemical quenching (NPQ) respectively, reflected the light energy absorbed by PS II in the form of heat dissipation and the maximum photosynthetic capacity of PS II (Farquhar et al., 1989; Tan et al., 2019). After being placed in the dark for 20 min, 2 mL samples were transferred to a pulse amplitude-modulated (PAM) fluorometer (Water-PAM fluorometer, Walz, Effeltrich, Germany) to measure Chlorophyll fluorescence parameters of photosystem II (PSII). The values of *Fv/Fm* and NPQ were obtained by analyzing the induction curves.

## Measurements of Total Lipid Content and Productivity

Lipids were extracted according to a modified method described by Bligh and Dyer (1959). The microalgae liquid was collected by centrifugation at 4,500 × g and lyophilized overnight by an ALPHA 1–4 LD freeze dryer (Christ, Osterod, Germany). 50 mg of freeze-dried algal powder were weighed correctly into a 100 mL centrifuge tube and crushed three times with an ultrasonic cell crusher (25% power for 20 min). Extraction was performed using 3 mL of chloroform and methanol at a proportion of 2:1 (v/v). Next, 1.2 ml of 0.9% NaCl was added to the extract combined three times. Finally, the lower layer (sediment) of the mixture was collected with a weighted glass tube ($W_1$) and placed in a 60°C water bath pot overnight and then taken out for weighing ($W_2$). The lipid content (LC,%) and productivity (TLP, mg $L^{-1}$ $d^{-1}$) were calculated as follows:

$$LC = (W_2 - W_1)/50 * 100\% \quad (2)$$

$$TLP = W_A * LC/T \quad (3)$$

where $W_A$ is the biomass (mg $L^{-1}$) and T is the culture time (day).

## Measurements of Fucoxanthin Content and Productivity

Fx was extracted according to methods described by Kim et al. (2012a) with modifications. The whole process of extraction was carried out under dim conditions. 10 mg algae powder was accurately weighed and put into a 2 ml grinding tube together with six steel balls and treated with a biological sample homogenizer. The crushed samples were added with 1 ml absolute ethanol and extracted in an Oscillating incubator under ice bath conditions for 1 h. After the Oscillating extraction, the mixture was centrifuged at 5,000 × g for 8 min.

The supernate was filtered through 0.45 μm PTFE filters, and Fx was analyzed by RP-HPLC (reversed-phase high-performance liquid chromatography) using a YMC Carotenoid column (C30, 3.5, 150 × 4.6 mm I.D.). The column temperature was set at 25.0°C and the injection volume was 10 μL. For the Fx assay, 90% acetonitrile and ethyl acetate were used as the mobile phase and operated at a flow rate of 1 ml/min. Under these conditions, the maximum absorbance of standard Fx (Sigma Aldrich) was obtained at 440 nm. The Fx productivity (FxP, mg $L^{-1}$ $d^{-1}$) was calculated as follows:

$$FxP = W_A * FxC/T \quad (4)$$

where $W_A$ is the biomass (mg $L^{-1}$), FxC is the Fx content (mg $g^{-1}$), and T is the culture time (day).

## Determination of Fatty Acid Composition

Fatty acid methyl esters (FAME) were analyzed using gas chromatography (Agilent 6890 Series GC System; US10251016; Agilent, Santa Clara, CA, United States) after transmethylation according to a method described by Lepage and Roy (1984). The FAME composition was used to compute the degree of unsaturation (DU), the cetane number (CN), long-chain saturation factor (LCSF) and cold filter plugging point (CFPP), which were important indicators to expect the combustion performance of biofuel (Ramos et al., 2009).

## Statistical Analysis

Three replicates were set for each treatment, and all results were calculated by Origin 2018 and expressed as mean ± standard deviation (SD). SPSS Statistics software program (version 23) was used for one-way ANOVA at the significance level of $p < 0.05$ to calculate the salient difference between treatments.

# RESULTS

## Growth and Photosynthetic Performance

The Growth curves, specific growth rate and photosynthetic parameters during 7 days of batch growth for *Nitzschia* sp. NW129 under different nitrogen concentrations were summarized in **Figures 1A–D**. When the concentration was more than 29.41 mM, the growth rate of the experimental groups was fast, and there was no significant difference in the specific growth rate throughout the whole process of cultivation, which corresponded to a consistent trend in NPQ values. Although *Fv/Fm* always ranged approximately from 0.60 to 0.66 at nitrogen concentrations ≥ 1.84 mM, which the rapidly increasing NPQ values at concentrations of 1.84 and 7.35 mM from the third day indicated that increased damage to PSII and greater dissipation of absorbed light energy in the form of heat, in accordance with almost no growth or even death of algal cells on the last day. Besides that, it was observed that a strong decrease of the growth rate and *Fv/Fm* when algae were cultured at concentrations of 0.11 and 0.46 mM after 2 days, and the increase of NPQ values accelerated with more extension of cultivation time. Moreover, the lower the nitrogen concentration in the range of concentrations less than 29.41 mM at the end of the culture period, the higher the NPQ value, which indicated that the growth of algal cells was stressed by nitrogen limitation.

## Variation in Fucoxanthin Accumulation

As shown in **Table 1**, the higher nitrogen concentrations could dramatically promote the accumulation of Fx content of *Nitzschia* sp. NW129. Concentrations had no pronounced effect

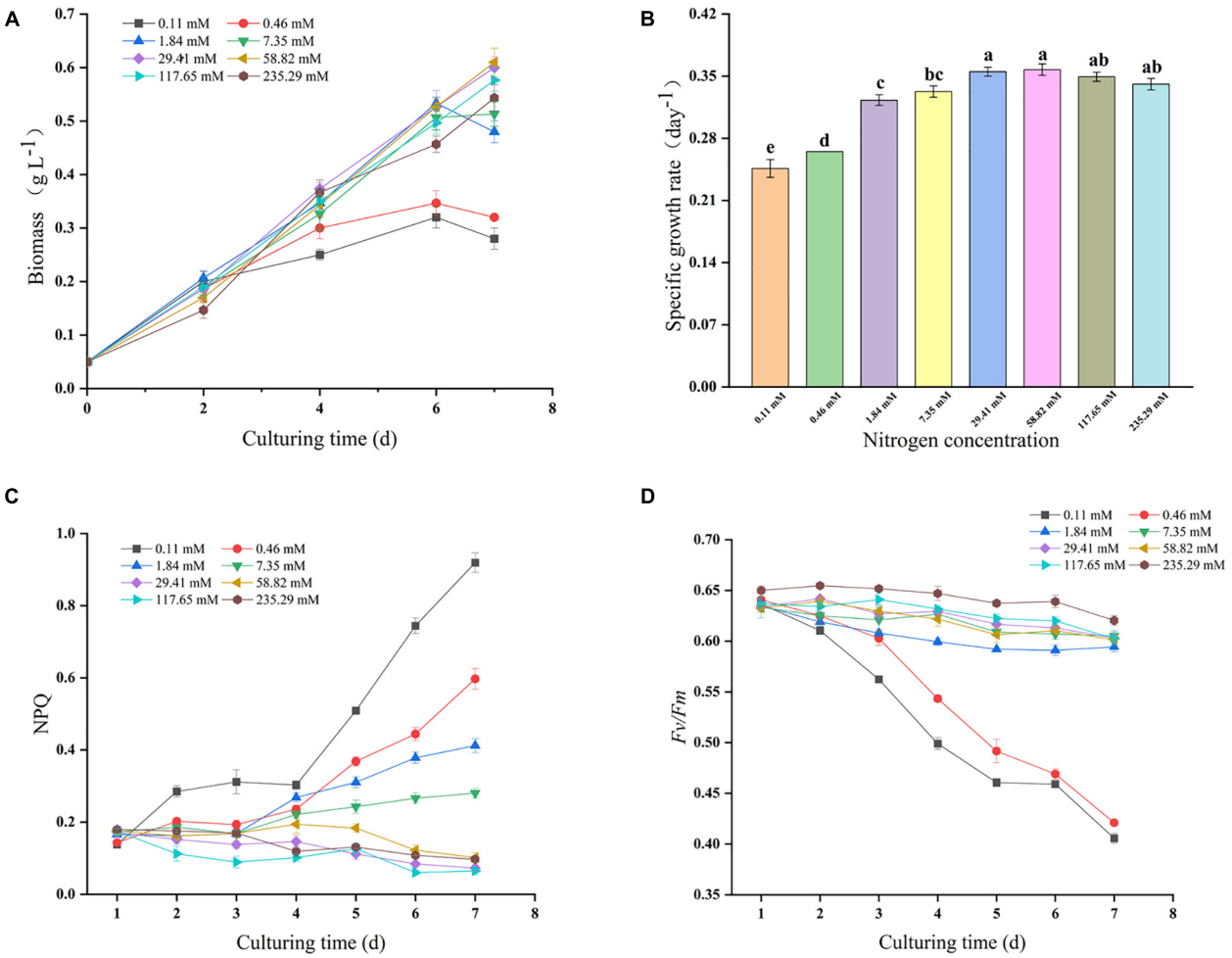


**FIGURE 1 |** Growth and photosynthetic performance of *Nitzschia* sp. NW129 under different nitrogen concentrations. Growth curves **(A)**. Specific growth rate **(B)**. Non-photochemical quenching (NPQ) **(C)**. Maximum quantum yield (*Fv/Fm*) **(D)**. Values are given as mean ± SD, $n = 3$. Letters indicate statistical differences, which was analyzed by a one-way ANOVA with an alpha value of 0.05.

on the Fx content at concentrations ≤ 0.46 mM, but when the concentration rose to 1.84 mM, the Fx content immediately increased to 9.11 ± 0.15 mg $g^{-1}$, which was 3.3 times higher than that of 0.46 mM (2.77 ± 0.06 mg $g^{-1}$). The maximum Fx content of 18.18 ± 0.10 mg $g^{-1}$ was observed at the concentration of 235.29 mM, which was 1.2 times than that at the standard nitrogen concentration of 117.65 mM. The Fx productivity increased apparently with increasing nitrogen concentrations from 0.11 to 117.65 mM, but there was no significant difference among the standard nitrogen concentration (1.32 ± 0.04 mg $d^{-1}$) and the higher concentrations except 117.65 mM (**Table 1**). The Fx content at the concentration of 235.29 mM had no prominent difference in comparison with that at the concentration of 117.65 mM, but its growth was inhibited by excessive nitrogen to a certain extent, bringing about a slightly lower productivity.

## Variation in Lipid Accumulation

Opposite to the Fx content, the lipid content of *Nitzschia* sp. NW129 was enhanced obviously within a certain range in response to the decrease of nitrogen concentration (**Table 1**). The maximum lipid content 40.67 ± 1.04% DW was observed at the concentration of 0.11 mM, which was 1.7 fold higher than that in the standard nitrogen concentration of Zarrouk medium. No considerable difference in lipid content was observed at concentrations ≤ 0.46 and ≥ 1.84 mM, respectively. With concentrations increased from 0.46 to 1.84 mM, the lipid content decreased from 36.50 ± 1.80 to 25.67 ± 2.67% DW (30%). Changes in productivities differed from the trend in content (**Table 1**). Due to the fact that low concentrations promoted an increase in content but markedly reduced biomass, lipid productivity showed an increase followed by a decrease with increasing nitrogen concentrations. Thus, the lipid productivity at the concentration of 0.11 mM was the lowest in spite that the lipid content at this concentration was maximum. The maximum lipid productivity attained 20.290 ± 0.902 mg $L^{-1}$ $d^{-1}$ at the concentration of 29.41 mM, but there were no significant difference among experimental groups of the nitrogen concentrations higher than 29.41 mM.

**TABLE 1 |** Final biomass, lipid and fucoxanthin (Fx) productivities of *Nitzschia* sp. NW129 grown under different nitrogen concentrations.

| Nitrogen concentration | Final Biomass (g $L^{-1}$) | Lipid content (% of dry weight) | Lipid productivity (mg $L^{-1}$ $d^{-1}$) | Fx content (mg $g^{-1}$) | Fx productivity (mg $L^{-1}$ $d^{-1}$) |
|---|---|---|---|---|---|
| 0.11 Mm | $0.28 \pm 0.02^{e}$ | $40.67 \pm 1.04^{a}$ | $16.26 \pm 1.15^{c}$ | $2.21 \pm 0.11^{e}$ | $0.09 \pm 0.01^{e}$ |
| 0.46 mM | $0.32 \pm 0.00^{e}$ | $36.50 \pm 1.80^{a}$ | $16.69 \pm 0.82^{bc}$ | $2.77 \pm 0.06^{e}$ | $0.13 \pm 0.00^{e}$ |
| 1.84 mM | $0.48 \pm 0.02^{d}$ | $25.67 \pm 2.47^{b}$ | $17.56 \pm 1.03^{abc}$ | $9.11 \pm 0.15^{d}$ | $0.63 \pm 0.02^{d}$ |
| 7.35 mM | $0.51 \pm 0.02^{cd}$ | $24.33 \pm 1.44^{b}$ | $17.88 \pm 1.89^{abc}$ | $12.44 \pm 0.19^{c}$ | $0.91 \pm 0.05^{c}$ |
| 29.41 mM | $0.60 \pm 0.02^{ab}$ | $23.67 \pm 0.29^{b}$ | $20.29 \pm 0.90^{a}$ | $15.44 \pm 0.14^{b}$ | $1.32 \pm 0.04^{b}$ |
| 58.82 mM | $0.61 \pm 0.03^{a}$ | $23.31 \pm 1.32^{b}$ | $20.28 \pm 0.33^{a}$ | $15.73 \pm 0.35^{b}$ | $1.37 \pm 0.06^{ab}$ |
| 117.65 mM | $0.58 \pm 0.02^{ab}$ | $23.98 \pm 2.10^{b}$ | $19.95 \pm 1.29^{a}$ | $17.55 \pm 1.13^{a}$ | $1.44 \pm 0.05^{a}$ |
| 235.29 mM | $0.54 \pm 0.03^{bc}$ | $25.19 \pm 2.18^{b}$ | $19.51 \pm 0.94^{ab}$ | $18.18 \pm 0.10^{a}$ | $1.41 \pm 0.06^{ab}$ |

*Values mean ± SD (n = 3). Values with the different letters indicate a significant difference between them ($p < 0.05$).*

## Variation in Fatty Acid Profiles and Biofuel Quality

The fatty acid profile and some biofuel indicators of *Nitzschia* sp. at three concentrations were summarized in **Table 2**. In this study, C14 to C16 were dominant in the FAME of isolated *Nitzschia* sp. Obviously, the content of saturated fatty acids (SFA) and unsaturated fatty acids was disparity under different nitrogen concentrations. Only eight fatty acids without polyunsaturated fatty acids (PUFA) were detected at the concentration of 0.11 mM, which contributed to the lowest DU of 10. Compared with the standard nitrogen concentration, the proportion of myristic acid (C14:0) decreased from 46.06 to 19.49% and pentadecanoic acid (C15:0) increased from 1.39 to 26.20% at the concentration of 0.11 mM. The percentage composition of SFA, Monounsaturated fatty acids (MUFA) and PUFA of *Nitzschia* sp. cultivated in the standard nitrogen concentration were 84.93, 12.59, and 2.21%, respectively. The increase of concentrations markedly contributed to the accumulation of unsaturated fatty acids, the highest values of 40.83% MUFA and 4.57% PUFA were observed at the concentration of 117.65 mM. Compared to the standard nitrogen concentration, the ginkgolic Acid (C15:1) and palmitoleic acid (C16:1) increased from 6.40 to 10.19% and from 0.37 to 25.58%, respectively, which led to higher DU value of 49.97 at the concentration of 117.65 mM. The nitrogen enrichment also promoted the increase of fatty acid species and the production of eicosapentaenoic acid (EPA). The CN value at the concentrations of 117.65 mM were saliently lower compared to standard nitrogen concentration. In addition, the extremely low content of long-chain saturated fatty acids under three treatments resulted in lower LCSF and CFPP.

# DISCUSSION

Nitrogen, known as "life element," is a macronutrient essential for algal growth and the production of lipids, pigments, terpenes and other substances. The genes encoding photosynthesis-related proteins in diatoms were significantly down-regulated under nitrogen deficiency conditions (Hockin et al., 2012; Yang et al., 2013). Meanwhile, the lack of nitrogen also triggered the degradation of nitrogen-containing compounds such as chlorophyll and entrained cellular chlorosis (Pancha et al., 2014). Therefore, the weakened photoreaction diminished the 5′-Adenylate triphosphate (ATP) and nicotinamide adenine dinucleotide phosphate (NADPH) necessary for carbon fixation, which led to the reduction of carbon dioxide fixed by algal cells and ultimately the reduction of biomass. NPQ mediated and *Fv/Fm* could be useful indicators for judging the nutritional limitation and stress degree of algal cells (Ruban et al., 2004). The high NPQ and low *Fv/Fm* values were frequently observed in plants under stress conditions, which indicated that the process of photosynthesis was hindered and more energy flew to heat dissipation (Li et al., 2020). In this study, the biomass and *Fv/Fm* at concentrations of 0.11 and 0.46 mM were significantly lower than those under higher concentrations, while NPQ was opposite. Compared with the nitrogen concentration of the standard nitrogen concentration of Zarrouk medium, the distinctly reduced specific growth rate concurred with the higher NPQ value at concentrations of 1.84 and 7.35 mM, which suggested that nitrogen deficiency restrained the growth and photosynthesis of algal cells. Furthermore, the biomass at concentrations $\geq$ 117.65 mM was slightly lower in comparison with that at the standard nitrogen concentration, which may be because the growth of algal cells was suppressed by the excessive nitrate in the culture medium (Feng et al., 2011).

It has been documented that Fx has high antioxidant capacity due to its allyl bond and six oxygen atoms, especially in a hypoxic environment (Peng et al., 2011). Heo et al. (2008) found that Fx could effectively inhibit the generation of reactive oxygen species by increasing catalase activity, thereby having antioxidant activity, preventing DNA damage and $H_2O_2$-induced fineness apoptosis. The gradual reduction of Fx content with decreasing the nitrogen concentrations in this study was similar to the response of *Phaeodactylum tricornutum* to nitrogen consumption (Gao et al., 2017). The mRNA level of genes encoding photosynthetic protein decreased remarkably under N restriction (Yang et al., 2013). Longworth et al. (2016) discovered that the relative abundances of light-harvesting proteins decreased under nitrogen stress. Fx combined with chlorophyll a/c to form fucoxanthin-chlorophyll a/c protein complex (FCP) in diatoms, the FCP existed in the thylakoid and played a role in light capture and light transmission (Wang et al., 2005), which had a high content of nitrogen. Therefore, under conditions of nitrogen scarcity, cells tend to degrade them actively to reuse nitrogen and transfer it to the synthesis of those proteins that are indispensable

**TABLE 2 |** Effects of different nitrogen concentrations on the fatty acid profiles and biofuel quality of *Nitzschia* sp. NW129.

| Fatty acid | Fatty acid content (% w/w) | | |
|---|---|---|---|
| | **0.11 mM** | **29.41 mM** | **117.65 mM** |
| C4:0 | $0.92 \pm 0.02^{a}$ | $0.05 \pm 0.01^{c}$ | $0.14 \pm 0.01^{b}$ |
| C6:0 | $4.81 \pm 0.04^{a}$ | $0.21 \pm 0.02^{c}$ | $0.29 \pm 0.02^{b}$ |
| C12:0 | ND | $0.19 \pm 0.01$ | ND |
| C14:0 | $19.49 \pm 0.73^{b}$ | $46.06 \pm 0.28^{a}$ | $13.48 \pm 0.15^{c}$ |
| C15:0 | $26.20 \pm 1.16^{a}$ | $1.39 \pm 0.05^{b}$ | $1.10 \pm 0.03^{b}$ |
| C16:0 | $37.89 \pm 0.64^{a}$ | $35.70 \pm 0.11^{b}$ | $35.98 \pm 0.45^{b}$ |
| C18:0 | ND | $0.62 \pm 0.03^{b}$ | $1.38 \pm 0.07^{a}$ |
| C20:0 | ND | $0.05 \pm 0.01^{b}$ | $0.26 \pm 0.02^{a}$ |
| C22:0 | ND | $0.26 \pm 0.03^{a}$ | $0.16 \pm 0.02^{b}$ |
| C23:0 | ND | ND | $1.02 \pm 0.02$ |
| C24:0 | ND | $0.22 \pm 0.01^{b}$ | $0.61 \pm 0.02^{a}$ |
| C14:n-5 | $0.43 \pm 0.01^{c}$ | $0.73 \pm 0.03^{b}$ | $1.14 \pm 0.06^{a}$ |
| C15:n-5 | $9.24 \pm 0.03^{b}$ | $6.40 \pm 0.07^{c}$ | $10.19 \pm 0.09^{a}$ |
| C16:n-7 | $0.33 \pm 0.02^{b}$ | $0.37 \pm 0.02^{b}$ | $25.58 \pm 0.16^{a}$ |
| C17:n-7 | ND | $2.26 \pm 0.07^{a}$ | $1.12 \pm 0.04^{b}$ |
| C18:n-9 | ND | $1.45 \pm 0.02^{b}$ | $1.71 \pm 0.05^{a}$ |
| C18:n-9 | ND | $0.70 \pm 0.01^{b}$ | $1.02 \pm 0.04^{a}$ |
| C22:n-9 | ND | $0.68 \pm 0.02^{b}$ | $0.08 \pm 0.01^{a}$ |
| C18:2n-6 | ND | $0.08 \pm 0.01^{b}$ | $0.24 \pm 0.01^{a}$ |
| C18:2n-6 | ND | $0.05 \pm 0.01^{b}$ | $0.26 \pm 0.02^{a}$ |
| C18:3n-6 | ND | $0.01 \pm 0.00^{b}$ | $0.15 \pm 0.01^{a}$ |
| C20:3n-3 | ND | $2.08 \pm 0.03^{a}$ | $1.00 \pm 0.02^{b}$ |
| C20:5n-3 | ND | ND | $2.82 \pm 0.09$ |
| SFA | $89.40 \pm 0.89^{a}$ | $84.93 \pm 0.45^{b}$ | $54.41 \pm 0.65^{c}$ |
| MUFA | $10.00 \pm 0.05^{c}$ | $12.59 \pm 0.07^{b}$ | $40.83 \pm 0.28^{a}$ |
| PUFA | ND | $2.21 \pm 0.03^{b}$ | $4.57 \pm 0.12^{a}$ |
| DU | $10.00 \pm 0.05^{c}$ | $17.01 \pm 0.11^{b}$ | $49.97 \pm 0.46^{a}$ |
| CN | $64.63 \pm 0.56^{b}$ | $66.79 \pm 0.26^{a}$ | $62.72 \pm 0.53^{c}$ |
| LCSF | $3.79 \pm 0.06^{c}$ | $4.76 \pm 0.07^{b}$ | $6.00 \pm 0.05^{a}$ |
| CFPP | $-4.57 \pm 0.20^{c}$ | $-1.52 \pm 0.22^{b}$ | $2.37 \pm 0.17^{a}$ |

*SFA, saturated fatty acids; MUFA, monounsaturated fatty acids; PUFA, polyunsaturated fatty acids; DU, degree of unsaturation, DU = (MUFA + 2 PUFA); CN, cetane number; LCSF, long chain saturated factor, LCSF = 0.1 × C16:0(%) + 0.5 × C18:0(%) + 1 × C20:0(%) + 1.5 × C22:0(%) + 2 × C24:0(%); CFPP, cold filter plugging point, CFPP = (3.1417 × LCSF) - 16.477; ND, below the limit of detection.*

*Each data value represents the mean ± SD of three replications. Values with the different letters indicate a significant difference between them ($p < 0.05$).*

for cell survival. *P. tricornutum* with high Fx content (0.2–16.51 mg $g^{-1}$) has been widely concerned, which was several times more abundant than that in macroalgae (Kim et al., 2012a; Gomez-Loredo et al., 2016; Wu et al., 2016; Ishika et al., 2017; Gao et al., 2020). It has been reported that Fx content obtained from *Nitzschia* sp. was from 0.49 to 12 mg $g^{-1}$ (Kim et al., 2012b; Guo et al., 2016; Lu et al., 2018; Sahin et al., 2019). The Fx content of *Nitzschia* sp. NW129 was higher under the nitrogen enrichment conditions, consistent with Sahin et al. (2019) on the noticeable increase in Fx content caused by nitrate supplementation to *Nitzschia* sp. Compared with other reports on *Nitzschia* sp., the highest Fx content of *Nitzschia* sp. NW129 was 18.176 mg $g^{-1}$, indicating that it cultured under high nitrogen conditions had better potential for Fx production.

In previous studies, the effects of nitrogen deficiency on lipid accumulation were species-specific. Carbohydrates, the primary energy storage substances in Odontella aurita and Arthrospira platensis under nitrogen-limited conditions, increased rather than lipids (Panyakampol et al., 2016; Xia et al., 2018). However, the lipid content of most microalgae increased under nitrogen limitation (Shifrin and Chisholm, 2010). For example, the lipid content of *Chlorella vulgaris* and *Nannochloropsis oculata* cultured under nutrients-stress conditions increased by 2–3-fold compared to the high nitrogen concentration (Converti et al., 2009). In agreement with the above results, in the present study, a lipid content of 40.67% was observed at the lowest nitrogen concentration, which was 1.7 times higher than that at standard nitrogen concentration. Under nitrogen-limited conditions, most genes related to photosynthesis and chlorophyll biosynthesis were inhibited, and a variety of roles in carbon metabolism were changed, such as the down-regulation of Calvin cycle, the up-regulation of glycolysis and tricarboxylic acid cycle, generating more carbon sources flowing into lipid metabolism (Alipanah et al., 2015). Nitrogen concentrations affected not only lipid content but also the fatty acid composition of diatoms greatly, which determined the quality of biofuel. CFPP, the temperature of filter blockage caused by crystallization of fuel, was generally acknowledged as an important indicator to measure the performance of biofuel in the global biofuel industry (Gomez-Rodriguez et al., 2021). The low CFPP obtained at three concentrations met European standards (EN14214) and represented a superior cold flow property of the biofuel (Stansell et al., 2012). The sum of SFA and MUFA contents of the *Nitzschia* sp. NW129 exceeded 90% under different nitrogen concentrations, which was in accordance with the previous results (Sahin et al., 2019). It was reported that high nitrogen concentration generated greater accumulation of MUFA while the higher percentage of SFA and PUFA were observed under nitrogen deficiency (Qiao et al., 2016). Compared to the standard nitrogen concentration, the proportion of C14:0 decreased markedly whereas C15:1 and C16:1 was significantly increased at the concentration of 117.65 mM, which contributed to a higher DU value. The high DU value represented that the biofuel was more difficult to form deposits and had better lubricity (Qiao et al., 2021). The maximum and minimum values of DU and CN should be 137 and 51, respectively (EN14214). DU and CN values under three nitrogen concentrations were in accordance with it. Furthermore, the content of linolenic acid (C18:3) under three treatments was less than 12% limited in EN14214 (Chisti, 2007). The fatty acid profile indicated that *Nitzschia* sp. NW129 was a potential candidate for biofuel production.

Productivity, determined by a combination of biomass and content, was a crucial quality in selecting strains for large-scale production of high-value materials (Griffiths and Harrison, 2009). Therefore, the effects of nutritional conditions on biomass and content needed to be taken into account together. The lipid content (3.44–31.96% DW) of thirty microalgal strains under nitrogen deprivation conditions was higher than that under nitrogen-sufficient. Interestingly, 24 of them showed lower lipid productivities (0.085–4.560 mg $L^{-1}$ $d^{-1}$) under nitrogen-free conditions. Andeden et al. (2021) reported that most microalgal strains in nitrogen-free cultivation showed

lower lipid productivities compared with the nitrogen-sufficient condition. However, as nitrogen deficiency affected the biomass and lipid content in different microalgal species to different degrees, higher lipid productivities of 10 algae species such as *Ankistrodesmus falcatus*, *Chlorella vulgaris,* and *Scenedesmus* sp. in low nitrate-stress induced cultures were observed (Griffiths et al., 2012). As to Fx, the nitrogen enrichment generally promoted the accumulation of biomass and Fx content at the same time, which would undoubtedly increase Fx productivity (Sun et al., 2019). Interestingly, it was found that the higher Fx content was caused by high biomass concentration and higher biomass and Fx productivities were induced by low biomass concentration (Gao et al., 2020). These results suggested the microalgae presented different responses in terms of the productivities of lipid and Fx under nitrogen replete and limited conditions, which it was difficult to obtain high Fx and lipid productivities in the meantime. In the present study, the increase in nitrogen concentration was accompanied by an increase in lipid productivity, yet there was no significant difference in productivities between different nitrogen concentrations when concentrations were higher than 1.84 mM. The maximum Fx productivity of the *Nitzschia* sp. NW129 was 1.44 $\pm$ 0.05 mg $L^{-1}$ $d^{-1}$ at the concentration of 117.65 mM, which was saliently higher than the standard nitrogen concentration and 2–3 times more than *P. tricornutum*, *Navicula* sp., and *Amphora* sp. (Ishika et al., 2017; Wang et al., 2018b). Thus, the concentration of 117.65 mM was considered the most suitable for simultaneous production of lipids and Fx in biorefinery. The overall performance of *Nitzschia* sp. NW129 at this concentration was equivalent to or higher than that of non-polar microalgae, which could be good producers of lipids or Fx.

## CONCLUSION

In this study, an appropriate nitrogen concentration of 117.65 mM was screened and excellent productivities of lipid ($19.95 \pm 1.29$ mg $L^{-1}$ $d^{-1}$) and Fx ($1.44 \pm 0.05$ mg $L^{-1}$ $d^{-1}$) were obtained from the alkalophilic microalga *Nitzschia* sp. NW129 simultaneously. Furthermore, this concentration induced the accumulation of unsaturated fatty acids, especially MUFA, resulting in superior biofuel properties. In a nutshell, these results demonstrated the feasibility of utilizing the alkalophilic microalgae for the integrated production of biofuels and Fx in biorefinery and emphasized the potential of *Nitzschia* sp. NW129 as a promising feedstock.

## DATA AVAILABILITY STATEMENT

The original contributions presented in the study are included in the article/supplementary material, further inquiries can be directed to the corresponding author/s.

## AUTHOR CONTRIBUTIONS

ZC: data curation and writing—original draft preparation. YL and BZ: writing—review and editing. XS: conceptualization. XW: formal analysis. YL: revision. KP: funding acquisition. All authors have read and agreed to the published version of the manuscript.

## FUNDING

This research was funded by the National Key Research and Development Program of China (2016YFB0601001).

## ACKNOWLEDGMENTS

We gratefully acknowledge the kind assistance of Ruihao Zhang and Xiufen Wang in writing the manuscript.

## REFERENCES

Alipanah, L., Rohloff, J., Winge, P., Bones, A. M., and Brembu, T. (2015). Whole-cell response to nitrogen deprivation in the diatom *Phaeodactylum tricornutum*. *J. Exp. Bot.* 66, 6281–6296. doi: 10.1093/jxb/erv340

Andeden, E. E., Ozturk, S., and Aslim, B. (2021). Evaluation of thirty microalgal isolates as biofuel feedstocks based on lipid productivity and triacylglycerol (TAG) content. *Curr. Microbiol.* 78, 775–788. doi: 10.1007/s00284-020-02340-5

Bligh, E. G., and Dyer, W. J. (1959). A rapid method of total lipid extraction and purification. *Can. J. Biochem. Physiol.* 37, 911–917. doi: 10.1139/o59-099

Bondioli, P., Della, B. L., Rivolta, G., Zittelli, G. C., Bassi, N., Rodolfi, L., et al. (2012). Oil production by the marine microalgae *Nannochloropsis* sp F&M-M24 and *Tetraselmis suecica* F&M-M33. *Bioresour. Technol.* 114, 567–572. doi: 10.1016/j.biortech.2012.02.123

Campenni', L., Nobre, B. P., Santos, C. A., Oliveira, A. C., Aires-Barros, M. R., Palavra, A. M. F., et al. (2013). Carotenoid and lipid production by the autotrophic microalga *Chlorella protothecoides* under nutritional, salinity, and luminosity stress conditions. *Appl. Microbiol. Biotechnol.* 97, 1383–1393. doi: 10.1007/s00253-012-4570-6

Chisti, Y. (2007). Biofuel from microalgae. *Biotechnol. Adv.* 25, 294–306. doi: 10.1016/j.biotechadv.2007.02.001

Converti, A., Casazza, A. A., Ortiz, E. Y., Perego, P., and Del Borghi, M. (2009). Effect of temperature and nitrogen concentration on the growth and lipid content of *Nannochloropsis oculata* and *Chlorella vulgaris* for biofuel production. *Chem. Eng. Process.* 48, 1146–1151. doi: 10.1016/j.cep.2009.03.006

Cui, J., Zhong, D. B., Zhao, Y. T., and Yu, X. Y. (2020). Melatonin and calcium act synergistically to enhance the coproduction of astaxanthin and lipids in *Haematococcus pluvialis* under nitrogen deficiency and high light conditions. *Bioresour. Technol.* 305:123069. doi: 10.1016/j.biortech.2020.123069

Farquhar, G. D., Wong, S. C., Evans, J. R., and Hubick, K. T. (1989). "Photosynthesis and gas exchange," in *Plants Under Stress*, eds H. G. Jones, T. J. Flowers, and M. B. Jones (Cambridge: Cambridge University Press), 47–69.

Feng, D. N., Chen, Z. A., Xue, S., and Zhang, W. (2011). Increased lipid production of the marine oleaginous microalgae *Isochrysis zhangjiangensis* (Chrysophyta) by nitrogen supplement. *Bioresour. Technol.* 102, 6710–6716. doi: 10.1016/j.biortech.2011.04.006

Gao, B. Y., Chen, A. L., Zhang, W. Y., Li, A. F., and Zhang, C. W. (2017). Co-production of lipids, eicosapentaenoic acid, fucoxanthin, and chrysolaminarin by phaeodactylum tricornutum cultured in a flat-plate photobioreactor under varying nitrogen conditions. *J. Ocean Univ. China* 16, 916–924. doi: 10.1007/s11802-017-3174-2

Gao, F. Z., Sa, M., Teles, I., Wijffels, R. H., and Barbosa, M. J. (2020). Production and monitoring of biomass and fucoxanthin with brown microalgae under

outdoor conditions. *Biotechnol. Bioeng.* 118, 1355–1365. doi: 10.1002/bit.27657

Gomez-Loredo, A., Benavides, J., and Rito-Palomares, M. (2016). Growth kinetics and fucoxanthin production of *Phaeodactylum tricornutum* and *Isochrysis galbana* cultures at different light and agitation conditions. *J. Appl. Phycol.* 28, 849–860. doi: 10.1007/s10811-015-0635-0

Gomez-Rodriguez, K. A., Chavarria-Hernandez, J. C., and Martinez-Tapia, G. E. (2021). Estimation of cold flow properties of biofuel from fatty acid composition. *Energ. Fuel.* 35, 1442–1448. doi: 10.1021/acs.energyfuels.0c03237

Griffiths, M. J., and Harrison, S. T. L. (2009). Lipid productivity as a key characteristic for choosing algal species for biofuel production. *J. Appl. Phycol.* 21, 493–507. doi: 10.1007/s10811-008-9392-7

Griffiths, M. J., van Hille, R. P., and Harrison, S. T. L. (2012). Lipid productivity, settling potential and fatty acid profile of 11 microalgal species grown under nitrogen replete and limited conditions. *J. Appl. Phycol.* 24, 989–1001. doi: 10.1007/s10811-011-9723-y

Guo, B. B., Liu, B., Yang, B., Sun, P. P., Liu, X., Liu, J., et al. (2016). Screening of Diatom strains and characterization of *Cyclotella cryptica* as a potential fucoxanthin producer. *Mar. Drugs* 14:125. doi: 10.3390/md14070125

Guo, H., Li, T., Zhao, Y. T., and Yu, X. Y. (2021). Role of copper in the enhancement of astaxanthin and lipid coaccumulation in *Haematococcus pluvialis* exposed to abiotic stress conditions. *Bioresour. Technol.* 335:125265. doi: 10.1016/j.biortech.2021.125265

Heo, S. J., Ko, S. C., Kang, S. M., Kang, H. S., Kim, J. P., Kim, S. H., et al. (2008). Cytoprotective effect of fucoxanthin isolated from brown algae *Sargassum siliquastrum* against H2O2-induced cell damage. *Eur. Food Res. Technol.* 228, 145–151. doi: 10.1007/s00217-008-0918-7

Hockin, N. L., Mock, T. F., Mulholland, F., Kopriva, S., and Malin, G. (2012). The response of Diatom central carbon metabolism to nitrogen starvation is different from that of green algae and higher plants. *Plant Physiol.* 158, 299–312. doi: 10.1104/pp.111.184333

Ishika, T., Moheimani, N. R., Bahri, P. A., Laird, D. W., Blair, S., and Parlevliet, D. (2017). Halo-adapted microalgae for fucoxanthin production: effect of incremental increase in salinity. *Algal Res.* 28, 66–73. doi: 10.1016/j.algal.2017.10.002

Kim, S. M., Jung, Y. J., Kwon, O. N., Cha, K. H., Um, B. H., Chung, D., et al. (2012a). A potential commercial source of fucoxanthin extracted from the microalga *Phaeodactylum tricornutum*. *Appl. Biochem. Biotechnol.* 166, 1843–1855. doi: 10.1007/s12010-012-9602-2

Kim, S. M., Kang, S. W., Kwon, O. N., Chung, D., and Pan, C. H. (2012b). Fucoxanthin as a major carotenoid in *Isochrysis aff. galbana*: characterization of extraction for commercial application. *J. Korean Soc. Appl. Biol. Chem.* 55, 477–483. doi: 10.1007/s13765-012-2108-3

Kuo, C. M., Lin, T. H., Yang, Y. C., Zhang, W. X., Lai, J. T., Wu, H. T., et al. (2017). Ability of an alkali-tolerant mutant strain of the microalga *Chlorella* sp. AT1 to capture carbon dioxide for increasing carbon dioxide utilization efficiency. *Bioresour. Technol.* 244, 243–251. doi: 10.1016/j.biortech.2017.07.096

Lai, Y. C., Karam, A. L., Sederoff, H. W., Ducoste, J. J., and de los Reyes, F. L. (2019). Relating nitrogen concentration and light intensity to the growth and lipid accumulation of *Dunaliella viridis* in a photobioreactor. *J. Appl. Phycol.* 31, 3397–3409. doi: 10.1007/s10811-019-01897-4

Lepage, G., and Roy, C. C. (1984). Improved recovery of fatty acid through direct transesterification without prior extraction or purification. *J. Lipid Res.* 25, 1391–1396. doi: 10.1089/jir.1984.4.635

Li, J., Tang, X. X., Pan, K. H., Zhu, B. H., Li, Y., Ma, X. B., et al. (2020). The regulating mechanisms of CO2 fixation and carbon allocations of two *Chlorella* sp. strains in response to high CO2 levels. *Chemosphere* 247:125814. doi: 10.1016/j.chemosphere.2020.125814

Liu, J., Mao, X. M., Zhou, W. G., and Guarnieri, M. T. (2016). Simultaneous production of triacylglycerol and high-value carotenoids by the astaxanthin-producing oleaginous green microalga *Chlorella zofingiensis*. *Bioresour. Technol.* 214, 319–327. doi: 10.1016/j.biortech.2016.04.112

Longworth, J., Wu, D. Y., Huete-Ortega, M., Wright, P. C., and Vaidyanathan, S. (2016). Proteome response of *Phaeodactylum tricornutum*, during lipid accumulation induced by nitrogen depletion. *Alagl Res.* 18, 213–224. doi: 10.1016/j.algal.2016.06.015

Lu, X., Sun, H., Zhao, W. Y., Cheng, K. W., Chen, F., and Liu, B. (2018). A hetero-photoautotrophic two-stage cultivation process for production of fucoxanthin by the marine diatom *Nitzschia laevis*. *Mar. Drugs* 16:219. doi: 10.3390/md16070219

Malviya, S., Scalco, E., Audic, S., Vincenta, F., Veluchamy, A., Poulain, J., et al. (2016). Insights into global diatom distribution and diversity in the world's ocean. *Proc. Natl. Acad. Sci. U.S.A.* 113, E1516–E1525. doi: 10.1073/pnas.1509523113

Mohamadnia, S., Tavakoli, O., Faramarzi, M. A., and Shamsollahi, Z. (2020). Production of fucoxanthin by the microalga *Tisochrysis lutea*: a review of recent developments. *Aquaculture* 516:734637. doi: 10.1016/j.aquaculture.2019.734637

Pancha, I., Chokshi, K., George, B., Ghosh, T., Paliwal, C., Maurya, R., et al. (2014). Nitrogen stress triggered biochemical and morphological changes in the microalgae *Scenedesmus* sp. CCNM 1077. *Bioresour. Technol.* 156, 146–154. doi: 10.1016/j.biortech.2014.01.025

Panyakampol, J., Cheevadhanarak, S., Senachak, J., Dulsawat, S., Siangdung, W., and Tanticharoen, M. (2016). Different effects of the combined stress of nitrogen depletion and high temperature than an individual stress on the synthesis of biochemical compounds in *Arthrospira platensis* C1 (PCC 9438). *J. Appl. Phycol.* 28, 2177–2186. doi: 10.1007/s10811-015-0765-4

Peng, J., Yuan, J. P., Wu, C. F., and Wang, J. H. (2011). Fucoxanthin, a marine carotenoid present in brown seaweeds and Diatoms: metabolism and bioactivities relevant to human health. *Mar. Drugs* 9, 1806–1828. doi: 10.3390/md9101806

Peng, L. C., Lan, C. Q., Zhang, Z. S., Sarch, C., and Laporte, M. (2015). Control of protozoa contamination and lipid accumulation in *Neochloris oleoabundans* culture: effects of pH and dissolved inorganic carbon. *Bioresour. Technol.* 197, 143–151. doi: 10.1016/j.biortech.2015.07.101

Qiao, H. J., Cong, C., Sun, C. X., Li, B. S., Wang, J. Y., and Zhang, L. M. (2016). Effect of culture conditions on growth, fatty acid composition and DHA/EPA ratio of *Phaeodactylum tricornutum*. *Aquaculture* 452, 311–317. doi: 10.1016/j.aquaculture.2015.11.011

Qiao, T. S., Zhao, Y. T., Han, B. Y., Li, T., Zhao, P., Xu, J. W., et al. (2021). Myo-inositol promotes lipid production and nutrients removal by microalga under molasses wastewater. *Renew. Energ.* 172, 327–335. doi: 10.1016/j.renene.2021.03.051

Qu, D. H., and Miao, X. L. (2021). Carbon flow conversion induces alkali resistance and lipid accumulation under alkaline conditions based on transcriptome analysis in Chlorella sp. BLD. *Chemosphere* 265:129046. doi: 10.1016/j.chemosphere.2020.129046

Ramos, M. J., Fernandez, C. M., Casas, A., Rodriguez, L., and Perez, A. (2009). Influence of fatty acid composition of raw materials on biofuel properties. *Bioresour. Technol.* 100, 261–268. doi: 10.1016/j.biortech.2008.06.039

Riccioni, G. (2012). Marine carotenoids and oxidative stress. *Mar. Drugs* 10, 116–118. doi: 10.3390/md10010116

Ruban, A. V., Lavaud, J., Rousseau, B., Guglielmi, G., Horton, P., and Etienne, A. L. (2004). The super-excess energy dissipation in diatom algae: comparative analysis with higher plants. *Photosynth. Res.* 82, 165–175. doi: 10.1007/s11120-004-1456-1

Sahin, M. S., Khazi, M. I., Demirel, Z., and Dalay, M. C. (2019). Variation in growth, fucoxanthin, fatty acids profile and lipid content of marine diatoms *Nitzschia* sp. and *Nanofrustulum shiloi* in response to nitrogen and iron. *Biocatal. Agric. Biotechnol.* 17, 390–398. doi: 10.1016/j.bcab.2018.12.023

Santos, A. M., Lamers, P. P., Janssen, M., and Wijffels, R. H. (2013). Biomass and lipid productivity of *Neochloris oleoabundans* under alkaline-saline conditions. *Algal Res.* 2, 204–211. doi: 10.1016/j.algal.2013.04.007

Sathasivam, R., and Ki, J. S. (2018). A review of the biological activities of microalgal carotenoids and their potential use in healthcare and cosmetic industries. *Mar. Drugs* 16:26. doi: 10.3390/md16010026

Shifrin, N. S., and Chisholm, S. W. (2010). Phytoplankton lipids: interspecific differences and effects of nitrate, silicate and light-dark cycles. *J. Phycol.* 17, 374–384. doi: 10.1111/j.1529-8817.1981.tb00865.x

Stansell, G. R., Gray, V. M., and Sym, S. D. (2012). Erratum to: microalgal fatty acid composition: implications for biofuel quality. *J. Appl. Phycol.* 24, 985–985. doi: 10.1007/s10811-012-9824-2

Sun, Z., Wang, X. F., and Liu, J. (2019). Screening of *Isochrysis* strains for simultaneous production of docosahexaenoic acid and fucoxanthin. *Alagal Res.* 41:101545. doi: 10.1016/j.algal.2019.101545

Tan, L. J., Xu, W. J., He, X. L., and Wang, J. T. (2019). The feasibility of Fv/Fm on judging nutrient limitation of marine algae through indoor simulation and in situ experiment. *Estuar. Coast. Shelfs* 229:106411. doi: 10.1016/j.ecss.2019.106411

Tanaka, T., Shnimizu, M., and Moriwaki, H. (2012). Cancer chemoprevention by carotenoids. *Molecules* 17, 3202–3242. doi: 10.3390/molecules17033202

Vadlamani, A., Viamajala, S., Pendyala, B., and Varanasi, S. (2017). Cultivation of microalgae at extreme alkaline pH conditions: a novel approach for biofuel production. *ACS. Sustain. Chem. Eng.* 5, 7284–7294. doi: 10.1021/acssuschemeng.7b01534

Wang, S., Said, I. H., Thorstenson, C., Thomsen, C., Ullrich, M. S., Kuhnert, N., et al. (2018a). Pilot-scale production of antibacterial substances by the marine diatom *Phaeodactylum tricornutum* Bohlin. *Algal Res.* 32, 113–120. doi: 10.1016/j.algal.2018.03.014

Wang, S., Verma, S. K., Said, I. H., Thomsen, L., Ullrich, M. S., and Kuhnert, N. (2018b). Changes in the fucoxanthin production and protein profiles in *Cylindrotheca closterium* in response to blue light-emitting diode light. *Microb. Cell Fact.* 17:110. doi: 10.1186/s12934-018-0957-0

Wang, W. J., Wang, G. C., Zhang, M., and Tseng, C. K. (2005). Isolation of fucoxanthin from the rhizoid of *Laminaria japonica* Aresch. *J. Integr. Plant Biol.* 47, 1009–1015. doi: 10.1111/j.1744-7909.2005.00054.x

Wang, X. J., Jin, G. Y., Wang, X. F., Ma, X. B., and Liu, Q. K. (2019). Separation, identification and assessing of potential application of a strain of *Nitzschia* sp. in Hamatai Lake. *Hebei Fish.* 11, 8–12+16. doi: 10.3969/j.issn.1004-6755.2019.11.002

Wensel, P., Helms, G., Hiscox, B., Davis, W. C., Kirchhoff, H., Bule, M., et al. (2014). Isolation, characterization, and validation of oleaginous, multi-trophic, and haloalkaline-tolerant microalgae for two-stage cultivation. *Algal Res.* 4, 2–11. doi: 10.1016/j.algal.2013.12.005

Wu, H. L., Li, T., Dai, S. K., He, H., and Xiang, W. Z. (2016). A comparative analysis of fatty acid composition and fucoxanthin content in six *Phaeodactylum tricornutum* strains from diff erent origins. *Chin. J. Oceanol. Limnol.* 34, 391–398. doi: 10.1007/s00343-015-4325-1

Xia, S., Gao, B. Y., Fu, J. Q., Xiong, J. H., and Zhang, C. W. (2018). Production of fucoxanthin, chrysolaminarin, and eicosapentaenoic acid by *Odontella aurita* under different nitrogen supply regimes. *J. Biosci. Bioeng.* 126, 723–729. doi: 10.1016/j.jbiosc.2018.06.002

Xia, S., Wang, K., Wan, L. L., Li, A. F., Hu, Q., and Zhang, C. W. (2013). Production, characterization, and antioxidant activity of fucoxanthin from the marine diatom, *Odontella aurita*. *Mar. Drugs* 11, 2667–2681. doi: 10.3390/md11072667

Yang, Z. H., Zhao, Y., Liu, Z. Y., Liu, C. F., Hu, Z. P., and Hou, Y. Y. (2017). A mathematical model of neutral lipid content in terms of initial nitrogen concentration and validation in coelastrum sp HA-1 and application in *Chlorella sorokiniana*. *Biomed. Res. Int.* 2017:9253020. doi: 10.1155/2017/9253020

Yang, Z. K., Niu, Y. F., Ma, Y. H., Xue, J., Zhang, M. H., Yang, W. D., et al. (2013). Molecular and cellular mechanisms of neutral lipid accumulation in diatom following nitrogen deprivation. *Biotechnol. Biofuels* 6:67. doi: 10.1186/1754-6834-6-67

Zarekarizi, A., Hoffmann, L., and Burritt, D. (2019). Approaches for the sustainable production of fucoxanthin, a xanthophyll with potential health benefits. *J. Appl. Phycol.* 31, 281–299. doi: 10.1007/s10811-018-1558-3

Zeng, J., Zhang, Y. P., Ruan, J. P., Yang, Z. G., Wang, C. G., Hong, Z., et al. (2018). Protective effects of fucoxanthin and fucoxanthinol against tributyltin-induced oxidative stress in HepG2 cells. *Environ. Sci. Pollut. Res.* 25, 5582–5589. doi: 10.1007/s11356-017-0661-3

Zeng, X. H., Danquah, M. K., Chen, X. D., and Lu, Y. H. (2011). Microalgae bioengineering: from CO2 fixation to biofuel production. *Renew. Sust. Energ. Rev.* 15, 3252–3260. doi: 10.1016/j.rser.2011.04.014

Zhang, C. W., Zmora, O., Kopel, R., and Richmond, A. (2001). An industrial-size flat plate glass reactor for mass production of *Nannochloropsis* sp (Eustigmatophyceae). *Aquaculture* 195, 35–49. doi: 10.1016/S0044-8486(00)00533-0

**Conflict of Interest:** The authors declare that the research was conducted in the absence of any commercial or financial relationships that could be construed as a potential conflict of interest.

**Publisher's Note:** All claims expressed in this article are solely those of the authors and do not necessarily represent those of their affiliated organizations, or those of the publisher, the editors and the reviewers. Any product that may be evaluated in this article, or claim that may be made by its manufacturer, is not guaranteed or endorsed by the publisher.

frontiers in Marine Science

ORIGINAL RESEARCH
published: 09 February 2022
doi: 10.3389/fmars.2021.836370

# Integration Bioprocess of B-Phycoerythrin and Exopolysaccharides Production From Photosynthetic Microalga *Porphyridium cruentum*

*Hao-Chan Yin[1†], Ji-Kang Sui[1†], Tian-Li Han[1,2], Tian-Zhong Liu[1] and Hui Wang[1*]*

[1] Key Laboratory of Biofuels, Qingdao Institute of Bioenergy and Bioprocess Technology, Chinese Academy of Sciences (CAS), Qingdao, China, [2] School of Chemical Engineering, University of Chinese Academy of Sciences, Beijing, China

OPEN ACCESS

**Edited by:**
*Shuhao Huo,*
*Jiangsu University, China*

**Reviewed by:**
*Xupeng Cao,*
*Dalian Institute of Chemical Physics, Chinese Academy of Sciences (CAS), China*
*Changhong Yao,*
*Sichuan University, China*

***Correspondence:**
*Hui Wang*
*wanghui@qibebt.ac.cn*

*[†] These authors have contributed equally to this work*

**Specialty section:**
*This article was submitted to Marine Fisheries, Aquaculture and Living Resources, a section of the journal Frontiers in Marine Science*

**Received:** *15 December 2021*
**Accepted:** *29 December 2021*
**Published:** *09 February 2022*

**Citation:**
*Yin H-C, Sui J-K, Han T-L, Liu T-Z and Wang H (2022) Integration Bioprocess of B-Phycoerythrin and Exopolysaccharides Production From Photosynthetic Microalga Porphyridium cruentum. Front. Mar. Sci. 8:836370. doi: 10.3389/fmars.2021.836370*

Red microalga *Porphyridium cruentum* has great potential for converting $CO_2$ into high-value bioactive compounds, such as B-phycoerythrin (B-PE) and extracellular polysaccharides or exopolysaccharides (EPS). This study aimed to establish the integration bioprocess of B-PE and EPS production from *P. cruentum*. First, different kinds of growth medium and $CO_2$ concentration were assessed indoor in terms of high biomass and B-PE and EPS contents. As follows, *P. cruentum* cells were outdoor scale-up cultured in 700 L pressurized tubular reactors for 9 days till the biomass reached 0.85 g/L and then separated from supernatants *via* centrifugation. Three different methods were adopted to extract phycobiliproteins, and the highest PE contents were extracted from cells by repeated freeze-thawing treatment along with the optimization of significant variables, and finally, 7.99 mg/L B-PE (16,500 Da) with a purity index of 0.82 was obtained. Moreover, analysis of physicochemical properties of EPS extracted from *P. cruentum* showed that the sulfate content was 14.85% and the uronic acid content was 9.36%.

**Keywords: *Porphyridium*, biomass production, phycoerythrin, exopolysaccharide, outdoor scale-up culture**

## INTRODUCTION

Microalgae are photoautotrophic microorganisms that use light energy, $CO_2$, and inorganic nutrients to synthesize valuable biomass compounds. These photosynthetic microorganisms have the positive advantages of high growth rate and high photosynthetic rate, and their capacity to fix carbon dioxide is 10 times that of terrestrial plants (Lalibertè and Noüie, 2010). In addition, because of the abundant active products, microalga is a good raw material for the production of biofuel and is widely used in food nutraceutical, pharmaceutical, and cosmetic industries as an antioxidant, antimicrobial, and anti-inflammatory product (Li et al., 2008; Francisco et al., 2010; John et al., 2011; Markou and Georgakakis, 2011; Zhu et al., 2016).

*Porphyridium cruentum* (Rhodophyta, Porphyridiophyceae, Porphyridiales, Porphyridiaceae, *Prophyridium*) is a spherical unicellular red alga without an organized cell wall (Arad et al., 1985; Adda et al., 1986; Vonshak, 1988; Arad and Levy-Ontman, 2010). This microalga is

photoautotrophic and can capture light and $CO_2$ into cells to convert them into abundant active molecules. And among these molecules, high contents of B-phycoerythrin (B-PE) and extracellular polysaccharides or exopolysaccharides (EPS) attract more attention. PE is one of the fluorescent substances that host photosynthesis, which shows maximal absorbance at the wavelength range 540–570 nm (Bermejo Román et al., 2002). PE has the advantages of high fluorescence intensity, anti-oxidation, scavenging free radicals, and high chroma. Thus, it has a wide range of commercial value in food (Fuentes et al., 2000; Gonzalez-Ramirez et al., 2014; Bueno et al., 2020), cosmetics, and pharmaceutical industries and is used as a fluorescent marker, which is dependent on its purity (Koller et al., 1977; Ayyagari et al., 1995; Qiu et al., 2004). Many methods, such as ultrastructure, salting out, column chromatography, and aqueous two-phase system, have been developed for the recovery and purification of B-PE ( Breccia et al., 1998; Romána et al., 2002; Benavides and Rito-Palomares, 2004; Parmar et al., 2011).

Furthermore, *Porphyridium* polysaccharides are another high-value compound, which is wrapped on the cell surface in the form of sulfated polysaccharides. In the liquid culture, the tropical part of polysaccharides is dissolved from the cell surface into the medium (Arad and Levy-Ontman, 2010). The average molecular weight of EPS from *P. cruentum* ranges from $1.4 \times 10^6$ Da to $1.7 \times 10^6$ Da, and EPS is negatively charged due to the presence of glucuronic acid and sulfate groups (Bernaerts et al., 2018). In addition, EPS is composed of numerous monosaccharides, the abundant glucose, and lactose's characters endow *Porphyridium* polysaccharide had antiviral and antioxidant activities and effectively inhibit the replication and cell transformation of some retroviruses (Dvir et al., 2000; Talyshinsky et al., 2002).

However, large-scale cultivation and commercial applications of *P. cruentum* have not achieved extensive use. To our knowledge, there is a crucial problem about how to promote the biomass and the yield of B-PE and EPS for large-scale cultivation (Spolaore et al., 2006). Moreover, despite the purification methods of B-PE and EPS from *P. cruentum* being developed, respectively, in previous studies, the joint extraction process of B-PE and EPS from *P. cruentum* culture is still rare, especially on a large scale. Therefore, in this study, microalga *P. cruentum* was initially cultured indoors with different mediums, and $CO_2$ concentration was considered as a key parameter to assess the accumulation of biomass, PE, and EPS production. As follows, outdoor scale cultivation with 700 L was carried out with optimal medium and $CO_2$ supply to obtain a large amount of biomass. After centrifugation, PE from biomass and EPS from culture were extracted and their basic performance analysis was investigated. The results will supply integration and optimal strategy for the customized production of B-PE and EPS from *P. cruentum*.

# MATERIALS AND METHODS

## Subsection Microalgal Growth Conditions Indoor

Photoautotrophic red microalga *P. cruentum* was maintained in 30 ml of f/2 medium in 100 ml Erlenmeyer flasks without aeration. Light at an intensity of 100 μmol photon/$m^2$ s was continuously supplied with pH adjusted at 7.6 and temperature at 25 ±°C. Continuous shaking of the culture flasks was done, 2–3 times a day, to prevent sticking of the culture to the bottom of the flask.

## Subsection Microalgal Growth With Different Conditions Indoor

For the medium treatment experiment, starter cultures in the logarithmic phase were gently centrifuged (5,000 rpm for 10 min) and washed with sterile distilled water. The microalgal pellets were resuspended in a small volume of sterile distilled water. The suspensions were then used to inoculate different mediums (700 ml) present in a glass column photobioreactor (PBR): artificial seawater (ASW) (Jones et al., 2010), BG11-seawater (S-BG11) (Liu et al., 2013), f/2 (Guillard and Ryther, 1962), and 4f (8 × f/2). Illumination was provided by single-side fluorescent lamps, which produced 100 μmol photon/$m^2$ s. The carbon source and agitation were supplied by bubbling $CO_2$-enriched compressed air (1% $CO_2$, v/v), which was filtered through the disposable sterile filter.

At the base optimal medium, cultures (700 ml) of *P. cruentum* were grown in the optimal medium with 100 μmol photon/$m^2$ s, and compressed air containing different levels of $CO_2$ (0.04%, 1%, 3%, and 5%) was aerated continuously into the cultivation medium. The concentration of the starting biomass was ca. 0.2 g/L, and all the experiments were carried out at 25 ± 1°C.

## Growth and Active Compounds Accumulation

Microalgal dry weight (DW) was measured according to a method previously reported (Talyshinsky et al., 2002). A certain volume of microalgal culture was filtered to a pre-weighted 0.45 μm GF/C filter membrane (Whatman, DW0). The membrane was oven-dried at 105°C overnight and then weighted (DW1). The DW was calculated as:

$$\mathrm{DW} = \frac{DW_1 - DW_0}{\mathrm{V}} \quad (1)$$

For the determination of EPS concentration, a 10 ml aliquot of microalgal culture was originally centrifuged at 8,000 rpm for 10 min. The supernatant was collected and stored at −4°C for the determination of EPS concentration. The EPS content was measured using the phenol-sulfuric acid method as described by Dubois et al. (1956).

Freeze-dried biomass was used to determine the PE content. The phycobiliproteins were extracted with 0.1 M phosphate buffer (pH 6.8) using a freeze-thawing technique as described below (Bermejo et al., 2003). Repeatedly extract the cells until the algae residue has no obvious red color and combine the extracts to a final volume of 50 ml. The absorbance of the solution was measured at 455, 564, and 592 nm with an ultraviolet spectrophotometer. The content of PE is calculated according to the formula used in the method of Beer and Eshel (1985).

## Large Cultivation of Microalgal Culture Outdoor

At the basis of indoor cultivation, microalga *P. cruentum* was cultivated in a 700 L pressurized tubular PBR with optimal medium and $CO_2$ supply. The PBR was set outdoor, and the intensity of natural light was set using curtains. The pH set point of 7.6 was automatically controlled by $CO_2$ injection (3%) and monitored by an inline Fermprobe pH probe. Air was injected continuously at a rate of 35 L/min. After 10 days, cells were harvested by bowl centrifugation at 6,000 rpm at room temperature and concentrated at a rate of ca. 10% dry weight. The biomass was then dispatched in aliquots in airtight glass bottles at −20°C away from light. And the supernatants were kept in the plastic drum at cold storage.

## Phycobiliproteins Extraction

Phycobiliprotein crude exact was obtained from *P. cruentum* with different methods:

1) *Repeated freezing and thawing treatment*: Suspend the microalgal particles and wash them with 18 MΩ Milli-Q pure water, then centrifuge for 10 min (12,000 × *g*, *T* = 10°C), and remove the supernatant. The pellet was suspended in 10 ml of extracting solution [phosphate-buffered saline (PBS): 10 mM phosphate, 100 mM NaCl, pH7] and was freeze-thawed 3 times between −20°C and room temperature (20–25°C). After repeating freeze-thawing treatments for 3 times, the suspension was kept at 4°C for 24 h and then centrifuged for 10 min (12,000 × *g*, *T* = 10°C). Collect the supernatant containing phycobiliprotein (crude extract) and store it at 4°C (Bermejo et al., 2003).
2) *Liquid nitrogen grinding treatment*: Proper amount of microalgal biomass was loaded into a mortar and mixed with the appropriate amount of liquid nitrogen and ground into powder, during which the liquid nitrogen is continuously loaded. Deionized water was added to dissolve the power, and the suspension was finally centrifuged for 10 min (12,000 × *g*, *T* = 10°C) to collect the supernatant (Chopin et al., 2000).
3) *Sonication treatment with bead milling*: This method was used as described by Zheng et al. (2011). The proper amount of microalgal biomass was dissolved in deionized water, and then a small steel ball with 3 mm diameter was added. Then, the mixture was sonicated four times for 60 s in a water/ice bath, with a 60 s pause in-between (to avoid phycobiliprotein degradation). The suspension was finally centrifuged, and the supernatant containing the phycobiliproteins (crude extract) was collected and stored at 4°C.

## Phycoerythrin Purification and Identification

In this study, we used algal mud or powder for extraction; accordingly, 10 ml of 18 MΩ Milli-Q pure water was added for 0.3 g. The method of Romána et al. (2002) was used to purify the crude PE extract. First, ammonium sulfate was added to the aqueous phycobiliproteins extract to make the saturation reach 20% for 3 h, and then, the mixture was centrifuged at 8,500 × *g* for 10 min to remove impurities. Next, ammonium sulfate was added to reach 60% saturation overnight at 4°C and then centrifuged again to obtain PE precipitate. Then, the target PE was re-dissolved in a small amount of ionized water and stored at 4°C. The PE content was calculated as described above, and the purity was calculated as the absorbance ratio of 545/280 nm.

Phycoerythrin identification was determined using the SDS-PAGE method and spectroscopic methods. For SDS-PAGE, electrophoresis was carried out in a vertical slab gel apparatus (Miniprotean III, Bio-Rad) according to the tricine buffer system described by Schagger and Jagow (1987) using a 16.5% polyacrylamide slab gel containing 0.1% (w/v) SDS with a stacking gel of 4% polyacrylamide. Samples were pre-incubated with buffer at ratio 4:1 at 95°C for about 10 min. Gels were run 45 min with 120 V constant voltage at room temperature and visualized by staining for 30 min with 0.1% (w/v) Coomassie Brilliant Blue R-250, 40% methanol (v/v) with 7% (v/v) acetic acid, and destained in dilute acetic acid. For the spectroscopic method, the PE was fully wavelength scanned.

## Exopolysaccharides Extraction and Analysis

As described above, microalgal culture was centrifuged and the supernatant was collected. A volume of ethanol was added to the supernatant [supernatant:ethanol = 1:3 (v/v)] and fully mixed overnight, and the temperature was kept at 4°C. To avoid the disturbance of monosaccharides and oligosaccharides, the supernatant was dialyzed using a dialysis bag of 8 kDa. After that, the dialyzed sugar solution was precipitated with ethanol once again. Finally, the EPS was freeze-dried *in vacuo*.

The physicochemical properties of EPS were determined. First of all, the sulfate content was determined using the barium sulfate turbidity method (Zhang, 2003). The concentration of glucuronic acid was measured using the sulfuric acid-carbazole colorimetry method (Dodgson and Price, 1962). The rheological properties of polysaccharide aqueous solutions were measured using an NDJ-8S digital viscometer with a 2-size rotor (Shanghai, China).

# RESULTS

## Growth and Active Compounds Accumulation Indoor

Microalga *P. cruentum* was cultivated in different mediums for 15 days, and the biomass, PE, and EPS contents were analyzed every 3 days. On the whole, *P. creuntum* showed marked differences in growth and active compounds accumulation in ASW, BG11-seawater, f/2, and 4f culture medium (**Figure 1**). Under a light intensity of 100 μmol photon/$m^2$ s, a lag phase of 4 days, 8 days of exponential phase, and 3 days of reduction phase were observed for the four culture mediums evaluated. The lowest biomass production was observed at the f/2 culture medium, the maximum specific growth rate and productivity

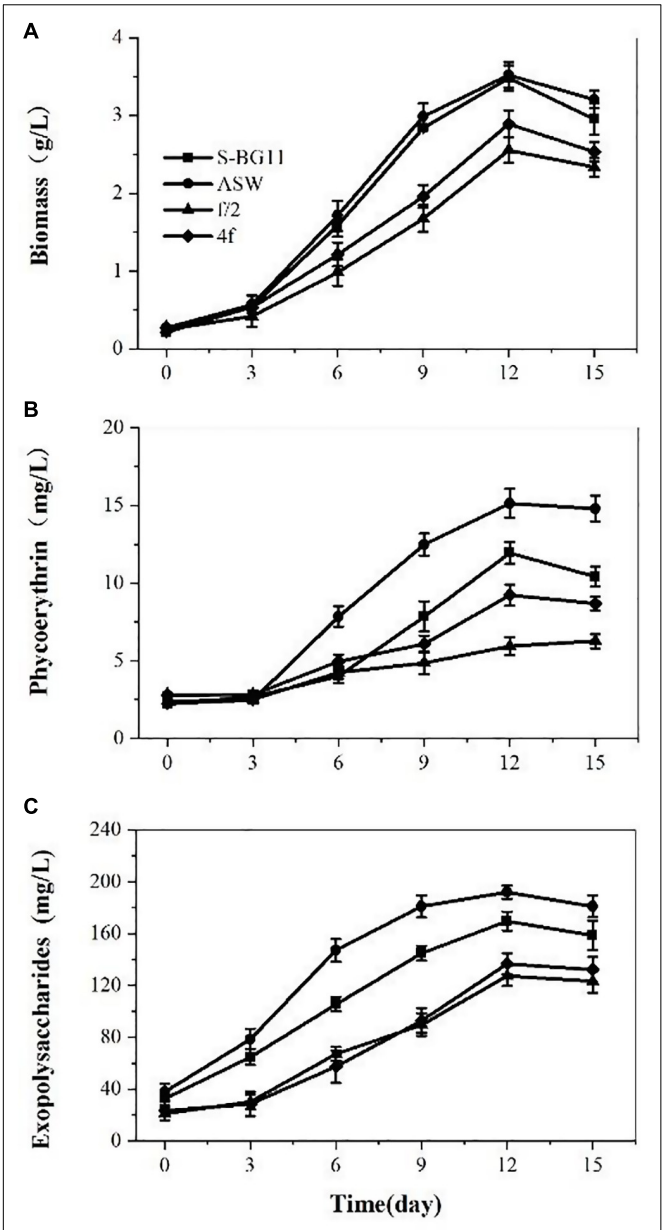


**FIGURE 1 |** Biomass **(A)**, phycoerythrin **(B)**, and exopolysaccharides **(C)** contents of *P. cruentum* in different culture mediums.

values were higher for the biomass with a culture medium of ASW, and the multiplication time of microalgal cells was shorter, compared with the condition of the other culture medium. Overall, the culture reached a maximum biomass concentration at day 12 with 3.48, 3.52, 2.55, and 2.88 g/L for ASW, S-BG11, f/2, and 4f, respectively.

Phycoerythrin production by *P. cruentum* was also analyzed under different culture mediums, and it showed similar lag phases among these culture mediums (**Figure 1B**). A maximum PE concentration of 15.14 mg/L was observed in the ASW culture medium on the 12th day. Lower PE content was observed in the f/2 culture medium. The EPS production by *P. cruentum* under different culture mediums is presented in **Figure 1C**. The four culture mediums showed a similar trend, and EPS production increased at the first 12 days of culture and showed a downward trend in the last 3 days. The maximum EPS concentration was observed on the 12th day of culture with 169.72, 191.88, 127.24, 136.67 mg/L, respectively. These could be associated with the fact that the mediums had different nutrient factors and concentrations.

At the base of the optimal medium, we investigated the effects of $CO_2$ concentration on *P. cruentum* growth, PE, and EPS production (**Figure 2**). The biomass production from the culture of the *P. cruentum* under different $CO_2$ concentrations is presented in **Figure 2A**. Overall, a lag phase of 3 days was observed, the culture reached a maximum biomass concentration at day 12, and then, the growth inhibited in the last 3 days. When the concentration of $CO_2$ was 3%, it resulted in the maximum biomass production of 4.52 g/L. The maximal biomass production for treatments with $CO_2$ concentrations of 0.04, 1, and 5 were 2.94, 3.68, and 4.24 g/L, respectively. The PE production by *P. cruentum* under different $CO_2$ concentrations is presented in **Figure 2B**. A maximum PE concentration of 18.37 mg/L was observed at 5% $CO_2$ on the 12th day of culture. Similarly, 18.17 mg/L PE was determined at 3% $CO_2$ on the 12th day. The PE content was lower when the concentration of $CO_2$ was 0.04% in the first 6 days. Similar to the biomass, the highest values of PE content were observed under 3% $CO_2$ concentration. The results of EPS concentration under different $CO_2$ concentrations are shown in **Figure 2C**. Overall, the culture reached a maximum EPS concentration at day 12, with 137.17, 152.15, 202.39, and 218.4 mg/L. Furthermore, the highest values of EPS content were obtained under the $CO_2$ concentration of 5%. The high EPS content was determined at 3% $CO_2$ obtained on the 12th day. The EPS content was lower when the concentration of $CO_2$ was 0.04%. The experiments performed in ASW culture medium at 3% $CO_2$ concentration resulted in a maximum PE and biomass production after 12 days.

## Growth and Active Compounds Accumulation Outdoor

On the above results indoor, we cultivated *P. cruentum* in ASW medium in the 700 L pressurized tubular PBR and offered compressed air with 3% $CO_2$ outdoor. The biomass and EPS production of *P. cruentum* were continuously monitored during the cultivation period. Five days of lag stage and 4 days of growth stage were observed (**Figure 3B**). *P. cruentum* reached its maximum biomass production of 0.85 g/L on the 9th day of culture. During the last 2 days of cultivation, the growth rate reduced and the biomass was inhibited. The EPS concentration for *P. cruentum* culture in the tubular PBR is shown in **Figure 3A**; a slow growth phase for 5 days and a stable growth phase were observed. The maximum EPS concentration of 11.41 mg/L was obtained on the 9th day of culture (**Figure 3C**). The difference in the results obtained between outdoor and indoor experiments may be due to uncontrollable factors, such as light intensity and temperature and the low inoculation.

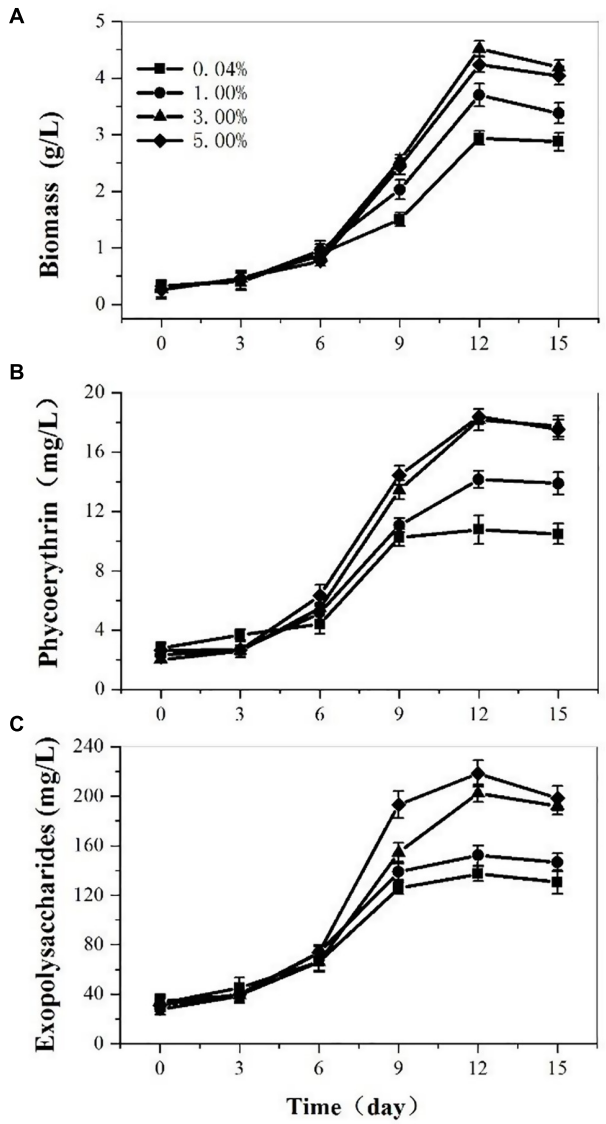


**FIGURE 2 |** Biomass **(A)**, phycoerythrin **(B)**, and exopolysaccharides **(C)** contents of *Porphyridium cruentum* in ASW with different $CO_2$ concentrations.

## Extraction of Phycoerythrin *via* Different Methods

In this study, we used three different methods to extract PE from *P. cruentum* cells and measured its concentrations and purity (**Figure 4**). The concentrations of PE from *P. cruentum* were 7.99, 5.27, and 6.34 mg/L for repeated freeze-thawing treatment, liquid nitrogen grinding, and sonication with bead milling, respectively. From the data, the repeated freeze-thawing treatment, which we adopted in indoor cultivation, could reach the highest extraction efficiency. Being different from the PE extraction concentrations, the three extraction methods did not show significant effects on the purities of PE. As illustrated in **Figure 4**, the PE purities of 0.82, 0.91, and 0.83 were obtained, respectively, from *P. cruentum* for the abovementioned three extraction methods.

## Analysis of Phycoerythrin Extraction

Ultraviolet absorption spectra of PE extraction *via* liquid nitrogen grinding method are presented in **Figure 5A**. The spectrum of PE displayed two maxima, namely, 545 and 564 nm; and exhibited only a slight shoulder at 499 nm. According to the ultraviolet absorption characteristics, there are mainly two types of PE in red microalga, namely, B-PE and R-phycoerythrin (R-PE). B-PE exhibits two absorption peaks at 545 and 564 nm, and one absorption shoulder at 499 nm; R-PE exhibits two characteristic absorption peaks at 499 and 564 nm, and one absorption shoulder at 545 nm (Glazer, 1984; Hilditch et al., 1991; Galland-Irmouli et al., 2000). It can be concluded that the PE fraction extracted and purified in this study is B-PE.

The purification was followed by electrophoretic experiments to confirm it. In this way, the electrophoretic analysis was carried out using the fraction obtained above (**Figure 5B**). By comparison with standards, we mainly obtained a molecular mass of 16,500 Da. It is similar to the band of the PE complex extracted from the marine red alga *Griffithsia pacifica* (Zhang et al., 2017).

## Analysis of Exopolysaccharides

In this study, we used the ultraviolet spectrum scanning method to evaluate the EPS extraction. According to the examination, there was no obvious characteristic absorption peak at 280 nm; it can be concluded that the crude polysaccharide contains no protein (data not shown). The biological activity of polysaccharides is usually related to their sulfate group and uronic acid content. In this study, the crude polysaccharide was configured into a 1 g/L solution for sulfate group and uronic acid content detection. The sulfate group content and the uronic acid content of the crude polysaccharide were 14.85% and 9.36%, respectively.

The rheological properties of polysaccharides are related to their concentration. The viscosity of the solution increased with the increment of the concentrations of the polysaccharide solution which indicated thickening performance (**Figure 6**). The polysaccharide solution showed significant shear-thinning behavior; the viscosity of the solution decreased with the increasing shear rate and exhibited the characteristics of pseudoplastic fluids. With the increase in temperature (25–75°C), the viscosity does not change much, which indicates that the polysaccharide solution has higher heat resistance.

# DISCUSSION

The culture medium can indicate the growth, PE, and EPS accumulation of *P. cruentum*. This study showed that biomass or growth rate of *P. cruentum* could reach its higher value in artificial seawater water (ASW) medium and BG11-seawater (S-BG11) (**Figure 1A**), which is in agreement with the results of the previous study for *Prophyridium* (Coward et al., 2016). During the cultivation period, the ASW and S-BG11 groups reached up to 3.48 and 3.52 g/L of biomass concentration, which was mostly higher than the concentrations reported in previous studies. The maximum biomass concentrations in *P. cruentum* reported in the studies by Razaghi et al. (2014) and Hu et al. (2018) were 1.61 and

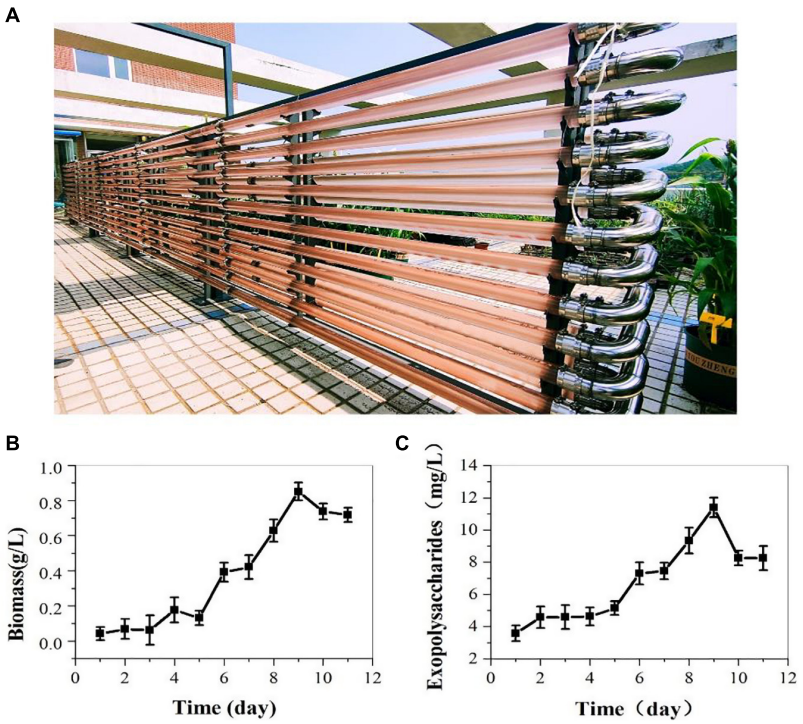


**FIGURE 3 |** Biomass **(B)** and exopolysaccharides **(C)** contents of *P. cruentum* in large-scale cultivation outdoor **(A)**.

1.22 g/L, respectively. This may be due to the continuous supply of available carbon during the entire cultivation period of this study. Besides biomass, PE and EPS contents were significantly different among these tested culture mediums due to abundant nutrients. Overall, ASW results in significantly higher contents in PE (15.14 mg/L) and EPS (191.88 mg/L) accumulation of *P. cruentum* than S-BG11 and other mediums. Therefore, ASW as the appropriate culture medium was used further in the following studies.

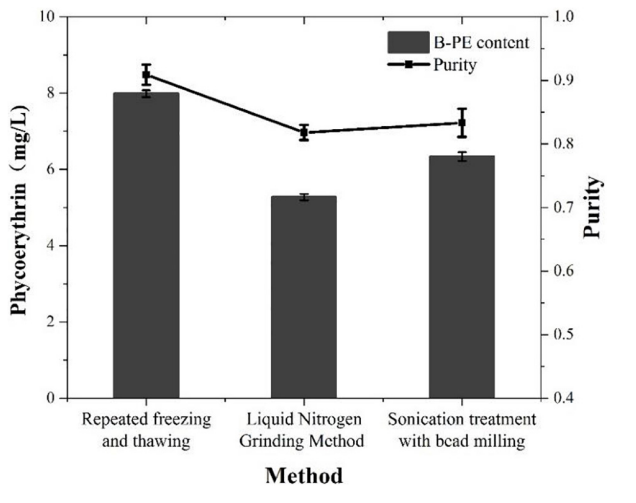


**FIGURE 4 |** Phycoerythrin contents and purities of *Porphyridium cruentum* with different extraction methods.

Besides culture medium, environmental factors, such as temperature, $CO_2$ concentration, and light regime, can directly influence the photosynthetic rate and metabolic activity of the microalga, thereby affecting the biomass and the overall accumulation of active compounds in the microalga. Among these, in scale cultivation outdoor, $CO_2$ concentration could be easily adjustable, while light intensity and temperature are not controllable. Therefore, in this study, the effect of $CO_2$ concentration on biomass and active compounds was also determined. Overall, with the increase of $CO_2$ concentration, the biomass, PE, and EPS contents of *P. cruentum* increased. The highest concentrations of PE (18.37 mg/L) and EPS (218.5 mg/L) were achieved with 5% $CO_2$; however, there was no significant difference in biomass and PE between 3% and 5% $CO_2$.

According to the abovementioned results, *P. cruentum* was cultivated outdoor in a 700 L pressurized tubular PBR with 3% $CO_2$ supply in ASW (**Figure 3**). In this section, the biomass of *P. cruentum* was significantly lower than those in indoor cultivation, because of the intermittent illumination and uncontrollable temperature outdoor. Light is an essential source for autotrophic growth, and photosynthetic activity in microalga, light intensity, and light regime leads to different changes, such as photo-inhibition and photo-insufficient, even in dense culture and thus can be detrimental to the final yield (Papageorgiou et al., 2007). Moreover, the temperature is another major factor that affects the growth rate and chemical composition of microalga. Previous studies performed with microalgal strains have shown

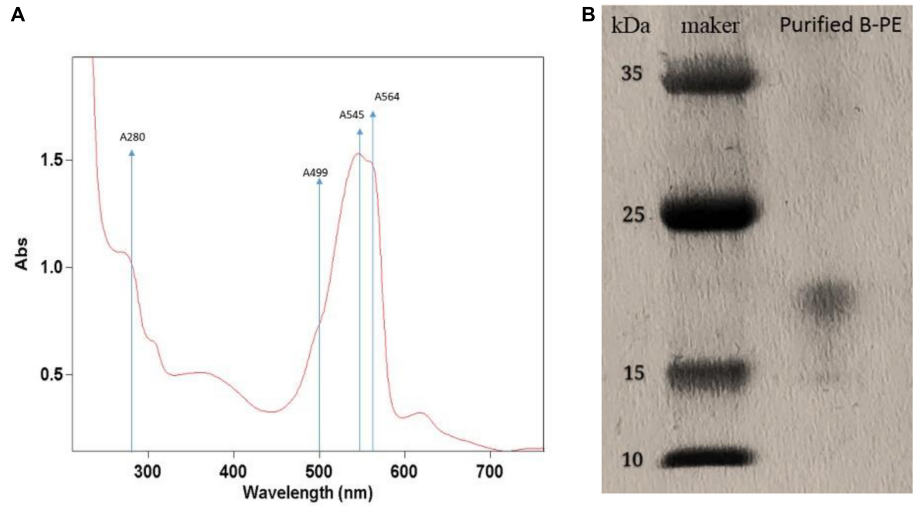


**FIGURE 5 |** Identification of phycoerythrin of *Porphyridium cruentum via* ultraviolet absorption spectra **(A)** and SDS-PAGE method **(B)**.

that the optimal temperature was 18–25°C (Srirangan et al., 2015). In outdoor cultivation, the temperature fluctuates up and down and results in biomass reduction. *P. cruentum* cells secrete EPS, which is considered an optimal ingredient in cosmetics because of its excellent moisturizing properties. Our results showed that the concentration of EPS gradually increased with the culture time, but the accumulation of EPS indicated a significant difference between indoor and outdoor cultivation because the biomass was reduced outdoor (**Figure 3B**).

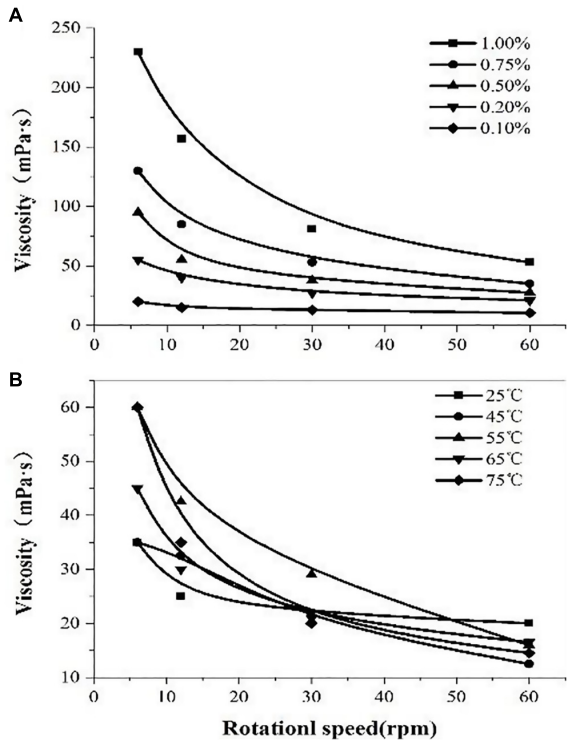


**FIGURE 6 |** The viscosity of polysaccharides extracted from *Porphyridium cruentum*. **(A)** Viscosity of polysaccharides at different concentrations. **(B)** Viscosity of polysaccharides at different temperatures.

Microalga *P. cruentum* contains three types of phycobiliproteins, namely, B-PE, PC, and APC (Marsac, 2003). Among these, B-PE is one of the most well-known pigment–protein complexes that are involved in photosynthesis in microalgal cells (Gough and Kannangara, 1979), and thus, the PE accumulation is closely related to the change of light quality (spectra composition), light intensity, and light regime (Barth et al., 2014). Concerning the target production of phycobiliproteins, it has been widely described as a preference for low and medium intensities of light for the production of these pigments (Rizzo et al., 2015). This can be explained by the function of these compounds in the photosynthetic apparatus. However, light intensity outdoor could reach a light intensity higher than 4,000 lux; the phycobiliproteins, like carotenoids, are not required to produce an increase in the range of light absorption.

To obtain target phycobiliproteins, extraction and purification procedures are required. According to the previous study (Mittal et al., 2017), a crude extraction can be done by mechanical disruption of the cell (ultrasonication, bead mill, or high-pressure systems) or even by chemical osmotic extraction. In this study, we used three methods (e.g., repeated freeze-thawing treatment, liquid nitrogen grinding treatment, and sonication treatment with beading milling) to extract the phycobiliprotein crude from microalgal cells that were cultivated outdoor and compared the extraction efficiency and purity of PE. As illustrated in **Figure 4**, the highest extraction efficiency of PE was obtained *via* repeated freeze-thawing treatment, while the highest purity of PE was got *via* liquid nitrogen grinding treatment. The in-depth research and optimization of extraction of phycobiliproteins to get higher extraction efficiency and purity will be studied in the future. Although the most utilized criterion to check the purity of

biliprotein solutions is absorbance, the purity and identification must be followed by electrophoretic experiments to confirm it. In this way, the spectroscopic and electrophoretic analysis of crude phycobiliprotein obtained from *P. cruentum* was carried out. Electrophoretic analysis revealed broadband between 15 and 25 kDa, which could be assigned to subunits α and β, which was consistent with the value reported previously (Zhang et al., 2017). **Figure 5** shows visible absorption, fluorescence emission, and anisotropy spectra of purified B-PE from *P. cruentum*. Absorbance maximum is 545 nm, whereas the fluorescence emission maximum is 564 nm and the anisotropy spectrum is similar to those earlier published for PEs from another red alga (Maccoll, 1991).

In addition, the fundamental characteristics of EPS extracted from *P. cruentum* were evaluated in this study (**Figure 6**). Former literature introduced that EPS from red alga contains β-1,3-glycosidic bonds and sulfates, which endow EPS with antiviral, antioxidant, and radical-scavenging functions (Sun et al., 2009). Our results showed that the sulfate content of EPS from *P. cruentum* was 14.85% and the uronic acid content was 9.36%. Moreover, the polysaccharide solution shows a significant shear-thinning behavior and has higher heat resistance.

## CONCLUSION

It is clear from this study that culture medium, $CO_2$ concentration, and light regime can affect the growth and active compounds accumulation of *P. cruentum*. According to the indoor experiment, optimal medium and $CO_2$ concentration were chosen to cultivate *P. cruentum* in a 700 L pressurized tubular PBR outdoor. However, uncontrollable factors including light intensity and temperature, and the low inoculation resulted in the low biomass, PE, and EPS contents. In addition, the results of this study indicated that the proper extraction and purification method made a significant contribution to the high yield and purity of PE. Therefore, an integrated process was proposed to produce biomass and active compounds (B-PE and EPS) from photosynthetic microalga *P. cruentum*.

## DATA AVAILABILITY STATEMENT

The original contributions presented in the study are included in the article/supplementary material, further inquiries can be directed to the corresponding author/s.

## AUTHOR CONTRIBUTIONS

HW and T-ZL conceptualized the study. H-CY, J-KS, and T-LH validated the study. H-CY contributed to the manuscript writing and prepared the original draft of the manuscript. J-KS contributed to the manuscript writing and reviewed and edited the manuscript. All authors contributed to the article and approved the submitted version.

## FUNDING

We would like to thank the National Key R&D Program of China (Grant No. 2018YFA0902503), Shangdong Taishan Scholars Program (No. tsqn202103144), and the Innovation Foundation of QIBEBT (Grant: QIBEBT I201920) CAS.

## REFERENCES

Adda, M., Merchuk, J. C., and Arad, S. (1986). Effect of nitrate on growth and production of cell-wall polysaccharide by the unicellular red alga Porphyridium. *Biomass* 10, 131–140. doi: 10.1016/0144-4565(86)90061-2

Arad, S. M., Adda, M., and Cohen, E. (1985). The potential of production of sulfated polysaccharides from Porphyridium. *Plant Soil* 89, 117–127.

Arad, S. M., and Levy-Ontman, O. (2010). Red microalgal cell-wall polysaccharides. biotechnological. aspects. *Curr. Opin. Biotechnol.* 21, 358–364. doi: 10.1016/j.copbio.2010.02.008

Ayyagari, M. S., Pande, R., Kamtekar, S., Marx, K. A., Tripathy, S. K., Gao, H., et al. (1995). Molecular assembly of proteins and conjugated polymers: Toward the development of biosensors. *Biotechnol. Bioeng.* 45, 116–121. doi: 10.1002/bit.260450204

Barth, J., Bergner, S. V., Jaeger, D., Niehues, A., Schulze, S., Scholz, M., et al. (2014). The interplay of light and oxygen in the reactive oxygen stress response of Chlamydomonas reinhardtii dissected by quantitative mass spectrometry. *Mol. Cell. Proteomics* 13, 969–989. doi: 10.1074/mcp.M113.032771

Beer, S., and Eshel, A. (1985). Determining phycoerythrin and phycocyanin concentrations in aqueous crude extracts of the red alga. *Australi. J. Mar. Freshw. Res.* 36, 785–792. doi: 10.1071/mf9850785

Benavides, J., and Rito-Palomares, M. (2004). Bioprocess intensification: a potential aqueous two-phase process for the primary recovery of B-phycoerythrin from Porphyridium cruentum. *J. Chromatogr B Analyt. Technol. Biomed. Life Sci.* 807, 33–38. doi: 10.1016/j.jchromb.2004.01.028

Bermejo, R., Acién, F. G., Ibáñez, M. J., Fernández, J. M., Molina, E., and Alvarez-Pez, J. M. (2003). Preparative purification of B-phycoerythrin from the microalga Porphyridium cruentum by expanded-bed adsorption chromatography. *J. Chromatogr B Analyt. Technol. Biomed. Life Sci* 790, 317–325.

Bermejo Román, R., Alvárez-Pez, J. M., Acién Fernández, F. G., and Molina Grima, E. (2002). Recovery of pure B-phycoerythrin from the microalga Porphyridium cruentum. *J. Biotechnol.* 93, 73–85. doi: 10.1016/s0168-1656(01)00385-6

Bernaerts, T., Gheysen, L., Kyomugasho, C., Kermani, Z. J., and Loey, A. (2018). Comparison of microalgal biomasses as functional food ingredients: Focus on the composition of cell wall-related polysaccharides. *Algal Res.* 32, 150–161.

Breccia, D., Siñeriz, F., Baigori, D., and Castro, G. R. (1998). Purification and characterization of a thermostable xylanase from Bacillus amyloliquefaciens. *Enzyme Microb. Technol.* 22, 42–49. doi: 10.1007/s13205-017-0615-y

Bueno, M., Gallego, R., and Chourio, A. M. (2020). Green ultra-high pressure extraction of bioactive compounds from Haematococcus Pluvialis and Porphyridium cruentum microalgae[J]. *Innov. Food Sci. Emerg. Technol.* 66:102532. doi: 10.1016/j.ifset.2020.102532

Chopin, T., Yarish, C., Wilkes, R., Belyea, E., Lu, S., and Mathieson, A. J. J. (2000). Developing Porphyra/salmon integrated aquaculture for bioremediation and diversification of the aquaculture industry. *J. Appl. Phycol.* 12, 99–99.

Coward, T., Fuentes-Grunewald, C., Llewellyn, G., Lovitt, R. W., and Silkina, A. (2016). Utilising light-emitting diodes of specific narrow wavelengths for the optimization and co-production of multiple high-value compounds in Porphyridium purpureum. *Bioresour. Technol.* 221, 607–615. doi: 10.1016/j.biortech.2016.09.093

Dodgson, K., and Price, R. G. (1962). A note on the determination of the ester sulfate content of sulfated polysaccharides. *Biochem. J.* 84, 106–110. doi: 10.1042/bj0840106

Dubois, M., Gilles, K. A., Hamilton, J. K., Rebers, P. T, and Smith, F. (1956). Colorimetric method for determination of sugars and related substances. *Anal. Chem.* 28, 350–356. doi: 10.1021/ac60111a017

Dvir, I., Chayoth, R., Sod-Moriah, U., Shany, S., Nyska, A., Stark, A. H., et al. (2000). Soluble polysaccharide and biomass of red microalga Porphyridium sp. alter intestinal morphology and reduce serum cholesterol in rats. *Br. J. Nutr.* 84, 469–476.

Francisco, E. C., Neves, D. B., Jacob-Lopes, E., and Franco, T. T. (2010). Microalgae as feedstock for biodiesel production: carbon dioxide sequestration, lipid production, and biofuel quality. *Chem. Technol. Biotechnol.* 85, 395–403. doi: 10.1016/j.jphotobiol.2018.01.003

Fuentes, M., Fernández, G. G. A., and Pérez, J. A. (2000). Biomass nutrient profiles of the microalga Porphyridium cruentum. *Food Chem.* 70, 345–353. doi: 10.1007/s00449-016-1676-8

Galland-Irmouli, A. V., Pons, L., Lucon, M., Villaume, C., Mrabet, N. T., Guéant, J. L., et al. (2000). One-step purification of R-phycoerythrin from the red macroalga Palmaria palmata using preparative polyacrylamide gel electrophoresis. *J. Chromatogr B Biomed. Sci. Appl.* 739, 117–123. doi: 10.1016/s0378-4347(99)00433-8

Glazer, A. N. (1984). Phycobilisome a macromolecular complex optimized for light energy transfer. *Biochim. Biophys. Acta* 768, 29–51. doi: 10.1016/0304-4173(84)90006-5

Gonzalez-Ramirez, E., Andujar-Sanchez, M., and Ortiz-Salmeron, E. (2014). Thermal and pH Stability of the B-Phycoerythrin from the Red Algae Porphyridium cruentum. *Food Biophys.* 9, 184–192. doi: 10.1007/s11483-014-9331-x

Gough, S. P., and Kannangara, C. G. (1979). Biosynthesis of Δ-aminolevulinate in greening barley leaves III: The formation of Δ-aminolevulinate in Tigrigna mutants of barley. *Carlsberg Res. Commun.* 44, 403–416. doi: 10.1007/bf02906189

Guillard, R. R., and Ryther, J. H. (1962). Studies of marine planktonic diatoms: i. Cyclotella nana hustedt, and detonula confervacea (cleve) gran. *Can. J. Microbiol.* 8, 229–239. doi: 10.1139/m62-029

Hilditch, C., Balding, P., Jenkins, R., Smith, A., and Rogers, L. J. (1991). R-phycoerythrin from the macroalgaCorallina Officinalis (Rhodophyceae) and application of a derived phycofluor probe for detecting sugar-binding sites on cell membranes. *J. Appl. Phycol.* 3, 345–354. doi: 10.1007/bf02392888

Hu, H., Wang, H. F., Ma, L. L., Shen, X. F., and Zeng, R. J. (2018). Effects of nitrogen and phosphorous stress on the formation of high-value LC-PUFAs in Porphyridium cruentum. *Appl. Microbiol. Biotechnol.* 102, 5763–5773. doi: 10.1007/s00253-018-8943-3

John, R. P., Anisha, G. S., Nampoothiri, K. M., and Pandey, A. (2011). Micro, and macroalgal biomass: A renewable source for bioethanol. *Bioresour. Technol.* 102, 186–193. doi: 10.1016/j.biortech.2010.06.139

Jones, R. F., Speer, H. L., and Kury, W. (2010). Studies on the Growth of the Red Alga Porphyridium cruentum. *Physiol. Plant*. 16, 636–643. doi: 10.1104/pp.91.3.1179

Koller, K. P., Wehrmeyer, W., and Schneider, H. (1977). Isolation, and characterization of disc-shaped phycobilisomes from the red alga Rhodella violacea. *Arch. Microbiol.* 12, 61–67. doi: 10.1007/BF00446655

Lalibertè, G., and Noüie, J. D. L (2010). Auto-, Hetero-, And Mixotrophic Growth Of Chlamydomonas Humicola (Cmloroimiyckak) On Acetate. *J. Phycol.* 29, 612–620.

Li, Y., Horsman, M., Wu, N., Lan, C. Q., and Calero, N. D. (2008). Biofuels from microalga. *Biotechnol. Pro.* 24, 815–820.

Liu, T., Wang, J., Hu, Q., Cheng, P., Bei, J., Liu, J., et al. (2013). Attached cultivation technology of microalga for efficient biomass feedstock production. *Bioresour. Technol.* 127, 216–222. doi: 10.1016/j.biortech.2012.09.100

Maccoll, R. (1991). Fluorescence studies on R-phycoerythrin and C-phycoerythrin. *J. Fluoresc.* 1, 135–140.

Parmar, A., Singh, K. N., Kaushal, A., Madamwar, D. (2011). Characterization of intact phycoerythrin and its cleaved 14 kDa functional subunit from marine cyanobacterium Phormidium sp. A27DM. *Process Biochem.* 46, 1793–1799.

Markou, G., and Georgakakis, D. (2011). Cultivation of filamentous cyanobacteria (blue-green alga) in agro-industrial wastes and wastewaters: a review. *Appl. Energy* 88, 3389–3401. doi: 10.1016/j.apenergy.2010.12.042

Marsac, N. (2003). Phycobiliproteins and phycobilisomes: the early observations. *Photosynth. Res.* 76, 193. doi: 10.1023/A:1024954911473

Mittal, R., Tavanandi, H. A., Mantri, V. A., and Raghavarao, K. (2017). Ultrasound-assisted methods for enhanced extraction of Phycobiliproteins from marine macro-alga. *Ultrason. Sonochem.* 38, 92. doi: 10.1016/j.ultsonch.2017.02.030

Papageorgiou, G. C., Tsimilli-Michael, M., and Stamatakis, K. (2007). The fast and slow kinetics of chlorophyll a fluorescence induction in plants, alga, and cyanobacteria: a viewpoint. *Photosynth. Res*. 94, 275–290. doi: 10.1007/s11120-007-9193-x

Qiu, J., Madoz-Gurpide, J., Misek, D. E., Kuick, R., Brenner, D. E., Michailidis, G., et al. (2004). Development of natural protein microarrays for diagnosing cancer-based on antibody response to tumor antigens. *J. Proteome Res.* 3, 261–267. doi: 10.1021/pr049971u

Razaghi, A., Godhe, A., and Albers, E. (2014). Effects of nitrogen on growth and carbohydrate formation in Porphyridium cruentum. *Cent. Eur J. Biol.* 9, 156–162. doi: 10.2478/s11535-013-0248-z

Rizzo, R. F., Santos, B., Castro, G. F. P., Passos, T. S., Nascimento, M., Guerra, H. D., et al. (2015). Production of phycobiliproteins by Arthrospira platensis under different light conditions for application in food products. *Food Sci. Technol.* 35, 247–252. doi: 10.1590/1678-457x.6463

Romána, R. B., Alvárez-Pez, J. M., Acién Fernándezc, F. G., and Grimac, E. M. (2002). Recovery of pure B-phycoerythrin from the microalga Porphyridium cruentum. *J. Biotechnol.* 93, 73–85. doi: 10.1016/s0168-1656(01)00385-6

Schagger, H., and Jagow, G. V. (1987). Tricine-sodium dodecyl sulfate-polyacrylamide gel electrophoresis for the separation of proteins in the range from 1 to 100 kDa. *Anal. Biochem.* 166, 368–379. doi: 10.1016/0003-2697(87)90587-2

Spolaore, P., Joannis-Cassan, C., Duran, E., and Isambert, A. (2006). Commercial applications of microalga. *J. Biosci. Bioeng.* 101, 87–96.

Srirangan, S., Sauer, M. L., Howard, B., Dvora, M., Dums, J., Backman, P., et al. (2015). Interaction of Temperature and Photoperiod Increases Growth and Oil Content in the Marine Microalga Dunaliella Viridis. *PLoS One* 10:e0127562. doi: 10.1371/journal.pone.0127562

Sun, L., Wang, C., Shi, Q., and Ma, C. (2009). Preparation of different molecular weight polysaccharides from Porphyridium cruentum and their antioxidant activities. *Int. J. Biol. Macromol.* 45, 42–47. doi: 10.1016/j.ijbiomac.2009.03.013

Talyshinsky, M. M., Souprun, Y. Y., and Huleihel, M. M. (2002). Anti-viral activity of red microalgal polysaccharides against retroviruses. *Cancer Cell Int.* 2:8. doi: 10.1186/1475-2867-2-8

Vonshak, A. (1988). "Porphyridium," in *Microalgal Biotechnology*, eds, M. A. Borowitzka, and L. J. Borowitzka (Cambridge: Cambridge University Press), 122–134.

Zhang, J., Ma, J., Liu, D., Qin, S., Sun, S., Zhao, J., et al. (2017). Structure of phycobilisome from the red alga Griffithsia Pacifica. *Nature* 551, 57–63. doi: 10.1038/nature24278

Zhang, Z. U. (2003). *Saccharide Complex Biochemical Research Technology*, 2nd edtion, China: Zhejiang University, 11–16.

Zheng, H., Yin, J., Gao, Z., Huang, H., Ji, X., and Dou, C. J. A. B. (2011). Biotechnology, Disruption of Chlorella Vulgaris Cells for the Release of Biodiesel-Producing Lipids: A Comparison of Grinding, Ultrasonication, Bead Milling, Enzymatic Lysis, and Microwaves. *Appl. Biochem. Biotechnol.* 164, 1215–1224. doi: 10.1007/s12010-011-9207-1

Zhu, L., Yan, C., and Li, Z. (2016). Microalgal cultivation with biogas slurry for biofuel production. *Bioresour. Technol*. 220, 629–636 doi: 10.1016/j.biortech.2016.08.111

**Conflict of Interest:** The authors declare that the research was conducted in the absence of any commercial or financial relationships that could be construed as a potential conflict of interest.

**Publisher's Note:** All claims expressed in this article are solely those of the authors and do not necessarily represent those of their affiliated organizations, or those of the publisher, the editors and the reviewers. Any product that may be evaluated in this article, or claim that may be made by its manufacturer, is not guaranteed or endorsed by the publisher.

frontiers | Frontiers in Marine Science

ORIGINAL RESEARCH
published: 24 May 2022
doi: 10.3389/fmars.2022.909237

# Effects of Nitrogen and Light Intensity on the Astaxanthin Accumulation in Motile Cells of *Haematococcus pluvialis*

*Feng Li*[1,2,3,4], *Minggang Cai*[2,3,4], *Yanqi Wu*[1], *Qingsheng Lian*[1], *Zuyuan Qian*[1], *Jiansen Luo*[1], *Yulei Zhang*[1], *Ning Zhang*[1], *Changling Li*[1]* and *Xianghu Huang*[1]*

[1] College of Fisheries, Guangdong Ocean University, Zhanjiang, China, [2] Fujian Provincial Key Laboratory for Coastal Ecology and Environmental Studies, Xiamen University, Xiamen, China, [3] Key Laboratory of Marine Chemistry and Applied Technology, Xiamen University, Xiamen, China, [4] College of Ocean and Earth Science, Xiamen University, Xiamen, China

OPEN ACCESS

**Edited by:**
Pengfei Cheng,
Ningbo University, China

**Reviewed by:**
Fatimah Md Yusoff,
Putra Malaysia University, Malaysia
Jianhua Fan,
East China University of Science and Technology, China

***Correspondence:**
Changling Li
licl@gdou.edu.cn
Xianghu Huang
huangxh@gdou.edu.cn

**Specialty section:**
This article was submitted to Marine Fisheries, Aquaculture and Living Resources, a section of the journal Frontiers in Marine Science

**Received:** 31 March 2022
**Accepted:** 27 April 2022
**Published:** 24 May 2022

**Citation:**
Li F, Cai M, Wu Y, Lian Q, Qian Z, Luo J, Zhang Y, Zhang N, Li C and Huang X (2022) Effects of Nitrogen and Light Intensity on the Astaxanthin Accumulation in Motile Cells of Haematococcus pluvialis. Front. Mar. Sci. 9:909237. doi: 10.3389/fmars.2022.909237

The dietary supplementation of *Haematococcus pluvialis* is a natural, safe, and sustainable method for fish pigmentation. However, astaxanthin-rich *H. pluvialis* cysts have a poor effect in pigmenting salmonid flesh due to their rigid and thick cell wall. *H. pluvialis* thin-walled motile cells have recently attracted attention due to their potential advantages in maintaining compound stability, easy digestion, enhancing the bioavailability of carotenoids, and reducing production costs. This study aimed to investigate the effect of various nitrogen concentrations and light intensities on astaxanthin production in motile cells. We first investigated the effect of four different concentrations of nitrogen on astaxanthin accumulation in motile cells. According to the results, the motile cells had the highest astaxanthin concentration and content under the 0 N condition. Then, we compared the differences in astaxanthin production in motile cells under three different light intensities under 0 N conditions. The results showed that after four days of treatment, the protoplasts of the motile cells in the medium light (ML) group and the high light (HL) group had distinct granularity. The cell mortality rate in the HL group reached more than 15%, which was significantly higher than that in the low light (LL) and ML groups, indicating that high light intensity was not suitable for inducing motile cells to accumulate astaxanthin. There were no significant differences between the LL and ML groups in astaxanthin content, motile cells percentage, and cell mortality rate. Considering these indicators, we recommended inducing motile cells to produce astaxanthin under low light conditions because it is more economical in terms of electricity consumption. This study added to the knowledge that nitrogen and light affects the accumulation of astaxanthin in *H. pluvialis* motile cells. The results would help determine the optimal nitrogen and light conditions in astaxanthin production from motile cells.

**Keywords: astaxanthin, *Haematococcus pluvialis*, motile cells, nitrogen starvation, light intensity**

# 1 INTRODUCTION

Farmed fish is globally recognized as one of the healthiest foods (Tacon and Metian, 2013) and plays a significant role in global food security and nutrition strategies. With the continuous increase in the scale of aquaculture, people have higher and higher requirements for farmed fish. Fish flesh color plays an important role in consumer sensory evaluation and sales price (Hart and Colombo, 2022). While flesh color doesn't directly affect flesh quality, consumers often consider it as a sign that fish is fresh and tasty or not (Yesilayer, 2020). Astaxanthin is the main carotenoid responsible for the red or pink pigmentation of most wild salmonids (Nogueira et al., 2021), and accounts for more than 85% of the total carotenoid content in salmonids fresh (Torrissen et al., 1995). Feeding salmonids' diets containing astaxanthin has become the main means of improving their flesh and skin color (Tejera et al., 2007; Kalinowski et al., 2011; Rahman et al., 2016). At present, synthetic astaxanthin occupies more than 95% of the market share astaxanthin (Shah et al., 2016), which is widely used in aquaculture due to its lower production cost (Panis and Garreon, 2016; Li et al., 2020a). However, it has raised consumer concerns about food safety, pollution, and sustainability due to synthetic astaxanthin derived from petrochemicals (Li et al., 2011; Stachowiak and Szulc, 2021). Consumer preference is shifting towards nature astaxanthin (Young et al., 2017; Viera et al., 2018).

Microalgae as fish feed additives have advantages in terms of safe availability of ingredients, ease of cultivation operations, and sustainability of production. *H. pluvialis* could accumulate high levels of astaxanthin (3-5% dry weight) (Lorenz and Cysewski, 2000; Ambati et al., 2014) and is regarded as the most potent natural source of astaxanthin (Bowen et al., 2002). Several studies indicated that dietary supplementation of *H. pluvialis* would improve the color, immune and antioxidant capacity of fish (Moretti et al., 2006; Sheikhzadeh et al., 2012; Li et al., 2018; Yu et al., 2021). However, *H. pluvialis* red cysts typically have thick and less digestible cell walls (Hagen et al., 2002; Shah et al., 2016), which reduce the bioavailability of astaxanthin (Sommer et al., 1991; Choubert et al., 2006). As a result, the tissue pigmentation levels of fish fed *H. pluvialis* were generally lower than those in fish fed synthetic astaxanthin (Choubert et al., 2006; Li et al., 2014). Recent studies suggested that whole-celled *H. pluvialis* with thin cell walls achieves the same efficiency at pigmenting the flesh of rainbow trout as synthetic astaxanthin (Hart and Colombo, 2022). It was attributed to the ease of digestion of *H. pluvialis* thin-walled cells.

There are various types of cells in the *H. pluvialis* life cycle, including motile cells, nonmotile cells, and red cyst cells (Li et al., 2019a), and only motile cells have thin cell walls. More attention has been paid in the past periods to enhancing astaxanthin accumulation in the thick-walled cysts (Boussiba and Vonshak, 1991; Kobayashi et al., 1997; Li et al., 2019b; Fang et al., 2020), but less attention has been paid to motile cells. Previous studies have shown that nitrogen and light intensity play critical roles in the astaxanthin accumulation in *H. pluvialis* (Borowitzka et al., 1991; Fábregas et al., 1998; Orosa et al., 2005). However, little is known about the effects of nitrogen and light intensity on astaxanthin accumulation in motile cells. In this study, we first investigated the effect of four different concentrations of nitrogen on the accumulation of astaxanthin in motile cells and determined the optimal nitrogen concentration to induce motile cells to produce astaxanthin. The effect of three light intensities on the astaxanthin accumulation in motile cells were then investigated at this nitrogen concentration. The results would help determine the optimal nitrogen and light conditions in the production of astaxanthin from *H. pluvialis* motile cells.

# 2 MATERIALS AND METHODS

## 2.1 *H. pluvialis* Strain and Growth Conditions

*H. pluvialis* CCMA-451 (Genbank accession number MG847145) was acquired from the Center for Collections of Marine Algae of Xiamen University (CCMA). The motile cells were grown photoautotrophically in liquid 3N-BBM (Bold Basal Medium) at 30 μmol $m^{-2}$ $s^{-1}$ (side, white light) for 10 days.

## 2.2 Experimental Design

The first experiment was the effect of different nitrogen concentrations on astaxanthin accumulation in motile cells. Four different nitrogen ($NaNO_3$) concentrations were tested, including 0 N, 0.5-fold N, 1-fold N (250 mg/L), and 3N. The experiment was carried out under the condition of 30 μmol $m^{-2}$ $s^{-1}$ light intensity.

For the second experiment, under the conditions of nitrogen concentration screened in experiment 1, motile cells were treated under the conditions of nitrogen concentration screened in experiment 1 with three light intensities: 30, 80, and 150 μmol $m^{-2}$ $s^{-1}$, representing a low (LL), medium (ML), and high light (HL), respectively.

The 10-day-old motile cells were collected by centrifugation (3000 rpm, 2 min) for experiments. All experimental groups were performed in 1 L glass columns (inner diameter 5 cm) at an initial optical density of 0.5 ($OD_{680}$) in 25 ± 1°C for 4 days, with three parallels per group. The cultures were mixed by continuous bubbling with 1.5% $CO_2$ gas at 0.5 vvm.

## 2.3 Analytical Methods

For cell numbers determination, samples were fixed with Lugol's iodine solution first, and then the cell number was counted by a Neubauer improved cell counting chamber under Olympus BX53 light microscope.

Dry weight (DW) is determined daily according to Li et al. (2019a). Briefly, 10 mL algal suspension were filtered by passing through a pre-weighed ($m_1$) filter paper (47 mm, 1.2 μm, Whatman GF/C). Then dry the filter paper overnight at 90 °C to a constant weight ($m_2$). The DW was calculated with Eq. 1.

$$DW = (m_2 - m_1) \times 10^3/10 \quad (1)$$

Astaxanthin concentration (AC) is determined by the photometric method (Li et al., 2020b). Briefly, algal cells were collected from a 10 mL sample by centrifugation (3000 rpm, 2 min) and then treated with 5% (w/v) KOH in 30% (v/v) methanol at 75 °C for 10 min. The remaining pellet was added 25 μL acetic acid first and then extracted

with 5 mL DMSO for 10 min in a water bath at 75 °C. The supernatant was collected after centrifugation (10000 rpm, 5 min). The extraction procedure was repeated several times until the pellet became colorless. Finally, the absorbance of the extract was measured at a wavelength of 492 nm.

$$AC = 4.5 \times A_{492} \times V_a/10 \quad (2)$$

where $A_{492}$ was the absorbance of extracts at 492 nm and $V_a$ was the volume of extracts.

The morphological changes of algal cells were examined daily using Olympus BX53 light microscope and the microphotographs were taken with an Olympus DP74 digital camera. Since the shape of motile cells is irregular, the cell size is characterized by the protoplast length and measured by Olympus application software with an internal reticle scale. No less than 300 cells per group were used for cell size statistics.

All data were subjected to an analysis of variance (ANOVA), and differences at $p \leq 0.05$ were considered statistically significant.

# 3 RESULTS

## 3.1 The Effect of Different Nitrogen Concentrations on Astaxanthin Production in Motile Cells

### 3.1.1 Microalgae Growth

The effect of different nitrogen concentrations on the dry weight is shown in **Figure 1B**. During the first three days of culture, the dry weight development trend of the four groups was the same, and no significant differences were observed. However, on the 4th day of treatment, the dry weight growth of the 0 N group slowed down significantly, while the other three groups continued to maintain a sustained increase. After four days of cultivation, the maximum dry weight of the 0 N, 0.5 N, 1 N and 3 N groups reached 1.02 ± 0.08 g $L^{-1}$, 1.25 ± 0.02 g $L^{-1}$, 1.15 ± 0.02 g $L^{-1}$ and 1.19 ± 0.04 g $L^{-1}$, respectively.

### 3.1.2 Astaxanthin Production

It can be seen from **Figure 1C** that the astaxanthin concentration of the 0 N and 0.5 N groups shows a similar growth trend, and the astaxanthin concentration growth trend of the 1 N and 3 N groups is similar. The 0 N and the 0.5 N groups showed rapid growth at first and then slowed down after one day of treatment, while the astaxanthin concentration of the 1 N group and the 3 N group showed a stable growth trend within four days. After four days of treatment, the astaxanthin concentration in the 0 N group has the highest value of 3.50 ± 0.10 mg $L^{-1}$, followed by the 0.5 N group and the 1 N group with the value of 3.12 ± 0.19 mg $L^{-1}$ and 2.93 ± 0.05 mg $L^{-1}$. The 3 N group had the lowest astaxanthin concentration with a value of 2.76 ± 0.09 mg $L^{-1}$.

The astaxanthin content of the four cultures at the end of cultivation is calculated, and the results is shown in **Figure 1D**. A trend is observed that the lower the nitrogen concentration, the higher the astaxanthin content. The 0 N group had the highest astaxanthin content at 0.31 ± 0.02%, while the 3N group had the lowest at 0.20 ± 0.01%.

## 3.2 The Effect of Different Light Intensity on Astaxanthin Production in Motile Cells Under Nitrogen Starvation

### 3.2.1 The Cell Morphological Changes

As shown in **Figure 2A**, the motile cell morphological changes at different light intensities are observed under the light microscope. The motile cells protoplast was enclosed by a

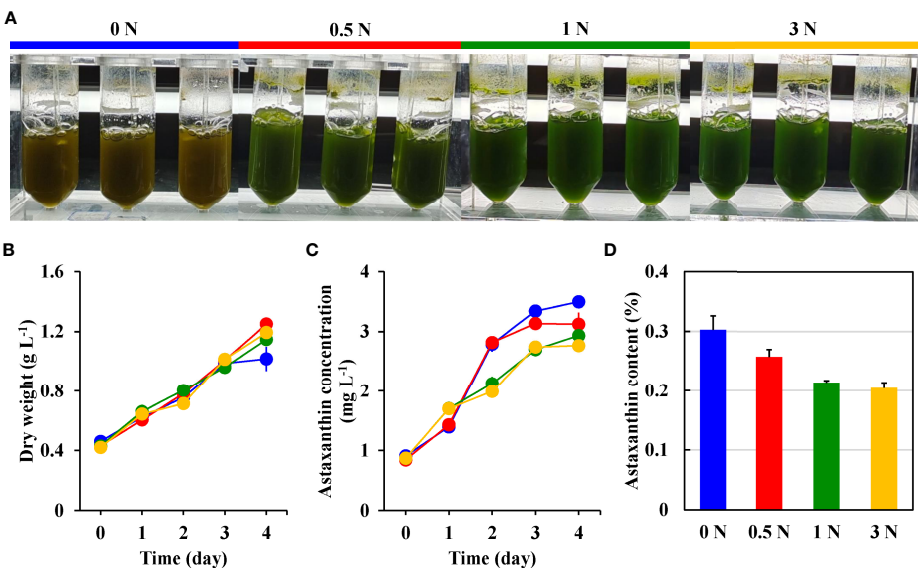


**FIGURE 1** | The color changes **(A)**, dry weight **(B)**, astaxanthin concentration **(C)**, and astaxanthin content **(D)** of *H. pluvialis* motile cells in the 0 N (blue), 0.5 N (red), 1 N (green), and 3 N (yellow) group.

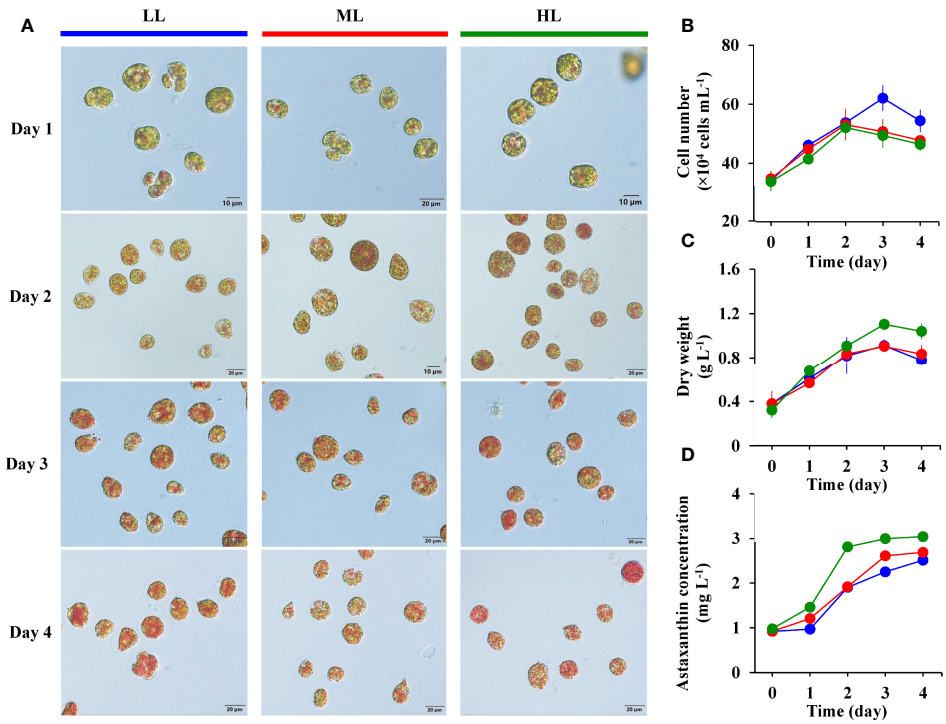


**FIGURE 2** | The cell morphological changes **(A)**, cell number **(B)**, dry weight **(C)**, and astaxanthin concentration **(D)** of *H. pluvialis* in the LL (blue), ML (red), and HL (green) group.

swollen and gelatinous cell wall layer. After culturing for one day under nitrogen starvation, a small amount of orange-red pigment was observed in the motile cells treated with different light intensities. With the increase of treatment time, the motile cells of the three groups gradually changed from green to red due to astaxanthin accumulation. After being exposed to HL for two days, the gelatinous extracellular matrix outside the protoplasts of some motile cells disappeared, and a few motile cells developed into cysts with thickened cell walls. After four days of treatment, the protoplasts of motile cells in the ML and HL groups had distinct granularity, but the granularity of cells in the LL group was weak.

### 3.2.2 Microalgae Growth

The effect of light intensity on the cell number of motile cells under nitrogen starvation is shown in **Figure 2B**. During the first two days of culture under nitrogen starvation conditions, the number of cells in the three groups showed an upward trend. The cell number in the ML and HL groups reached the maximum value on the second day, at $5.3\times10^5$ cells $mL^{-1}$ and $5.2\times10^5$ cells $mL^{-1}$, respectively, and then rapidly decreased until the end. However, the number of cells in the LL group reached a maximum value of $6.2\times10^5$ cells $mL^{-1}$ after three days of culture, significantly higher than the ML and HL group.

**Figure 2C** shows the changes in dry weight in different light intensity groups. Dry weights of the three groups show a similar trend, increasing with culture time, peaking on the third day, and then decreasing until the end of the 4-day cultivation. After four days of cultivation, the HL group showed the highest dry weight, followed by the ML group, and the LL group had the lowest dry weight. All the maximum dry weight of each group appeared on the third day of culture, and it was 1.11 ± 0.05 g $L^{-1}$ in the HL group, 0.91 ± 0.02 g $L^{-1}$ in the ML group, and 0.91 ± 0.06 g $L^{-1}$ in the LL group (**Table 1**).

### 3.2.3 Astaxanthin Production

The changes in astaxanthin concentration in different light intensity groups are shown in **Figure 2D**. The concentrations of astaxanthin in the three groups showed an upward trend with the increase of culture time. A significant difference in astaxanthin concentrations among the three groups was observed, with the highest in the HL group, followed by the ML group, and the lowest in the LL group. The maximum astaxanthin concentration values of the three groups all appeared at the end of the 4-day cultivation. As shown in **Table 1**, the maximum astaxanthin concentration of the HL group reached 3.04 ± 0.04 mg $L^{-1}$, the ML group was 2.69 ± 0.05 mg $L^{-1}$, and the LL group was 2.51 ± 0.02 mg $L^{-1}$.

We calculated the astaxanthin content of the three cultures at the end of cultivation. As shown in **Table 1**, no difference in astaxanthin content was observed between LL and ML groups, with values of 0.32 ± 0.02% and 0.32 ± 0.04%, respectively, while the astaxanthin content in the HL group was lower than that in the other two groups, with a value of 0.29 ± 0.02%.

**TABLE 1** | The maximum dry weight and astaxanthin concentration, percentage of motile cells, cell mortality rate, and cell size in the LL, ML, and HL group.

| Parameters | LL | ML | HL |
|---|---|---|---|
| The maximum dry weight (g $L^{-1}$) | 0.91 ± 0.06 | 0.91 ± 0.02 | 1.11 ± 0.05 |
| The maximum astaxanthin concentration (mg $L^{-1}$) | 2.51 ± 0.02 | 2.69 ± 0.05 | 3.04 ± 0.04 |
| Astaxanthin content (%) | 0.32 ± 0.02 | 0.32 ± 0.04 | 0.29 ± 0.02 |
| Percentage of motile cells (%) | 87.7 ± 1.6 | 88.1 ± 1.5 | 82.8 ± 1.4 |
| Cell mortality rate (%) | 10.5 ± 1.6 | 9.8 ± 1.3 | 15.1 ± 0.7 |
| Cell size (μm) | 21.72 ± 3.82 | 23.67 ± 4.63 | 23.22 ± 5.05 |

### 3.2.4 Motile Cells Percentage, Cell Mortality Rate, and Cell Size

The motile cells percentage, cell mortality rate, and cell size at the end of the 4-day cultivation were analyzed, and the results are shown in **Table 1**. Among the three groups, the motile cells percentage and cell size in the ML group were 88.1 ± 1.5% and 23.67 ± 4.63 μm, which were higher than those in the LL and HL groups, respectively, while the cell mortality rate in the ML group reached 9.8 ± 1.3%, which was smaller than that in the other two groups. The HL group had the lowest motile cells percentage and highest cell mortality rate among the three groups, with the value of 82.8 ± 1.4% and 15.1 ± 0.7%, respectively. The cell size in the LL group was the lowest among the three groups, with a value of 21.72 ± 3.82 μm.

## 4 DISCUSSION

Astaxanthin accumulation in *H. pluvialis* is normally accompanied by the formation of encystment (Boussiba, 2000). During encystment, a voluminous multilayered cell wall, including trilaminar sheath and secondary wall, is formed with a significantly hardening and thickening (Monstsant et al., 2001; Hagen et al., 2002; Wang et al., 2003). Although the formation of thick cell walls is favorable for the large quality astaxanthin accumulation in *H. pluvialis* (Li et al., 2019a), it is regarded as one of the main factors in reducing the coloration efficiency and bioavailability of astaxanthin when fed to salmonids and other commercial species (Sommer et al., 1991; Young et al., 2017). Previous studies have shown that breaking *H. pluvialis* cysts can improve the astaxanthin deposition rate in trout flesh (Sommer et al., 1991). But, disruption of *H. pluvialis* cyst cell walls often require mechanical, chemical, or enzymatic means, and all of these processes are currently highly energy-intensive and expensive (Tibbetts, 2018). In addition, these processes can decrease the stability of astaxanthin and reduce the shelf life of the compound (Han et al., 2013). In contrast, thin-walled *H. pluvialis* can use whole cells as a source of astaxanthin, which has potential advantages in maintaining compound stability, easy digestion, enhance bioavailability of carotenoids, and reducing production costs.

Astaxanthin is accumulated in *H. pluvialis* under growth-limiting conditions, such as nutrient deprivation, high light, and/or high salinity (Lemoine & Schoefs, 2010; Chekanov et al., 2014; Scibilia et al., 2015; Solovchenko, 2015; Oslan et al., 2021). Nitrogen is one of the essential nutrients that affect cell growth and enzymatic activity of *H. pluvialis* (Zhang et al., 2018). Previous studies showed that nitrogen deficiency inhibited *H. pluvialis* chlorophyll biosynthesis and promoted chlorophyll b degradation, PTOX activity, and cyclic electron transport (Scibilia et al., 2015). The reduction of chlorophyll content resulted in the limitation of the cell's ability to maintain photosynthetic function (Young and Beardall, 2003). In this case, *H. pluvialis* accumulated large amounts of carbon in the form of carotenoids and lipids (Sun et al., 2018). In the present study, we observed that the lower the nitrogen concentration, the higher the astaxanthin content in motile cells. The results are consistent with previous reports that nitrogen deficiency can stimulate astaxanthin synthesis (Borowitzka et al., 1991; Fábregas et al., 1998).

Light intensity is another one of the most significant factors in the induction of astaxanthin accumulation (Oslan et al., 2021). It can cause oxidative stress and promote the excess of reactive oxygen species in algal cells, thereby activating the biosynthesis of astaxanthin (Han et al., 2012). It has been reported that within the first three days of high light induction, the non-photochemical quenching (NPQ) of *H. pluvialis* cells decreased dramatically, while the chlorophyll a/b ratio increased transiently. In contrast, under the high light combined with nitrogen starvation, cells exhibited a sustained increase in chlorophyll a/b ratio and a rapid rise in NPQ induction. In addition, the PSII quantum yield decreased by 20% under high light conditions, while the Fv/Fm remained stable under the combined induction of high light and nitrogen deficiency (Scibilia et al., 2015). Scibilia et al. (2015) believed that nitrogen starvation enhanced the stress response of *H. pluvialis*, inducing cells to rapidly counteract high-irradiation-induced photooxidative stress, thereby improving the resistance of cells to photo-oxidation. However, motile cells of *H. pluvialis* are sensitive to light intensity, and the PSII core subunits of cells are degraded when exposed to high light conditions (Han et al., 2012). In this study, after four days of culture, the cell mortality rate in the HL group reached more than 15%, which was significantly higher than that in the LL and ML groups, indicating that high light intensity was not suitable for inducing motile cells to accumulate astaxanthin. In addition, no significant differences were observed in astaxanthin content, motile cells percentage, and cell mortality rate between the LL and ML groups. Considering low light is more economical in terms of electricity consumption, we recommend that low light as the light condition for motile cells to accumulate astaxanthin under nitrogen starvation.

We have to point out that the astaxanthin content obtained in the current study was not high. It may account for the short irradiation time. Considering that prolonged induction can lead to an increase in the number of thick-walled cysts, further work investigating the relationship between the induction period and the percentage of motile cells and astaxanthin content is needed with the aim to determine the optimal induction period. In addition,

according to Butler et al. (2018), the intracellular astaxanthin content of *H. pluvialis* motile cells can reach up to 2.7% of dry weight. It is indicated that there is still large improvement room for astaxanthin content in motile cells. Therefore, more effort to optimize induction conditions would be needed for improving astaxanthin production by motile cells. Phosphorus deficiency (Imamoglu et al., 2009) or high salt (Tam et al., 2012) can promote astaxanthin accumulation. However, phosphorus deficiency (Boussiba and Vonshak, 1991; Li et al., 2021) and high salt (Droop, 1955; Li et al., 2021) can induce cyst formation in *H. pluvialis*. Further study on optimizing the astaxanthin production by motile cells should take into account this aspect.

## DATA AVAILABILITY STATEMENT

The original contributions presented in the study are included in the article/supplementary material. Further inquiries can be directed to the corresponding authors.

## AUTHOR CONTRIBUTIONS

FL: data curation, methodology, and writing-original draft. YW: investigations. MC: writing-review and editing. QL: investigations. ZQ: investigations. JL: investigations. YZ: methodology. NZ: methodology. XH: project administration and resources. CL: project administration and resources. All authors contributed to the article and approved the submitted version.

## FUNDING

This research was mainly supported by Program for Scientific Research Start-up Funds of Guangdong Ocean University (grant number 060302022102) and Marine Economic Development Special Fund of Fujian Province (FJHJF-L-2021-5).

## REFERENCES

Ambati, R. R., Phang, S. M., Ravi, S., and Aswathanarayana, R. G. (2014). Astaxanthin: Sources, Extraction, Stability, Biological Activities and Its Commercial Applications—A Review. *Mar. Drugs* 12 (1), 128–152. doi: 10.3390/md12010128

Borowitzka, M. A., Huisman, J. M., and Osborn, A. (1991). Culture of The Astaxanthin-Producing Green Alga Haematococcus Pluvialis 1. Effects of Nutrients on Growth and Cell Type. *J. Appl. Phycol.* 3 (4), 295–304. doi: 10.1007/BF02392882

Boussiba, S. (2000). Carotenogenesis in The Green Alga *Haematococcus Pluvialis*: Cellular Physiology and Stress Response. *Physiol. Plantar.* 108 (2), 111–117. doi: 10.1034/j.1399-3054.2000.108002111.x

Boussiba, S., and Vonshak, A. (1991). Astaxanthin Accumulation in The Green Alga *Haematococcus Pluvialis*. *Plant Cell Physiol.* 32 (7), 1077–1082. doi: 10.1093/oxfordjournals.pcp.a078171

Bowen, J., Soutar, C., Serwata, R. D., Lagocki, S., White, D. A., and Davies, S. J. (2002). Utilization of (3S, 3′S) Astaxanthin Acyl Esters in Pigmentation of Rainbow Trout (*Oncorhynchus Mykiss*). *Aquacult. Nutr.* 8 (1), 59–68. doi: 10.1046/j.1365-2095.2002.00190.x

Butler, T. O., McDougall, G. J., Campbell, R., Stanley, M. S., and Day, J. G. (2018). Media Screening for Obtaining *Haematococcus Pluvialis* Red Motile Macrozooids Rich in Astaxanthin and Fatty Acids. *Biology* 7 (1), 2. doi: 10.3390/biology7010002

Chekanov, K., Lobakova, E., Selyakh, I., Semenova, L., Sidorov, R., and Solovchenko, A. (2014). Accumulation of Astaxanthin by A New *Haematococcus Pluvialis* Strain BM1 From The White Sea Coastal Rocks (Russia). *Mar. Drugs* 12 (8), 4504–4520. doi: 10.3390/md12084504

Choubert, G., Mendes-Pinto, M. M., and Morais, R. (2006). Pigmenting Efficacy of Astaxanthin Fed to Rainbow Trout *Oncorhynchus Mykiss*: Effect of Dietary Astaxanthin and Lipid Sources. *Aquaculture* 257 (1-4), 429–436. doi: 10.1016/j.aquaculture.2006.02.055

Droop, M. R. (1955). Some Factors Governing Encystment in *Haematococcus Pluvialis*. *Arch. Für. Mikrobiol.* 21, 267–272. doi: 10.1007/BF00412349

Fábregas, J., Domínguez, A., Álvarez, D. G., Lamela, T., and Otero, A. (1998). Induction of Astaxanthin Accumulation by Nitrogen and Magnesium Deficiencies in *Haematococcus Pluvialis*. *Biotechnol. Lett.* 20 (6), 623–626. doi: 10.1023/A:1005322416796

Fang, L., Zhang, J., Fei, Z., and Wang, M. (2020). Astaxanthin Accumulation Difference Between Non-Motile Cells and Akinetes of *Haematococcus Pluvialis* Was Affected by Pyruvate Metabolism. *Biores. Bioprocess.* 7 (1), 1–12. doi: 10.1186/s40643-019-0293-1

Hagen, C., Siegmund, S., and Braune, W. (2002). Ultrastructural And Chemical Changes in The Cell Wall of *Haematococcus Pluvialis* (Volvocales, Chlorophyta) During Aplanospore Formation. *Eur. J. Phycol.* 37 (2), 217–226. doi: 10.1017/S0967026202003669

Han, D., Li, Y., and Hu, Q. (2013). Astaxanthin in Microalgae: Pathways, Functions and Biotechnological Implications. *Algae* 28 (2), 131–147. doi: 10.4490/algae.2013.28.2.131

Han, D., Wang, J., Sommerfeld, M., and Hu, Q. (2012). Susceptibility And Protective Mechanisms of Motile and Non-Motile Cells of *Haematococcus Pluvialis* (Chlorophyceae) to Photooxidative Stress. *J. Phycol.* 48 (3), 693–705. doi: 10.1111/j.1529-8817.2012.01147.x

Hart, B., and Colombo, S. M. (2022). Effects of a Novel Weakened Whole-Cell Form of *Haematococcus Pluvialis* on Flesh Pigmentation of Rainbow Trout (*Oncorhynchus Mykiss*) When Compared to Synthetic Astaxanthin. *Aquacult. Res.* 53 (6), 2408–2319. doi: 10.1111/are.15758

Imamoglu, E., Dalay, M. C., and Sukan, F. V. (2009). Influences of Different Stress Media and High Light Intensities on Accumulation of Astaxanthin in The Green Alga *Haematococcus Pluvialis*. *New Biotechnol.* 26 (3-4), 199–204. doi: 10.1016/j.nbt.2009.08.007

Kalinowski, C. T., Robaina, L. E., and Izquierdo, M. S. (2011). Effect of Dietary Astaxanthin on The Growth Performance, Lipid Composition and Post-Mortem Skin Colouration of Red Porgy *Pagrus Pagrus*. *Aquacult. Int.* 9 (5), 811–823. doi: 10.1007/s10499-010-9401-0

Kobayashi, M., Kurimura, Y., and Tsuji, Y. (1997). Light-Independent, Astaxanthin Production by The Green Microalga *Haematococcus Pluvialis* Under Salt Stress. *Biotechnol. Lett.* 19 (6), 507–509. doi: 10.1023/A:1018372900649

Lemoine, Y., and Schoefs, B. (2010). Secondary Ketocarotenoid Astaxanthin Biosynthesis in Algae: A Multifunctional Response to Stress. *Photosynthesis. Res.* 106 (1), 155–177. doi: 10.1007/s11120-010-9583-3

Li, F., Cai, M., Lin, M., Huang, X., Wang, J., Ke, H., et al. (2019a). Differences Between Motile and Nonmotile Cells of *Haematococcus Pluvialis* in The Production of Astaxanthin at Different Light Intensities. *Mar. Drugs* 17 (1), 39. doi: 10.3390/md17010039

Li, F., Cai, M., Lin, M., Huang, X., Wang, J., Ke, H., et al. (2020b). Enhanced Biomass and Astaxanthin Production of *Haematococcus Pluvialis* by A Cell Transformation Strategy With Optimized Initial Biomass Density. *Mar. Drugs* 18 (7), 1–7. doi: 10.3390/md18070341

Li, F., Cai, M., Lin, M., Huang, X., Wang, J., Zheng, X., et al. (2019b). Accumulation of Astaxanthin Was Improved by The Nonmotile Cells of *Haematococcus Pluvialis*. *BioMed. Res. Int.* 2019, 1–7. doi: 10.1155/2019/8101762

Li, F., Huang, S., Lu, X., Wang, J., Lin, M., An, Y., et al. (2018). Effects of Dietary Supplementation With Algal Astaxanthin on Growth, Pigmentation, And

Antioxidant Capacity of The Blood Parrot (*Cichlasoma Citrinellum* × *Cichlasoma Synspilum*). *J. Oceanol. Limnol.* 36 (5), 1851–1859. doi: 10.1007/s00343-019-7172-7

Li, X., Wang, X., Duan, C., Yi, S., Gao, Z., Xiao, C., et al. (2020a). Biotechnological Production of Astaxanthin From The Microalga *Haematococcus Pluvialis*. *Biotechnol. Adv.* 43, 107602. doi: 10.1016/j.biotechadv.2020.107602

Li, M., Wu, W., Zhou, P., Xie, F., Zhou, Q., and Mai, K. (2014). Comparison Effect of Dietary Astaxanthin and *Haematococcus Pluvialis* On Growth Performance, Antioxidant Status and Immune Response of Large Yellow Croaker *Pseudosciaena Crocea*. *Aquaculture* 434, 227–232. doi: 10.1016/j.aquaculture.2014.08.022

Li, F., Zhang, N., Zhang, Y., Lian, Q., Qin, C., Qian, Z., et al. (2021). NaCl Promotes the Efficient Formation of *Haematococcus Pluvialis* Nonmotile Cells Under Phosphorus Deficiency. *Mar. Drugs* 19 (6), 337. doi: 10.3390/md19060337

Li, J., Zhu, D., Niu, J., Shen, S., and Wang, G. (2011). An Economic Assessment of Astaxanthin Production by Large Scale Cultivation of *Haematococcus Pluvialis*. *Biotechnol. Adv.* 29 (6), 568–574. doi: 10.1016/j.biotechadv.2011.04.001

Lorenz, R. T., and Cysewski, G. R. (2000). Commercial Potential for *Haematococcus* Microalgae as A Natural Source of Astaxanthin. *Trends Biotechnol.* 18 (4), 160–167. doi: 10.1016/S0167-7799(00)01433-5

Montsant, A., Zarka, A., and Boussiba, S. (2001). Presence Of a Nonhydrolyzable Biopolymer in The Cell Wall of Vegetative Cells and Astaxanthin-Rich Cysts of *Haematococcus Pluvialis* (Chlorophyceae). *Mar. Biotechnol.* 3 (6), 515–521. doi: 10.1007/s1012601-0051-0

Moretti, V. M., Mentasti, T., Bellagamba, F., Luzzana, U., Caprino, F., Turchini, G. M., et al. (2006). Determination of Astaxanthin Stereoisomers and Colour Attributes in Flesh of Rainbow Trout (*Oncorhynchus Mykiss*) As A Tool to Distinguish the Dietary Pigmentation Source. *Food Additive. Contaminant.* 23 (11), 1056–1063. doi: 10.1080/02652030600838399

Nogueira, N., Canada, P., Caboz, J., Andrade, C., and Cordeiro, N. (2021). Effect of Different Levels of Synthetic Astaxanthin on Growth, Skin Color and Lipid Metabolism of Commercial Sized Red Porgy (*Pagrus Pagrus*). *Anim. Feed. Sci. Technol.* 276, 114916. doi: 10.1016/j.anifeedsci.2021.114916

Orosa, M., Franqueira, D., Cid, A., and Abalde, J. (2005). Analysis and Enhancement of Astaxanthin Accumulation in *Haematococcus Pluvialis*. *Biores. Technol.* 96 (3), 373–378. doi: 10.1016/j.biortech.2004.04.006

Oslan, S. N. H., Shoparwe, N. F., Yusoff, A. H., Rahim, A. A., Chang, C. S., Tan, J. S., et al. (2021). A Review on *Haematococcus Pluvialis* Bioprocess Optimization of Green and Red Stage Culture Conditions for The Production of Natural Astaxanthin. *Biomolecules* 11 (2), 256. doi: 10.3390/biom11020256

Panis, G., and Carreon, J. R. (2016). Commercial Astaxanthin Production Derived by Green Alga *Haematococcus Pluvialis*: A Microalgae Process Model and A Techno-Economic Assessment All Through Production Line. *Algal. Res.* 18, 175–190. doi: 10.1016/j.algal.2016.06.007

Rahman, M. M., Khosravi, S., Chang, K. H., and Lee, S. M. (2016). Effects of Dietary Inclusion of Astaxanthin on Growth, Muscle Pigmentation and Antioxidant Capacity of Juvenile Rainbow Trout (*Oncorhynchus Mykiss*). *Prev. Nutr. Food Sci.* 21 (3), 281–288. doi: 10.3746/pnf.2016.21.3.281

Scibilia, L., Girolomoni, L., Berteotti, S., Alboresi, A., and Ballottari, M. (2015). Photosynthetic Response to Nitrogen Starvation and High Light in *Haematococcus Pluvialis*. *Algal. Res.* 12, 170–181. doi: 10.1016/j.algal.2015.08.024

Shah, M. M. R., Liang, Y., Chen, J. J., and Daroch, M. (2016). Astaxanthin-Producing Green Microalga *Haematococcus Pluvialis*: From Single Cell to High Value Commercial Products. *Front. Plant Sci.* 7. doi: 10.3389/fpls.2016.00531

Sheikhzadeh, N., Tayefi-Nasrabadi, H., Khani Oushani, A., and Enferadi, M. H. N. (2012). Effects of *Haematococcus Pluvialis* Supplementation on Antioxidant System and Metabolism in Rainbow Trout (*Oncorhynchus Mykiss*). *Fish. Physiol. Biochem.* 38 (2), 413–419. doi: 10.1007/s10695-011-9519-7

Solovchenko, A. E. (2015). Recent Breakthroughs in the Biology of Astaxanthin Accumulation by Microalgal Cell. *Photosynthesis. Res.* 125 (3), 437–449. doi: 10.1007/s11120-015-0156-3

Sommer, T. R., Potts, W. T., and Morrissy, N. M. (1991). Utilization of Microalgal Astaxanthin by Rainbow Trout (*Oncorhynchus Mykiss*). *Aquaculture* 94 (1), 79–88. doi: 10.1016/0044-8486(91)90130-Y

Stachowiak, B., and Szulc, P. (2021). Astaxanthin for the Food Industry. *Molecules* 26 (9), 26. doi: 10.3390/molecules26092666

Sun, X. M., Ren, L. J., Zhao, Q. Y., Ji, X. J., and Huang, H. (2018). Microalgae for the Production of Lipid and Carotenoids: A Review With Focus on Stress Regulation and Adaptation. *Biotechnol. Biofuels.* 11 (1), 1–16. doi: 10.1186/s13068-018-1275-9

Tacon, A. G. J., and Metian, M. (2013). Fish Matters: Importance of Aquatic Foods in Human Nutrition and Global Food Supply. *Rev. Fish. Sci.* 21 (1), 22–38. doi: 10.1080/10641262.2012.753405

Tam, L. T., Hoang, D. D., Mai, D. T. N., Thu, N. T. H., Anh, H. T. L., and Dang, D. H. (2012). Study on the Effect of Salt Concentration on Growth and Astaxanthin Accumulation of Microalgae *Haematococcus Pluvialis* As the Initial Basis for Two Phase Culture of Astaxanthin Production. *Academia. J. Biol.* 34 (2), 213–223. doi: 10.15625/0866-7160/v34n2.964

Tejera, N., Cejas, J. R., Rodríguez, C., Bjerkeng, B., Jerez, S., Bolaños, A., et al. (2007). Pigmentation, Carotenoids, Lipid Peroxides and Lipid Composition of Skin of Red Porgy (*Pagrus Pagrus*) Fed Diets Supplemented With Different Astaxanthin Sources. *Aquaculture* 270 (1-4), 218–230. doi: 10.1016/j.aquaculture.2007.01.019

Tibbetts, S. M. (2018). "The Potential for 'Next-Generation', Microalgae-Based Feed Ingredients for Salmonid Aquaculture in Context of The Blue Revolution," in *Microalgal Biotechnology*. Eds. E. Jacob-Lopes, L. Q. Zepka and M. I. Queiroz, 151–175. London, United Kingdom: IntechOpen. doi: 10.5772/intechopen.73551

Torrissen, O. J., Christiansen, R., Struksnæs, G., and Estermann, R. (1995). Astaxanthin Deposition in the Flesh of Atlantic Salmon, *Salmo Salar* L, in Relation to Dietary Astaxanthin Concentration and Feeding Period. *Aquacult. Nutr.* 1 (2), 77–84. doi: 10.1111/j.1365-2095.1995.tb00022.x

Viera, I., Pérez-Gálvez, A., and Roca, M. (2018). Bioaccessibility of Marine Carotenoids. *Mar. Drugs* 16 (10), 397. doi: 10.3390/md16100397

Wang, B., Zarka, A., Trebst, A., and Boussiba, S. (2003). Astaxanthin Accumulation in *Haematococcus Pluvialis* (Chlorophyceae) As an Active Photoprotective Process Under High Irradiance[1]. *J. Phycol.* 39 (6), 1116–1124. doi: 10.1111/j.0022-3646.2003.03-043.x

Yeşilayer, N. (2020). Comparison of Flesh Colour Assessment Methods for Wild Brown Trout (*Salmo Trutta Macrostigma*), Farmed Rainbow Trout (*Oncorhynchus Mykiss*) and Farmed Atlantic Salmon (*Salmo Salar*). *Pakistan J. Zool.* 52 (3), 1007–1014. doi: 10.17582/journal.pjz/20190520140524

Young, E. B., and Beardall, J. (2003). Photosynthetic Function in *Dunaliella Tertiolecta* (Chlorophyta) During a Nitrogen Starvation and Recovery Cycle. *J. Phycol.* 39 (5), 897–905. doi: 10.1046/j.1529-8817.2003.03042.x

Young, A. J., Pritchard, J., White, D., and Davies, S. (2017). Processing of Astaxanthin-Rich *Haematococcus* Cells for Dietary Inclusion and Optimal Pigmentation in Rainbow Trout, *Oncorhynchus Mykiss* L. *Aquacult. Nutr.* 23 (6), 1304–1311. doi: 10.1111/anu.12505

Yu, W., Lin, H., Yang, Y., Zhou, Q., Chen, H., Huang, X., et al. (2021). Effects of Supplemental Dietary *Haematococcus Pluvialis* on Growth Performance, Antioxidant Capacity, Immune Responses and Resistance to *Vibrio Harveyi* Challenge of Spotted Sea Bass *Lateolabrax Maculatus*. *Aquacult. Nutr.* 27 (2), 355–365. doi: 10.1111/anu.13189

Zhang, W., Zhou, X., Zhang, Y., Cheng, P., Ma, R., Cheng, W., et al. (2018). Enhancing Astaxanthin Accumulation in *Haematococcus Pluvialis* by Coupled Light Intensity and Nitrogen Starvation in Column Photobioreactors. *J. Microbiol. Biotechnol.* 28 (12), 2019–2028. doi: 10.4014/jmb.1807.07008

**Conflict of Interest:** The authors declare that the research was conducted in the absence of any commercial or financial relationships that could be construed as a potential conflict of interest.

**Publisher's Note:** All claims expressed in this article are solely those of the authors and do not necessarily represent those of their affiliated organizations, or those of the publisher, the editors and the reviewers. Any product that may be evaluated in this article, or claim that may be made by its manufacturer, is not guaranteed or endorsed by the publisher.

frontiers | Frontiers in Marine Science

ORIGINAL RESEARCH
published: 23 June 2022
doi: 10.3389/fmars.2022.907065

# Identification of Interacting Proteins of Transcription Factor DpAP2 Related to Carotenoid Biosynthesis From Marine Microalga *Dunaliella parva*

*Changhua Shang[1,2,3*†], Bingbing Pang[1,2†], Jin Zhang[1,2], Lihong Yu[1,2], Shanling Gan[1,2], Yujia Li[1,2] and Haifeng Wu[1,2]*

[1] College of Life Sciences, Guangxi Normal University, Key Laboratory of Ecology of Rare and Endangered Species and Environmental Protection (Guangxi Normal University), Ministry of Education, Guilin, China, [2] Guangxi Key Laboratory of Landscape Resources Conservation and Sustainable Utilization in Lijiang River Basin (Guangxi Normal University), Guilin, China, [3] School of Life Sciences, Sun Yat-sen University, Guangzhou, China

OPEN ACCESS

**Edited by:**
Shuhao Huo,
Jiangsu University, China

**Reviewed by:**
Xupeng Cao,
Dalian Institute of Chemical Physics (CAS), China
Jichang Han,
Ningbo University, China
Ang Ren,
Nanjing Agricultural University, China
Qiuning Liu,
Yancheng Teachers University, China

***Correspondence:**
Changhua Shang
shangchanghua@mailbox.gxnu.edu.cn

[†]These authors have contributed equally to this work

**Specialty section:**
This article was submitted to Marine Fisheries, Aquaculture and Living Resources, a section of the journal Frontiers in Marine Science

**Received:** 29 March 2022
**Accepted:** 19 May 2022
**Published:** 23 June 2022

**Citation:**
Shang C, Pang B, Zhang J, Yu L, Gan S, Li Y and Wu H (2022) Identification of Interacting Proteins of Transcription Factor DpAP2 Related to Carotenoid Biosynthesis From Marine Microalga Dunaliella parva. Front. Mar. Sci. 9:907065. doi: 10.3389/fmars.2022.907065

Carotenoids are widely distributed and structurally diverse, which have significant roles in the photosynthesis of plants. As a precursor of vitamin A, carotenoids are also antioxidants that reduce various chronic diseases, which are beneficial for human health. Currently, the existing studies concerned the biological roles of *APETALA2 (AP2)/ethylene-responsive factor (ERF)* genes originated from higher plants. The AP2 superfamily of the transcriptional regulator was identified in higher plants, which was related to growth, development, carotenoid metabolism, and responses to various stresses. However, the regulatory mechanisms of the AP2-modulating carotenoid metabolism have not been reported in microalgae, which remain to be elucidated. *Dunaliella parva* AP2 (i.e., DpAP2), an important transcription factor, promotes carotenoid accumulation by binding to the promoter of target gene. Here, we identified an important AP2/ERF transcription factor, DpAP2, which could promote carotenoid accumulation by binding to the promoter of target gene. To demonstrate the function of DpAP2, the interacting proteins were identified by the yeast two-hybrid system. The results showed that DpAP2 could interact with three proteins with different activities (DNA-binding transcription factor activity, protein kinase activity, and alpha-D-phosphohexomutase activity); these proteins may be associated with multiple biological processes. This paper laid a good foundation for a deep understanding of the regulatory mechanisms of DpAP2 and genetic engineering breeding in *D. parva*.

**Keywords: *Dunaliella parva*, AP2, yeast two-hybrid system, interacting proteins, carotenoid biosynthesis**

## INTRODUCTION

Microalgae have been utilized commercially in the Far East for healthy foodstuffs such as *Arthrospira platensis* and in the United States for wastewater treatment (Oswald, 2003). At present, in response to the increasing concern around global warming, the microalgal culture was again considered for a carbon-neutral process to obtain third-generation biofuels such as biodiesel (Gilmour, 2019). Biomass productivity, oil content, and energy-intensive harvesting were the major constraints for biodiesel production from microalgae on a large scale (Shahid et al., 2020). Nitrogen limitation has been widely used to increase oil content in microalgae (Kumari et al., 2021; Zhang et al., 2021). When *Scenedesmus acuminatus* grew under nitrogen-limited conditions, oil productivity was enhanced (Zhang et al., 2021). Nitrogen limitation increased oil content in *Chlorella vulgaris*, which might be related to the upregulation of mRNA levels of several oil biosynthesis genes (Kumari et al., 2021). Our previous study also showed that nitrogen limitation could induce an increase in oil content from 25% to 40% in *D. parva* (Shang et al., 2016). However, nitrogen limitation also hampered the growth, photosynthetic antennae size, and maximum photosynthetic efficiency in algae (Jiang et al., 2021; Kamalanathan et al., 2021), which was also demonstrated by our previous study (Shang et al., 2016). The biochemical engineering approach depended on physiological stresses such as nitrogen limitation to channel metabolic fluxes to lipid accumulation. However, an inherited shortcoming of the biochemical engineering approach was the reduced cell division, which limited the application of this approach (Ratledge, 2002). Compared with the biochemical engineering approach, the transcription factor engineering approach was an emerging technology to improve the yield of the specific metabolites by overexpressing transcription factors regulating the metabolic pathways related to the accumulation of target metabolites (Courchesne et al., 2009).

A comprehensive utilization of microalgae could significantly reduce the cost of microalgae biofuels, which included microalgae cultivation using wastewaters in outdoor raceway ponds (Arora et al., 2016; Gao et al., 2018; Keerthana et al., 2020) and the production of bioactive substances such as polysaccharides (Li et al., 2019), antiviral substances (Fritzsche et al., 2021), bioactive peptides (Donadio et al., 2021), and carotenoids (du Preez et al., 2021; Todorović et al., 2021).

Carotenoid biosynthesis involves a complex pathway (Narang et al., 2021). Our previous study also cloned and characterized several carotenoid synthesis genes such as *GGPS* encoding geranylgeranyl diphosphate synthase (Shang et al., 2016b), *Psy* encoding phytoene synthase, and *Pds* encoding phytoene desaturase (Shang et al., 2018). In *D. parva*, the *PSY* gene played important roles in carotenoid metabolism (Ismaiel et al., 2018). These genes played a key role in the carotenoid biosynthesis pathway because they catalyzed the rate-limiting step. The current studies focused on the regulators (especially transcription factors) of the metabolic pathway rather than the key enzyme (Li et al., 2021). A lot of transcription factors (TFs) regulating the carotenoid biosynthesis pathway were identified in higher plants, which included MADS-box (Kang et al., 2021), NAC (Gong et al., 2021), AP2/ERF (Dang et al., 2021), and MYB families (Shi et al., 2021). These TFs can bind to the promoter of the target gene. The putative carotenoid biosynthetic pathway in microalgae is shown in **Figure 1**. The metabolic enzymes were encoded by the structural genes in the carotenoid biosynthesis pathway, which included zeta-carotene desaturase (ZDS), carotenoid isomerase (CRTISO), ζ-carotene isomerase (ZISO), lycopene β-cyclase (LCY-β), beta-carotene hydroxylase (CHY-β), lycopene ϵ-cyclase (LCY-ϵ), and zeaxanthin epoxidase (ZEP) (Ampomah-Dwamena C et al., 2019).

The APETALA2/ethylene-responsive factor (AP2/ERF) superfamily in plants contains four subfamilies including AP2, CBF/DREB, ERF, and RAV according to the number of AP2/ERF domains and the sequence (Xing et al., 2021). TFs played important regulatory roles in the development, growth, and responses to various stresses in plants. The AP2/ERF, a complex TF family, is one of the largest families, which efficiently regulates carotenoid accumulation in plants. In *Auxenochlorella protothecoides*, AP2, ERF, and R2R3-MYB promoted triacylglycerol accumulation by triggering the lipid biosynthesis pathway (Xing et al., 2021). Previous studies have reported that AP2/ERF TF could modulate carotenoid accumulation. In apple, MdAP2-34 was able to enhance carotenoid accumulation by binding to the *MdPSY2-1* promoter (Dang et al., 2021). SIERF6 could exactly regulate carotenoid accumulation in tomato (Lee et al., 2012). The TFs (AP2, AP2-like) related to phytohormones potentially affected carotenoid metabolism in apricot (Zhang et al., 2019). RAP2.2 could efficiently regulate carotenoid accumulation by binding to the selected site of the promoter region in tomato (Koul et al., 2019). In *Arabidopsis*, RAP2.2 could also accelerate carotenoid accumulation by binding to the *PSY* promoter (Welsch et al., 2007). In addition, we have overexpressed *DpAP2* genes in *D. parva* in our subsequent experiments. The total carotenoid content increased to 0.85 μg/g of dry cell weight. However, the regulatory mechanism of AP2/ERF TF for carotenoid metabolism is currently unknown in *D. parva*.

*D. parva* is an oleaginous halophilic green alga without a cell wall, which can also accumulate large amounts of carotenoids (mainly β-carotene) (Shang et al., 2016). The simultaneous production of biodiesel and carotenoids using *D. parva* is more attractive compared with the model microalgae. As a new type of bioreactor, *D. parva* has been widely used because of its characteristics including rapid growth, rapid reproduction, easy culture, the ease of controlling pollution, high efficiency, and low price (Shang et al., 2016). *D. parva* is rich in natural carotenoids, folic acid, calcium, and other trace elements required for human health. Carotenoids can be utilized as a colorant, provitamin, precursor of abscisic acid, chemopreventive substance against cancer, and antioxidant (Mohsin et al., 2021). AP2/ERF TF plays significant roles in carotenoid accumulation in plants, but these roles remain unknown in *D. parva*.

In a previous study, we identified a gene fragment *DpAP2* encoding AP2/ERF TF. The role of *DpAP2* is still unclear in

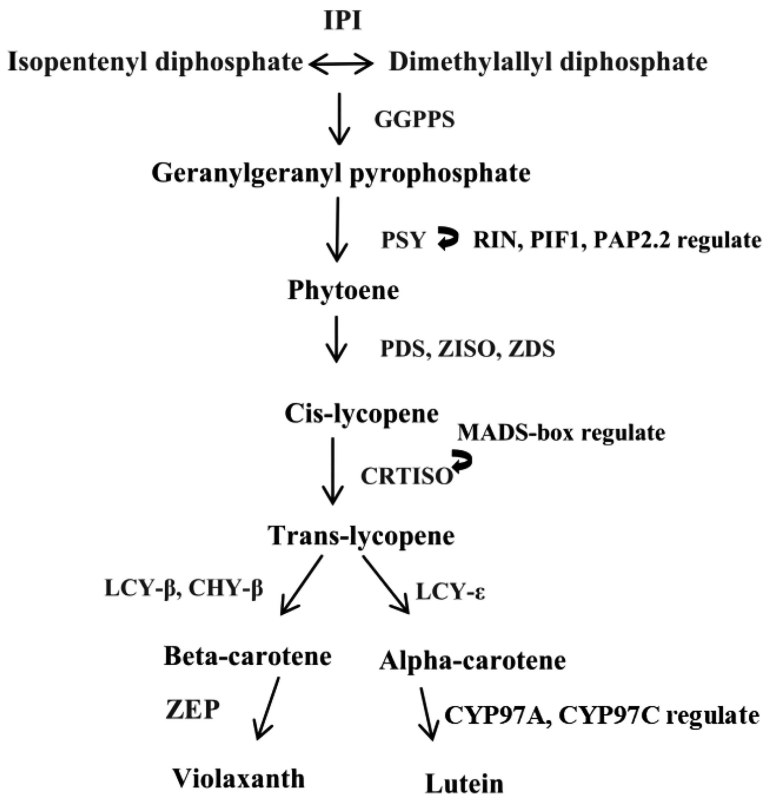


**FIGURE 1** | A graphic representation depicting the putative carotenoid biosynthetic pathway in microalgae. IPI, isopentenyl diphosphate isomerase; GGPPS, geranylgeranyl diphosphate synthase; PSY, phytoene synthase; PDS, phytoene desaturase; ZDS, zeta-carotene desaturase; CRTISO, carotenoid isomerase; ZISO, ζ-carotene isomerase; LCY-β, lycopene β-cyclase; CHY-β, beta-carotene hydroxylase; LCY-ε, lycopene ε-cyclase; ZEP, zeaxanthin epoxidase.

carotenoid metabolism in *D. parva*. In view of a correlation between *DpAP2* and carotenoid production, it is of interest to study the function of *DpAP2* at the molecular level. Here, we reported the cloning of the full-length complementary DNA (cDNA) of *DpAP2*. Then, the DpAP2-interacting proteins were identified by yeast two-hybrid systems and subjected to bioinformatics analysis and further discussion.

# MATERIALS AND METHODS

## Microalgal Material and Growth Conditions

*D. parva* FACHB-815 was purchased from Freshwater Algae Culture Collection at the Institute of Hydrobiology (Wuhan, China). The cells of *D. parva* grew in the Dunaliella medium under the light intensity of 34 μmol of photons $m^{-2}$ $s^{-1}$ illumination at 26°C with 14 h light/10 h dark cycle. The algae bottles were gently swirled one or three times each day by hand.

## First-Strand cDNA Synthesis

Total RNA was extracted from *D. parva* cells using a Total RNA Extractor (Trizol) (Sangon Biotech, Shanghai, China). To ensure that the enough and qualified samples were obtained, the RNA quantity and quality were determined with a Nanophotometer NP80 Spectrophotometer (Geneflow, Lichfield, United Kingdom). First-stand cDNA was synthesized using PrimeScript II Reverse Transcriptase (Takara Bio, Dalian, China) and Oligo (dT) primer. A total amount of 1.5 μg of total RNA was used for reverse transcription reaction.

## Full-Length cDNA Cloning

An attempt was made to gain full-length cDNA by the rapid amplification of cDNA ends (RACE) method. Based on the previous 582 bp cDNA fragment of *DpAP2*, four specific primers (**Table 1**), AP2(3w)/AP2(3n) for 3' RACE and AP2(5w)/AP2(5n) for 5' RACE, were designed. The 5' and 3' RACE were firstly performed using the 5'/3'-Full RACE Kit (Takara) according to the manufacturer's protocol. The outer and inner PCR were conducted with LA Taq (Takara) under the following conditions, respectively: 94°C 3 min, 25 cycles (94°C 30 s, 55°C 30 s, 72°C 2 min), 72°C 10 min for outer PCR, and 94°C 3 min, 35 cycles (94°C 30 s, 55°C 30 s,72°C 2 min), 72°C 10 min for inner PCR. The resulting products were detected with 1% agarose gel electrophoresis and ligated into the pMD19-T vector. However, the resulting 5' nucleotide sequence was shorter than the expected 5' end sequence. In order to obtain the entire 5′ sequence, the second 5' RACE was carried out using the

**TABLE 1** | Primers used in this study.

| Primer name | Primer sequence (5'-3') |
|---|---|
| AP2-5-W | GGCTCAGTTCCTCCGTGT |
| AP2-5-N | CGCTTCCTCCTGAGTTCCA |
| AP2-3-W | GGAGGCAGTGAGACAGAAGG |
| AP2-3-N | GTAGGAGGAGCAGGAACAACT |
| AP2-5-GSP | GATTACGCCAAGCTTGCCGCTTCCTCCTGAGTTCCAAA |
| Long primer | CTAATACGACTCACTATAGGGCAAGCAGTGGTATCAACGCAGAGT |
| AP2-N | CATGCAGGCCTTGCCATTGCATGAC |
| AP2-C | CTATGATCGCTTTAAGCTTAGGGG |
| AP2-JHN2 | CATGGAGGCCGAATTCAAGTACAAGGGCGTGACACGACAT |
| AP2-JHC2 | GCAGGTCGACGGATCCCTCCGTGTACATGTCCAGGGAGAA |
| 5' PCR primer | TTCCACCCAAGCAGTGGTATCAACGCAGAGTGG |
| 3' PCR primer | GTATCGATGCCCACCCTCTAGAGGCCGAGGCGGCCGACA |

specific primer AP2(GSP) and Long Primer from the SMARTer RACE 5'/3' Kit (**Table 1**) (Zhu et al., 2001). The primer AP2(GSP) was designed according to the obtained sequence in the first 5' RACE. According to the assembled full-length sequence, specific primers AP2(N) and AP2(C) (**Table 1**) were synthesized to obtain the accurate full-length cDNA of *DpAP2*. PCR products were purified, cloned, and sequenced as described above (Abid et al., 2012).

## Construction of cDNA Library of *D. parva*

Total RNA was isolated from *D. parva* using the MiniBEST Plant RNA Extraction Kit (Takara). This kit is more efficient, fast, and convenient. The construction of the cDNA library of *D. parva* requires a high concentration and purity of RNA. Up to 10 μg of total RNA with high purity could be extracted from 50~100 mg plant tissue by this kit. The degradation and contamination of RNA were detected by 1% agarose gel electrophoresis. The RNA concentration was determined with the Nanophotometer NP80 Spectrophotometer. The cDNA library was constructed according to the instructions from the SMART cDNA Library Construction Kit (Takara) (Mendelsohn and Brent, 1994). First-strand cDNA was synthesized using CDS (complementary determining region) III Oligo (dT) primer and MMLV reverse transcriptase. Double-strand cDNA was synthesized by LD PCR with specific primers (5' PCR Primer and 3' PCR Primer) (**Table 1**). The cDNA size was fractionated by CHROMA SPIN+TE-400 Column to select cDNA molecules (>200 bp). Finally, cDNA fragments were cloned into the pGADT7-Rec plasmid through homologous recombination *in vivo*, transformed into the competent yeast strain Y187, and selected on the selective medium by the yeast two-hybrid assay.

## Subtraction Efficiency of the Library

The purified double-strand cDNA and pGADT7-Rec were co-transformed into Y187 yeast competent cells. Then, all liquids were combined in a single sterile flask. The library broth was diluted $10^{-2}$ and $10^{-4}$ times, and 100 μl was spread onto the SD/–Leu plate for 3–5 days. The number of colonies on plates were counted. PCR amplification was used to evaluate recombination efficiency (Zheng et al., 2005). PCR was performed with universal sequencing primers designed for PGADT7-REC using 24 colonies as templates, which were randomly selected on SD/-Leu plates. PCR was performed using Green Taq Mix 12.5 μl, T7 Primer (10 μM) 1 μl, 3'AD Primer (10 μM) 1 μl, yeast culture 1 μl, $ddH_2O$ 9.5 μl. The procedures were as follows: 94°C for 3 min, 35 cycles (98°C for 10 s, 42°C for 30 s, 72°C for 2 min), 72°C for 10 min. PCR products were analyzed by 1% agarose gel electrophoresis. The size and recombination rate of inserted fragments were measured and analyzed.

## Generation of Yeast Bait Strain

All plasmids and strains used in the two-hybrid experiment were included in the Matchmaker Gold Yeast Two-Hybrid System Kit (Takara). To confirm the binding region required for the interaction of DpAP2, cDNA fragments corresponding to N-terminus (67–252 and 349–537 bp) and C-terminus (537–2,331 bp) of DpAP2 were amplified by PCR, respectively. A PCR-amplified bait was obtained using primers AP2-JHN2 and AP2-JHC2 that contained 24 bp homology to the bait sequence and 15 bp homology to the linear end of pGBKT7. The 5' terminus of *DpAP2* was cloned in-frame into the pGBKT7 plasmid at *Bam*H I and *Eco*R I sites. In order to confirm that the fusion construct was in frame, the construct was sequenced using the T7 Primer. It is imperative to confirm that the bait does not autonomously activate reporter genes and is not toxic in Y2HGold in the absence of a prey protein. The pGBKT7 and pGBKT7-AP2N3 plasmids were used in a series of transformation tests to exclude false activation and the toxicity of reporter gene of the system (Chung et al., 2021). The yeast strains Y2HGold and Y187 were transformed using a slightly modified method. In brief, one colony was inoculated into 3 ml of the YPDA medium at 30°C with shaking at 250 rpm for 8–12 h. Then, 5 μl of the culture was transferred to 50 ml of the YPDA medium, and it was continued to be incubated until $OD_{600}$ reaches 0.15–0.3. Cells were centrifuged at 700 g for 5 min at room temperature. The supernatant was discarded and each pellet was resuspended in 30 ml of sterile $ddH_2O$ and centrifuged again using the same condition. Cells were resuspended in freshly prepared LiAc/TE. Plasmid DNA, carrier DNA, and DMSO were added; then, the mixture was centrifuged with 14,000 g at room temperature after incubation. The yeast sediment was resuspended in YPD plus the medium in a shaker at 30°C for 90 min. Yeast cells were resuspended in 0.9% NaCl, and 100 μl of 1/10 and 1/100 diluted cells were spread on the SD selection medium plate at 30°C for 3–6 days.

## Library Screening

Library screening was done *via* the yeast mating of one aliquot of Y187 cDNA library with 5 ml (an $OD_{600}$ : Optical Density (OD) of at least 2.0) of the Y2HGold culture transformed with pGBKT7-AP2N3 (Zhang et al., 2020). Two cultures were combined in a sterile 2 L flask, and 45 ml of the 2×YPDA liquid medium (with 50 μg/ml kanamycin) was added. The

culture was incubated at 30°C with slow shaking (30–50 rpm) for 20–24 h to prevent cells from settling at the base of the flask. After 20 h, we checked for the presence of zygotes under the phase contrast microscope (×40). The mating culture was centrifuged at 1,000 g for 10 min, washed with 100 ml of 0.5×YPDA containing 50 μg/ml of kanamycin, and resuspended in 10 ml of 0.5×YPDA with 50 μg/ml of kanamycin. For the mated culture, 100 μl of undiluted, 1:100 and 1:10,000 diluted cultures were spread on each of the SD/-Trp, SD/-Leu, and SD/-Leu/-Trp (DDO) agar plates to calculate the mating efficiency. The remaining culture was spread on SD/-Leu/-Trp (with X-α-Gal/AbA) and SD/-Ade/-His/-Leu/-Trp (with X-α-Gal/AbA) and incubated at 30°C for 3–5 days. Colonies were numbered and restreaked on the SD/-Ade/-His/-Leu/-Trp (with X-α-Gal/AbA) (QDO/X/A) master plate and then grown for another 4–6 days. All QDO/X/A-positive interactions must be further analyzed to identify duplicates and verify the genuineness of the interaction.

## Yeast Colony PCR

Positive colonies were selected and incubated on the QDO/X/A liquid medium. PCR amplification was performed with primers T7 and 3'AD under the following conditions: 94°C for 3 min; 35 cycles (98°C for 10 s, 42°C for 30 s, and 72°C for 2 min). Plasmid was isolated from yeast using the MiniBEST Plasmid Purification Kit (Takara) and transformed into *Escherichia coli*. Positive colonies were subjected to sequencing and similarity searches in the National Center for Biotechnology Information (NCBI) database. All identified colonies were checked for the right frame and orientation.

# RESULTS AND DISCUSSION

## Full-Length cDNA Cloning

A 582 bp cDNA fragment of differentially expressed *DpAP2* gene associated with the regulation of carotenoid biosynthesis in *D. parva* was obtained by a comparison between SCH-5.0mMA (nitrogen-sufficient control sample) and SCH-0.5mMA (nitrogen limitation-treated sample) using transcriptome technology. To obtain the full-length cDNA, we performed 5' RACE and 3' RACE with gene-specific primers designed from the obtained 582 bp fragment. Then, using primers AP2(GSP) and the Long Primer, a 405 bp cDNA fragment was obtained. The full-length cDNA was 3,129 bp with an open reading frame (ORF) of 2,331 bp encoding 776 amino acids, a 3' untranslated region (UTR) of 582 bp, and a 5' UTR of 216 bp (**Figure 2**). The agarose gel electrophoresis analysis of the product amplified by primers AP2(N) and AP2 (C) detected a band of approximately 2,331 bp (**Figure 3**). The Blastx search suggested that the PCR product was homologous to a number of known *AP2* genes. The detailed sequence of *DpAP2* is shown in **Supplementary Figure 1**.

## Phylogenetic Analysis of AP2

The conserved amino acid residues in the AP2 domain from *D. parva* and *Arabidopsis thaliana* AP2/ERF superfamily proteins were identified by MEME online software (**Figure 4**). The AP2 subfamily in *D. parva* contains two AP2 domains such as AP2-R1 and AP2-R2. The results displayed that both *D. parva* and *A. thaliana* have RAYD, WLG/YLG, AA, and YRG elements. The analysis of the AP2 domain between *D. parva* and *A. thaliana* suggested that the domain was highly conserved. The AP2-R1 domain includes $G_{22}$, $E_{29}$, $F_{24}$, $L_{21}$, and $T_{26}$, and the AP2-R2 domain includes $E_{15}$, $S_{16}$, $F_7$, and $H_{17}$. We constructed an evolutionary tree to analyze the evolutionary relationship of AP2/ERF TFs (**Figure 5**). The results indicated that *Scenedesmus* sp. And *D. parva* shared the closest relationship, which was consistent with the traditional classification.


**FIGURE 2** | Full-length cDNA of the *DpAP2* gene. The graphic was constructed base on a complete sequence of the *DpAP2* gene using the DOG 2.0 program. The full-length cDNA was 3,129 bp with an ORF of 2,331 bp encoding 776 amino acids, a 3' UTR of 582 bp, and a 5' UTR of 216 bp.

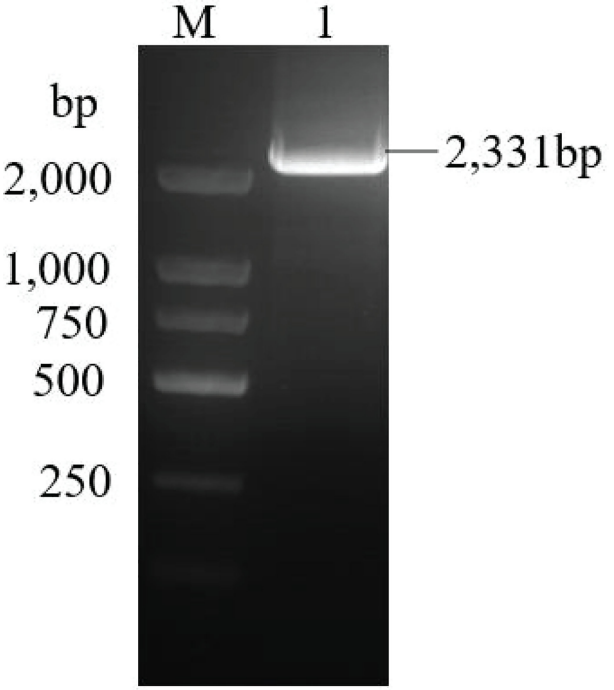


**FIGURE 3** | ORF amplification of the *DpAP2* gene. M: DL 2000 Marker, 1: ORF of the *DpAP2* gene. The ORF of *DpAP2* gene was amplified by primers AP2(N) and AP2 (C).

## Construction of Two-Hybrid cDNA Library

In order to hunt for the interaction partners of DpAP2, we generated an appropriate cDNA library well suited for the yeast two-hybrid system. Total RNA was extracted from *D. parva* cells

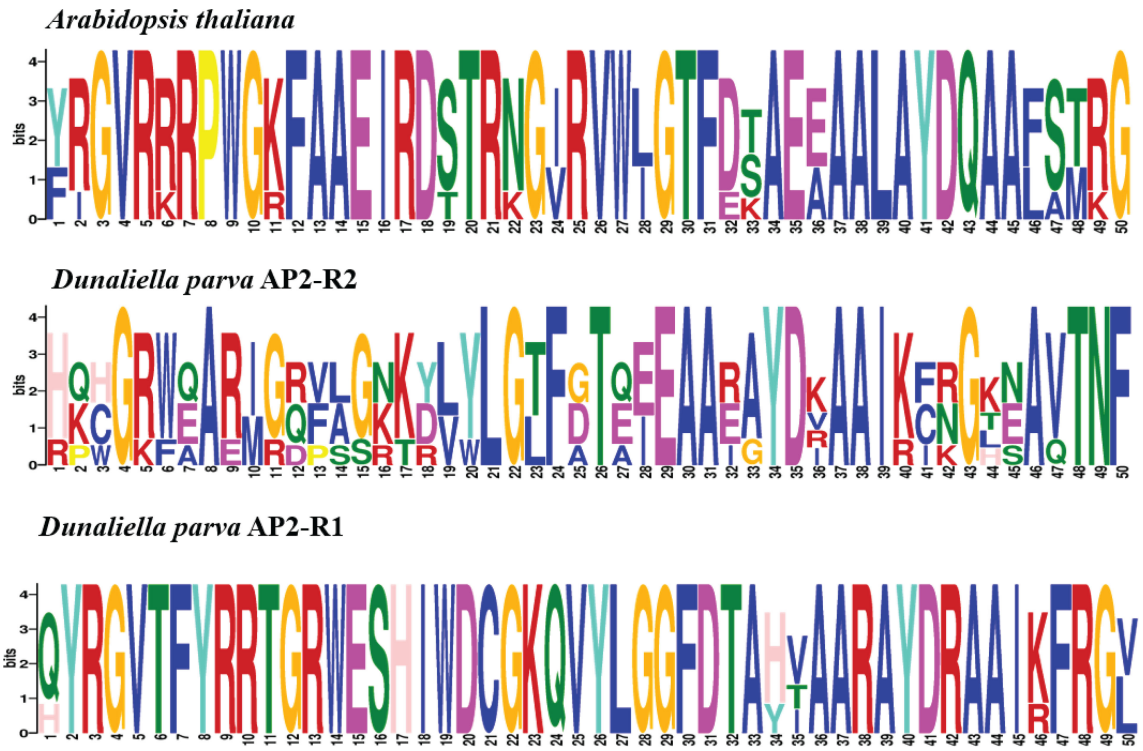


**FIGURE 4** | The conserved amino acid residues in the AP2 domain from the *D. parva* and *A. thaliana* AP2 subfamily. The domain was analyzed by MEME software. The horizontal number indicates the amino acid site; each site represents a stack. The height of character represents the frequency of the amino acid.

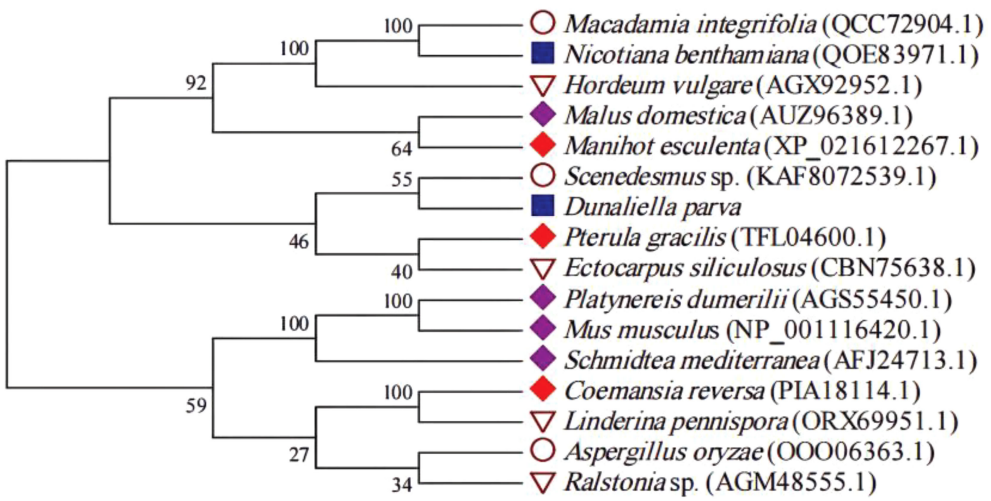


**FIGURE 5** | Phylogenetic tree of AP2 proteins. The tree was constructed based on the complete protein sequences of AP2 proteins by the neighbor-joining method of the MEGA program.

(**Figure 6**). Approximately 2.0 μg of total RNA was transcribed to form first-strand cDNA using SMART technology, and second-strand cDNA was amplified using long-distance PCR with the universal primers (**Figure 7**). The CHROMA SPIN TE-400 Column was used to select DNA molecules more than 200 bp that were likely to encode the translated region of mRNAs. The cDNA was cloned into yeast strain Y187 along with AD plasmid pGADT7-Rec. Plasmid pGADT7-Rec and cDNA fragments were

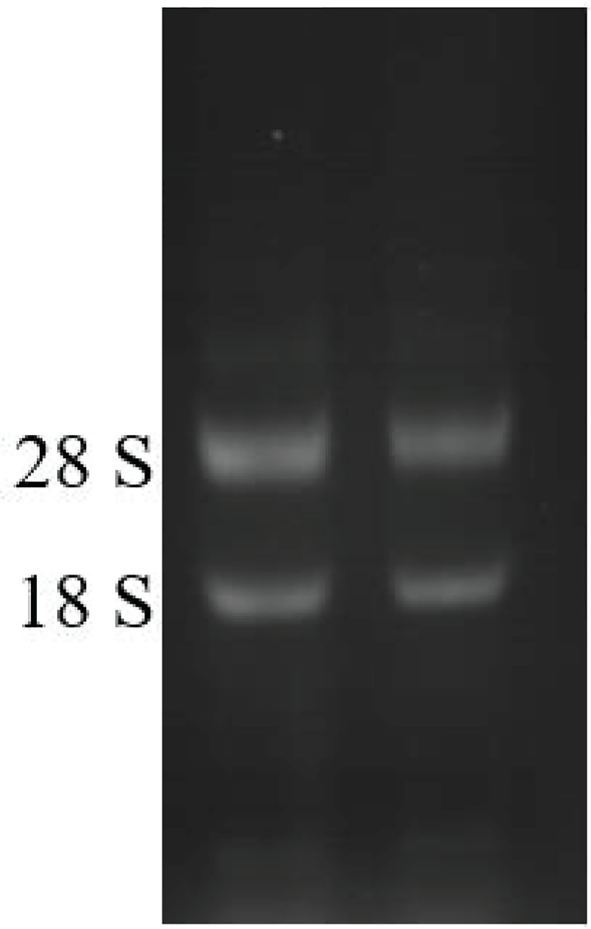


**FIGURE 6** | Total RNA from *D. parva* cells. Lanes 1 and 2 represented the total RNA of *D. parva* cells. The integrity of RNA was detected by 1% agarose gel electrophoresis.

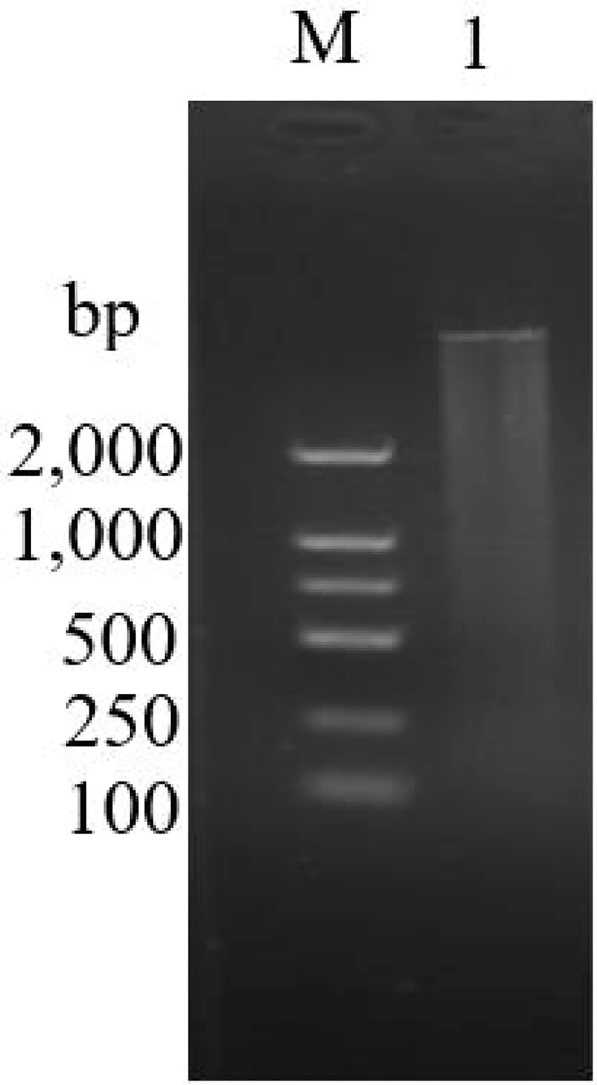


**FIGURE 7** | Long-distance PCR for second-strand cDNA synthesis. M: DL 2000 Marker. 1: Second-strand cDNA. The length of cDNA molecules was more than 200 bp.

combined *in vivo* through homologous recombination. Transformation efficiency was identified by calculating the number of colonies on a plate with a 1:1,000 dilution of transformation (**Figure 8**). PCR was performed to evaluate recombination efficiency (**Figure 9**). Transformation efficiency could be calculated with the data shown in **Table 2**. Cell density was more than $2 \times 10^7$ per milliliter of the cDNA library.

## Generation of Bait Strain Y2HGold

To confirm the binding region required for the interaction of DpAP2, the cDNA fragments of the N-terminus (67–252 and 349–537 bp) and C-terminus (537–2,331 bp) was amplified using gene-specific primers, respectively (**Figure 10**). Plasmid pGBKT7-AP2N3 (537–2,331 bp) was transformed into the yeast strain Y2HGold. pGBKT7 and pGBKT7-AP2N3 were used in a series of transformation tests to exclude the false activation and toxicity of the reporter gene of the system. Then, the self-activation of the recombinant vector was determined by testing the autoactivation of Aureobasidin A and beta-galactosidase reporter. The recombinant bait plasmid had no toxic effect on yeast Y2HGold cells without the self-activation of reporter genes. The yeast strains of Y2HGold-pGBKT7-AP2N3 and Y2HGold-pGBKT7 could grow on the SD/-Trp medium without a significant difference in the colony size and number, which suggested that plasmid pGBKT7-AP2N3 had no effect on yeast growth and no toxicity to yeast (**Figure 11**). Furthermore, the blue Y2HGold-pGBKT7-AP2N3 colonies were detected on the SD/-Trp/X-α-Gal agar medium; however, they were absent on the SD/-Ade/-Trp/X-α-gal plate. Therefore, the DpAP2 protein had no autonomous activation effect. Yeast strains Y2HGold and Y187 were transformed by a slightly modified method.

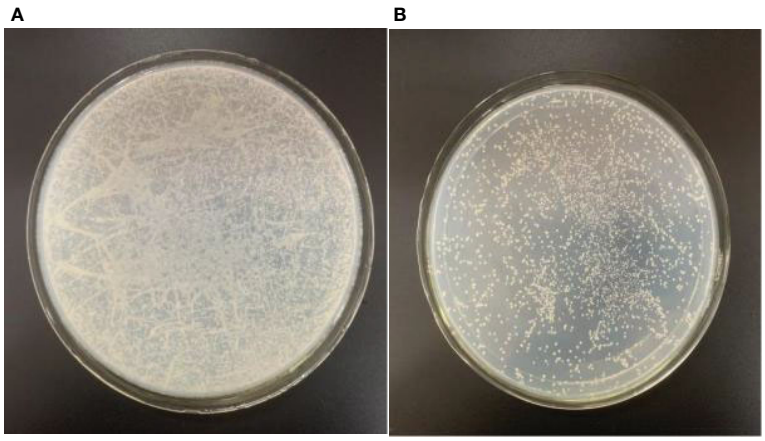


**FIGURE 8** | Colony number was counted for the cDNA library. **(A)** 1/1,000 dilution. **(B)** 1/10,000 dilution. The colony number on plate was approximately 600 under the condition of 1:10,000 dilution.

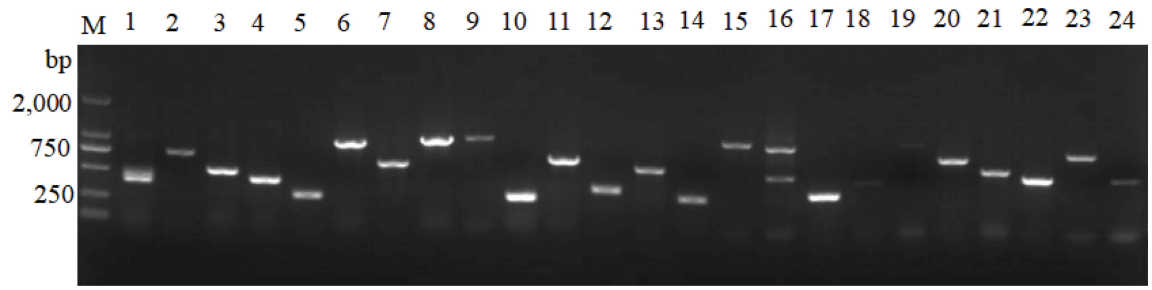


**FIGURE 9** | Identification of the integrity of the recombinant sequence of the cDNA library. M: DL 2000 Marker. 1–24: PCR verification of positive colonies. Positive colonies were selected to evaluate recombination efficiency by PCR amplification with primers T7 and 3'AD.

## Screening of Positive Colonies

One aliquot of cDNA library containing more than $2 \times 10^7$ transformed Y187 cells were mated with more than $1 \times 10^8$ Y2HGold cells transformed with pGBKT7-AP2N3. The zygotes were detected under a phase contrast microscope (40×) after 24 h of co-incubation, which showed that yeast mating was successful. The mating culture was centrifuged and resuspended on the SD/-Leu/-Trp (with X-α-Gal/AbA) plate. The mating efficiency was counted by analyzing the SD/-Leu, SD/-Trp and SD/-Leu/-Trp plates on which different dilutions of the mating mixture were spread. The mating efficiency of the two-hybrid screen was approximately 2%. Many positive colonies grew on the SD/-Leu/-Trp/X-α-Gal/AbA agar medium and were restreaked for three times on SD/-Ade/-His/-Leu/-Trp/X-α-Gal/AbA plates (**Figure 12**). Finally, 34 putative positive yeast colonies were obtained.

## Bioinformatical Analysis of Sequencing Information

To select for stable expression of interaction partners, the colonies of mating screen were restreaked on the 4×Dropout medium, and 34 positive yeast colonies were obtained. A total of 34 cDNA inserts were verified by a colony PCR using universal primers T7 and 3'AD, and 24 cDNA fragments were determined. Plasmid was isolated from 24 yeast strains and purified, then transformed into *E. coli* DH5α (**Figure 13**). The transformants containing only pGADT7-DpAP2 plasmids from the cDNA library were obtained on the Luria-Bertani (LB) agar medium with 50 μg/ml of ampicillin. The sequencing results were subjected to the Blastx search. Three proteins interacting with DpAP2 were identified, including protein 1 (alpha-D-phosphohexomutase), protein 2 (protein serine/threonine kinase activity), and protein 3 (DNA-binding transcription factor activity) in *D. parva* (**Table 3**). The detailed sequences of three proteins interacting with DpAP2 are shown in **Supplementary Figure 2**. The functions of three interacting proteins of DpAP2 were analyzed by NetGO 2.0 software, which are shown in **Supplementary Figure 3**.

The yeast two-hybrid system was widely used to identify the interacting protein of specific proteins. Chen et al. found that the AP2/ERF transcription factor SlERF.F5 functioned in leaf senescence in tomato, and SlERF.F5 and SlMYC2 (a transcription factor downstream of the jasmonic acid receptor) could physically interact by the yeast two-hybrid experiment (Chen et al., 2022). Transcription factor SHE1 was identified as an

**TABLE 2 |** Calculation of the transformation efficiency of the cDNA library.

| **Number of colonies on plate (1:10,000)** | **600** |
|---|---|
| Transformant density of undiluted transformation mix | 6,000,000/plate |
| Number of plates used for streaking out transformants | 94 |
| Total number of transformants | $5.6 \times 10^8$ cfu/ml |

interacting protein of cucumber mosaic virus 1a protein in the yeast two-hybrid system (Yoon and Palukaitis, 2021). AP2/ERF family transcription factors ORA59 and RAP2.3 interacted in the nucleus identified by yeast two-hybrid technology and functioned together in ethylene responses (Kim et al., 2018). Zander et al. reported that at least 17 plant-specific glutaredoxins interacted with TGA2 by the yeast two-hybrid system in *Arabidopsis* (Zander et al., 2012).

The ubiquitous and ancient alpha-D-phosphohexomutases are a large enzyme superfamily that exists in three domains of organisms (Backe et al., 2020). Enzymes in alpha-D-phosphohexomutases superfamily catalyze the reversible conversion of phosphosugars, such as glucose 1-phosphate and glucose 6-phosphate (Stiers et al., 2017). The phosphoglucomutase 5 (PGM5) of the alpha-D-phosphohexomutase family is a structural muscle protein in humans (Gong et al., 2020). In the Atlantic herring, *PGM5* is a gene closely related to ecological adaptation to the brackish Baltic Sea (Gustafsson et al., 2020). In our study, *D.*

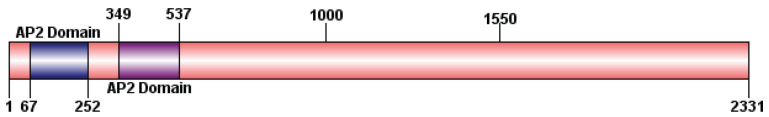


**FIGURE 10** | Prediction of conserved domains in DpAP2. The diagram was constructed based on a complete protein sequence of DpAP2 using the DOG 2.0 program. The conserved domain was analyzed by the NCBI CD-Search tool.

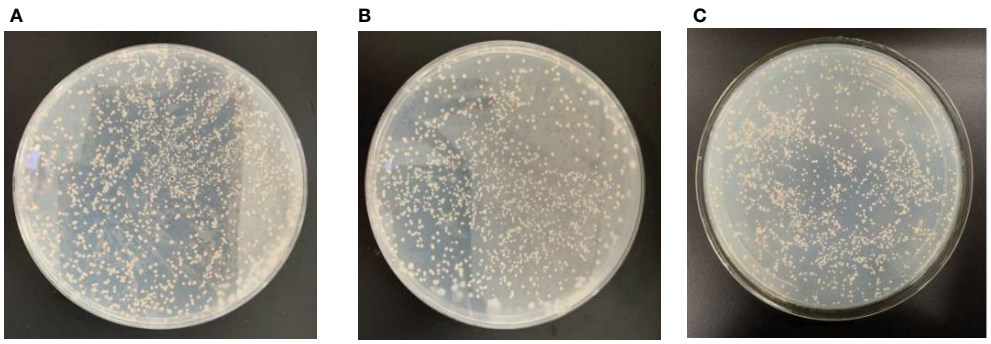


**FIGURE 11** | The toxicity assays of DpAP2 protein in yeast cells. **(A)** PGBKT7-AP2N3. **(B)** pGBKT7-AP2N2. **(C)** PGBKT7. Yeast strains containing plasmids pGBKT7-AP2N3 and pGBKT7 could grow without significant differences in the colony size and number, which suggested that plasmid pGBKT7-AP2N3 had no effect on yeast growth and no toxicity to yeast.

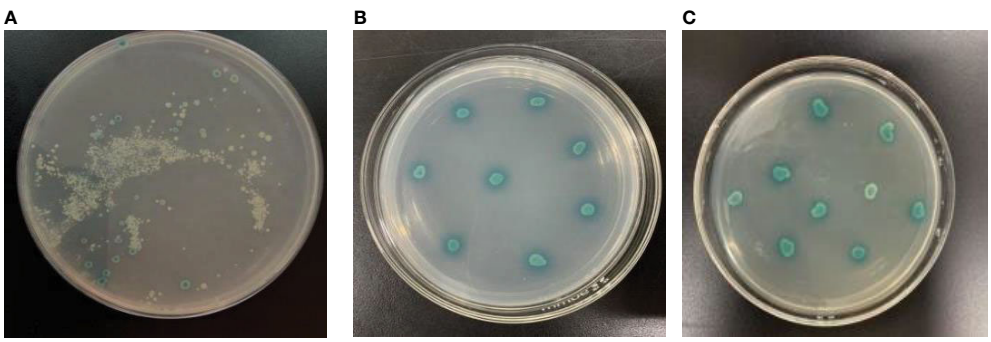


**FIGURE 12** | Screening of positive colonies. The positive colonies were restreaked for three times on SD/-Ade/-His/-Leu/-Trp/X-α-Gal/AbA plates. **(A)** The initial screening. **(B)** The second screening. **(C)** The third screening.

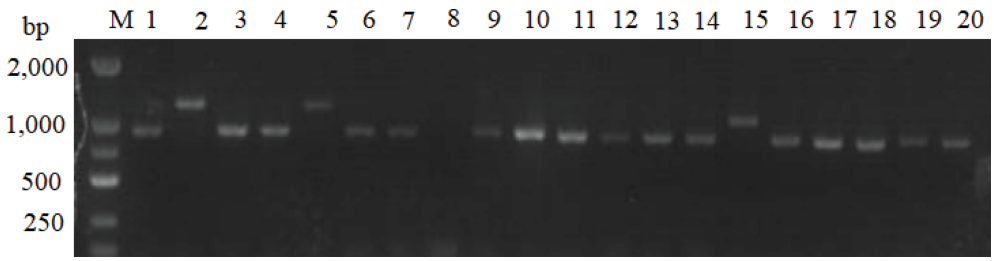


**FIGURE 13** | Verification of positive colonies by PCR. M: DL2000 Marker. 1-20: PCR verification of positive yeast colonies.

**TABLE 3** | Proteins interacting with DpAP2.

| Protein No. | Annotation |
|---|---|
| Protein 1 | Alpha-D-phosphohexomutase |
| Protein 2 | Protein kinase activity |
| Protein 3 | DNA-binding transcription factor activity |

*parva* also lives in the brackish environment. Perhaps protein 1 (alpha-D-phosphohexomutase) is related to the halophilic characteristic in *D. parva*. However, a detailed understanding of its function is lacking in *D. parva*.

The interacting protein 2 of DpAP2 with protein serine/threonine kinase activity was also identified. The serine/threonine kinase Akt is a key factor regulating glucose and lipid energy metabolism, which is activated in response to various stimuli such as cell stress and various hormones and drugs (Miao et al., 2022). The eukaryotic-like serine/threonine protein kinases play important roles in cell growth and signal transduction in *Mycobacterium tuberculosis* (Burastero et al., 2022). Protein kinase G regulates the carbon and nitrogen metabolism by the phosphorylation of the glycogen accumulation regulator (GarA) at Thr21 (Burastero et al., 2022). Protein kinase B is related to the formation of the cell shape, cell wall synthesis, and phosphorylation of GarA at Thr22 (Burastero et al., 2022). In a word, protein serine/threonine kinase plays an important role in cell metabolism. However, the function of protein 2 remains unclear in *D. parva*.

The analysis of interacting protein 3 by NetGO 2.0 software indicated that protein 3 had a DNA-binding transcription factor activity. Transcription factors are proteins that help turn specific target genes "on" or "off" by binding to the nearby DNA. The previous studies have suggested that the AP2/ERF transcription factor could interact with other transcription factors, which was consistent with our study (Kim et al., 2018; Chen et al., 2022). However, the function and interacting target genes of protein 3 remain unclear in *D. parva*. ChIP and ChIP-Seq will be used to identify the target genes of protein 3 in the future.

## CONCLUSION

DpAP2 is a key regulator of carotenoid biosynthesis. The *DpAP2* encoding TF DpAP2 has been identified in our former study. However, the target proteins of DpAP2 remain unknown. The interacting proteins of DpAP2 were identified by the yeast two-hybrid system in order to further demonstrate the function of DpAP2 in this study. The results showed that three target proteins were identified. This study laid a good foundation for the further understanding of the regulatory mechanism of carotenoid biosynthesis related to DpAP2.

## DATA AVAILABILITY STATEMENT

The data presented in the study are deposited in the National Center for Biotechnology Information repository, accession number ON548534, ON548535, ON548536, ON548537.

## AUTHOR CONTRIBUTIONS

CS is the corresponding author. CS contributed to the conception, design, data acquisition, and drafting of the article. BP is the co-first author. BP contributed to the data acquisition and drafting of the article. JZ, LY, SG, YL, and HW contributed to partial data acquisition and drafting of the article. All authors read and approved the final manuscript.

## FUNDING

This study was financially supported by National Natural Science Foundation of China (31860010), Innovation Project of Guangxi Graduate Education (YCSW2022178 and XJCY2022011), National Training Program of Innovation and Entrepreneurship for Undergraduates (202210602064), Guangxi Key Research and Development Program (AB21220057, 2021AB27009), Research Funds of the Guangxi Key Laboratory of Landscape Resources Conservation and Sustainable Utilization in Lijiang River Basin, Guangxi Normal University (LRCSU21Z0207). Research Funds of Key Laboratory of Ecology of Rare and Endangered Species and Environmental Protection (Guangxi Normal University), Ministry of Education, China (ERESEP2022Z11).

## SUPPLEMENTARY MATERIAL

The Supplementary Material for this article can be found online at: https://www.frontiersin.org/articles/10.3389/fmars.2022.907065/full#supplementary-material

**Supplementary Figure 1 |** Full-length cDNA sequence of *DpAP2* gene. The initiation and termination codons were **ATG** and **TAG**, respectively. The ORF of *DpAP2* was 2,331 bp

**Supplementary Figure 2 |** Full-length cDNA encoding three interacting proteins of DpAP2. The initiation and termination codons were underlined. **(A)** Interacting protein of DpAP2 (alpha-D-phosphohexomutase activity). **(B)** Interacting protein of DpAP2 (protein kinase activity). **(C)** Interacting protein of DpAP2 (DNA-binding transcription factor activity).

**Supplementary Figure 3 |** Function prediction of three interacting proteins of DpAP2 by NetGO 2.0 software. **(A)** Interacting protein of DpAP2 (alpha-D-phosphohexomutase activity). **(B)** Interacting protein of DpAP2 (protein kinase activity). **(C)** Interacting protein of DpAP2 (DNA-binding transcription factor activity).

## REFERENCES


Abid, G., Muhovski, Y., Jacquemin, J. M., Mingeot, D., Sassi, K., Toussaint, A., et al. (2012). Characterization and Expression Profile Analysis of a Sucrose Synthase Gene From Common Bean (*Phaseolus Vulgaris* L.) During Seed Development. *Mol. Biol. Rep.* 39, 1133–1143. doi: 10.1007/s11033-011-0842-y

Ampomah-Dwamena, C., Thrimawithana, A. H., Dejnoprat, S., Lewis, D., Espley, R. V., and Allan, A. C. (2019). A Kiwifruit (*Actinidia Deliciosa*) R2R3-MYB Transcription Factor Modulates Chlorophyll and Carotenoid Accumulation. *New Phytol.* 221, 309–325. doi: 10.1111/nph.15362

Arora, N., Patel, A., Sartaj, K., Pruthi, P. A., and Pruthi, V. (2016). Bioremediation of Domestic and Industrial Wastewaters Integrated With Enhanced Biodiesel Production Using Novel Oleaginous Microalgae. *Environ. Sci. Pollut. Res. Int.* 23, 20997–21007. doi: 10.1007/s11356-016-7320-y

Backe, P. H., Laerdahl, J. K., Kittelsen, L. S., Dalhus, B., Mørkrid, L., and Bjørås, M. (2020). Structural Basis for Substrate and Product Recognition in Human Phosphoglucomutase-1 (PGM1) Isoform 2, a Member of the α-D-Phosphohexomutase Superfamily. *Sci. Rep.* 10, 5656. doi: 10.1038/s41598-020-62548-0

Burastero, O., Cabrera, M., Lopez, E. D., Defelipe, L. A., Arcon, J. P., Durán, R., et al. (2022). Specificity and Reactivity of *Mycobacterium Tuberculosis* Serine/Threonine Kinases PknG and PknB. *J. Chem. Inf. Model.* 62, 1723–1733. doi: 10.1021/acs.jcim.1c01358

Chen, Y., Feng, P., Tang, B., Hu, Z., Xie, Q., Zhou, S., et al. (2022). The AP2/ERF Transcription Factor SlERF.F5 Functions in Leaf Senescence in Tomato. *Plant Cell Rep.* 41, 1181–1195. doi: 10.1007/s00299-022-02846-1

Chung, I. Y. W., Li, L., Tyurin, O., Gagarinova, A., Wibawa, R., Li, P., et al. (2021). Structural and Functional Study of *Legionella Pneumophila* Effector RavA. *Protein Sci.* 30, 940–955. doi: 10.1002/pro.4057

Courchesne, N. M., Parisien, A., Wang, B., and Lan, C.Q. (2009). Enhancement of Lipid Production Using Biochemical, Genetic and Transcription Factor Engineering Approaches. *J. Biotechnol.* 141, 31–41. doi: 10.1016/j.jbiotec.2009.02.018

Dang, Q., Sha, H., Nie, J., Wang, Y., Yuan, Y., and Jia, D. (2021). An Apple (*Malus Domestica*) AP2/ERF Transcription Factor Modulates Carotenoid Accumulation. *Hortic. Res.* 8, 223. doi: 10.1038/s41438-021-00694-w

Donadio, G., Santoro, V., Dal Piaz, F., and De Tommasi, N. (2021). Food Matrices Affect the Peptides Produced During the Digestion of *Arthrospira Platensis*-Based Functional Aliments. *Nutrients* 13, 3919. doi: 10.3390/nu13113919

du Preez, R., Majzoub, M. E., Thomas, T., Panchal, S. K., and Brown, L. (2021). *Nannochloropsis Oceanica* as a Microalgal Food Intervention in Diet-Induced Metabolic Syndrome in Rats. *Nutrients* 13, 3991. doi: 10.3390/nu13113991

Fritzsche, S., Blenk, P., Christian, J., Castiglione, K., and Becker, A. M. (2021). Inhibitory Properties of Crude Microalgal Extracts on the *In Vitro* Replication of Cyprinid Herpesvirus 3. *Sci. Rep.* 11, 23134. doi: 10.1038/s41598-021-02542-2

Gao, F., Peng, Y. Y., Li, C., Yang, G. J., Deng, Y. B., Xue, B., et al. (2018). Simultaneous Nutrient Removal and Biomass/Lipid Production by *Chlorella* Sp. In Seafood Processing Wastewater. *Sci. Total Environ.* 640-641, 943–953. doi: 10.1016/j.scitotenv.2018.05.380

Gilmour, D. J. (2019). Microalgae for Biofuel Production. *Adv. Appl. Microbiol.* 109, 1–30. doi: 10.1016/bs.aambs.2019.10.001

Gong, J., Zeng, Y., Meng, Q., Guan, Y., Li, C., Yang, H., et al. (2021). Red Light-Induced Kumquat Fruit Coloration Is Attributable to Increased Carotenoid Metabolism Regulated by FcrNAC22. *J. Exp. Bot.* 72, 6274–6290. doi: 10.1093/jxb/erab283

Gong, J., Zeng, Y., Meng, Q., Guan, Y., Li, C., Yang, H., et al. (2020). Structure and Characterization of Phosphoglucomutase 5 From Atlantic and Baltic Herring-An Inactive Enzyme With Intact Substrate Binding. *Biomolecules* 10, 1631. doi: 10.3390/biom10121631

Gustafsson, R., Eckhard, U., Ye, W., Enbody, E. D., Pettersson, M., Jemth, P., et al. (2020). Structure and Characterization of Phosphoglucomutase 5 from Atlantic and Baltic Herring-An Inactive Enzyme with Intact Substrate Binding. *Biomolecules* 10, 1631. doi: 10.3390/ biom10121631

Ismaiel, M. M. S., El-Ayouty, Y. M., Said, A. A., and Fathey, H. A. (2018). Transformation of *Dunaliella Parva* With PSY Gene: Carotenoids Show Enhanced Antioxidant Activity Under Polyethylene Glycol and Calcium Treatments. *Biocatal. Agric. Biotechnol.* 16, 378–384. doi: 10.1016/j.bcab.2018.09.011

Jiang, X., Zhang, Y., Hutchins, D. A., and Gao, K. (2021). Nitrogen-Limitation Exacerbates the Impact of Ultraviolet Radiation on the Coccolithophore *Gephyrocapsa Oceanica*. *J. Photochem. Photobiol. B.* 226, 112368. doi: 10.1016/j.jphotobiol.2021.112368

Kamalanathan, M., Hillhouse, J., Claflin, N., Rodkey, T., Mondragon, A., Prouse, A., et al. (2021). Influence of Nutrient Status on the Response of the Diatom *Phaeodactylum Tricornutum* to Oil and Dispersant. *PLoS One* 16, e0259506. doi: 10.1371/journal.pone.0259506

Kang, J., Gong, J., Zhang, L., Gao, Z., Xie, Q., Hu, Z., et al. (2021). A Novel E6-Like Gene, E6-2, Affects Fruit Ripening in Tomato. *Plant Sci.* 313, 111066. doi: 10.1016/j.plantsci.2021.111066

Keerthana, S., Sekar, S., Kumar, S. D., Santhanam, P., Divya, M., Krishnaveni, N., et al. (2020). *Scenedesmus Pecsensis* Cultivation in Rice Mill Effluent Using Commercial Scale Nutrient Sources. *Bioresource Tech. Rep.* 9, 100379. doi: 10.1016/j.biteb.2019.100379

Kim, N. Y., Jang, Y. J., and Park, O. K. (2018). AP2/ERF Family Transcription Factors ORA59 and RAP2.3 Interact in the Nucleus and Function Together in Ethylene Responses. *Front. Plant Sci.* 9. doi: 10.3389/fpls.2018.01675

Kumari, K., Samantaray, S., Sahoo, D., and Tripathy, B. C. (2021). Nitrogen, Phosphorus and High $CO_2$ Modulate Photosynthesis, Biomass and Lipid Production in the Green Alga *Chlorella Vulgaris*. *Photosynth. Res.* 148, 17–32. doi: 10.1007/s11120-021-00828-0

Koul, A., Sharma, D., Kaul, S., and Dhar, M. K.. (2019). Identification and *In Silico* Characterization of Cis-Acting Elements of Genes Involved in Carotenoid Biosynthesis in Tomato. *3 Biotech.* 9, 287. doi: 10.1007/s13205-019-1798-1

Lee, J. M., Joung, J. G., McQuinn, R., Chung, M. Y., Fei, Z., Tieman, D., et al. (2012). Combined Transcriptome, Genetic Diversity and Metabolite Profiling in Tomato Fruit Reveals That the Ethylene Response Factor SlERF6 Plays an Important Role in Ripening and Carotenoid Accumulation. *Plant J.* 70, 191–204. doi: 10.1111/j.1365-313X.2011.04863.x

Li, S., Ji, L., Shi, Q., Wu, H., and Fan, J. (2019). Advances in the Production of Bioactive Substances From Marine Unicellular Microalgae *Porphyridium* Spp. *Bioresour. Technol.* 292, 122048. doi: 10.1016/j.biortech.2019.122048

Li, R., Tan, Y., and Zhang, H. (2021). Regulators of Starch Biosynthesis in Cereal Crops. *Molecules* 26, 7092. doi: 10.3390/molecules26237092

Mendelsohn, A. R., and Brent, R. (1994). Biotechnology Applications of Interaction Traps/Two-Hybrid Systems. *Curr. Opin. Biotechnol.* 5, 482–486. doi: 10.1016/0958-1669(94)90061-2

Miao, R., Fang, X., Wei, J., Wu, H., Wang, X., and Tian, J. (2022). Akt: A Potential Drug Target for Metabolic Syndrome. *Front. Physiol.* 13. doi: 10.3389/fphys.2022.822333

Mohsin, A., Hussain, M. H., Zaman, W. Q., Mohsin, M. Z., Zhang, J., Liu, Z., et al. (2021). Advances in Sustainable Approaches Utilizing Orange Peel Waste to Produce Highly Value-Added Bioproducts. *Crit. Rev. Biotechnol.* 2, 1–20. doi: 10.1080/07388551.2021.2002805

Narang, P. K., Dey, J., Mahapatra, S. R., Roy, R., Kushwaha, G. S., Misra, N., et al. (2021). Genome-Based Identification and Comparative Analysis of Enzymes

for Carotenoid Biosynthesis in Microalgae. *World J. Microbiol. Biotechnol.* 38, 8. doi: 10.1007/s11274-021-03188-y

Oswald, W. J. (2003). My Sixty Years in Applied Algology. *J. Appl. Phycol.* 15, 99–106. doi: 10.1023/A:1023871903434

Ratledge, C. (2002). Regulation of Lipid Accumulation in Oleaginous Micro-Organisms. *Biochem. Soc Trans.* 30, 1047–1050. doi: 10.1042/bst0301047

Shahid, A., Rehman, A. U., Usman, M., Ashraf, M. U. F., Javed, M. R., Khan, A. Z., et al. (2020). Engineering the Metabolic Pathways of Lipid Biosynthesis to Develop Robust Microalgal Strains for Biodiesel Production. *Biotechnol. Appl. Biochem.* 67, 41–51. doi: 10.1002/bab.1812

Shang, C., Bi, G., Yuan, Z., Wang, Z., Alam, M. A., and Xie, J. (2016). Discovery of Genes for Production of Biofuels Through Transcriptome Sequencing of *Dunaliella Parva*. *Algal Res.* 13, 318–326. doi: 10.1016/j.algal.2015.12.012

Shang, C., Wang, W., Zhu, S., Wang, Z., Qin, L., Alam, M. A., et al. (2018). The Responses of Two Genes Encoding Phytoene Synthase (Psy) and Phytoene Desaturase (Pds) to Nitrogen Limitation and Salinity Up-Shock With Special Emphasis on Carotenogenesis in *Dunaliella Parva*. *Algal Res.* 32, 1–10. doi: 10.1016/j.algal.2018.03.002

Shang, C., Xu, X., Yuan, Z., Wang, Z., Hu, L., Alam, M. A., et al. (2016). Cloning and Differential Expression Analysis of Geranylgeranyl Diphosphate Synthase Gene From *Dunaliella Parva*. *J. Appl. Phycol.* 28, 2397–2405. doi: 10.1007/s10811-015-0767-2

Shi, Y., Pang, X., Liu, W., Wang, R., Su, D., Gao, Y., et al. (2021). SlZHD17 is Involved in the Control of Chlorophyll and Carotenoid Metabolism in Tomato Fruit. *Hortic. Res.* 8, 259. doi: 10.1038/s41438-021-00696-8

Stiers, K. M., Muenks, A. G., and Beamer, L. J. (2017). Biology, Mechanism, and Structure of Enzymes in the α-D-Phosphohexomutase Superfamily. *Adv. Protein Chem. Struct. Biol.* 109, 265–304. doi: 10.1016/bs.apcsb.2017.04.005

Todorović, B., Grujić, V. J., Krajnc, A. U., Kranvogl, R., and Ambrožič-Dolinšek, J. (2021). Identification and Content of Astaxanthin and its Esters From Microalgae Haematococcus Pluvialis by HPLC-DAD and LC-QTOF-MS After Extraction With Various Solvents. *Plants (Basel).* 10, 2413. doi: 10.3390/plants10112413

Welsch, R., Maass, D., Voegel, T., Dellapenna, D., and Beyer, P. (2007). Transcription Factor RAP2.2 and its Interacting Partner SINAT2: Stable Elements in the Carotenogenesis of *Arabidopsis* Leaves. *Plant Physiol.* 145, 1073–1085. doi: 10.1104/pp.107.104828

Xing, G., Li, J., Li, W., Lam, S. M., Yuan, H., Shui, G., et al. (2021). AP2/ERF and R2R3-MYB Family Transcription Factors: Potential Associations Between Temperature Stress and Lipid Metabolism in *Auxenochlorella Protothecoides*. *Biotechnol. Biofuels* 14, 22. doi: 10.1186/s13068-021-01881-6

Yoon, J. Y., and Palukaitis, P. (2021). Cucumber Mosaic Virus 1a Protein Interacts With the Tobacco SHE1 Transcription Factor and Partitions Between the Nucleus and the Tonoplast Membrane. *Plant Pathol. J.* 37, 182–193. doi: 10.5423/PPJ.FT.03.2021.0045

Zander, M., Chen, S., Imkampe, J., Thurow, C., and Gatz, C. (2012). Repression of the *Arabidopsis Thaliana* Jasmonic Acid/Ethylene-Induced Defense Pathway by TGA-Interacting Glutaredoxins Depends on Their C-Terminal ALWL Motif. *Mol. Plant* 5, 831–840. doi: 10.1093/mp/ssr113

Zhang, L., Zhang, Q., Li, W., Zhang, S., and Xi, W. (2019). Identification of Key Genes and Regulators Associated With Carotenoid Metabolism in Apricot (*Prunus Armeniaca*) Fruit Using Weighted Gene Coexpression Network Analysis. *BMC Genomics* 20, 876. doi: 10.1186/s12864-019-6261-5

Zhang, H., Zhao, L., Chen, Y., Zhu, M., Xu, Q., Wu, M., et al. (2021). Trophic Transition Enhanced Biomass and Lipid Production of the Unicellular Green Alga *Scenedesmus Acuminatus*. *Front. Bioeng. Biotechnol.* 9. doi: 10.3389/fbioe.2021.638726

Zhang, Z. M., Zhuang, M., Wang, B. T., Jin, L., and Jin, F. J. (2020). Identification and Characterization of a DevR-Interacting Protein in *Aspergillus Oryzae*. *Fungal Biol.* 124, 155–163. doi: 10.1016/j.funbio.2020.01.001

Zheng, M., Wu, Y. J., Cai, W. M., Weng, H. L., and Liu, R. H. (2005). Construction of a Hepatic Stellate Cells Subtracted cDNA Library of Differentially Expressed Genes in Normal Mice and Mice With *Schistosomiasis Japonica*. *J. Zhejiang Univ. Sci. B.* 6, 280–287. doi: 10.1631/jzus.2005.B0280

Zhu, Y. Y., Machleder, E. M., Chenchik, A., Li, R., and Siebert, P. M. (2001). Reverse Transcriptase Template Switching: A SMART™ Approach for Full-Length cDNA Library Construction. *BioTechniques* 30, 892–897. doi: 10.2144/01304pf02

**Conflict of Interest:** The authors declare that the research was conducted in the absence of any commercial or financial relationships that could be construed as a potential conflict of interest.

**Publisher's Note:** All claims expressed in this article are solely those of the authors and do not necessarily represent those of their affiliated organizations, or those of the publisher, the editors and the reviewers. Any product that may be evaluated in this article, or claim that may be made by its manufacturer, is not guaranteed or endorsed by the publisher.

frontiers | Frontiers in Marine Science

ORIGINAL RESEARCH
published: 13 July 2022
doi: 10.3389/fmars.2022.939745

# Three Mitochondrial Markers Reveal Genetic Diversity and Structure of Rock Carp (*Procypris rabaudi*) Endemic to the Upper Yangtze: Implications for Pre-release Genetic Assessment

*Wenping He*[1], *Zhiling Dong*[1], *Tingting Ma*[1], *Huiguo Yan*[1], *Zhenxin Chen*[1], *Weizhi Yao*[1] *and Fei Cheng*[2*]

[1]Key Laboratory of Freshwater Fish Reproduction and Development (Ministry of Education), College of Fisheries, Southwest University, Chongqing, China, [2]Key Laboratory of Aquatic Biodiversity and Conservation of Chinese Academy of Sciences, Institute of Hydrobiology, Chinese Academy of Sciences, Wuhan, China

OPEN ACCESS

**Edited by:**
Pengfei Cheng,
Ningbo University, China

**Reviewed by:**
Shengjie Ren,
Queensland University of Technology, Australia
Zhenhua Ma,
Chinese Academy of Fishery Sciences (CAFS), China

***Correspondence:**
Fei Cheng
chengfei@ihb.ac.cn

**Specialty section:**
This article was submitted to Marine Fisheries, Aquaculture and Living Resources, a section of the journal Frontiers in Marine Science

**Received:** 09 May 2022
**Accepted:** 06 June 2022
**Published:** 13 July 2022

**Citation:**
He W, Dong Z, Ma T, Yan H, Chen Z, Yao W and Cheng F (2022) Three Mitochondrial Markers Reveal Genetic Diversity and Structure of Rock Carp (Procypris rabaudi) Endemic to the Upper Yangtze: Implications for Pre-release Genetic Assessment. Front. Mar. Sci. 9:939745. doi: 10.3389/fmars.2022.939745

Rock carp, Procypris rabaudi, is a vulnerable carp endemic to the upper reaches of the Yangtze River and included in the National Key Protected Wildlife in 2021 as a second-class aquatic animal. Evaluating the genetic makeup of released individuals before a restocking activity is carried out is essential, and a molecular marker with simple, rapid, and universal characteristics will be helpful to the evaluation. In this study, the genetic diversity and structure of rock carp from two representative hatcheries [Yibin (YB) and Wanzhou (WZ)] and a section of the upper Yangtze [Zhuyang (ZY)] were investigated using three mtDNA markers to select one marker instead of genetic evaluation of release. The results of three mtDNA markers revealed basically the same, indicating that the level of genetic diversity in rock carp was low, and there was significant genetic differentiation between the ZY and YB. Except for Cyt b–labeled YZ (0.81) and D-loop–labeled WZ (0.59), most of the haplotypic diversity values (h) were below 0.5, the nucleotide diversity values ($\pi$) of each group were lower than 0.5 × 10-2, and the haplotype number of rock carp is 1 to 4. Among the three mtDNA markers selected, D-loop marker detected higher diversity, more haplotypes, and private haplotypes, and significant differences between the YB and WZ. The results in this study pointed out the importance of pre-release genetic evaluation and the urgency of protecting the genetic diversity of rock carp, and the D-loop marker was preferentially selected in the pre-release genetic evaluation of fish. Hatchery release is the main strategy for the recovery of rock carp populations, similar to more than 20 endemic fish species in the upper Yangtze River. This study has guiding significance for the protection and restoration of other endemic fishes in the Yangtze River by hatchery release.

**Keywords: Cyt b, CO I, D-loop, hatchery release, population differentiation, rock carp**

## INTRODUCTION

Rock carp, *Procypris rabaudi*, is an endemic and vulnerable Cyprinid fish in the upper Yangtze River (Yang et al., 2009). The fish is demersal, inhabits mainly slow-flowing areas with rocky substrate, and spawns under rocky shelters in rushing streams (Wang et al., 2015). Rock carp had relatively extensive distribution records in the mainstem of the upper Yangtze and its tributaries, such as the Jinsha River, Jialing River, and Minjiang River (Yang et al., 2009; Wang et al., 2015). The upper mainstem and its tributaries are typical canyon rivers with steep gradients, staggered shoals, and rapids (Cheng et al., 2015). Hence, the fish have extensive distribution in the upper Yangtze, and its suitable habitats may be limited. A lot of dams have been or are being constructed in the upper Yangtze, such as 10 cascade dams in the middle and lower reaches of the Jinsha River, which have dramatically degraded the habitats of the fish (Cheng et al., 2015). Combining other anthropogenic effects including the construction of shipping channels, water pollution, and overfishing, wild populations of rock carp have dramatically declined and become extremely rare in its native habitats (Yang et al., 2009; Cheng et al., 2011; Wang et al., 2015). As a result, the fish has been listed as a second-class aquatic animal in the National List of Key Protected Wild Animals in 2021 (Zhang et al., 2022). Furthermore, many endemic fishes in the upper Yangtze River, such as *Acipenser dabryanus*, *Percocypris pingi*, and *Myxocyprinus asiaticus*, have similar threats to rock carp. Population conservation and restoration of these endemic fishes have greatly been concerning.

Hatchery release is one of the major techniques for fish stock enhancement and has been practiced as a major strategy for population conservation and restoration of endemic fishes in the upper Yangtze River (Cheng et al., 2011; Yang and Wei, 2021; Zhang et al., 2022). A total of $2.77 \times 10^7$ and $1.65 \times 10^7$ endemic fishes were resealed into the upper Yangtze River in replenishment activities in Sichuan province and Chongqing city only in 2019 and 2020, respectively (Fishery Supervision and Administration Office of the Yangtze River Basin, 2019; 2020). Rock carp are the main component of these released endemic fish. For example, at least $2.29 \times 10^7$ rock carp were released by replenishment activities in Wanzhou district, Chongqing city, between 2013 and 2017 (Zhang et al., 2022). However, when the release of individuals with substantially different genetic backgrounds contributes to gene flow in wild populations, hatchery release may have potentially adverse effects such as loss of genetic diversity, alteration in genetic structure, and a decrease in effective population size (Cross, 1999; Bert et al., 2001; Grant et al., 2017). To rock carp, Cheng et al. (2011) found lower genetic diversity in hatchery individuals and hybrids with released individuals in the wild population. Zhang et al. (2022) demonstrated the genetic effects of hatchery release, which resulted in a substantial change in the genetic structure of the wild population and the threat of inbreeding decline of this vulnerable fish. Both studies used different microsatellite loci to compare population genetics between wild and hatchery groups of rock carp (Cheng et al., 2011; Zhang et al., 2022). Microsatellite marker can reveal abundant genetic information for analysis, is laborious and time-consuming, and needs a specific primer for loci amplification (Liu and Cordes, 2004; Portnoy and Heist, 2012). Evaluating the genetic makeup of released individuals and their genetic effects on wild counterparts prior to restocking activity is critical to ensuring population conservation and restoration of endemic fishes in the upper Yangtze River, and a molecular marker with simple, rapid, and universal characteristics will be helpful to the evaluation of pre-released.

Mitochondrial (mtDNA) markers are frequently used to reveal genetic diversity and structure, population origins and mixing, and hybrid introgression of fishes (Jackson et al., 2012). This has been attributed to its practical advantages such as simpler operation, universal primer, and quick and comparable results, in part due to faster accumulating of sequence divergence in vertebrate than in nuclear DNA (Brown, 1985; Liu and Cordes, 2004). Common mtDNA markers applied in fish include the cytochrome oxidase I (CO I), cytochrome b (Cyt b), and the control region (D-loop). Among these markers, the D-loop is a non-coding region and exhibits generally higher genetic variations relative to coding regions such as the CO I and Cyt b (Keeney and Heist, 2006; Jackson et al., 2012; Portnoy and Heist, 2012). Furthermore, the genetic diversity and structure of rock carp are relatively clear (Cheng et al., 2011; Song et al., 2014; Zhang et al., 2022). In general, wild populations of the fish showed a moderate level of genetic diversity and no obvious geographical distribution patterns in the Yangtze River (He et al., 2008; Zhu et al., 2008; Zhang et al., 2020); hatchery-raised individuals showed lower genetic diversity and significant genetic differentiation with wild populations and among different hatcheries (Cheng et al., 2011; Yue et al., 2021). In addition, impacts of hatchery release on the genetic makeup of wild rock carp in the upper Yangtze have already been demonstrated (Cheng et al., 2011; Zhang et al., 2022).

Hatchery releases have not always achieved the anticipated population conservation and restoration of endemic fishes in the Yangtze River (Wei, 2020; Xie, 2020; Yang and Wei, 2021). One reason may be that many individuals in released fishes are genetically inferior to wild individuals (Cheng et al., 2011; Grant et al., 2017). A molecular marker with practical advantages will be helpful to evaluate rapidly genetic makeup of released individuals before restocking activity which is important to improve the restocking plan and to predict genetic effects on wild counterparts. In this study, samples of rock carp were collected from representative hatcheries and the upper reaches of the Yangtze River, and the genetic diversity and structure of sampling groups were investigated using three mtDNA markers. The aim of this study was to prioritize mtDNA markers for pre-released genetic evaluation of rock carp, which would also be helpful to hatchery release protect the population conservation and restoration of other endemic fishes in the upper Yangtze River.

## MATERIALS AND METHODS

A total of 21 adult individuals as a wild population (ZY) were collected from fishers located in the Zhuyang section of the upper Yangtze River in 2020 (**Figure 1**). ZY section is a main habitat and spawning ground of the fish and is an important part of the

National Natural Reserve Areas of Rare and Special Fishes in the upper reaches of the Yangtze River (Cheng et al., 2011). Two released groups of the fish were sampled from the Yibin hatchery of Sichuan province (YB) and Wanzhou hatchery of Chongqing city (WZ) in 2020. Fin specimens were collected from 30 adult individuals for each hatchery. The Yibin hatchery collected the original broodstock of rock carp from the Zhuyang section in the 1990s and produced the majority of released rock carp for Sichuan province, China (Cheng et al., 2011). The Wanzhou hatchery is a major supplied hatchery for released activities of Chongqing city; however, the information on the original broodstock of the Wanzhou hatchery is unknown (Zhang et al., 2022). All specimens were collected and fixed immediately with 95% ethanol and stored at −20°C in the laboratory.

Total DNA was extracted using an animal genomic DNA extraction kit (Sangon, Shanghai, China). DNA quality and concentration were determined by agarose gel electrophoresis and spectrophotometer (Eppendorf, Germany). For partial sequences of the mtDNA CO I marker, universal primers were FishF1 and FishR1, and amplification was performed following Ward et al. (2005). For partial sequences of the mtDNA Cyt b marker, universal primers were L14724 and H15915, and amplification was performed following Xiao et al. (2001). For partial sequences of the mtDNA D-loop marker, universal primers were MitD1-F and MitD1-R, and amplification was performed following Dong et al. (2014). Products of polymerase chain reaction (PCR) products were detected by agarose gel electrophoresis and purified and sequenced by a commercial sequencing company (BGI, Shenzhen, China).

The Clustal X software (version 1.83) was used to edit and align sequences of the three markers (Thompson et al., 1997). The MEGA 5.0 software translated sequences into amino acids to check for sequencing errors and pseudogene presences for the mtDNA CO I and Cyt b markers (Tamura et al., 2011). The DnaSP v5.1 software calculated standard genetic diversity indices for sequences of the three mtDNA markers such as the haplotype number ($k$), haplotypic diversity ($h$), average pairwise sequence differences ($\Pi$), and nucleotide diversity ($\pi$) (Librado and Rozas, 2009). The ARLEQUIN v3.1 software estimated genetic differentiation among the three sampling groups through mean pairwise differences ($N_{ST}$) for each marker (Excoffier et al., 2005), and $p < 0.05$ was used to screen out the significant differences between different populations. The TCS v1.21 software constructed a minimum-spanning haplotype network to evaluate relationships between sampling groups and the distribution of haplotypes for each marker using a statistical parsimony procedure with 95% connection limits (Clement et al., 2000). The DnaSP v5.1 software also evaluated the historical dynamics of the population through the mismatch distribution analysis and implemented Tajima's $D$ test and Fu's $Fs$ statistic for the neutrality test in the wild population. The ARLEQUIN v3.1 software assessed the goodness of fit by the raggedness index ($r$) and the sum of square deviations ($SSD$) between the observed and expected mismatch with 1,000 parametric bootstrap replicates for the wild population.

## RESULTS

Partial sequences of the mtDNA CO I, Cyt b, and D-loop markers were extracted from about 900, 997, and 637 base pairs for furthermore analysis, respectively. No indels, sequencing errors, and pseudogenes were detected from the CO I and Cyt b sequences. The D-loop sequence showed relatively higher variations and diversities than the CO I and Cyt b sequences. Haplotypes were detected in four (GenBank: 2562447) from the CO I sequences, five (GenBank: 2563182) from the Cyt b sequences, and six (GenBank: 2562496) from the D-loop sequences. Variable sites, parsimony informative sites, and G+C content were 7, 5, and 45.0% in the CO I sequence; 6, 4, and 41.7% in the Cyt b sequences; and 22, 8, and 27.8% in the D-loop sequences, respectively. Haplotypic and nucleotide diversity indices were 0.31 and $0.16 \times 10^{-2}$ in the CO I sequence, 0.37 and

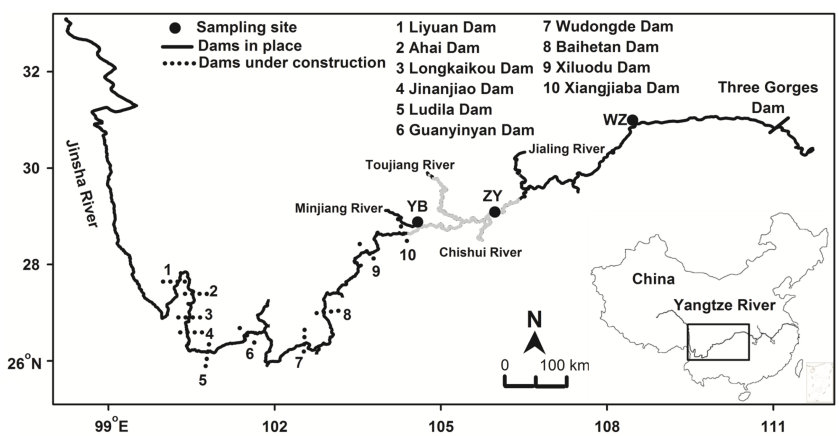


**FIGURE 1 |** Sampling sites of *Procypris rabaudi* for the wild population (ZY), Yibin hatchery (YB), and Wanzhou hatchery (WZ) in the upper Yangtze River. Main section of the National Natural Reserve Areas of Rare and Special Fishes of the Upper Yangtze River is shown using gray, and main tributaries, the Three Gorges Dam, and 10 cascade dams in the middle and lower reaches of the Jinsha River are located

$0.79 \times 10^{-3}$ in the Cyt b sequences, and 0.39 and $0.35 \times 10^{-2}$ in the D-loop sequences, respectively.

Among the sampling groups, the *k*, *h*, *Π*, and π values of the CO I sequences were lowest in the YB and similar between the ZY and the WZ and ranged from 1 to 4, 0.00 to 0.47, 0.00 to 2.00, and 0.00 to $0.22 \times 10^{-2}$, respectively (**Table 1**). The diversity indices also were lowest in the YB and highest in the ZY, and the *k*, *h*, *Π*, and π values ranged from 1 to 4, 0.00 to 0.81, 0.00 to 1.90, and 0.00 to $0.19 \times 10^{-2}$, respectively (**Table 1**). However, the genetic diversity indices of the D-loop regions were relatively higher than the other two markers' sequences in all groups and ranged from 2 to 4, 0.11 to 0.59, 1.26 to 2.67, and $0.20 \times 10^{-2}$ to $0.42 \times 10^{-2}$, respectively (**Table 1**).

Significant genetic differences were detected between the YB and other groups and not found between the ZY and WZ by the three mtDNA markers ($p < 0.05$) (**Table 2**). The D-loop marker also detected significant genetic differences between the YB and WZ ($p < 0.05$) (**Table 2**). The minimum-spanning haplotype network of the three mtDNA markers indicated a segregating trend between the wild population and hatchery groups (**Figure 2**). Among four haplotypes of rock carp detected by the CO I marker, the ZY processed two private (Hap 2 and Hap 4) and shared Hap 3 with the WZ and Hap 1 with the YB and WZ, and similar haplotype networks among the three sampling groups are also detected by the Cyt b and D-loop markers (**Figure 2**). Furthermore, the D-loop marker detected more private haplotypes among the groups than the other two markers, which showed the three groups had, respectively, one private haplotype (**Figure 2**).

Similar results in historical dynamics of the wild population were revealed by the three mtDNA markers, which failed to reject the raw hypothesis of population inflation and neutrality theory. The mismatch distribution analysis showed multimodal distribution (**Figure 3**). The goodness of fit and neutrality tests did not detect a significant departure from the raw hypothesis, except for the mtDNA CO I and D-loop–labeled markers SSDs ($p < 0.05$) (**Table 3**).

## DISCUSSION

The three mtDNA markers revealed consistent results and indicated a low level of genetic diversity in rock carp and significant genetic differentiation between the wild population and the YB hatchery group. These results pointed out the importance of genetic evaluation of pre-released and the urgency in protecting the genetic diversity of rock carp. Among the three mtDNA markers, the D-loop marker showed higher genetic variations and more effective detection in genetic makeups among different groups of rock carp, which may be preferred in pre-released genetic evaluation for the fish. Hatchery release is a major strategy for population conservation and restoration of rock carp, similar to over 20 endemic fishes in the upper Yangtze River (Yin and Zhang, 2008). Application of pre-released genetic evaluation is suggested for protecting the genetic diversity of rock carp and avoiding genetic risks of hatchery-raised fish released based on our results. This study also is instructive for hatchery release for population conservation and restoration of other endemic fishes in the upper Yangtze River.

A low level of genetic diversity in rock carp was revealed by the mtDNA markers, which may be related to the genetic impacts of released hatchery-raised individuals. Most of the *h* values were below 0.5, except for the YZ (0.81) by the Cyt b marker and the WZ (0.59) by the D-loop marker; the π values of all groups were below $0.5 \times 10^{-2}$, and the *k* values ranged from 1 to 4 in rock carp. All these results showed low genetic diversity, which was consistent with the recent results of rock carp (Zhang et al., 2020; Yue et al., 2021). The *h* and π values of the D-loop marker were 0.41 and $0.13 \times 10^{-2}$ and 0.40 and $0.13 \times 10^{-2}$ for two released hatcheries of Chongqing city (Yue et al., 2021), and the *h* and π values of the Cyt b marker were 0.63 and $0.14 \times 10^{-2}$ and 0.46 and $0.10 \times 10^{-2}$ for wild populations from the Wanzhou section and the Chishui River of the upper Yangtze, respectively (Zhang et al., 2020). Compared with earlier results of wild populations, our results showed a sharp decrease in genetic diversity in the last decade with the implementation of the mass-scale release of hatchery fish. The *h* and π values of the D-loop marker ranged from 0.60 to 0.97 with a mean of 0.86 and from $0.25 \times 10^{-2}$ to $1.60 \times 10^{-2}$ with a mean of $0.79 \times 10^{-2}$ for eight wild populations collected from 2002 to 2006 (Song et al., 2014). Research studies before 2010 also showed high genetic diversity of rock carp, such as three wild populations with average $h = 0.86$ using the D-loop marker and two wild populations with average $h = 0.88$ using the Cyt b marker (He et al., 2008; Zhu et al., 2008). The research using microsatellite markers had identified the negative effects of hatchery release on the genetic diversity and structure of rock carp (Cheng et al., 2011; Zhang et al., 2022). Combined with

**TABLE 1 |** Genetic diversity indices for partial sequences of the mtDNA CO I, Cyt b, and D-loop markers in the wild population (ZY), Yibin hatchery (YB), and Wanzhou hatchery (WZ) of *Procypris rabaudi*.

| mtDNA Marker | Sampling Group | Haplotype Number (*k*) | Haplotype Diversity (*h*) | Ave. Nucleotide Dif. (*Π*) | Nucleotidic Diversity (π) |
|---|---|---|---|---|---|
| CO I | ZY | 4 | 0.47 | 1.98 | $0.22 \times 10^{-2}$ |
| | YB | 1 | 0.00 | 0.00 | 0.00 |
| | WZ | 2 | 0.40 | 2.00 | $0.22 \times 10^{-2}$ |
| Cyt b | ZY | 4 | 0.81 | 1.90 | $0.19 \times 10^{-2}$ |
| | YB | 1 | 0.00 | 0.00 | 0.00 |
| | WZ | 3 | 0.38 | 0.91 | $0.91 \times 10^{-3}$ |
| D-loop | ZY | 4 | 0.45 | 2.67 | $0.42 \times 10^{-2}$ |
| | YB | 2 | 0.11 | 1.26 | $0.20 \times 10^{-2}$ |
| | WZ | 4 | 0.59 | 2.63 | $0.41 \times 10^{-2}$ |

**TABLE 2 |** Pairwise differences ($N_{ST}$) among the wild population (ZY), Yibin hatchery (YB), and Wanzhou hatchery (WZ) of *Procypris rabaudi* using partial sequences of the mtDNA CO I, Cyt b, and D-loop markers.

| | CO I | | Cyt b | | D-loop | |
|---|---|---|---|---|---|---|
| **Sampling group** | **YB** | **WZ** | **YB** | **WZ** | **YB** | **WZ** |
| ZY | 0.16* | −0.12 | 0.05* | −0.05 | 0.25* | −0.14 |
| YB | | 0.25 | | 0.04 | | 0.18* |

*$p < 0.05$.

other research, our results may be indicated that hatchery release is likely to important reason for the sharp decrease in genetic diversity of rock carp, which is consistent with the reference of Zhang et al. (2020). Genetic diversity is closely associated with population adaptation and fitness and is important to the long-term persistence of a species (Schindler et al., 2010; Grant et al., 2017). Thus, our results pointed out the importance of pre-released genetic evaluation and the urgency of protecting the genetic diversity of rock carp.

Significant genetic differences were detected between the ZY and YB, which were consistent with the results using microsatellite markers and cautioned the genetic impacts of released hatchery-raised rock carp (Cheng et al., 2011). The observed segregating trend of the haplotype network between the wild population and hatchery groups also supported the results of population differentiation. Previous research showed that no genetic differentiation and obvious geographical distribution patterns were found in wild populations of the fish using the mtDNA markers (He et al., 2008; Song et al., 2014; Zhang et al., 2020). However, recent research demonstrated genetic differentiation between the Wanzhou population and other natural populations due to long-term released activities of hatchery-raised rock carp in Wanzhou, Chongqing city (Zhang et al., 2022). Furthermore, the YB, the same broodstock in Cheng et al. (2011), showed extremely low genetic diversity and dramatically homogenizing of genetic variability in the last decade. Broodstock is generally small for economic efficiency to reduce the costs in hatchery practices, which inevitably produces a cohort of individuals that differs genetically from the wild population (Araki et al., 2007; Araki et al., 2008; Grant et al., 2017). Hybridizations with released hatchery-raised individuals like the YB have the potential to lower the fitness of wild counterparts. In addition, our results in historical dynamics indicated that the wild population complied with the neutrality theory and held relatively stable. Protecting the genetic resources of wild populations is an important mission in implementing stock restoration (Teletchea and Fontaine, 2014; Grant et al., 2017). Combined with this research, our results underscored the importance of broodstock management in the

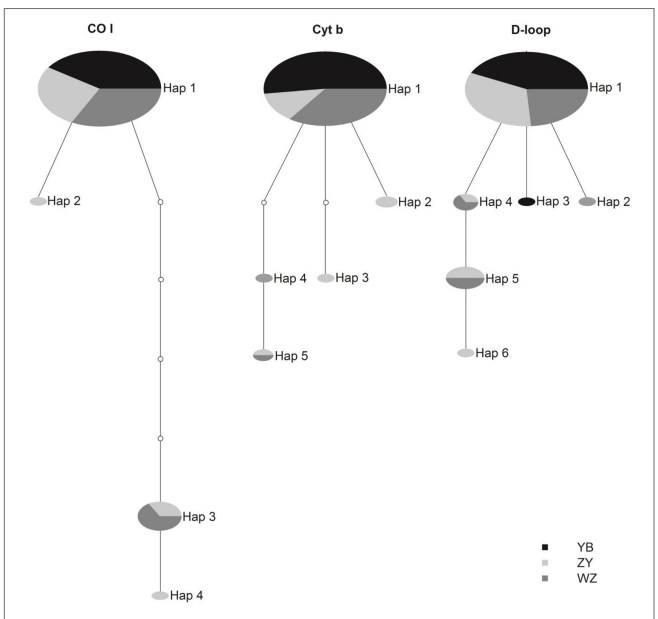


**FIGURE 2 |** Statistical parsimony network based on haplotype frequencies of the mtDNA CO I, Cyt b, and D-loop markers among the wild population (ZY), Yibin hatchery (YB), and Wanzhou hatchery (WZ) of *Procypris rabaudi*.

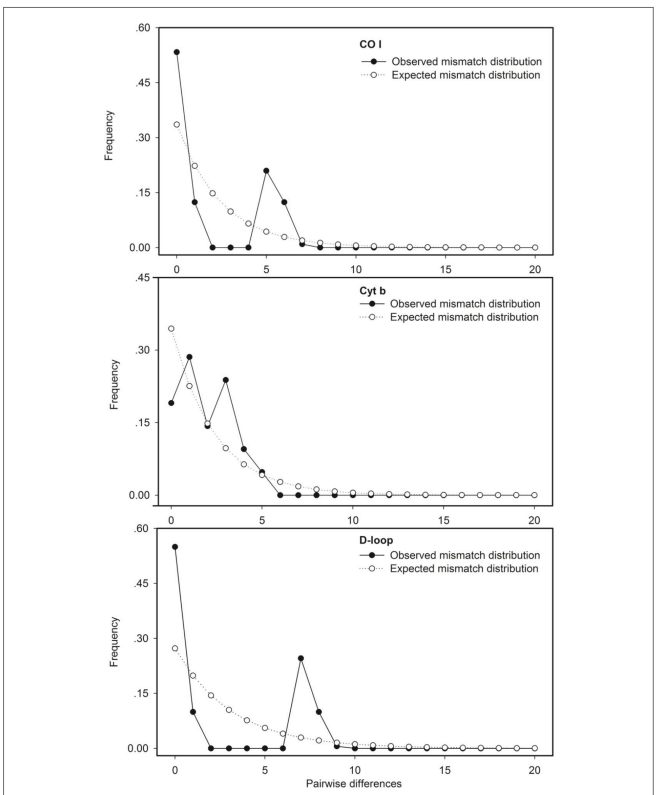


**FIGURE 3 |** Mismatch distribution of partial sequences of the mtDNA CO I, Cyt b, and D-loop markers for the wild population of *Procypris rabaudi*.

**TABLE 3 |** Goodness of fit and neutrality tests for partial sequences of the mtDNA CO I, Cyt b, and D-loop markers in the wild population of *Procypris rabaudi*.

| | Raggedness Index | Sum of Square Deviations | Tajima's *D* | Fu' *Fs* |
|---|---|---|---|---|
| CO I | 0.23 | 0.33* | –0.29 | 1.29 |
| Cyt b | 0.06 | 0.01 | –1.13 | –0.23 |
| D-loop | 0.30 | 0.28* | 0.12 | 2.63 |

*$p < 0.05$.

released hatchery. Broodstock management, especially effective broodstock size for rock carp, is central to successful hatchery release and then stock restoration (Grant et al., 2017). The Ryman–Laikre model with its extensions can be used to estimate appropriate broodstock size (Ryman and Laikre, 1991; Waples et al., 2016), which should be applied in broodstock management of released hatcheries, especially in the YB for rock carp. A careful evaluation of the genetic makeup of released individuals before restocking activity is needed to avoid the genetic impacts of released hatchery-raised rock carp.

The D-loop marker results revealed higher genetic variations and more effective detection of the genetic makeups of different groups of rock carp, which may be preferred in pre-release genetic assessment for the fish. Compared with other mtDNA markers, the D-loop marker detected higher diversity, more haplotypes and private haplotypes, and significant differences between the YB and WZ. As the non-coding region in mtDNA, the D-loop marker generally exhibits higher genetic variations and the fastest evolution rate relative to coding regions such as the CO I and Cyt b markers (Keeney and Heist, 2006; Jackson et al., 2012; Portnoy and Heist, 2012). In addition, the D-loop marker was also the most widely used molecular marker in rock carp and had comprehensively depicted the genetic background of two hatchery groups and all wild populations across the natural range of the fish (Song et al., 2014; Zhang et al., 2020; Yue et al., 2021). It is impossible to implement a risk-free program for population conservation and restoration (Waples and Drake, 2004). On the basis of our results, pre-released genetic evaluation is proposed for protecting the genetic diversity of rock carp and for avoiding the genetic risks of released hatchery-raised individuals. The D-loop marker with its practical advantages may be preferred in the evaluation for rock carp.

## CONCLUSION

Rock carp (*Procypris rabaudi*) is included in the National Key Protected Wildlife in 2021 as a second-class aquatic animal. Hatchery release is the main strategy for the recovery of rock carp populations. In this study, we presented that the D-loop marker was preferentially selected in the pre-release genetic evaluation from three mtDNA markers; the D-loop marker detected higher diversity, more haplotypes, and private haplotypes, and significant differences between the two hatcheries: YB and WZ. This study pointed out the importance of pre-release genetic evaluation and the urgency of protecting the genetic diversity of rock carp. Hatchery release has been practiced for more than 20 endemic fishes including rock carp, and the results of this study are also instructive to hatchery release for population conservation and restoration of other endemic fishes in the upper Yangtze River.

## DATA AVAILABILITY STATEMENT

The datasets presented in this study can be found in online repositories. The names of the repository/repositories and accession number(s) can be found in the article/supplementary material.

## ETHICS STATEMENT

The animal study was reviewed and approved by Institutional Animal Care and Use Committee(IACUC) of Southwest University. Written informed consent was obtained from the owners for the participation of their animals in this study.

## AUTHOR CONTRIBUTIONS

WH, methodology, genetic analysis and writing-original draft. ZD performed the field and laboratory work. TM, performed the field and laboratory work. HY, performed the field and laboratory work. ZC, performed the field and laboratory work. FC, conceptualization, supervision, writing-review & editing. All authors contributed to the article and approved the submitted version.

## FUNDING

This research was supported by the Fundamental Research Funds for the Central Universities (XDJK2019C025), the National Natural Science Foundation of Chongqing (cstc2020jcyj-msxmX0438), and the National Natural Science Foundation of China (32071651).

## REFERENCES


Araki, H., Berejikian, B. A., Ford, M. J. and Blouin, M. S. (2008). Fitness of Hatchery-Reared Salmonids in the Wild. *Evol. Appl.* 1, 342–355. doi: 10.1111/j.1752-4571.2008.00026.x

Araki, H., Cooper, B. and Blouin, M. S. (2007). Genetic Effects of Captive Breeding Cause a Rapid, Cumulative Fitness Decline in the Wild. *Science* 318, 100–103. doi: 10.1126/science.1145621

Bulletin on Hydrobiological Resources and Habitat in the Yangtze River Basin. (2020) Fishery Supervision and Administration Office of the Yangtze River Basin. http://www.cjyzbgs.moa.gov.cn/.

Bert, T. M., Tringali, M. D. and Baker, J. (2001). "Considerations for Sustainable Aquaculture, Biodiversity, and Ecosystem Processes a Genetics Perspective," in: *Promoting Global Innovation of Agricultural Science and Technology and Sustainable Agriculture Development*. Ed. ICAST Organizing Committee (Beijing: Proceedings of the International Conference on Agriculture Science and Technology), 238–254.

Brown, W. M. (1985). "The Mitochondrial Genome of Animals," in *Molecular Evolutionary Genetics*. Ed. MacIntyre, R. J., 95–130. Plenum. (New York: Springer), 95-130.

Cheng, F., Li, W., Castello, L., Murphy, B. R. and Xie, S. G. (2015). Potential Effects of Dam Cascade on Fish: Lessons From the Yangtze River. *Rev. Fish Biol. Fisher.* 25, 569–585. doi: 10.1007/s11160-015-9395-9

Cheng, F., Wu, Q. J., Liu, M., Radhakrishnan, K. V., Murphy, B. R. and Xie, S. G. (2011). Impacts of Hatchery Release on Genetic Structure of Rock Carp *Procypris Rabaudi* in the Upper Yangtze River, China. *Fish. Sci.* 77, 765–771. doi: 10.1007/s12562-011-0383-2

Clement, M., Posada, D. and Crandall, K. A. (2000). TCS: A Computer Program to Estimate Gene Genealogies. *Mol. Ecol.* 9, 1657–1659. doi: 10.1046/j.1365-294x.2000.01020.x

Cross, T. F. (1999). "Genetic Considerations in Enhancement and Ranching of Marine and Anadromous Species," in *Stock Enhancement and Sea Ranching*. Ed. r, K. M., Kitada, S., Blankenship, H. L. and Svasand, T. (Oxford: Blackwell), 37–48.

Dong, X. P., Mu, S. M., Zhou, N., Kang, X. J., Lou, Q. and Bai, J. J. (2014). Structure Analysis of mtDNA D-Loop Region and the Genetic Diversity of *Chanan Argu* in Different Populations. *J. Fish. China* 38 (9), 1277–1285. doi: 10.3724/SP.J. 1231.2014.49331

Excoffier, L., Laval, G. and Schneider, S. (2005). Arlequin Ver. 3.0: An Integrated Software Package for Population Genetics Data Analysis. *Evol. Bioinform.* 1, 47–50. doi: 10.1177/117693430500100003

Grant, W. S., Jasper, J., Bekkevold, D. and Adkison, M. (2017). Responsible Genetic Approach to Stock Restoration, Sea Ranching and Stock Enhancement of Marine Fishes and Invertebrates. *Rev. Fish Biol. Fish.* 27, 615–649. doi: 10.1007/s11160-017-9489-7

He, Y. F., Tang, Q. Y., Wang, J. W., Liu, H. Z. and Tan, D. Q. (2008). Population Differentiation of *Procypris Rabaudi* (Tchang) in the Upper Reaches of the Yangtze River Revealed by Mitochondrial DNA and RAPD Markers. *Genes Genom.* 30, 223–233. Available from https://www.researchgate.net/publication/259782818

Jackson, A. J., Laikre, L., Baker, C. S. and Kendall, C. K. (2012). Guidelines for Collecting and Maintaining Archives for Genetic Monitoring. *Conserv. Genet. Res.* 4 (2), 527–536. doi: 10.1007/s12686-011-9545-x

Keeney, D. B. and Heist, E. J. (2006). Worldwide Phylogeography of the Blacktip Shark (*Carcharhinus Limbatus*) Inferred From Mitochondrial DNA Reveals Isolation of Western Atlantic Populations Coupled With Recent Pacific Dispersal. *Mol. Eco.* 15, 3669–3679. doi: 10.1111/j.1365-294X.2006.03036.x

Librado, P. and Rozas, J. (2009). DnaSP V5: A Software for Comprehensive Analysis of DNA Polymorphism Data. *Bioinformatics* 25 (11), 1451–1452. doi: 10.1093/bioinformatics/btp187

Liu, Z. J. and Cordes, J. F. (2004). DNA Marker Technologies and Their Applications in Aquaculture Genetics. *Aquaculture* 238, 1–37. doi: 10.1016/j.aquaculture.2004.05.027

Portnoy, D. S. and Heist, E. J. (2012). Molecular Markers: Progress and Prospects for Understanding Reproductive Ecology in Elasmobranchs. *J. Fish Biol.* 80, 1120–1140. doi: 10.1111/j.1095-8649.2011.03206.x

Ryman, N. and Laikre, L. (1991). Effects of Supportive Breeding on the Genetically Effective Population Size. *Conserv. Biol.* 5, 325–329. doi: 10.1111/j.1523-1739.1991.tb00144.x

Schindler, D., Hilborn, R., Chasco, B., Boatright, C., Quinn, T., Rogers, L., et al. (2010). Population Diversity and the Portfolio Effect in an Exploited Species. *Nature* 465, 609–613. doi: 10.1038/nature09060

Song, J., Hou, F. X., Zhang, X. Y., Yue, B. S. and Song, Z. B. (2014). Mitochondrial Genetic Diversity and Population Structure of a Vulnerable Freshwater Fish, Rock Carp (*Procypris Rabaudi*) in Upper Yangtze River Drainage. *Biochem. Syst. Ecol.* 55, 1–9. doi: 10.1016/j.bse.2014.02.008

Tamura, K., Peterson, D., Peterson, N., Stecher, G., Nei, M. and Kumar, S. (2011). MEGA5: Molecular Evolutionary Genetics Analysis Using Maximum Likelihood, Evolutionary Distance, and Maximum Parsimony Methods. *Mol. Biol. Evol.* 28, 2731–2739. doi: 10.1093/molbev/msr121

Teletchea, F. and Fontaine, P. (2014). Levels of Domestication in Fish: Implications for the Sustainable Future of Aquaculture. *Fish* 15, 181–195. doi: 10.1111/faf.12006

Thompson, J. D., Gibson, T. J., Plewniak, F., Jeanmougin, F. and Higgins, D. G. (1997). The Clustal X Windows Interface: Flexible Strategies for Multiple Sequences Alignment Aided by Analysis Tools. *Nucleic Acids Res.* 25, 4876–4882. doi: 10.1093/nar/25.24.4876

Wang, T., Gao, X., Wang, J., Jakovlic, I., Dan, S. G. and Liu, H. Z. (2015). Life History Traits and Implications for Conservation of Rock Carp *Procypris Rabaudi* Tchang, an Endemic Fish in the Upper Yangtze River, China. *Fish. Sci.* 81, 515–523. doi: 10.1007/s12562-015-0872-9

Waples, R. S. and Drake, J. (2004)."Risk-benefit Consideration for Marine Stock Enhancement: a Pacific Salmon Perspective," in *Stock Enhancement and Sea Ranching*. Ed. Leber, K. M., Kitada, S., Blankenship, H. L. and Svasand, T. (Oxford: Blackwell), 160–306.

Ward, R. D., Zemlak, T. S., Bronwyn, H., Last, P. R. and Hebert, P. D. N. (2005). DNA Barcoding Australia's Fish Species. *Philos. Trans. R. Soc Lond. B. Biol. Sci.* 360, 1847–1857. doi: 10.1098/rstb.2005.1716

Wei, Q. W. (2020). Conservation of Chinese Sturgeon (*Acipenser Sinensis*) Based on its Life History: Dilemma and Breakthrough. *J. Lake Sci.* 32 (5), 1297–1319. doi: 10.18307/2020.0509

Xiao, W. H., Zhang, Y. P. and Liu, H. Z. (2001). Molecular Systematics of Xenocyprinae (Teleostei: Cyprinidae): Taxonomy, Biogeography, and Coevolution of a Special Group Restricted in East Asia. *Mol. Phylogenet. Evol.* 18, 163–173. doi: 10.1006/mpev.2000.0879

Xie, P. (2020). How to Evaluate and Rescue Endangered Species? *J. Lake Sci.* 32 (2), 281–293.

Yang, L., Mayden, R. L. and Cai, Y. (2009). Threatened Fishes of the World: *Procypris Rabaudi* (Tchang 1930) (Cyprinidae). *Environ. Biol. Fish.* 84, 275–276. doi: 10.1007/s10641-008-9417-8

Yang, H. L. and Wei, Q. W. (2021). Suppressive and Active Protective Actions in Aquatic Wildlife Conservation. *J. Lake Sci.* 33 (1), 1–10. doi: 10.18307/2021.0102

Yin, Z. Q. and Zhang, S. Y. (2008). Thoughts About Released and Proliferation of Fisheries Resources in China. *Fish Sin.* 3, 9–11. doi: 10.3969/j.issn.1002-6681.2008.03.009

Yue, H. M., Ruan, R., Cao, H., Zhou, L., Jiang, W., Li, S., et al. (2021). Analysis on Genetic Diversity of Cultured Rock Carp (*Procypris Rabaudi*) From Chongqing City Based on the mtDNA D-Loop Sequences. *Acta Hydrobiol. Sin.* 45 (4), 846–850. doi: 10.7541/2021.2020.082

Zhang, X. Y., Ouyang, M., Zhang, F. T. and Wang, J. W. (2022). Study on the Genetic Structure of Wild and Hatchery Populations of *Procypris Rabaudi* Tchang, an Endemic Fish in the Upper Yangtze River. *Fish Res.* 245, 106134. doi: 10.1016/j.fishres.2021.106134

Zhang, X. Y., Zhang, F. T., Yao, F. C. and Wang, J. W. (2020). Study on Genetic Diversity and Population Historical Dynamics of *Procypris Rabaudi* (Tchang) Endemic in the Upper Yangtze River. *Acta Hydrobiol. Sin.* 44, 330–338. doi: 10.7541/2020.040

Zhu, C. K., Zhang, Q. Z., Juan, Y. and Luo, F. (2008). Analysis of Genetic Diversity of the Mitochondrial DNA D-Loop Control Region of Rock Carp (*Procypris Rabaudi*

(Tchang)) in the Three Gorges Reservoir. *J. Southwest Univ.* 30, 126–133. doi: 10.13718/j.cnki.xdzk.2008.12.012

**Conflict of Interest:** The authors declare that the research was conducted in the absence of any commercial or financial relationships that could be construed as a potential conflict of interest.

**Publisher's Note:** All claims expressed in this article are solely those of the authors and do not necessarily represent those of their affiliated organizations, or those of the publisher, the editors and the reviewers. Any product that may be evaluated in this article, or claim that may be made by its manufacturer, is not guaranteed or endorsed by the publisher.

frontiers | Frontiers in Marine Science

TYPE Original Research
PUBLISHED 16 August 2022
DOI 10.3389/fmars.2022.947726



OPEN ACCESS

EDITED BY
Shuhao Huo,
Jiangsu University, China

REVIEWED BY
Yi Cui,
Jiangsu University, China
Fengzheng Gao,
Wageningen University and Research, Netherlands

*CORRESPONDENCE
Dong Wei
fewd304@scut.edu.cn

SPECIALTY SECTION
This article was submitted to Marine Fisheries, Aquaculture and Living Resources, a section of the journal Frontiers in Marine Science

RECEIVED 19 May 2022
ACCEPTED 20 July 2022
PUBLISHED 16 August 2022

CITATION
Yang R, Wei D and Pohnert G (2022) Nitrogen utilization analysis reveals the synergetic effect of arginine and urea in promoting fucoxanthin biosynthesis in the mixotrophic marine diatom *Phaeodactylum tricornutum*. *Front. Mar. Sci.* 9:947726. doi: 10.3389/fmars.2022.947726



# Nitrogen utilization analysis reveals the synergetic effect of arginine and urea in promoting fucoxanthin biosynthesis in the mixotrophic marine diatom *Phaeodactylum tricornutum*

Runqing Yang[1], Dong Wei[1]* and Georg Pohnert[2]

[1]Guangdong Province Key Laboratory for Green Processing of Natural Products and Product Safety, Engineering Research Center of Starch and Vegetable Protein Processing Ministry of Education, Research Institute for Food Nutrition and Human Health, School of Food Science and Engineering, South China University of Technology, Guangzhou, China, [2]Institute for Inorganic and Analytical Chemistry, Bioorganic Analytics, Friedrich Schiller University Jena, Jena, Germany

Fucoxanthin is a new dietary ingredient applied in healthy foods with specific benefits of body weight loss and liver fat reduction. The marine diatom *Phaeodactylum tricornutum* is a highly suitable species for fucoxanthin production. In the present study, aiming to promote fucoxanthin biosynthesis in mixotrophic *P. tricornutum*, $NaNO_3$, tryptone, and urea were evaluated as nitrogen sources with 0.10 mol $L^{-1}$ of glycerol as the organic carbon source for mixotrophic growth in shake flasks. Compared to $NaNO_3$, the mixture of tryptone and urea (referred to as T+U, 1:1, mol N:mol N) as organic nitrogen sources could induce a higher biomass and fucoxanthin production. Through nitrogen utilization analysis, leucine, arginine, lysine, and phenylalanine in the T+U medium were identified as the amino acids that primarily support cell growth. Among those amino acids, arginine causes the highest rate of nitrogen utilization and cell growth promotion. After 12 days of cultivation, the highest biomass concentration (3.18 g $L^{-1}$), fucoxanthin content (12.17 mg $g^{-1}$), and productivity (2.68 mg $L^{-1}$ $day^{-1}$) were achieved using 25 mmol N $L^{-1}$ of arginine and 5 mmol N $L^{-1}$ of urea as nitrogen sources, indicating that arginine and urea performed synergistically on enhancing biomass and pigment production. This study provides new insights into the promotion of fucoxanthin biosynthesis by nitrogen utilization analysis and verifies the synergetic effect of arginine and urea on facilitating the development of a promising strategy for efficient enhancement of fucoxanthin production through mixotrophic cultivation of *P. tricornutum*.

KEYWORDS

**fucoxanthin, *Phaeodactylum tricornutum*, amino acids, arginine, urea**

## Introduction

Fucoxanthin is a carotenoid that is widely distributed in diatoms, brown algae, and golden algae (Yang et al., 2020). Given its antioxidant, anticancer, anti-obesity, anti-diabetes, and anti-Alzheimer's disease properties (Lourenco-Lopes et al., 2021; Seth et al., 2021), fucoxanthin draws a growing attention and an increasing demand in the global market. Due to its health benefits and non-toxicity, fucoxanthin obtained the acknowledgement from the U.S. Food and Drug Administration (FDA) as a new dietary ingredient in 2017 for application in human health food (https://www.fda.gov/media/108748/download), especially for body weight management and liver health improvement (Yang et al., 2020; Sun et al., 2022). For example, fucoxanthin has been applied in commercial products of whole milk and skimmed milk as a weight loss drink (Mok et al., 2016; de Gonzalez et al., 2021). Currently, the commercial source of fucoxanthin is mainly brown seaweeds, but the very low content (<0.1% DW) of fucoxanthin and the difficulties of extraction result in the low quality and high cost of fucoxanthin-rich oil products (Rajauria et al., 2017).

Marine diatoms are microalgae that produce bioactive compounds like long-chain polyunsaturated fatty acids [eicosapentaenoic acid (EPA) and docosahexaenoic acid (DHA)], natural pigments (fucoxanthin and other high-value carotenoids, phycobiliproteins), and polysaccharides (chrysolaminarin, etc.), with broad applications in aquaculture, health foods, pharmaceuticals, and cosmetics (Yang et al., 2020). The marine diatom *Phaeodactylum tricornutum* is recognized as a suitable fucoxanthin producer due to its high content of fucoxanthin (Yang and Wei, 2020), and the highest level of fucoxanthin could reach 59 mg $g^{-1}$ using flat panel photobioreactors (McClure et al., 2018). It can be cultivated at a large scale under autotrophic conditions for industrial purposes (Gao et al., 2017; Delbrut et al., 2018). The mixotrophic cultivation of *P. tricornutum* could achieve higher biomass productivity (1.01 g $L^{-1}$ $day^{-1}$) compared to autotrophic conditions, but the photosynthetic system was significantly inhibited, causing the low content of carotenoids (<0.7% DW) (Ceron-Garcia et al., 2013). As fucoxanthin is the main carotenoid in *P. tricornutum*, the content was even lower in the mixotrophic biomass. The results above suggested that it is hard to accumulate biomass and fucoxanthin simultaneously. Therefore, the development of a high-efficient manufacturing technology is an urgent demand for the commercial production of fucoxanthin by mixotrophic marine diatoms.

Since fucoxanthin exists in the form of a fucoxanthin–chlorophyll–protein complex (FCP) in the photosynthetic system of diatoms (Wang et al., 2019), nitrogen plays a vital role in FCP formation during cultivation. In diatoms, fucoxanthin biosynthesis requires nitrogen-rich conditions (Jauffrais et al., 2016; McClure et al., 2018; Wang et al., 2018). The fucoxanthin content was increased immediately after nitrate addition and then decreased with the consumption of nitrate (Pajot et al., 2022). The increase of nitrogen concentration from 40 to 400 μmol $L^{-1}$ promoted a two-fold increase in pigment contents (including chlorophyll and fucoxanthin) (Jauffrais et al., 2016). The highest level of fucoxanthin content (5.92% DW) was reported under 10-fold $NO_3^-$ addition (McClure et al., 2018). Biomass concentration and fucoxanthin content were also significantly enhanced around 50% and 70%, respectively, by extra nitrogen supply in the growth of *P. tricornutum* (Wang et al., 2018). Transcriptome analysis indicated that genes involved in the photosynthesis system and fucoxanthin biosynthesis pathway were upregulated under nitrogen-replete conditions (Alipanah et al., 2015; Remmers et al., 2018), and RNA-seq analysis demonstrated that the expression of light-harvesting complex genes (including FCP genes) was decreased with nitrogen depletion, resulting in the reduction of fucoxanthin content (Pajot et al., 2022). Thus, sufficient nitrogen is an essential nutrient for both cell growth and fucoxanthin biosynthesis in *P. tricornutum*.

*Phaeodactylum tricornutum* can utilize not only inorganic nitrogen sources like nitrate, nitrite, and ammonium but also organic nitrogen sources like urea, tryptone, and amino acids (Smith et al., 2019; Contreras and Gillard, 2021; Yang and Wei, 2020). Compared with nitrate and ammonium, *P. tricornutum* preferred to use urea, achieving a higher biomass concentration with no significant difference in fucoxanthin content (Zhang et al., 2016). Furthermore, the fucoxanthin production was 3.45-fold higher than that in the presence of urea when tryptone was used as a nitrogen source (Wang et al., 2021), and *P. tricornutum* could utilize most of the amino acids, in which the maximum uptake rate of nitrogen was reached by using arginine (Rees and Allison, 2006; Contreras and Gillard, 2021). Among 20 proteinogenic amino acids, arginine has four amino moieties, leading to the highest nitrogen to carbon ratio in the molecule. It is thus regarded as an effective storage of organic nitrogen *in vivo* (Winter et al., 2015). However, the impact of different types and concentrations of amino acids as well as the synergetic effect with other nitrogen sources on fucoxanthin biosynthesis is still not known clearly.

*Phaeodactylum tricornutum* cells assimilate nitrogen through glutamine synthetase (GS) and glutamine 2-oxoglutarate aminotransferase (GOGAT) cycle working with transport systems (Smith et al., 2019). Nitrate, nitrite, ammonium, and several amino acids that are metabolized extracellularly are assimilated in the chloroplast *via* GSII-$GOGAT_{Fd}$ and shuttle nitrogen to the mitochondria through the aspartate system (Smith et al., 2019; Contreras and Gillard, 2021). In contrast, urea, arginine, and lysine are assimilated by mitochondrial GSIII-$GOGAT_{a,b}$, and amino moieties are transported to the chloroplast through the alanine system (Flynn and Syrett, 1986; Smith et al., 2019). The aspartate and alanine systems both utilize the pyruvate carbon skeleton to transport nitrogen between organelles (Smith et al., 2019). In addition, pyruvate is an important precursor of photosynthetic

pigment synthesis (Yang et al., 2020). To improve the efficiency of nitrogen assimilation, adequate carbon source and glycolysis capacity are required for the fast growth of cells. Previous studies indicated that mixotrophic conditions using glycerol as the organic carbon source could upregulate the pathway of glycolysis and provide more pyruvate in cells (Villanova et al., 2017), potentially supporting the biomass accumulation and fucoxanthin biosynthesis in *P. tricornutum*. For example, with glycerol and sufficient nitrogen addition, biomass productivity and fucoxanthin concentration were increased 43.5% and 97.5% in *P. tricornutum*, respectively (Wang et al., 2021). Therefore, it is feasible to improve nitrogen consumption rate and induce fucoxanthin biosynthesis by optimizing the types and concentrations of nitrogen sources with glycerol supply.

In this study, cell growth and fucoxanthin production were evaluated using inorganic ($NaNO_3$) and organic nitrogen sources (the mixture of tryptone and urea) in mixotrophic *P. tricornutum*. Then, arginine was proven as the preferred amino acid by free amino acid consumption analysis in the medium using the mixture of tryptone and urea as nitrogen sources. Different concentrations of arginine, urea, and their mixture were investigated and optimized to develop a promising strategy for the efficient enhancement of fucoxanthin production. The proposed nitrogen assimilation pathway in *P. tricornutum* was fully discussed to explain the promotion of fucoxanthin biosynthesis.

# Materials and methods

## Microalgal strain and seed culture

The diatom *P. tricornutum* CCMP 1327 was kindly donated by Dr. Hanhua Hu from the Institute of Hydrobiology, Chinese Academy of Sciences (CAS), Wuhan, China. The seed culture was grown in 250-ml shake flasks containing 100 ml of modified f/2 medium with 9.20 g $L^{-1}$ of glycerol and a mixture of 1.17 g $L^{-1}$ of tryptone and 3 g $L^{-1}$ of urea (1:1, N mol:N mol) in a shaking incubator with continuous illumination under 20 µmol $m^{-2}$ $s^{-1}$ by white LED light (OQ-PZP003050, 4,000 K, Guangdong Ocean Quantum Lighting Company, China) at 20°C and 160 rpm according to our previous work (Yang and Wei, 2020). The seed culture at the logarithmic phase was used as the inoculum for further experiments.

## Evaluation of nitrogen sources on cell growth and fucoxanthin production

To investigate the effect of inorganic and organic nitrogen sources on cell growth and fucoxanthin accumulation, sufficient nitrogen concentrations (20 mmol $L^{-1}$) of $NaNO_3$ and the mixture of tryptone and urea (1:1, N mol:N mol, presented as T+U) selected from our previous study (Wang et al., 2021) were evaluated in mixotrophic growth with an initial cell density of $1 \times 10^7$ cells $ml^{-1}$ (Yang and Wei, 2020) in shake flasks, respectively. Cell density, pH value, and nitrogen concentration were detected by sampling every 2 days during the cultivation. The biomass productivity and fucoxanthin content were detected at the end of cultivation according to our previous work (Yang and Wei, 2020).

## Identification of the preferred amino acids in the T+U medium

During the cultivation above, the free amino acid concentrations in the T+U medium were analyzed by sampling every 2 days. According to the results of free amino acid consumption, the top 4 amino acids with high nitrogen consumption rate were identified as the preferred amino acids, in which the top 2 amino acids (lysine and arginine) at nitrogen contents of 0.3, 0.6, 0.9, and 1.2 mmol N $L^{-1}$ based on the initial concentration in the T+U medium were then selected to compare their effects on cell density, biomass concentration, and chlorophyll fluorescence, as well as on the consumption rate of carbon and nitrogen. Nitrogen concentrations were selected according to the initial concentration of the top 2 amino acids identified in the T+U medium.

## Synergetic effects of the preferred amino acids with urea

After the comparison of the top 2 preferred amino acids above, arginine, the dominant one, was investigated for its effect at the final nitrogen contents of 5, 10, 15, 20, 25, and 30 mmol N $L^{-1}$ by comparing to urea at final nitrogen contents of 5, 10, 15, and 20 mmol N $L^{-1}$. Moreover, their mixture at total nitrogen contents of 10, 15, 20, 25, and 30 mmol N $L^{-1}$, in which urea was at 5 mmol N $L^{-1}$, was carried out to investigate the synergetic effects by comparing with the solo nitrogen medium. Cell density, pH, and nitrogen concentration were monitored during the cultivation. Biomass concentration and productivity, pigment content, and fucoxanthin productivity were analyzed with glycerol consumption rate at the end of cultivation.

## Analytical methods

### Cell density and biomass concentration

A 1-ml cell suspension was collected for cell density and chlorophyll fluorescence determination by CytoFLEX flow cytometry (Beckman Coulter, USA) according to the operation manual. The fluorescence intensity of chlorophyll was recorded

in channel PC5.5 (excitation at 488 nm, emission at 690/50 nm through a BP filter).

The biomass concentration (g $L^{-1}$) was determined by the gravimetric method. A 2-ml cell suspension was collected in a preweighed tube and biomass was measured after centrifuging, washing, and drying in a 60°C oven to a constant weight.

The specific growth rate ($\mu$, $day^{-1}$) and biomass productivity (mg $L^{-1}$ $day^{-1}$) were calculated using formulae (1) and (2):

$$\mu = (\ln N_t - \ln N_0)/(t - t_0) \quad (1)$$

$$\text{Biomass productivity (mg L}^{-1}\text{ day}^{-1}) = (W_t - W_0)/t \times 1{,}000 \quad (2)$$

where $N_t$ and $N_0$ are the cell densities (cells $ml^{-1}$) at time $t$ and time $t_0$; $W_t$ and $W_0$ are the biomass concentrations (g $L^{-1}$) at time $t$ and time $t_0$, respectively.

## Glycerol and nitrogen concentrations

The glycerol concentration was determined by an M-100 biosensor analyzer (Siemens, China). $NO_3^-$ and total nitrogen (TN) concentrations were determined using a water quality analyzer (HI83200, Hanna, Italy) and DR2700 spectrophotometer (HACH, USA), respectively (Luo et al., 2020; Yang and Wei, 2020).

The urea concentration was determined by the urease kit (C013-2-1, Jianyang, China). The reaction solution was prepared according to the kit's instructions, and the absorbance was measured at 640 nm. The urea concentration was calculated using formula (3):

$$\text{Urea concentration mmol L}^{-1} = (A_{sample} - A_{blank}) \div (A_{standard} - A_{blank}) \times C_{standard} \quad (3)$$

where $A_{sample}$, $A_{blank}$, and $A_{standard}$ are the absorbance of the sample, blank, and standard solution, while $C_{standard}$ is the concentration of the standard (mmol $L^{-1}$).

## Profile and concentration of amino acids

The profile and concentration of free amino acids in the T+U medium were determined by an automatic amino acid analyzer (L8900, Hitachi, Japan) (Shim et al., 2013). A 2-ml cell-free culture broth of the T+U medium was collected every 48 h, and 0.5 ml of 15% sulfosalicylic acid was added for deproteinization. After mixing, the solution was stored at 2°C–4°C for 60 min. The supernatant was collected by centrifugation at 10,000×*g* for 15 min and then filtered through a 0.22-μm syringe membrane for further detection. The samples were detected by standard procedure with the MCI* buffer L-8500 pH kit, and then the free amino acids were identified and quantified by standard curves (Shen et al., 2021).

The arginine and lysine concentrations in the medium were determined by the ninhydrin colorimetric method (Tu, 2018). A 2× pH 5.6 buffer was prepared by 4.15 g of $Na_2HPO_4{\cdot}12H_2O$ and 0.88 g of citric acid monohydrate. A 2% ninhydrin solution (w/v) was prepared using 1× pH 5.6 buffer. Two hundred microliters of 2× pH 5.6 buffer; a 200-μl supernatant of arginine, lysine standard, or sample; and a 400-μl ninhydrin solution were added in a glass tube and then put in a 100°C water bath for 15 min. Then, 2 ml of double-distilled $H_2O$ ($ddH_2O$) was added to the tube after cooling at room temperature, and absorbance was measured at 570 nm. The arginine and lysine concentrations were calculated using arginine and lysine standard curves, respectively.

## Natural pigments

Natural pigments were extracted by organic solvents and measured by high-performance liquid chromatography (HPLC, DIONEX P680, Thermo Scientific, Waltham, USA) equipped with a PDA detector and a YMC™ Carotenoid column (150 mm × 4.6 mm, 3 μm) (Yang and Wei, 2020). The fucoxanthin productivity (mg $L^{-1}$ $day^{-1}$) was calculated by the following formula:

$$\text{Fucoxanthin productivity (mg L}^{-1}\text{day}^{-1}) = (W_t \times C_t - W_0 \times C_0)/t \quad (4)$$

where $W_t$ and $W_0$ are the biomass concentrations (g $L^{-1}$) at time $t$ and time $t_0$; $C_t$ and $C_0$ are the fucoxanthin contents (mg $g^{-1}$) at time $t$ and time $t_0$, respectively.

## Statistical analysis

The data were performed by triple biological replicates and presented as mean ± SD (standard deviation). The Origin V9.0 software was used for drawing the figures. The statistical analysis was carried out by one-way analysis of variance (ANOVA) and LDS *t*-test with SPSS V22.0. Different letters indicate significant differences ($p < 0.05$).

# Results and discussion

## Effects of nitrogen sources on cell growth and fucoxanthin production

$NaNO_3$ and the mixture of tryptone and urea (T+U) affected the cell growth of *P. tricornutum*. Higher cell density ($10.86 \times 10^7$ cells $ml^{-1}$) and specific growth rate (0.17 $day^{-1}$) were observed in the T+U medium compared to the $NaNO_3$ medium ($p < 0.05$) (Figure 1A; Table 1). It is coincident with the previous studies that *P. tricornutum* performed better in terms of cell growth with tryptone or urea addition (Wang et al., 2021). Compared with nitrate, it was reported that organic nitrogen sources, including leucine, isoleucine, and valine, could induce higher cell density in *P. tricornutum* (Hu et al., 2019). The pH

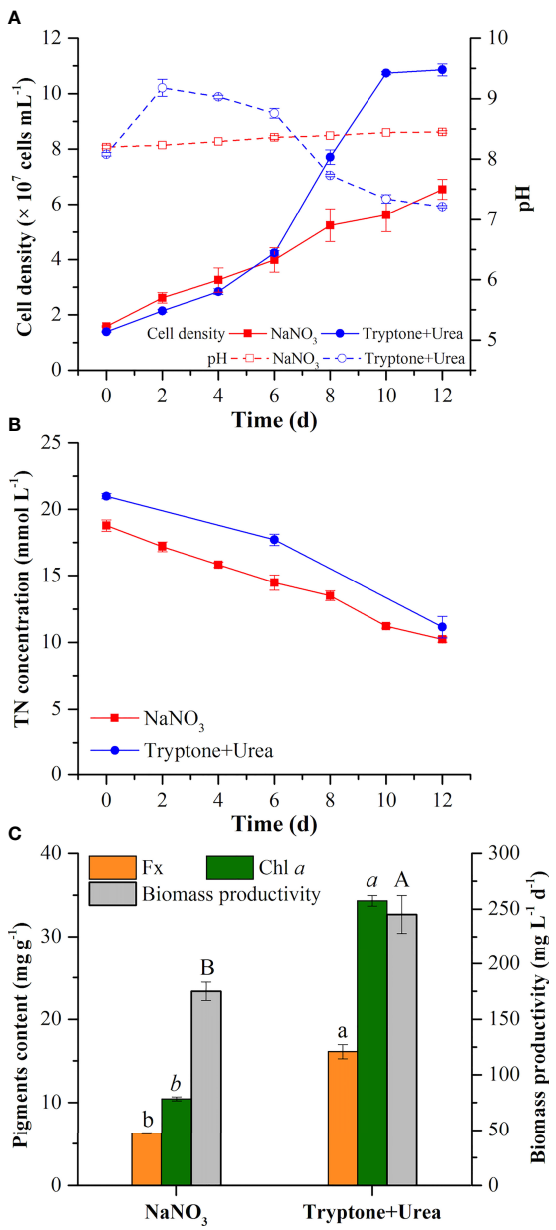


FIGURE 1
Cell density and pH value **(A)**, total nitrogen concentration in the medium **(B)**, pigment (fucoxanthin and chlorophyll *a*) contents, and biomass productivity **(C)** in the mixotrophic growth of *Phaeodactylum tricornutum* using inorganic ($NaNO_3$) and organic nitrogen (tryptone:urea = 1:1, mol N:mol N) sources at 20 mmol N $L^{-1}$. Different letters indicate a significant difference ($p< 0.05$).

value in the $NaNO_3$ medium remained around 8.20~8.40 during the cultivation (Figure 1A), like in previous reports (Yongmanitchai and Ward, 1991; Eustance et al., 2013). In the T+U medium, pH was increased sharply to peak at 9.18 and then gradually decreased to 7.3 with faster cell growth in the logarithmic phase (Figure 1A). This pH fluctuation might

TABLE 1 The specific growth rate, carbon and nitrogen consumption rate, and pigment content in the mixotrophic growth of *P. tricornutum* using $NaNO_3$ and the mixture of tryptone and urea (1:1, mol N:mol N) as nitrogen source at 20 mmol N $L^{-1}$ in shaking flasks.

| Index | $NaNO_3$ | Tryptone + urea |
|---|---|---|
| Specific growth rate ($day^{-1}$) | $0.12 \pm 0.01^b$ | $0.17 \pm 0.00^a$ |
| Glycerol consumption rate (mg $L^{-1}$ $day^{-1}$) | $183.33 \pm 6.80^b$ | $233.33 \pm 16.67^a$ |
| Nitrogen consumption rate (mg $L^{-1}$ $day^{-1}$) | $10.00 \pm 0.43^b$ | $11.50 \pm 0.50^a$ |
| Fucoxanthin content (pg $cell^{-1}$) | $0.32 \pm 0.03^b$ | $0.51 \pm 0.01^a$ |
| Chlorophyll *a* content (pg $cell^{-1}$) | $0.53 \pm 0.04^b$ | $1.10 \pm 0.07^a$ |

Different letters (a, b) indicate significant difference ($p< 0.05$). Glycerol (0.10 mol $L^{-1}$) was used as the organic carbon source in the mixotrophic medium.

relate to the priority utilization of nitrogen in the mixture of urea and free amino acids in the T+U medium. Moreover, the decline in nitrogen concentration was positively correlated with the increase of cell growth (Figures 1A, B). The consumption rate of total nitrogen (11.50 mg $L^{-1}$ $day^{-1}$) in the T+U medium was 15% higher than that in the $NaNO_3$ medium ($p< 0.05$) (Table 1).

In the T+U medium, the biomass productivity, glycerol consumption rate, fucoxanthin content, and chlorophyll *a* content were 245.2 mg $L^{-1}$ $day^{-1}$, 233.3 mg $L^{-1}$ $day^{-1}$, 16.11 mg $g^{-1}$, and 34.33 mg $g^{-1}$ (Figure 1C; Table 1), which were 40%, 27%, 157%, and 229% higher those in the $NaNO_3$ medium, respectively ($p< 0.05$). Notably, the increase of biomass productivity was higher than the increase of glycerol consumption rate, which indicated that the higher biomass accumulation in the T+U medium might be caused by the additional carbon supply from the organic nitrogen sources. A previous study demonstrated that carbon and nitrogen tend to flow toward carbohydrate and protein synthesis rather than the photosynthetic system under glycerol and $NaNO_3$ supply, which might explain the low content of photosynthetic pigments (fucoxanthin and chlorophyll *a*) in the $NaNO_3$ medium (Villanova et al., 2017). It is reported that urea induced higher biomass productivity than nitrate in *P. tricornutum* (Zhang et al., 2016), and higher biomass was obtained using tryptone compared with both nitrate and urea in the diatom *Nitzschia laevis* (Wen and Chen, 2001). Earlier research also demonstrated that a 36% increase of biomass and a 28% increase of fucoxanthin were obtained using the mixture of tryptone and urea compared to tryptone (Wang et al., 2021). It is noteworthy that cellular chlorophyll *a* (1.10 pg $cell^{-1}$) in the T+U medium was twice that in the nitrate medium with a 59% increase of cellular fucoxanthin ($p< 0.05$) (Table 1), indicating that the organic nitrogen source significantly promoted cellular pigment biosynthesis. Ammonium induced higher intracellular chlorophyll *a* concentrations in *P. tricornutum* compared with nitrate (Frada et al., 2013), and *Entomoneis paludosa* also reached the highest level of fucoxanthin content under ammonium compared to nitrate (Jauffrais et al., 2016) due to the high activities of the GS and GOGAT systems (Rees, 2003). Most of the available nitrogen (free amino acids and urea) in the T

+U medium was finally utilized intracellularly as ammonium (Smith et al., 2019; Contreras and Gillard, 2021), which might promote intracellular nitrogen metabolism and contribute to the increased biosynthesis of photosynthetic pigments including FCP.

Therefore, the mixture of tryptone and urea was the optimal nitrogen source for enhancing biomass and fucoxanthin production, in which tryptone provided a complex nutrition (free amino acids, peptides, vitamins, and growth factors). However, high cost and lower bioavailability limit its industrial-scale application. Thus, the following experiments were carried out to determine the dominant nitrogen components for utilization and simplify of the medium.

## Identification of the preferred amino acids in the T+U condition

To explore the amino acid utilization in the T+U medium, the concentration of free amino acids was monitored during the cultivation. As shown in Figure 2, leucine, lysine, arginine, and phenylalanine were the most abundant amino acids in the T+U medium (Figure 2A). When preferentially used up in 4~6 days, their nitrogen consumption rates reached 0.83, 2.09, 2.09, and 0.44 mg $L^{-1}$ $day^{-1}$, respectively (Figure 2C). Methionine, tyrosine, histidine, glutamate, and aspartic acid could be utilized to support cell growth as well (Figure 2A). A similar phenomenon was observed in previous studies, in which arginine, glutamate, leucine, and isoleucine could be used as sole nitrogen sources in *P. tricornutum*, and cells performed best by using arginine (Contreras and Gillard, 2021). A higher cell density was achieved by using arginine in *E. paludosa* compared with that using glutamine and glycine (Jauffrais et al., 2016). Interestingly, the rapid consumption of leucine, lysine, arginine, and phenylalanine was observed as the preferred amino acids (Figure 2A). Valine, serine, threonine, and alanine levels remained stable during the first 2 days and then increased sharply within the following 2 days (Figure 2B). Though the isoleucine content dropped slightly in the first 2 days, it reached the highest level on the fourth day. When the preferred amino acids were used up in the T+U medium after 6 days (Figure 2A), valine, serine, threonine, alanine, and isoleucine started to be consumed (Figure 2B). However, proline and glycine were secreted into the medium on the 4th and 10th day, respectively, without consumption during the cultivation (Figure 2B). The results were coincident with a previous report on *E. paludosa* where glycine was the worst nitrogen source for cell growth and pigment production (Jauffrais et al., 2016). A similar phenomenon was observed in *P. tricornutum* since proline and serine were hardly utilized after nitrogen deprivation (Rees and Allison, 2006). The intracellular glycine was reported as the only amino acid that increased in *P. tricornutum* after 4 days of cultivation (Ge et al., 2014), which was consistent with the trend of glycine in this study. Therefore, leucine, lysine, arginine, and

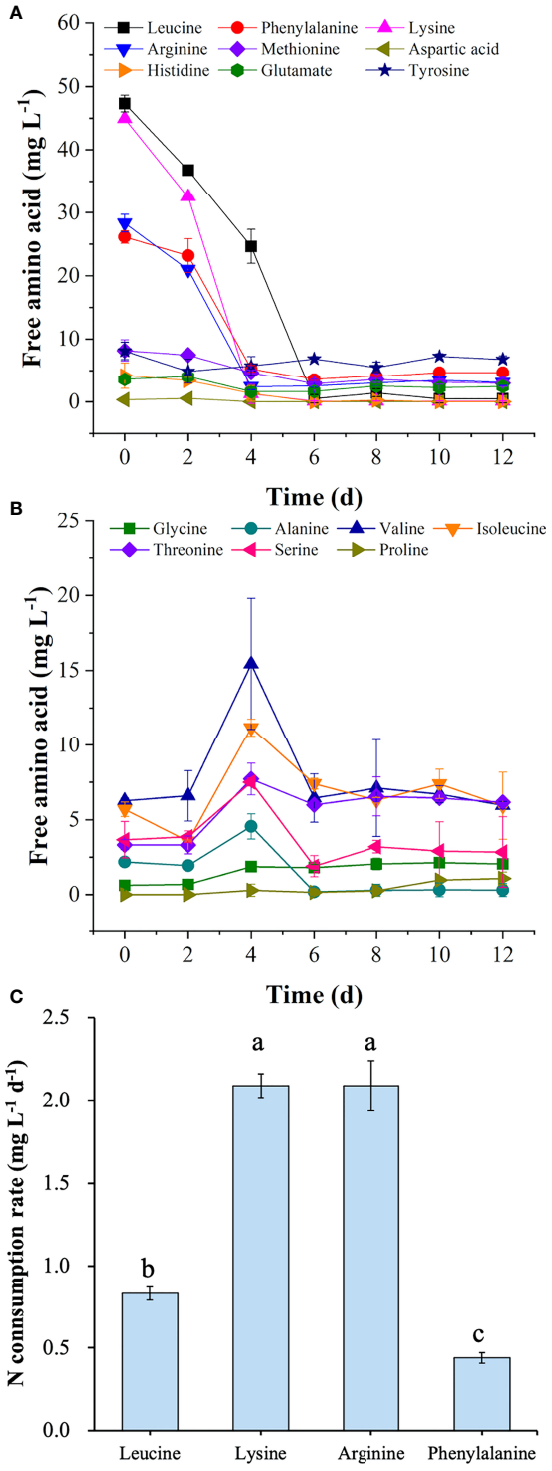


FIGURE 2
Concentrations of preferred free amino acids **(A)** and other free amino acids **(B)** in the medium and nitrogen consumption rates of four preferred amino acids **(C)** in the mixotrophic growth of *Phaeodactylum tricornutum* using organic nitrogen source (tryptone:urea = 1:1, mol N:mol N) at 20 mmol N $L^{-1}$. Different letters represent significant difference ($p<0.05$).

phenylalanine were identified as the preferred amino acids for *P. tricornutum* utilization.

To deeply understand nitrogen assimilation in *P. tricornutum*, the proposed assimilation pathway of amino acids and other nitrogen sources is summarized in Figure 3 according to the literature. In *P. tricornutum*, amino acids can be utilized mainly in two ways (Rees and Allison, 2006). On the one hand, amino acids are transported into cells by amino acid-specific transporters on the membrane systems and metabolized intracellularly (Flynn and Syrett, 1986). On the other hand, amino acids are oxidized to $NH_4^+$, α-keto acid, and hydrogen peroxide by extracellular L-amino acid oxidase (LAAO), then taken up by $NH_4^+$ transporters (AMT) on the membrane systems (Rees and Allison, 2006; Contreras and Gillard, 2021). Arginine and lysine can be assimilated by transporters directly and metabolized *in vivo* (Flynn and Wright, 1986; Rees and Allison, 2006). After entering the cells, arginine is converted to urea and ornithine by arginase (ARG) in the urea cycle in the mitochondrial membrane, and then urea is metabolized to $NH_4^+$ participating in the GS III-$GOGAT_{a,b}$ cycle in the mitochondria (Smith et al., 2019), contributing to cell growth and protein synthesis (Zhang et al., 2015). Meanwhile, lysine is transported into cells directly and catabolized by the α-amino adipic acid pathway to produce glutamate joining in the GS III-$GOGAT_{a,b}$ cycle (Arruda and Barreto, 2020), as well as acetyl-CoA, which finally enters the tricarboxylic acid (TCA) cycle contributing to carbohydrate accumulation (Zhang et al., 2015; Pan et al., 2020). In contrast, alanine, methionine, leucine, glutamate, valine, and asparagine are oxidized exclusively by LAAO extracellularly, and histidine is partially oxidized by LAAO in *P. tricornutum* (Rees and Allison, 2006; Contreras and Gillard, 2021). Phenylalanine, tyrosine, isoleucine, serine, threonine, aspartic acid, and glycine are also catalyzed by LAAO in other microalgae (Calatrava et al., 2019). It was reported that hydrogen peroxide produced by LAAO could not be utilized by cells and remained in the medium (Palenik and Morel, 1990), in which the accumulation of hydrogen peroxide triggered a massive cell death in *P. tricornutum* (Contreras and Gillard, 2021). Therefore, amino acids that are metabolized through LAAO are not considered favorable nitrogen sources for cell growth due to their indirect cell-damaging effect. All information above suggested that arginine and lysine are taken up by membrane transporters without hydrogen peroxide generation and have a great potential to be used as exclusive nitrogen sources for cell culturing and fucoxanthin production in *P. tricornutum*.

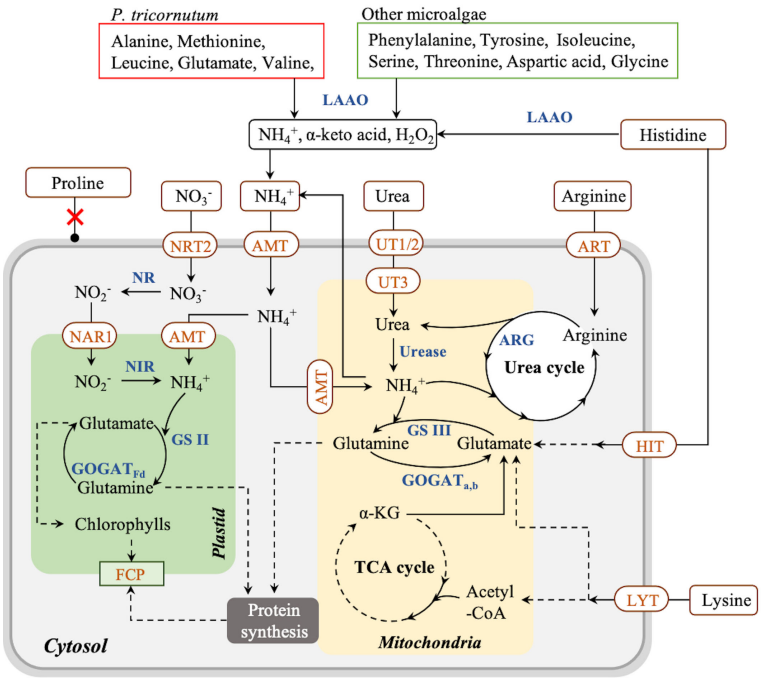


FIGURE 3
Proposed pathway of nitrogen assimilation in *Phaeodactylum tricornutum* and other microalgae. Solid arrow lines represent the direct reactions between the metabolites, and dash arrow lines represent the multistep reactions between those metabolites. Red boxes represent the amino acids consumed *via* LAAO by *P. tricornutum*; green boxes represent the amino acids consumed *via* LAAO by other microalgae. NRT, nitrate transporter; NAR, nitrite transporter; NR, nitrate reductase; NIR, nitrite reductase; GS, glutamine synthetase; GOGAT, glutamine 2-oxoglutarate aminotransferase; AMT, ammonium transporter; UT, urea transporter; ART, arginine transporter; ARG, arginase; HIT, histidine transporter; LYT, lysine transporter; LAAO, L-amino acid oxidase; FCP, fucoxanthin–chlorophyll–protein complex.

## Comparison of arginine and lysine on cell growth and chlorophyll fluorescent character

As the top 2 preferred amino acids in the T+U medium, arginine and lysine triggered the same nitrogen consumption rate (2.09 mg $L^{-1}$ $day^{-1}$) (Figure 2C). By taking into account the original nitrogen concentrations of arginine (0.61 mmol N $L^{-1}$) and lysine (0.65 mmol N $L^{-1}$) in the T+U medium (calculated from Figure 2A), the initial concentrations of arginine and lysine were set as 0.30, 0.60, 0.90, and 1.20 mmol N $L^{-1}$ for the comparative study. As shown in Figure 4A, the cell density was higher under arginine supply, and the higher concentration of nitrogen led to a higher biomass concentration, glycerol, and nitrogen consumption rate (Figures 4A–D). Compared with the lysine medium, the biomass concentration increased 6%~30% in the arginine medium with a 12%~42% increase of glycerol consumption rate (Figures 4B–D). After inoculation in the medium, both arginine and lysine were consumed immediately, and the maximum nitrogen consumption rate (7.93 mg $L^{-1}$ $day^{-1}$) on the second day was achieved in the 1.20 mmol N $L^{-1}$ arginine medium, which was 1.92-fold higher than the highest level in the 1.20 mmol N $L^{-1}$ lysine medium ($p< 0.05$) (Figure 4D). In the literature, cells also performed better in the arginine medium than in the lysine medium, and the uptake rate of arginine was 64% higher than that of lysine in *P. tricornutum* (Flynn and Syrett, 1986; Rees and Allison, 2006), indicating that cells preferred arginine to lysine. In *P. tricornutum*, arginine has four amino moieties and three of them finally participated in nitrogen metabolism through the urea cycle and the GS-GOGAT cycle (Smith et al., 2019), while lysine only has two amino moieties and one was transported to the nitrogen metabolism pathway *via* the saccharopine pathway to produce glutamate (Arruda and Barreto, 2020) (Figure 3), suggesting that arginine has a higher nitrogen conversion rate *in vivo*. According to the nitrogen consumption curves, arginine was consumed entirely, while lysine remained in trace amounts in the medium. Though cells reached a nitrogen-deficient state in later cultivation, the final chlorophyll fluorescence using arginine was still 36%~79% higher than lysine (Figure 4B). Contreras and Gillard reported that *P. tricornutum* obtained the highest chlorophyll *a* fluorescence under arginine supply compared to other amino acids. The photosynthetic capacity was positively correlated to fluorescence (Contreras and Gillard,

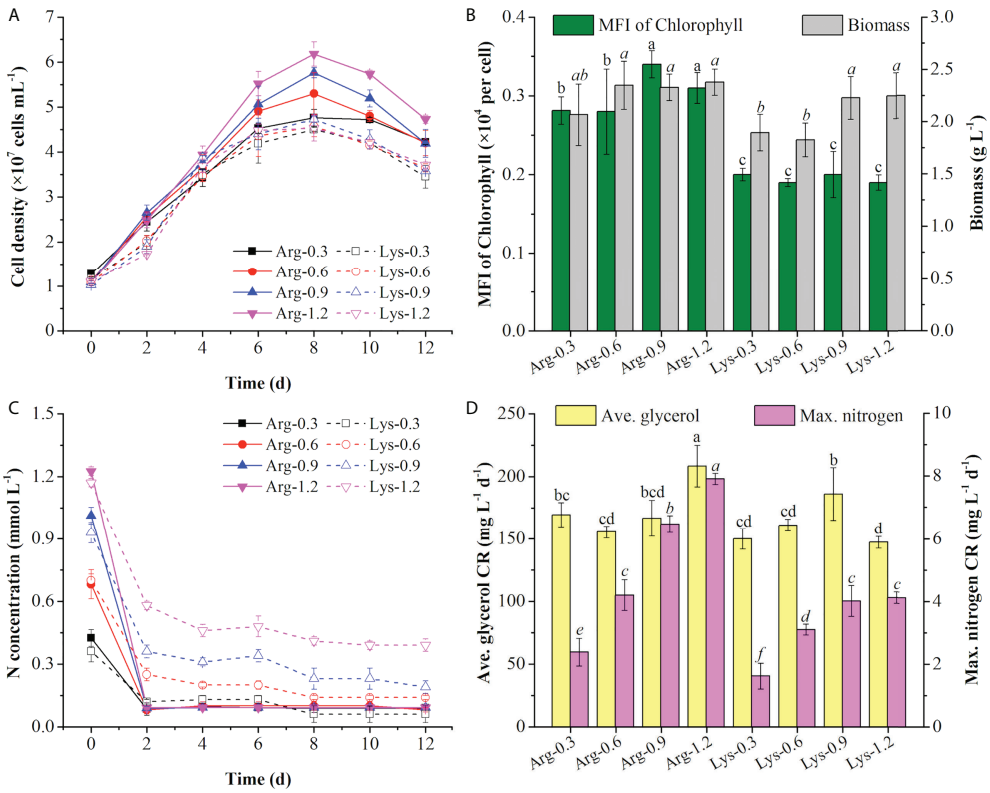


FIGURE 4
Cell density **(A)**, mean fluorescence intensity (MFI) of chlorophyll and biomass concentration **(B)**, nitrogen concentration **(C)**, and average (ave.) glycerol consumption rate and maximum (max.) nitrogen consumption rate **(D)** using arginine (Arg) and lysine (Lys) at 0.3, 0.6, 0.9, and 1.2 mmol N $L^{-1}$ in the mixotrophic medium. Different letters indicate a significant difference ($p< 0.05$).

2021), indicating that the photosynthetic system was more active in the arginine medium. Nitrogen starvation could significantly inhibit both growth and photosynthetic systems (including FCP) (Pajot et al., 2022); thus, the arginine supply was selected for an in-depth survey in the following experiments with the aim to obtain higher cell density, biomass, and photosynthetic capacity.

## Synergetic effect of arginine and urea on cell growth and pigment production

### Principal component analysis

To clarify the role of mixtures of organic nitrogen sources, urea was chosen to compare algal growth with or without the addition of arginine. The performance of cell growth under arginine, urea, and the mixture of arginine and urea (Arg + urea) in various concentrations is shown in Figure 5. Algal cultures showed a deeper brown color in the Arg + urea medium than in those media containing arginine or urea only. With the increase in nitrogen concentration, cells grew better in arginine and in the Arg + urea medium, but it was the opposite in the urea medium (Figure 5A–C). As shown in Figure 5D, a principal component analysis (PCA) was carried out according to the cell growth, nutrient consumption, pH change, and pigment production to understand the differences among various nitrogen sources. Principal component 1 (PC1) explained 77% of the total variation and showed a separated arginine cluster on the left, Arg + urea cluster on the right, and urea cluster in the middle. With the increase in nitrogen concentration, the dots in arginine and Arg + urea clusters exhibited a rightward shift, but the urea cluster showed the opposite trend. The separation in PC1 and PC2 suggested a significant difference between the three clusters with nitrogen types and concentrations.

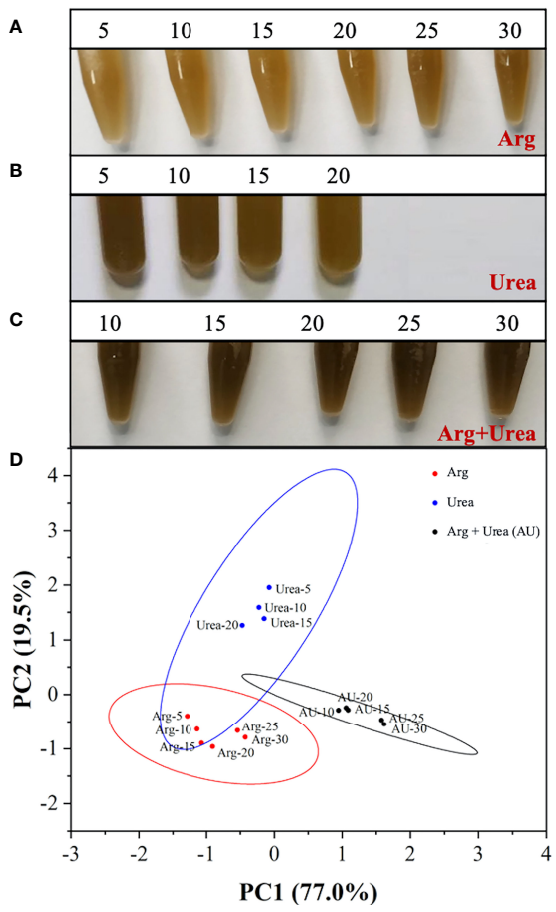


FIGURE 5
The images of the mixotrophic *Phaeodactylum tricornutum* at the end of cultivation using **(A)** Arg (5, 10, 15, 20, 25, 30 mmol N $L^{-1}$), **(B)** urea (5, 10, 15, 20 mmol N $L^{-1}$), and **(C)** the mixture of Arg and urea (10, 15, 20, 25, 30 mmol TN $L^{-1}$, in which urea was at 5 mmol N $L^{-1}$) as nitrogen source and **(D)** score plot of the principal component analysis (PCA) for cell growth performance and pigment production.

### Cell growth

The cell density increased rapidly after inoculating in both arginine and Arg + urea media. The specific growth rate was increased with the rise of nitrogen concentration, but it was the opposite in the urea medium (Figures 6A–C; Table 2) on the first 4 days, which were coincident with the color of algal cultures (Figure 5) and a previous report (Jauffrais et al., 2016). In the diatom *E. paludosa*, the cells obtained higher cell density under a higher concentration of arginine and achieved the maximum specific growth rate under a lower concentration of urea (Jauffrais et al., 2016). However, the cell growth became very slow after 4 days due to the sharp drop of pH in the arginine medium (Figure 6A). Though *P. tricornutum* continued to grow on the 10th day when adapted to low pH around 4.5, the cell densities (4.12~6.05 × $10^7$ cells $ml^{-1}$) on the 12th day were insignificantly different than those in the urea media (3.62~6.22 × $10^7$ cells $ml^{-1}$) but lower than those in the Arg + urea media. Obviously, the maximum cell density (9.21 × $10^7$ cells $ml^{-1}$) was obtained in the Arg + urea medium at 25 mmol N $L^{-1}$ even though the pH finally dropped to 5.23, which was 52% and 48% higher than those in the 30 mmol N $L^{-1}$ arginine and 5 mmol N $L^{-1}$ urea media, respectively (Figures 6A–C).

### pH and nitrogen consumption

Arginine is a basic amino acid with a positive charge in the side chain group, and the uptake of arginine results in the release of hydrogen ions resulting in the decrease of pH value (Allen et al., 2011). Under an acidic pH environment, the function of FCPs switched from light-harvesting to energy-quenching *via* regulation of energy transfer pathways (Nagao et al., 2020), which might explain why the cells stopped growing after 4 days at pH below 4.5 (Figures 6A, C). As shown in Figure 6D, arginine was fully consumed on the 4th day at 5 mmol N $L^{-1}$, and the Arg-N concentration curves in the other concentrations

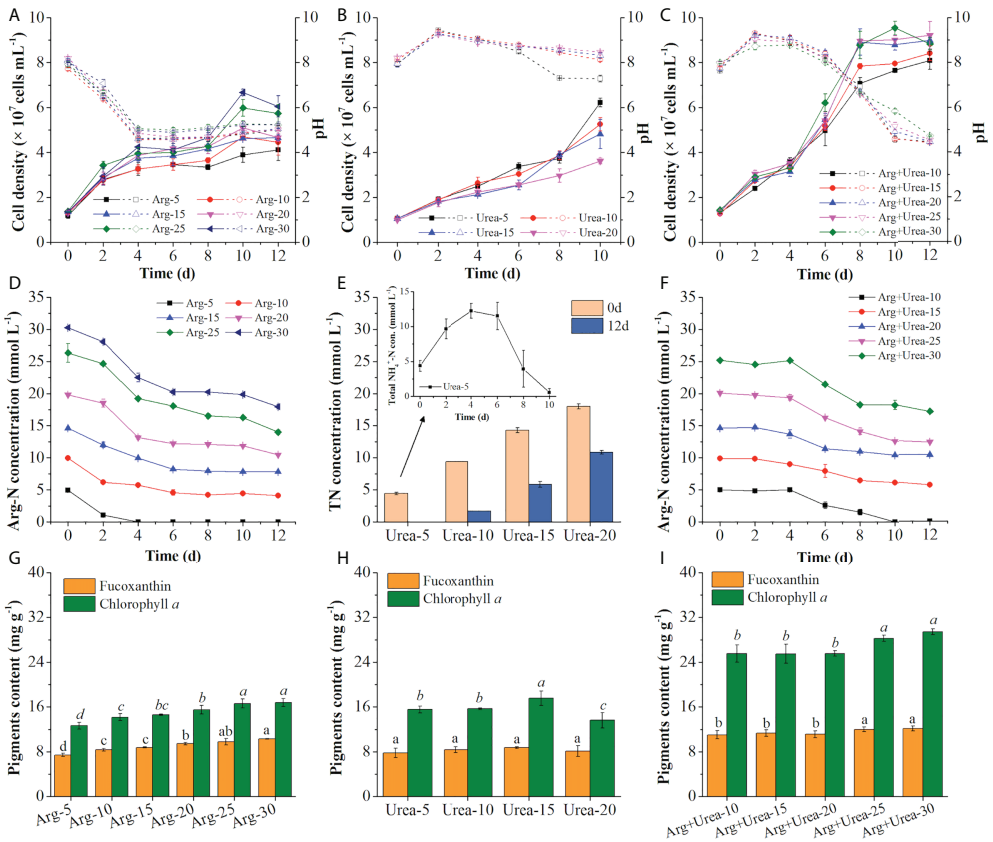


FIGURE 6
Cell density and pH value **(A–C)**, TN concentration in the medium **(D–F)**, and pigment contents **(G–I)** using Arg (5,10, 15, 20, 25, 30 mmol N $L^{-1}$) **(A, D, G)**, urea (5, 10, 15, 20 mmol N $L^{-1}$) **(B, E, H)**, and the mixture of Arg and urea (10, 15, 20, 25, 30 mmol TN $L^{-1}$, in which urea was at 5 mmol N $L^{-1}$) **(C, F, I)** as nitrogen sources. The solid and dotted lines represent cell density and pH value **(A–C)**, respectively. Total $NH_4^+$-N concentration (con.) represents $NH_4^+$ from the decomposed urea and secreted $NH_4^+$ from cells **(E)**. Different letters indicate a significant difference ($p < 0.05$).

indicated that the consumption rate of arginine also slowed down due to the decrease of pH, which was coincident with the cell growth curve (Figure 6A). pH showed an increase after inoculation of seed cultures in the urea medium within 48 h and then decreased slightly except in 5 mmol N $L^{-1}$ of urea, in which pH decreased to 7.28 after the 8th day (Figure 6B). Similar results were observed that the utilization of urea would not change the pH in the medium at the beginning (Eustance et al., 2013) and decreased to around 7.0 at the end of the culture period (Wen and Chen, 2001). It was reported that urea was metabolized intracellularly to form $NH_4^+$ and secreted it into the medium when urea was used as the only nitrogen source, causing an elevation of pH (Dhup et al., 2016). The medium with 5 mmol N $L^{-1}$ of urea showed a rise in total $NH_4^+$-N concentration during the first 4 days and complete consumption on the 12th day (Figure 6E). Because extracellular urea-N concentration in the medium was determined by the chromogenic reaction of $NH_4^+$ generated from urea *via* the urease kit, the fluctuating curve of total nitrogen demonstrated the secretion of extra $NH_4^+$ in the medium (Figure 6E). The secretion and consumption of extra $NH_4^+$ caused the rise and decline of pH in the medium with 5 mmol N $L^{-1}$ of urea (Wen and Chen, 2001; Eustance et al., 2013). Compared with the solo arginine media, the addition of 5 mmol N $L^{-1}$ of urea in the arginine medium increased cell density and also maintained the pH in the range of 7.96~9.30 during the first 6 days as expected (Figure 6C). As shown in Figure 6F, arginine was barely consumed on the first 4 days with an increase of pH (Figure 6C), indicating that cells preferred to uptake urea at the beginning in the Arg + urea medium. After the fourth day, cells entered the logarithmic phase in the Arg +urea medium and entered the stationary phase on the eighth day when the pH decreased to 6.60 (Figure 6C).

## Biomass and pigment production

As shown in Figures 6G–I; Table 2, biomass productivity, glycerol consumption rate, and pigment content were increased with the rise of nitrogen concentrations in arginine and Arg + urea

TABLE 2 The specific growth rate, biomass concentration, glycerol consumption rate (CR), and productivities of biomass and fucoxanthin in the mixotrophic growth of *Phaeodactylum tricornutum* using different types and concentrations of nitrogen sources in shaking flasks.

| N sources | $\mu$ (day$^{-1}$) | Biomass (g L$^{-1}$) | Glycerol CR (mg L$^{-1}$ day$^{-1}$) | Productivity (mg L$^{-1}$ day$^{-1}$) | |
|---|---|---|---|---|---|
| | | | | Biomass | Fucoxanthin |
| Arginine (mmol N L$^{-1}$) | | | | | |
| 5 | 0.10 ± 0.01$^{c}$ | 1.37 ± 0.14$^{b}$ | 77.78 ± 9.62$^{b}$ | 67.71 ± 9.28$^{b}$ | 0.31 ± 0.06$^{d}$ |
| 10 | 0.10 ± 0.01$^{c}$ | 1.37 ± 0.10$^{b}$ | 77.78 ± 4.81$^{b}$ | 61.86 ± 4.37$^{b}$ | 0.42 ± 0.05$^{c}$ |
| 15 | 0.10 ± 0.00$^{c}$ | 1.42 ± 0.07$^{b}$ | 80.56 ± 4.81$^{b}$ | 65.61 ± 1.24$^{b}$ | 0.49 ± 0.04$^{c}$ |
| 20 | 0.11 ± 0.01$^{bc}$ | 1.46 ± 0.04$^{b}$ | 80.56 ± 4.81$^{b}$ | 69.37 ± 2.26$^{b}$ | 0.61 ± 0.89$^{b}$ |
| 25 | 0.12 ± 0.01$^{ab}$ | 1.76 ± 0.12$^{a}$ | 88.89 ± 4.81$^{ab}$ | 99.61 ± 4.69$^{a}$ | 0.89 ± 0.03$^{a}$ |
| 30 | 0.12 ± 0.01$^{a}$ | 1.78 ± 0.10$^{a}$ | 100.00 ± 16.67$^{a}$ | 97.10 ± 6.89$^{a}$ | 0.99 ± 0.08$^{a}$ |
| Urea (mmol N L$^{-1}$) | | | | | |
| 5 | 0.18 ± 0.00$^{a}$ | 2.24 ± 0.24$^{a}$ | 103.33 ± 5.77$^{a}$ | 142.93 ± 21.43$^{a}$ | 0.31 ± 0.06$^{a}$ |
| 10 | 0.16 ± 0.01$^{ab}$ | 1.92 ± 0.14$^{a}$ | 103.33 ± 11.55$^{a}$ | 111.70 ± 13.95$^{b}$ | 0.19 ± 0.05$^{b}$ |
| 15 | 0.15 ± 0.02$^{b}$ | 2.04 ± 0.10$^{a}$ | 86.67 ± 5.77$^{b}$ | 120.01 ± 6.25$^{a}$ | 0.37 ± 0.02$^{a}$ |
| 20 | 0.13 ± 0.01$^{b}$ | 2.03 ± 0.14$^{a}$ | 90.00 ± 0.00$^{b}$ | 120.92 ± 11.51$^{a}$ | 0.23 ± 0.04$^{ab}$ |
| Arginine + urea (mmol N L$^{-1}$)* | | | | | |
| 10 | 0.15 ± 0.01$^{b}$ | 2.59 ± 0.08$^{b}$ | 236.11 ± 17.35$^{b}$ | 166.13 ± 4.62$^{c}$ | 1.83 ± 0.09$^{c}$ |
| 15 | 0.16 ± 0.01$^{ab}$ | 2.75 ± 0.08$^{b}$ | 230.56 ± 17.35$^{b}$ | 180.73 ± 3.48$^{b}$ | 2.05 ± 0.07$^{b}$ |
| 20 | 0.15 ± 0.00$^{b}$ | 2.82 ± 0.20$^{b}$ | 230.56 ± 4.81$^{b}$ | 180.52 ± 10.16$^{b}$ | 2.06 ± 0.04$^{b}$ |
| 25 | 0.16 ± 0.00$^{a}$ | 3.13 ± 0.17$^{a}$ | 260.11 ± 9.62$^{a}$ | 209.72 ± 11.78$^{a}$ | 2.59 ± 0.05$^{a}$ |
| 30 | 0.15 ± 0.00$^{b}$ | 3.18 ± 0.12$^{a}$ | 247.22 ± 4.81$^{ab}$ | 217.86 ± 4.69$^{a}$ | 2.68 ± 0.05$^{a}$ |

Different letters (a–d) indicate significant difference ($p< 0.05$). Glycerol (0.10 mol L$^{-1}$) was used as the organic carbon source in the mixotrophic medium.
*Total nitrogen amount, in which urea was at 5 mmol N L$^{-1}$.

media. The maximum biomass concentration (3.18 g L$^{-1}$) and productivity (217.9 mg L$^{-1}$ day$^{-1}$) with a glycerol consumption rate of 247.22 mg L$^{-1}$ day$^{-1}$ were achieved under 30 mmol TN L$^{-1}$ of Arg + urea medium, significantly higher than the solo arginine or urea medium ($p< 0.05$) (Table 2). In contrast, the biomass productivity in the urea media reached the highest level (142.93 mg L$^{-1}$ day$^{-1}$) at 5 mmol N L$^{-1}$, 47% higher than that at 30 mmol N L$^{-1}$ of arginine (Table 2). However, fucoxanthin content (7.79 mg g$^{-1}$) and productivity (0.31 mg L$^{-1}$ day$^{-1}$) were decreased by 24% and 69%, respectively, suggesting that urea addition could significantly promote biomass production but reduce the biosynthesis of fucoxanthin. A previous study reported that more arginine–carbon was respired with the same uptake rate when ammonium and arginine were both present in the medium (Flynn and Wright, 1986). In this study, the addition of urea in the arginine medium provided sufficient ammonium *in vivo*. It could induce the assimilation of arginine, which might explain the higher biomass accumulation in the Arg + urea media. Furthermore, the maximum contents of fucoxanthin (12.17 mg g$^{-1}$) and chlorophyll *a* (29.45 mg g$^{-1}$) were both obtained at the highest concentration (30 mmol TN L$^{-1}$) in the Arg + urea medium ($p< 0.05$), significantly increased by 18%~64% and 68%~133% compared with the solo arginine and urea media, respectively (Figures 6G–I). Fucoxanthin and chlorophyll *a* share the geranylgeranyl pyrophosphate building block that forms from pyruvate as a precursor. The biosynthesis of chlorophyll additionally requires the participation of glutamate (Bertrand, 2010; Meier et al., 2011). The synergetic effect of arginine and urea might promote the activity of the urea cycle, GS-GOGAT cycle, and TCA cycle (Figure 3), providing more substrate for the biosynthesis of photosynthetic pigments and proteins, leading to the higher contents of fucoxanthin and chlorophyll *a*. After 12 days of cultivation, the highest fucoxanthin productivity (2.68 mg L$^{-1}$ day$^{-1}$) was observed in the Arg + urea medium with 30 mmol TN L$^{-1}$, 2.71-fold and 8.64-fold higher than that in the arginine medium at 30 mmol N L$^{-1}$ and in the urea medium at 5 mmol N L$^{-1}$, respectively (Table 2), but had no significant difference with the Arg + urea medium at 25 mmol TN L$^{-1}$. In the literature, *P. tricornutum* was cultivated under complex organic carbon or nitrogen sources, but the bottleneck still remained for the simultaneous accumulation of biomass and fucoxanthin. For example, the fucoxanthin content achieved 17.55 mg g$^{-1}$ with the supplementation of 1.5 ml L$^{-1}$ of *Laminaria japonica* hydrolysate in *P. tricornutum*, while the biomass was only 1.59 g L$^{-1}$ (Wang et al., 2022). When the spruce hydrolysate and yeast extract (C/N = 60) were used as carbon and nitrogen sources, biomass concentration reached 3.31 g L$^{-1}$, but carotenoid concentration only achieved 16.92 mg L$^{-1}$, in which the fucoxanthin concentration was lower (Patel et al., 2019). In this study, the maximum biomass productivity (217.9 mg L$^{-1}$ day$^{-1}$) and fucoxanthin content (12.17 mg g$^{-1}$) in the Arg + urea medium at 30 mmol TN L$^{-1}$ were 24% and 94% higher than those in the nitrate medium (Figure 1). We could thus realize the simultaneous accumulation of biomass and fucoxanthin and provide an efficient strategy for fucoxanthin production by mixotrophic *P. tricornutum*. In future studies, a higher biomass

and fucoxanthin productivity could be expected with pH control in synergetic systems of arginine and urea by mixotrophic cultivation of *P. tricornutum*.

## Conclusion

In this study, various inorganic and organic nitrogen sources were evaluated for improving cell growth and fucoxanthin production by mixotrophic *P. tricornutum*. Arginine was proven as the dominant amino acid for promoting cell growth compared to other free amino acids in tryptone and urea media. The synergetic effect of arginine and urea in the mixotrophic medium with 0.1 mol $L^{-1}$ glycerol addition could promote biomass production and fucoxanthin biosynthesis simultaneously, achieving the highest productivity of biomass (217.9 mg $L^{-1}$ $day^{-1}$) and fucoxanthin (2.68 mg $L^{-1}$ $day^{-1}$). The present study provided new insights into fucoxanthin biosynthesis promoted by nitrogen metabolism, facilitating the development of an efficient process for enhancing fucoxanthin production by mixotrophic *P. tricornutum*.

## Author contributions

RY: investigation, data curation, formal analysis, methodology, conceptualization, and writing—original draft. DW: conceptualization, supervision, and writing—review and editing. GP: supervision and writing—review and editing. All authors contributed to the article and approved the submitted version.

## Funding

This work was supported by Guangdong Basic and Applied Basic Research Foundation (2019B1515120002). This work was partly supported by the 111 Project (B17018).

## Conflict of interest

The authors declare that the research was conducted in the absence of any commercial or financial relationships that could be construed as a potential conflict of interest.

## Publisher's note

All claims expressed in this article are solely those of the authors and do not necessarily represent those of their affiliated organizations, or those of the publisher, the editors and the reviewers. Any product that may be evaluated in this article, or claim that may be made by its manufacturer, is not guaranteed or endorsed by the publisher.

## References

Alipanah, L., Rohloff, J., Winge, P., Bones, A. M., and Brembu, T. (2015). ). whole-cell response to nitrogen deprivation in the diatom phaeodactylum tricornutum. *J. Exp. Bot.* 66 (20), 6281–6296. doi: 10.1093/jxb/erv340

Allen, A. E., Dupont, C. L., Obornik, M., Horak, A., Nunes-Nesi, A., McCrow, J. P., et al. (2011). Evolution and metabolic significance of the urea cycle in photosynthetic diatoms. *Nature* 473 (7346), 203–209. doi: 10.1038/nature10074

Arruda, P., and Barreto, P. (2020). Lysine catabolism through the saccharopine pathway: Enzymes and intermediates involved in plant responses to abiotic and biotic stress. *Front. Plant Sci.* 11. doi: 10.3389/fpls.2020.00587

Bertrand, M. (2010). Carotenoid biosynthesis in diatoms. *Photosynthesis Res.* 106 (1-2), 89–102. doi: 10.1007/s11120-010-9589-x

Calatrava, V., Hom, E. F. Y., Llamas, A., Fernandez, E., and Galvan, A. (2019). Nitrogen scavenging from amino acids and peptides in the model alga chlamydomonas reinhardtii. The role of extracellular l-amino oxidase. *Algal Research-Biomass Biofuels Bioproducts* 38, 11. doi: 10.1016/j.algal.2018.101395

Ceron-Garcia, M. C., Fernandez-Sevilla, J. M., Sanchez-Miron, A., Garcia-Camacho, F., Contreras-Gomez, A., and Molina-Grima, E. (2013). Mixotrophic growth of phaeodactylum tricornutum on fructose and glycerol in fed-batch and semi-continuous modes. *Bioresource Technol.* 147, 569–576. doi: 10.1016/j.biortech.2013.08.092

Contreras, J. A., and Gillard, J. T. F. (2021). Asparagine-based production of hydrogen peroxide triggers cell death in the diatom phaeodactylum tricornutum. *Bot. Lett.* 168(1), 6–17 doi: 10.1080/23818107.2020.1754289

de Gonzalez, M. T. N., Attaie, R., Mora-Gutierrez, A., Woldesenbet, S., and Jung, Y. (2021). Stability of fucoxanthin in pasteurized skim and whole goat milk. *Foods* 10 (7), 10. doi: 10.3390/foods10071647

Delbrut, A., Albina, P., Lapierre, T., Pradelles, R., and Dubreucq, E. (2018). Fucoxanthin and polyunsaturated fatty acids Co-extraction by a green process. *Molecules* 23 (4), 874. doi: 10.3390/molecules23040874

Dhup, S., Kannan, D. C., and Dhawan, V. (2016). Understanding urea assimilation and its effect on lipid production and fatty acid composition of scenedesmus sp. *SOJ Biochem.* 2 (1), 7. doi: 10.15226/2376-4589/2/1/00112

Eustance, E., Gardner, R. D., Moll, K. M., Menicucci, J., Gerlach, R., and Peyton, B. M. (2013). Growth, nitrogen utilization and biodiesel potential for two chlorophytes grown on ammonium, nitrate or urea. *J. Appl. Phycol* 25 (6), 1663–1677. doi: 10.1007/s10811-013-0008-5

Flynn, K. J., and Syrett, P. J. (1986). Utilization of l-lysine and l-arginine by the diatom phaeodactylum-tricornutum. *Mar. Biol.* 90 (2), 159–163. doi: 10.1007/bf00569122

Flynn, K. J., and Wright, C. R. N. (1986). The simultaneous assimilation of ammonium and l-arginine by the marine diatom phaeodactylum-tricornutum bohlin. *J. Exp. Mar. Biol. Ecol.* 95 (3), 257–269. doi: 10.1016/0022-0981(86)90258-3

Frada, M. J., Burrows, E. H., Wyman, K. D., and Falkowski, P. G. (2013). Quantum requirements for growth and fatty acid biosynthesis in the marine diatom phaeodactylum tricornutum (Bacillariophyceae) in nitrogen replete and limited conditions. *J. Phycol* 49 (2), 381–388. doi: 10.1111/jpy.12046

Gao, B. Y., Chen, A. L., Zhang, W. Y., Li, A. F., and Zhang, C. W. (2017). Co-Production of lipids, eicosapentaenoic acid, fucoxanthin, and chrysolaminarin by phaeodactylum tricornutum cultured in a flat-plate photobioreactor under varying nitrogen conditions. *J. Ocean Univ. China* 16 (5), 916–924. doi: 10.1007/s11802-017-3174-2

Ge, F., Huang, W. C., Chen, Z., Zhang, C. Y., Xiong, Q., Bowler, C., et al. (2014). Methylcrotonyl-CoA carboxylase regulates triacylglycerol accumulation in the model diatom phaeodactylum tricornutum. *Plant Cell* 26 (4), 1681–1697. doi: 10.1105/tpc.114.124982

Hu, H., Pan, Y., and Yu, C. (2019). *Use of branched chain amino acids for culturing phaeodactylum tricornutum having high neutral lipid content (in Chinese).* Hubei, China: Chinese Acad. Sci. Inst, Hydrobiology. CN110819536.

Jauffrais, T., Jesus, B., Meleder, V., Turpin, V., Russo, A., Raimbault, P., et al. (2016). Physiological and photophysiological responses of the benthic diatom entomoneis paludosa (Bacillariophyceae) to dissolved inorganic and organic nitrogen in culture. *Mar. Biol.* 163 (5), 14. doi: 10.1007/s00227-016-2888-9

Lourenco-Lopes, C., Fraga-Corral, M., Jimenez-Lopez, C., Carpena, M., Pereira, A. G., Garcia-Oliveira, P., et al. (2021). Biological action mechanisms of fucoxanthin extracted from algae for application in food and cosmetic industries. *Trends Food Sci. Technol.* 117, 163–181. doi: 10.1016/j.tifs.2021.03.012

Luo, X., Chen, J., and Wei, D. (2020). High efficient assimilation of NO3- -n with coproduction of microalgal proteins by chlorella pyrenoidosa (in Chinese). *Chin. J. Biotechnol.* 36 (06), 1150–1161. doi: 10.13345/j.cjb.190358

McClure, D. D., Luiz, A., Gerber, B., Barton, G. W., and Kavanagh, J. M. (2018). An investigation into the effect of culture conditions on fucoxanthin production using the marine microalgae phaeodactylum tricornutum. *Algal Research-Biomass Biofuels Bioproducts* 29, 41–48. doi: 10.1016/j.algal.2017.11.015

Meier, S., Tzfadia, O., Vallabhaneni, R., Gehring, C., and Wurtzel, E. T. (2011). A transcriptional analysis of carotenoid, chlorophyll and plastidial isoprenoid biosynthesis genes during development and osmotic stress responses in arabidopsis thaliana. *BMC Syst. Biol.* 5, 19. doi: 10.1186/1752-0509-5-77

Mok, I. K., Yoon, J. R., Pan, C. H., and Kim, S. M. (2016). Development, quantification, method validation, and stability study of a novel fucoxanthin-fortified milk. *J. Agric. Food Chem.* 64 (31), 6196–6202. doi: 10.1021/acs.jafc.6b02206

Nagao, R., Yokono, M., Ueno, Y., Shen, J.-R., and Akimoto, S. (2020). Acidic pH-induced modification of energy transfer in diatom fucoxanthin chlorophyll a/c-binding proteins. *J. Phys. Chem. B* 124 (24), 4919–4923. doi: 10.1021/acs.jpcb.0c04231

Pajot, A., Lavaud, J., Carrier, G., Garnier, M., Saint-Jean, B., Rabilloud, N., et al. (2022). The fucoxanthin chlorophyll a/c-binding protein in tisochrysis lutea: influence of nitrogen and light on fucoxanthin and chlorophyll a/c-binding protein gene expression and fucoxanthin synthesis. *Front. Plant Sci.* 13. doi: 10.3389/fpls.2022.830069

Palenik, B., and Morel, F. M. M. (1990). Amino-acid utilization by marine-phytoplankton - a novel mechanism. *Limnol Oceanogr* 35 (2), 260–269. doi: 10.4319/lo.1990.35.2.0260

Pan, Y., Hu, F., Yu, C., Li, C., Huang, T., and Hu, H. (2020). Amino acid catabolism during nitrogen limitation in phaeodactylum tricornutum. *Front. Plant Sci.* 11. doi: 10.3389/fpls.2020.589026

Patel, A., Matsakas, L., Hruzova, K., Rova, U., and Christakopoulos, P. (2019). Biosynthesis of nutraceutical fatty acids by the oleaginous marine microalgae phaeodactylum tricornutum utilizing hydrolysates from organosolv-pretreated birch and spruce biomass. *Mar. Drugs* 17 (2), 119. doi: 10.3390/md17020119

Rajauria, G., Foley, B., and Abu-Ghannam, N. (2017). Characterization of dietary fucoxanthin from himanthalia elongata brown seaweed. *Food Res. Int.* 99 (3), 995–1001. doi: 10.1016/j.foodres.2016.09.023

Rees, T. A. V. (2003). Mitochondrial oxidative phosphorylation is required for ammonium assimilation in light in a marine diatom. *Physiol Plantarum* 117 (4), 558–563. doi: 10.1034/j.1399-3054.2003.00074.x

Rees, T. A. V., and Allison, V. J. (2006). Evidence for an extracellular l-amino acid oxidase in nitrogen-deprived phaeodactylum tricornutum (Bacillariophyceae) and inhibition of enzyme activity by dissolved inorganic carbon. *Phycologia* 45 (3), 337–342. doi: 10.2216/04-92.1

Remmers, I. M., D'Adamo, S., Martens, D. E., de Vos, R. C. H., Mumm, R., America, A. H. P., et al. (2018). Orchestration of transcriptome, proteome and metabolome in the diatom phaeodactylum tricornutum during nitrogen limitation. *Algal Research-Biomass Biofuels Bioproducts* 35, 33–49. doi: 10.1016/j.algal.2018.08.012

Seth, K., Kumar, A., Rastogi, R. P., Meena, M., Vinayak, V., and Harish, (2021). Bioprospecting of fucoxanthin from diatoms-challenges and perspectives. *Algal Research-Biomass Biofuels Bioproducts* 60, 10. doi: 10.1016/j.algal.2021.102475

Shen, Y., Hu, L. T., Xia, B., Ni, Z. J., Elam, E., Thakur, K., et al. (2021). Effects of different sulfur-containing substances on the structural and flavor properties of defatted sesame seed meal derived maillard reaction products. *Food Chem.* 365, 11. doi: 10.1016/j.foodchem.2021.130463

Shim, Y. S., Yoon, W. J., Ha, J., Seo, D., Lee, K. W., Lee, W. Y., et al. (2013). Method validation of 16 types of structural amino acids using an automated amino acid analyzer. *Food Sci. Biotechnol.* 22 (6), 1567–1571. doi: 10.1007/s10068-013-0252-0

Smith, S. R., Dupont, C. L., McCarthy, J. K., Broddrick, J. T., Obornik, M., Horak, A., et al. (2019). Evolution and regulation of nitrogen flux through compartmentalized metabolic networks in a marine diatom. *Nat. Commun.* 10, 14. doi: 10.1038/s41467-019-12407-y

Sun, H., Yang, S. F., Zhao, W. Y., Kong, Q., Zhu, C. L., Fu, X. D., et al. (2022). Fucoxanthin from marine microalgae: A promising bioactive compound for industrial production and food application. *Crit. Rev. Food Sci. Nutr.*, 1–18. doi: 10.1080/10408398.2022.2054932

Tu, Y. (2018). Determination of total free amino acid in tea by ninhydrin (in Chinese). *Modern Agric. Sci. Technol.* 14, 238. Available at: https://kns.cnki.net/kcms/detail/34.1278.S.20180724.1139.290.html

Villanova, V., Fortunato, A. E., Singh, D., Dal Bo, D., Conte, M., Obata, T., et al. (2017). Investigating mixotrophic metabolism in the model diatom phaeodactylum tricornutum. *Philos. Trans. R. Soc. B-Biol Sci.* 372 (1728), 1–14. doi: 10.1098/rstb.2016.0404

Wang, Z. P., Wang, P. K., Ma, Y., Lin, J. X., Wang, C. L., Zhao, Y. X., et al. (2022). Laminaria japonica hydrolysate promotes fucoxanthin accumulation in phaeodactylum tricornutum. *Bioresource Technol.* 344, 4. doi: 10.1016/j.biortech.2021.126117

Wang, S., Yang, R., Song, P., and Wei, D. (2021). Improving production of biomass and fucoxanthin in mixotrophic phaeodactylum tricornutum by optimization of carbon and nitrogen sources (in Chinese). *J. Food Sci. Biotechnol.* 40 (10), 82–90. doi: 10.3969/j.issn

Wang, W. D., Yu, L. J., Xu, C. Z., Tomizaki, T., Zhao, S. H., Umena, Y., et al. (2019). Structural basis for blue-green light harvesting and energy dissipation in diatoms. *Science* 363 (6427), 598. doi: 10.1126/science.aav0365

Wang, H., Zhang, Y., Chen, L., Cheng, W., and Liu, T. (2018). Combined production of fucoxanthin and EPA from two diatom strains phaeodactylum tricornutum and cylindrotheca fusiformis cultures. *Bioprocess Biosyst. Eng.* 41 (7), 1061–1071. doi: 10.1007/s00449-018-1935-y

Wen, Z. Y., and Chen, F. (2001). Optimization of nitrogen sources for heterotrophic production of eicosapentaenoic acid by the diatom nitzschia laevis. *Enzyme Microb Technol.* 29 (6-7), 341–347. doi: 10.1016/s0141-0229(01)00385-4

Winter, G., Todd, C. D., Trovato, M., Forlani, G., and Funck, D. (2015). Physiological implications of arginine metabolism in plants. *Front. Plant Sci.* 6. doi: 10.3389/fpls.2015.00534

Yang, R., and Wei, D. (2020). Improving fucoxanthin production in mixotrophic culture of marine DiatomPhaeodactylum tricornutumby LED light shift and nitrogen supplementation. *Front. Bioengineering Biotechnol.* 8. doi: 10.3389/fbioe.2020.00820

Yang, R. Q., Wei, D., and Xie, J. (2020). Diatoms as cell factories for high-value products: chrysolaminarin, eicosapentaenoic acid, and fucoxanthin. *Crit. Rev. Biotechnol.* 40 (7), 993–1009. doi: 10.1080/07388551.2020.1805402

Yongmanitchai, W., and Ward, O. P. (1991). Growth of and omega-3-fatty-acid production by phaeodactylum-tricornutum under different culture conditions. *Appl. Environ. Microbiol.* 57 (2), 419–425. doi: 10.1128/aem.57.2.419-425.1991

Zhang, W., Gao, B., Li, A., and Zhang, C. (2016). Effects of different culture conditions on growth and accumulation of bioactive compounds by phaeodactylum tricornutum. *Mar. Sci.* 40 (5), 57–65. doi: 10.11759/hykx20150706002

Zhang, W. G., Zhang, Z. H., and Yan, S. H. (2015). Effects of various amino acids as organic nitrogen sources on the growth and biochemical composition of chlorella pyrenoidosa. *Bioresource Technol.* 197, 458–464. doi: 10.1016/j.biortech.2015.08.100

frontiers | Frontiers in Marine Science

TYPE Original Research
PUBLISHED 15 September 2022
DOI 10.3389/fmars.2022.934504



OPEN ACCESS

EDITED BY
Liandong Zhu,
Wuhan University, China

REVIEWED BY
Haiqing Yu,
Shandong University, China
Jeffrey Ren,
National Institute of Water and Atmospheric Research (NIWA), New Zealand

*CORRESPONDENCE
Xianyong Zhao
zhaoxy@ysfri.ac.cn

SPECIALTY SECTION
This article was submitted to Marine Fisheries, Aquaculture and Living Resources, a section of the journal Frontiers in Marine Science

RECEIVED 02 May 2022
ACCEPTED 17 August 2022
PUBLISHED 15 September 2022

CITATION
Zhao Y, Wang X, Zhao X and Ying Y (2022) A statistical assessment of the density of Antarctic krill based on "chaotic" acoustic data collected by a commercial fishing vessel. *Front. Mar. Sci.* 9:934504. doi: 10.3389/fmars.2022.934504



# A statistical assessment of the density of Antarctic krill based on "chaotic" acoustic data collected by a commercial fishing vessel

Yunxia Zhao[1], Xinliang Wang[1,2], Xianyong Zhao[1,2]* and Yiping Ying[1]

[1]Key Laboratory of Sustainable Development of Polar Fisheries, Ministry of Agriculture and Rural Affairs, Yellow Sea Fisheries Research Institute, Chinese Academy of Fishery Science, Qingdao, China, [2]Joint Laboratory for Open Sea Fishery Engineering, Pilot National Laboratory for Marine Science and Technology (Qingdao), Qingdao, China

With the development of acoustic data processing technology, it is possible to make full use of the "chaotic" acoustic data obtained by fishing vessels. The purpose of this study is to explore a feasible statistical approach to assess the Antarctic krill density rationally and scientifically based on the acoustic data collected during routine fishing operations. The acoustic data used in this work were collected from the surveys conducted by the Chinese krill fishing vessel F/V *Fu Rong Hai* since the 2015/16 fishing season in the Bransfield Strait. We first processed acoustic data into small units of 0.1 nm, then selected the location of the central fishing ground for grid processing. Because of many zero and low values, we established a Regional Gridding and Extended Delta-distribution (RGED) model to evaluate the acoustic density of the krill. We defined the selection coefficient of grid size by using the coefficient of variation (CV) of the mean density and the weight of the effective covered area of the grids. Through the comparison of selection indexes, cells of 5′S × 10′W were selected as a computational grid and applied to the hotspot in the Bransfield Strait. Acoustic data reveal the distribution of krill density to be spatially heterogeneous. The CV of the mean density for 4 months converges at ~15% for cells of 5′S × 10′W. Simulations estimate krill resource densities in February to be ~1990 $m^2$ $nm^{-2}$ and to increase to ~8760 $m^2$ $nm^{-2}$ in May (4.4 times higher). We deem the RGED model to be useful to explore dynamic changes in krill resources in the hotspot. It is not only of great significance for guiding krill fishery, but it also provides krill density data for studying the formation mechanism of the resource hotspots.

KEYWORDS

**Antarctic krill, acoustic data, Regional Gridding, Extended delta-distribution model, fishing vessel**

## Introduction

As a key species of the Southern Ocean ecosystem, Antarctic krill (*Euphausia superba*, hereinafter "krill") occupies a central position in pelagic food webs because it is the main food for many predators such as fish, penguins, seals, and whales (Murphy et al., 2007; Atkinson et al., 2009; Trathan and Hill, 2016). The Commission for the Conservation of Antarctic Marine Living Resources (CCAMLR) was established by international convention in 1982 with the objective of conserving Antarctic marine life. CCAMLR practices an ecosystem-based management approach and is responsible for the conservation of Antarctic marine ecosystem. This does not exclude harvesting as long as such harvesting is carried out in a sustainable manner and takes account of the effects of fishing on other components of the ecosystem (https://www.ccamlr.org/). CCAMLR is committed to precautionary, ecosystem-based management, especially in areas where a fishery is concentrated (Zhao et al., 2020; Zhao Y. X. et al., 2021; Trathan et al., 2022). Accordingly, CCAMLR has agreed that priority items for consideration by the Working Group on Acoustic Survey and Analysis Methods (WG-ASAM) and the Working Group on Statistics, Assessment and Modelling (WG-SAM) should be subarea-scale krill biomass estimates based on repeated regional surveys and a review of the open-source Generalized Yield Model (GYM) implementation for krill assessment, respectively (SC-CAMLR- XXXVIII, 2019, Paragraph 13.4).

According to the characteristics of krill fishery equipment, product type, and fishery management, the development process of the krill industry can be divided into three stages (Zhao et al., 2016; Figure 1): 1) a development period from 1972 to 1991 (including initial development and first peak periods), 2) a stagnation period from 1993 to 2006, and 3) a second development period from 2006 until the present. By the end of the 2019/20 fishing season, the total annual production of Antarctic krill (460,000 t) was at its highest level in nearly 30 years. With the development of krill fishery, working groups of the Scientific Committee (SC-CAMLR) have actively promoted development of technical specifications for acoustic data acquisition and processing of commercial fishing vessels, to enable the appropriate application of fishing vessel acoustic data in krill resource assessment (Watkins et al., 2016; Wang et al., 2019).

The vast circumpolar distribution of krill (many potential habitats, Atkinson et al., 2008) and complex food–web relationships (Trathan and Hill, 2016; Warwick-Evans et al., 2021) are the obstacles to krill resource assessment. Krill are a micro-nektonic and move with ocean currents; they do have some behavioral control of their position in the water column (Nicol, 2006; Thorpe et al., 2007; Trathan et al., 2022). Therefore, the size, mobility, and variable behavior of krill are challenges for acoustic or net sampling (Watkins et al., 2016). On the other hand, estimating the krill standing stocks based on the acoustic data is restricted by limited spatial and temporal coverage (Reiss et al., 2008; Kinzey et al., 2015), particularly in near-shore waters (Trathan et al., 2022). Although a large number of investigations (Atkinson et al., 2017) and studies have been conducted on the assessment of Antarctica krill resources, estimates of their total biomass and production are still uncertain (Atkinson et al., 2009). In the Southern Ocean, due to the limitations of various factors, the large-scale scientific investigations had been undertaken only twice, one in 2000 (Watkins et al., 2004) and the other in 2019 (Krafft et al., 2021), which were both conducted in Area 48 of CCAMLR in the Atlantic sector, mostly stations concentrated in subareas 48.1–48.3 (Supplementary Figure 1).

Generally, the evaluations of distribution and biomass of marine organisms are based on scientific surveys characterized by the use of full-time dedicated vessels and pre-planned sampling designs (Gunderson, 1993). With the increased interest in acoustic data from fishing vessels, relative noise-mitigation (Wang et al., 2016), krill identification (Wang et al., 2017a), and statistical techniques for density estimation (Niklitschek and Skaret, 2016; Zhao Y. X. et al., 2021) are already under development. The acoustic method to identify these swarms was established based on their biological characteristics using a biological swarm algorithm, which overcomes the limitations of having to use

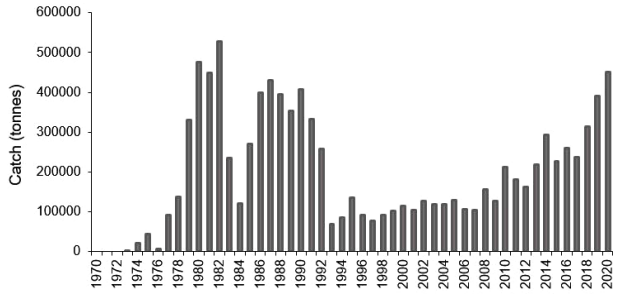


FIGURE 1
Antarctic krill catch 1970-2020 (CCAMLR, 2021).

multiple frequencies in traditional frequency-difference identification methods (Wang et al., 2017a). This method improved the utility of fishing-vessel-based acoustic data for a range of objectives, and it was applied and validated based on the Antarctic krill resources data in the 2019 International Joint survey (Krafft et al., 2021). Multiple works using commercial fishing vessel acoustic data were promoted by the ASAM (SG-ASAM-2017, 2017; SG-ASAM-2018, 2018; SG-ASAM-2019, 2019); the outcomes indicated that fishery-based acoustic data could be applied to assess krill abundance. The methods using these acoustic data rationally and scientifically are being increasingly discussed (Watkins et al., 2016; Niklitschek and Skaret, 2016; Zhao Y. X. et al., 2021).

Currently, to improve krill fishery monitoring and management, an important challenge is the estimation of krill population dynamics in the fishery hotspots (WG-EMM-2019, 2019; SC-CAMLR-XXXVIII, 2019). Thus, using fishery-based acoustic data in different spatiotemporal scales is useful to the assessment of krill density. However, the applications of the acoustic data collected during routine fishing operations remain in exploration (Watkins et al., 2016; Niklitschek and Skaret, 2016; Zhao Y. X. et al., 2021), and there is no commonly used method. Though the spatial coverage of these trace tracking acoustic data is less systematically collected than the data in the general acoustic survey, these data cover more primary fishing grounds. At the same time, these data cover the entire fishing season, which can show the dynamic changes of krill density in fishing hotspots, and are of value to fishery management. Our objective is to develop a simple statistical approach to assess the density of Antarctic krill and an associated coefficient of variation (CV) using acoustic data collected by the krill fishing vessel from routine fishing operations.

# Materials and methods

## Fishing area

Surveys were conducted by the Chinese krill fishing vessel F/V *Fu Rong Hai* during the 2015/16 fishing season. The acoustic data were recorded using a scientific echosounder (Simrad EK60) at 38, 70, and 120 kHz. The acoustic navigation routes are depicted in Figure 2. Most fishing effort occurred in the Bransfield Strait, especially in a hotspot (59.50–57.75°W, 63.50–62.90°S) within the red polygon (Figure 2B). The bathymetry of the Bransfield Strait is generally shallower than 1000 m and characterized by steep slopes between the deep basin alongside the South Shetland Islands and Antarctic Peninsula. This topography with large depth gradient changes also complicates the physical environment of this region, especially the flow field (Wang et al., 2017a).

## Acoustic data collection and processing

Acoustic data were collected using a Simrad EK60 echosounder system with hull-mounted transducers operating at 38, 70, and 120 kHz. Echosounder parameters were set in accordance with CCAMLR specifications (SC-CAMLR-XXX, 2011). Acoustic data were processed using Echoview (v 10.0.298). Krill backscatter was identified using a swarm-based method (Krafft et al., 2021) at 120 kHz, and a 'nautical area scattering coefficient' [acoustic density, NASC or $S_A$, $m^2$ nautical mile $(nm)^{-2}$] was integrated on a 0.1 nm horizontal resolution grid and exported for analysis. Detailed information of transducer specification and transceiver settings during data collection and the process of data analysis is described in Wang et al. (2017a).

## Statistical approach

After the preprocessing of the raw data, the chaotic acoustic data were gridded, and the mean value for each grid was calculated to evaluate acoustic density. In the further processing involved, we assumed the distribution of krill population to be relatively random; then we averaged the data during a month as the monthly mean value, filtering the effect of tides on krill migration. The processed acoustic data had many zero and lower values with the horizontal resolution grid of 0.1 nm. We designed the Regional Gridding and Extended Delta-distribution model (hereinafter RGED model) to make reasonable use of these data to evaluate dynamic changes of krill density. This statistical method was verified by the data collected during the 2015/16 fishing season.

## Regional gridding

According to the tracks of the fishing season vessel (to determine the study area boundary), we selected data from February–May 2016 from an area of ~1753 $nm^2$ (6013 $km^2$) within the Bransfield Strait as our study area (Figure 2B). We designed 10 scenario simulations with different grid sizes. We divided the grid cells on the basis of the length along the meridian direction, respectively 1'S (about 1 nm), 2'S,…, 10'S, with the corresponding length along the latitude direction being 2'W, 4'W, …, 20'W, respectively. Within each grid cell, data were averaged for each month and treated as independent observations for that grid and that month.

A principle of grid size selection is that the coefficient of variation (CV) of acoustic density is relatively small, at the same time the proportion of effective covered area is relatively optimal. Accordingly, we design a selection index calculated as CV/weight of the effective covered area. The weight of the effective

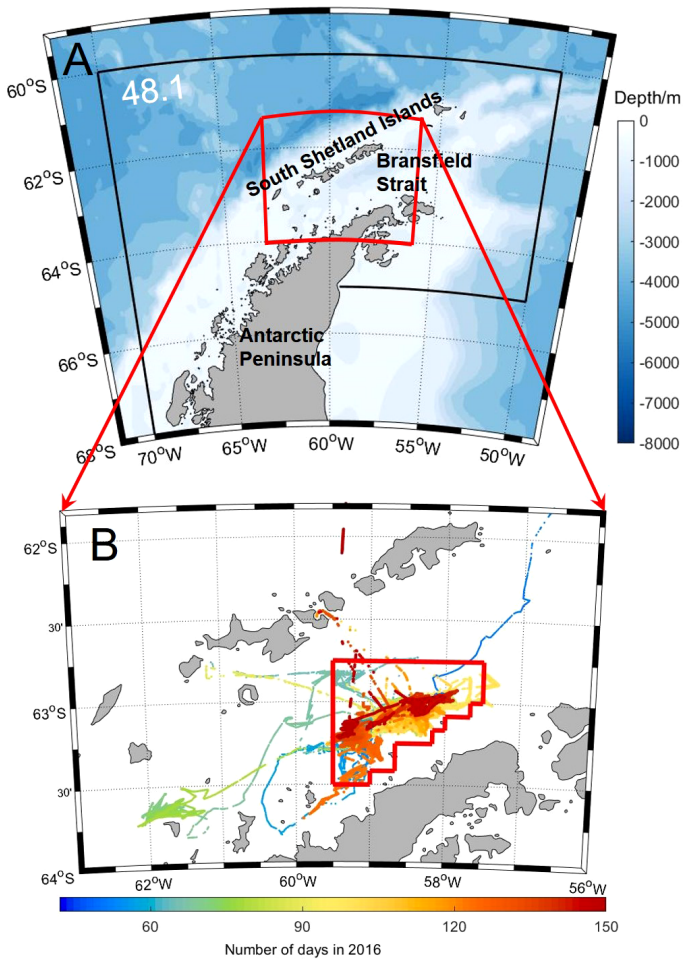


FIGURE 2
Study area: **(A)** CCAMLR Subarea 48.1 topography, **(B)**: F/V *Fu Rong Hai* track lines, February–May 2016 (color intensity indicates number of days). The red polygon denotes area within grid 59.50–57.75°W, 63.50–62.90° S.

covered area is the proportion of the acoustic data coverage to the total study area. The smaller the selection index, the better the grid design. Additionally, we also refer to the common space between stations and data analysis methods for the design of fishing resource bottom trawl survey stations.

## Extended delta-distribution model

Delta-distribution has been applied to the distribution of catch-per-tow data from trawl surveys for fish and plankton (Pennington, 1996; Pennington and Strømme, 1998; Li et al., 2008). The delta-distribution is a logarithmic normal distribution that includes data with a sample value of zero, and its non-zero value part is a logarithmic normal distribution, that is, the natural logarithm of non-zero value conforms to normal distribution. The statistical advantage of using the delta-distribution is that the estimator of the mean defined for this distribution is more efficient than the ordinary sample mean typically used to estimate abundance within study area strata (Smith, 1988). Smith and Pennington have conducted many studies on the application of this method in fisheries resource assessment (Smith, 1996; Pennington, 1983; 1986 and 1996). During the data analysis, density data (non-zero value part) are first converted to natural logarithm, with converted values then tested for goodness of fit to a normal distribution. The prerequisite for logarithmic transformation is that there can be no zeros in the sample. If they conform to a lognormal distribution, then the model is used for calculation.

Acoustic data are highly skewed to the right and usually have a cluster of smaller values relatively close to zero. Even after removing zero values, it is difficult to completely satisfy the normal/lognormal distribution. Myers and Pepin (1990) demonstrated that the sample mean and variance are more

robust than lognormal-based estimators of mean and variance of population abundance if the data don't follow a lognormal distribution. Because low values can severely bias lognormal-based estimators, we suppose the values greater than $k$ are distributed approximately lognormally (Pennington, 1991; Kappenman, 1999). Here, $k$ is a value to ensure that the values greater than it are approximately conforming to lognormal distribution. The basic principle of the method is as follows (Pennington, 1996; Folmer and Pennington, 2000).

Let $\rho_i$ be the NASC value of Grid $i$ ($i \in n$). An alternative estimator $\rho$, as the mean of $\rho_i$ is given by

$$\rho = \frac{n-m}{n}\bar{y} + \frac{m}{n}\exp(\bar{x})g_m\left(\frac{s_x^2}{2}\right) \quad (1)$$

Where $n$ is the number of sample values, $m$ is the number of sample values > $k$, $\bar{y}$ denotes the mean of the value ≤ $k$, and $\bar{x}$ and $s_x^2$ are the mean and variance, respectively. Here $x=ln(\rho_i)$ of the logged values > k, $g_m(t)$ is a function of $m$ and $t$ ( $t = \frac{s_x^2}{2}$) defined by

$$g_m(t) = 1 + \frac{m-1}{m}t + \sum_{j=2}^{\infty}\frac{(m-1)^{2j-1}}{m^j(m+1)(m+3)\ldots(m+2j-3)}\cdot\frac{t^j}{j^!} \quad (2)$$

The estimator of the variance of $\rho_i$ is given by

$$\mathrm{var}(\rho) = \mathrm{var}(\rho_x) + \left(\frac{n-m-1}{n(n-1)}\right)s_y^2 + \left(\frac{m(n-m)}{n(n-1)}\right)\bar{y}^2 - 2\left(\frac{n-m}{n(n-1)}\right)\bar{y}\rho_x \quad (3)$$

where $s_y^2$ is the variance of the values less than or equal to $k$, and $\rho_x$ is the mean of the values greater than $k$,

$$\rho_x = \frac{m}{n}exp(\bar{x})g_m\left(\frac{s_x^2}{2}\right) \quad (4)$$

and

$$\mathrm{var}(\rho_x) = \frac{m}{n}\exp(2\bar{x})\left\{\frac{m}{n}g_m^2\left(\frac{s_x^2}{2}\right) - \left(\frac{m-1}{n-1}\right)\cdot g_m\left(\frac{m-2}{m-1}s_x^2\right)\right\} \quad (5)$$

The standard error (SE) of the mean density is estimated by

$$\mathrm{SE}(\rho) = \sqrt{\mathrm{var}(\rho)} \quad (6)$$

An approximate 95% confidence interval for the mean density $\rho$ is calculated as

$$\rho \pm 1.96\mathrm{SE}(\rho) \quad (7)$$

The coefficient of variation (CV) is given as

$$\mathrm{CV} = \frac{\mathrm{SE}(\rho)}{\rho} \quad (8)$$

When determining $k$, we use a Kolmogorov–Smirnov (K–S) test to determine if the non-zero part of the original data is subject to a normal or lognormal distribution. For our data, we consider the $k$ value to be subject to a lognormal distribution.

# Results

## Sensitivity test of grid size

Using chaotic acoustic data during fishing operations from February 2016 as an example, the krill density scatter distributions in the study area in 10 different grid scenarios are illustrated in Figure 3. The scatter distributions in March–May 2016 are shown in the supplementary material (Supplementary Figures 2A–C). It can be seen that when the grid size is small, there are many zero and low values in the acoustic data, which is unsuitable for statistical analysis. With the increase of the grid size, the area covered by grid points accounts for a larger proportion of the total study area. The number of grid points and weights of effective areas within the research area in the 10 scenarios are presented in Figure 4.

Figure 4 also compares the CVs of the mean density for each scenario. When grid size decreased to<5 nm (meridian), CV values tended to converge. Few differences in CV were apparent among months at grid sizes<3 nm (meridian). At a grid size of 5′ S × 10′W, the selection index (CV/Weight of effective covered area) decreased, with results for the four months being relatively homogeneous. In the survey designs of fishery resource assessment, a distance of 5 nm between stations is more commonly used. Accordingly, we selected the 5′S × 10′W grid to calculate krill resource density for this region.

## Sensitivity test of the *k* value

The K-S test results of the extended delta-distribution model are shown in Table 1. After selecting the $k$ value, the distribution of these data larger than the $k$ value follows lognormal distribution and passes the hypothesis test of the significance level a = 0.05. Here the $k$ value is the minimum value, and p-value >0.05 means the data obey a lognormal distribution. Histogram of the number of samples with a grid cell of 5′S × 10′W is shown in the supplementary material (Supplementary Figure 3).

## Krill density

Estimated krill density at multiple grid sizes (Figure 5) reveals similar means, but with some variation in confidence intervals among grid sizes, especially in high-density months (April and May). CVs generally increased with changing grid size (Figure 4). As grid size increased, the sample size used to

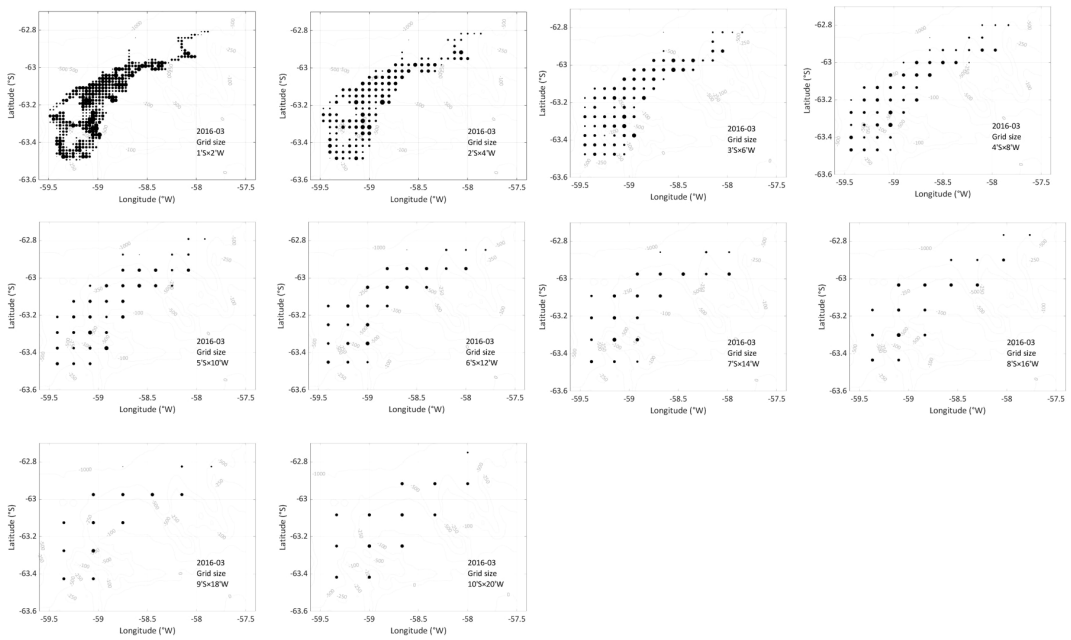


FIGURE 3
The scatter distributions of acoustic density for different grid sizes in February 2016. Circle diameter is proportional to krill density.

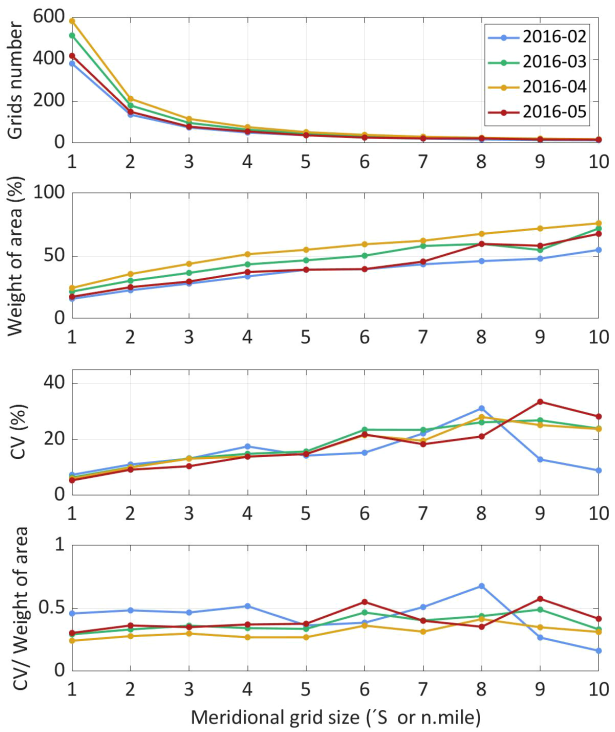


FIGURE 4
Gridded sample number, weight of effective covered area, coefficient of variation of the nautical area scattering coefficient (NASC), and grid selection index for different grid sizes.

TABLE 1 From February to May 2016, the p-values corresponding to *k* values of the four groups of data and test values at the significance level a = 0.05 are shown in Table 1.

| K-S test | Feb. 2016 | Mar. 2016 | Apr. 2016 | May 2016 |
|---|---|---|---|---|
| Number of samples | 37 | 44 | 52 | 37 |
| *k* | 0 | 0 | 0 | 3%×$\rho$ |
| p-Value | 0.0626 | 0.53 | 0.126 | 0.7420 |

The grid size is 5′S × 10′W.

estimate mean krill density decreased (Figure 3). Mean density was not strongly changing with grid size; however, a larger grid size resulted in greater variation (with larger confidence interval, CVs) in krill density estimates (Figure 5).

The spatial distributions of acoustic density $S_A^{1/2}$ throughout the study area are presented in Figure 6, wherein differences in spatial sample sizes used to estimate pooled mean krill density of krill in fishery hotspots are apparent, with discrepant distribution in formations. Averaged acoustic density estimated in the hotspot with a 5'S × 10'W grid cell in February–May 2016 is presented in Figure 7 and Table 2. Krill density in the fishing ground is dynamic, and density was very high toward the end of the fishing season (May). Krill density in February was 1987.4 $m^2$ $nm^{-2}$ and reached 8757.9 $m^2$ $nm^{-2}$ in May (4.4× February values).

# Discussion

## Statistical approaches

The overall characteristics of acoustic data collected during fishing operations are disordered. As for traditional bottom trawl survey data, a proportion of zero or small values exist for sampling points (nets), and a proportion of sampling points have high density values. While traditional empirical statistical

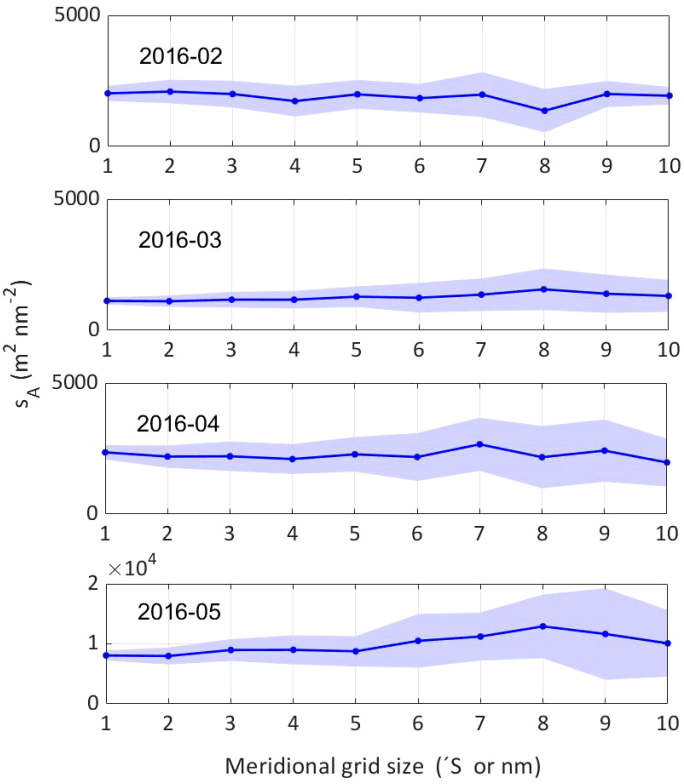


FIGURE 5
The estimations of nautical area scattering coefficient (NASC) in the hotspot with 10 gridding scenarios in February–May 2016. Error bars represent 95% confidence intervals of means.

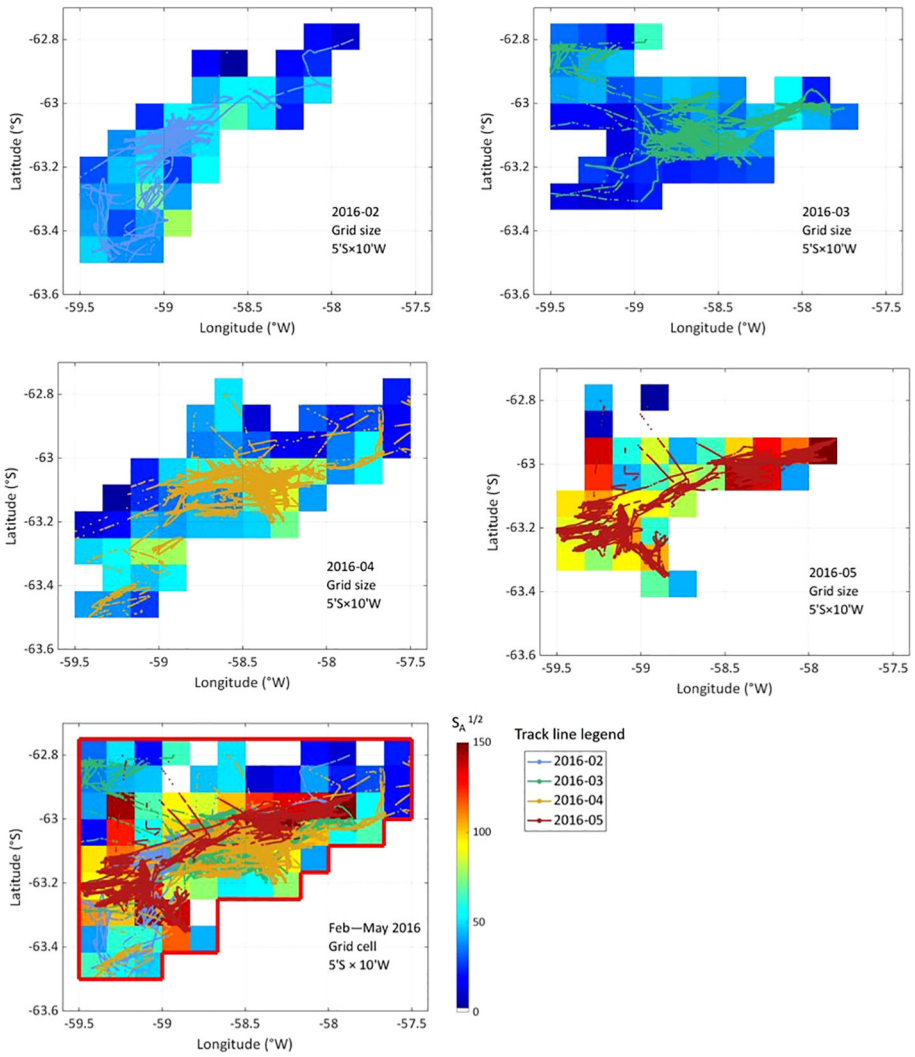


FIGURE 6
Monthly (February–May 2016) spatial distribution of nautical area scattering coefficient (NASC) values with a 5′S × 10′W grid cell.

methods generally combine these zero, low, and high values, model-based methods generally treat them separately and, by doing so, better describe the resource distribution for an entire region (Gunderson, 1993; Li et al., 2008). According to the spatial distribution of krill acoustic density (Figure 6), the difference between high- and low-density areas is 10 or more times larger. Areas with high resource densities are inherent manifestations of the spatial distribution characteristics of fish populations, with high catch values making the distribution of resource density very discrete (Pennington, 1996). The working paper WG-FSA-2021/56 (Zhao X. Y. et al., 2021) regarded high concentrations of, and high variation in, Antarctic krill resources to be natural characteristics of krill populations, for which reason the distribution of the Antarctic krill fishery must be highly concentrated, and the yield also highly variable.

Before using the extended delta-distribution model, we used the arithmetic average method, re-sampling (Bootstrap) method, delta-distribution model, and Gamma distribution models to perform relevant experimental simulations. Each approach has its pros and cons. When we use classical probability statistics in the study of data, data must be independent (random variables). However, the distribution of krill appears to have a degree of spatial correlation or continuity rather than being purely random. Here, we assume that the data is random and relatively independent. The mean density and CV calculated in our study using the arithmetic average method, Bootstrap method, and the extended delta-distribution model differed little (Supplementary Figure 4). On another side, if a data sample does not obey a normal distribution, the arithmetic mean method cannot accurately reflect the size characteristics

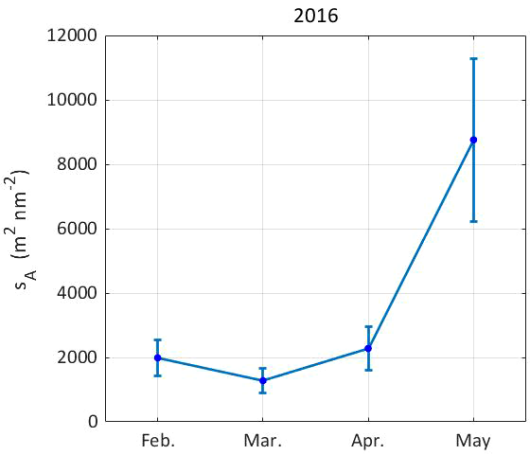


FIGURE 7
The estimations of the mean acoustic density in February–May 2016 in the fishing ground with a 5′S × 10′W grid cell. Error bars represent 95% confidence intervals of means.

of the variable, because this method is easily affected by the minimax value (Yuan et al., 2011). Taking this into account, the extended delta-distribution model in this paper has more advantages and stronger universality.

The delta-distribution model based on normal distribution has certain advantages over other methods in dealing with zero values (Smith, 1988; Pennington, 1996; Li et al., 2008). However, when processing acoustic data and simply using the delta-distribution model to analyze them, we find that non-zero data follow neither a normal nor logarithmic normal distribution, so CVs are large (Supplementary Figure 4). The extended delta-distribution model takes this problem into account.

The Gamma distribution model is not appropriate for analyzing samples with zero values (Smith, 1981). The average density and mean calculated using this model in monthly samples without zero values differ little from the extended delta-distribution model (Supplementary Figure 4). There is no zero value in the acoustic data of the 2015/16 fishing season applied, so the Gamma distribution model is applicable. However, if the data series has zero values, this method is not suitable (Supplementary Table 1).

The non-parametric Bootstrap method based on the resampling theory of EFRON (Efron, 1979) replicates observation information on the basis of the given original sample, does not need to make a distribution hypothesis or add new sample information, and can carry out statistical inference on the distribution characteristics of the whole population (Money and Duval, 1993; Zhao et al., 2010; Yuan et al., 2014). Although the spatial distribution of krill resources has not been determined, the Bootstrap method does not need to consider the overall distribution type. Therefore, this method can be used when there is uncertain data distribution, or the data layer distribution type is inconsistent (Zhao Y. X. et al., 2021). The fitting analysis of the simulation results between the extended delta-distribution model and the bootstrap method showed high agreement, with $R^2 = 0.9895$ (Figure 8). In the case of this study, when the grid size is confirmed with 5′S × 10′W, the number of samples is around 37–52 (Table 1), so the two methods are both applicable (Supplementary Table 1). The bootstrap distribution is greatly affected by the samples; especially when the sample size is small, the bootstrap distribution will be significantly different. In this case, the bootstrap distribution reflects more the characteristics of the sample (Hesterberg et al., 2005). Therefore, with the increase of samples, the extended delta-distribution model might be more widely applicable.

## Monthly variations of krill density

The Antarctic circumpolar current has a strong effect on the transportation of krill larvae, with the krill population

TABLE 2 Krill nautical area scattering coefficient (NASC) (= acoustic density), and coefficient of variation (CV) of the fishing ground in the Bransfield Strait in February–May 2016.

| | Feb. 2016 | Mar. 2016 | Apr. 2016 | May 2016 |
|---|---|---|---|---|
| NASC ($m^2$ $nm^{-2}$) | 1987.4 | 1280.0 | 2279.3 | 8757.9 |
| CV (%) | 14.2 | 15.7 | 14.8 | 14.8 |

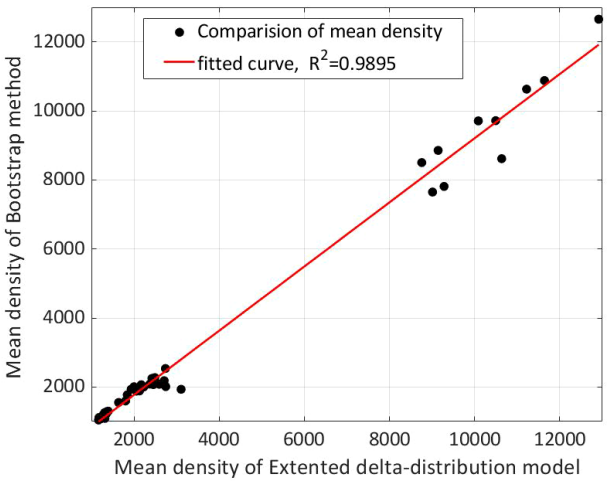


FIGURE 8
Fitting analysis of the simulation results (10 gridding scenarios) between extended the delta-distribution model and the bootstrap method.

distribution consistent with the overall current direction (Atkinson et al., 2008; Piñones et al., 2011; Piñones et al., 2013). For large-to-medium scale krill populations, ocean currents also influence their distribution, but how these currents retain or aggregate krill is not well understood (Reiss et al., 2008; Hinke et al., 2017). The Antarctic Ecosystem Research Division et al. (2016), indicated that seasonal horizontal migration of krill led to its accumulation in the Bransfield Strait, and the slower winter flow retained krill within it.

The krill hotspot that we report represents an important central fishing ground that for several months produces high yield (Ying et al., 2017; Wang et al., 2017b). Krill catch data statistics for this area reveals that with fishing season progression, krill fishery production sites gradually concentrated in the central Bransfield Strait, and by the end of summer and fishery closure, krill density in this hotspot trended significantly upward (Zhao Y. X. et al., 2021). The direction of flow in the northern Bransfield Strait is from west to east, from the Bellingshausen Sea coastal current to the Bransfield Strait Current. The southern regional current forms a branch of the northward Antarctic coastal current from the Weddell Sea into the interior of the strait (Trathan et al., 2022). Currents from the Bellingshausen Sea and Weddell Sea intrude into the strait, providing a source of krill, and affecting changes in their biomass and biological structure. The special topography of the Bransfield Strait produces many eddies that provide an environment for the accumulation and retention of the krill. However, there are few reports detailing specific inputs and outputs of krill for this fishery hotspot. The driving mechanisms for the accumulation and retention of the krill in this hotspot need further research.

## Krill fishery management

As krill is an important species in Antarctic marine ecosystems, the change of krill population will directly affect the entire ecosystem. Under the background of climate change, the health of the ecosystem has become a global concern. Striking a balance between conservation and sustainable fishery exploitation requires long-term monitoring and analysis of changes in the abundance and distribution of krill, which also presents a challenge for CCAMLR fisheries management (Wang et al., 2021). To promote the development of science-based management, the Commission endorsed a three-component strategy agreed upon by the Scientific Committee (CCAMLR-XXXVIII, 2019, para. 5.17; Ying et al., 2021): 1) the krill population is assessed to estimate a precautionary catch limit (i.e., the parameter gamma in the Generalized R Yield Model (GrYM) and the catch rate corresponding to a precautionary catch limit); 2) regular biomass estimate updates, initially at a subarea scale, but possibly at multiple scales; and 3) a risk-assessment framework to inform the spatial distribution of catches. It is not practical to regularly assess krill biomass by multi-year large-scale surveys. We explore how to apply acoustic data accumulated during routine commercial fishing operations to regionally assess krill density. Although this can only reflect the resource dynamic in the hotspot, it is a step towards achieving the goal of krill biomass assessment.

# Conclusion

We present RGED model to process and apply “chaotic” acoustic data collected during routine fishing operations.

Selection indexes calculated by the CV and weight of effective covered area of grids were screened using the Regional Gridding process. We then used an extended delta-distribution model to analyze the gridded data. Acoustic data collected by the Chinese krill fishing vessel F/V *Fu Rong Hai* since the 2015/16 fishing season in the Bransfield Strait were used as an application example. The results showed that the CV of the mean density for 4 months converged in a 5′S × 10′W grid cell at approximately 15%. Our method accurately reflects characteristics of the spatial and temporal distribution of krill density in the central Bransfield Strait fishing ground, with acoustic density in February of ~1990 $m^2$ $nm^{-2}$, reaching ~8760 $m^2$ $nm^{-2}$ in May. We demonstrate the RGED model to reasonably and scientifically analyze commercial fishery acoustic data collected during the production period to identify changes in Antarctic krill density and to provide a scientific basis upon which this fishery can be managed.

## Data availability statement

The raw data supporting the conclusions of this article will be made available by the authors, without undue reservation.

## Author contributions

YZ and XZ conceived the study. YZ led the study and writing of the manuscript. XW provided data and contributed substantially to writing the manuscript. YY contributed substantially to writing the manuscript. All authors read and approved the final manuscript.

## Funding

This work was funded by the National Natural Science Foundation of China (No.42006194 and 41706219); the Marine S&T Fund of Shandong Province for Pilot National Laboratory for Marine Science and Technology (Qingdao) (No. 2022QNLM030002-1); the Major Scientific and Technological Innovation Project of Shandong Provincial Key Research and Development Program (No.2019JZZY010819); the Central Public-interest Scientific Institution Basal Research Fund, YSFRI, CAFS, China (No.20603022021017); and the Central Public-interest Scientific Institution Basal Research Fund, CAFS, China (No.2021TD02).

## Acknowledgments

We would like to thank the fishing vessel F/V *Fu Rong Hai* for providing the acoustic data. We would also like to thank Steve O'Shea, PhD, from Liwen Bianji (Edanz) (www.liwenbianji.cn/), for editing the English text of a draft of this manuscript.

## Conflict of interest

The authors declare that the research was conducted in the absence of any commercial or financial relationships that could be construed as a potential conflict of interest.

## Publisher's note

All claims expressed in this article are solely those of the authors and do not necessarily represent those of their affiliated organizations, or those of the publisher, the editors and the reviewers. Any product that may be evaluated in this article, or claim that may be made by its manufacturer, is not guaranteed or endorsed by the publisher.

## Supplementary material

The Supplementary Material for this article can be found online at: https://www.frontiersin.org/articles/10.3389/fmars.2022.934504/full#supplementary-material

## References

Antarctic Ecosystem Research Division and Southwest Fisheries Science Center and NOAA Fisheries, et al (2016). *Background information to support development of a feedback management strategy for the krill fishery in subarea 48.1*, WG-EMM-16/45. Hobart, Tasmania, Australia: CCAMLR.

Atkinson, A., Hill, S., Pakhomov, E. A., Siegel, V., Anadon, R., Chiba, S., et al. (2017). KRILLBASE: a circumpolar database of Antarctic krill and salp numerical densitieS, 1926–2016. *Earth System Science Data* 9, 193–210. doi: 10.5194/essd-2016-52

Atkinson, A., Siegel, V., Pakhomov, E. A., Jessopp, M. J., and Loeb, V. (2009). A re-appraisal of the total biomass and annual production of Antarctic krill. *Deep-Sea Res. Part I: Oceanogr. Res. Papers* 56 (5), 727–740. doi: 10.1016/j.dsr.2008.12.007

Atkinson, A., Siegel, V., Pakhomov, E. A., Rothery, P., Loeb, V., Ross, R. M., et al. (2008). Oceanic circumpolar habitats of Antarctic krill. *Mar. Ecol. Prog. Ser.* 362, 1–23. doi: 10.3354/meps07498

CCAMLR-XXXVIII (2019). *Report of the thirty-eighth meeting of the commission* (Hobart, Australia: CCAMLR).

CCAMLR (2021). *Statistical Bulletin* (Hobart, Tasmania, Australia) Vol. 33. CCAMLR, Hobart, Tasmania, Australia. Available at: www.ccamlr.org.

Efron, B. (1979). Bootstrap methods: Another look at the jackknife. *Ann. Statist.* 7 (1), 1–26. doi: 10.1214/aos/1176344552

Folmer, O., and Pennington, M. (2000). A statistical evaluation of the design and precision of the shrimp trawl survey off West Greenland. *Fish. Res.* 49 (2), 165–178. doi: 10.1016/S0165-7836(00)00196-X

Gunderson, D. R. (1993). *Surveys of fisheries resources* (New York: Wiley).

Hesterberg, T., Moore, D., Monaghan, S., Clipson, A., and Epstein, R. (2005). "Bootstrap methods and permutation tests," in *Introduction to the practice of statistics*, *5th ed*. New York: WH Freeman & Co.

Hinke, J. T., Cossio, A. M., Goebel, M. E., Reiss, C. S., Trivelpiece, W. Z., and Watters, G. M. (2017). Identifying risk: concurrent overlap of the Antarctic krill fishery with krill-dependent predators in the Scotia Sea. *PloS One* 12, e0170132. doi: 10.1371/journal.pone.0170132

Kappenman, R. F. (1999). Trawl survey based abundance estimation using data sets with unusually large catches. *ICES J. Mar. Sci.* 56, 28–35. doi: 10.1006/jmsc.1998.0422

Kinzey, D., Watters, G. M., and Reiss, C. S. (2015). Selectivity and two biomass measures in an age-based assessment of Antarctic krill (*Euphausia superba*). *Fish. Res.* 168, 72–84. doi: 10.1016/j.fishres.2015.03.023

Krafft, B. A., Macaulay, G. J., Skaret, G., Knutsen, T., Bergstad, O. A., Lowther, A., et al. (2021). Standing stock of Antarctic krill (*Euphausia superba* Dana 1850) (Euphausiacea) in the Southwest Atlantic sector of the Southern Ocean 2018–19. *J. Crustacean Biol.* 41(3), 1–17. doi: 10.1093/jcbiol/ruab071

Li, F., Li, X., and Zhao, X. (2008). Bottom trawl survey data analysis based on delta-distribution model and its application in the estimation of small yellow croak and silver pomfret in yellow Sea. *J. Fish. China* 32 (1), 145–151. (in Chinese, with English abstract). doi: 10.3321/j.issn:1000-0615.2008.01.023

Money, C. Z., and Duval, R. D. (1993). "Bootstrapping: A nonparametric approach to statistical inference," in *Sage university paper series on quantitative applications in the social sciences* (Newbury Park: Sage).

Murphy, E. J., Watkins, J. L., Trathan, P. N., Reid, K., Meredith, M. P., Thorpe, S. E., et al. (2007). Spatial and temporal operation of the Scotia Sea ecosystem: a review of large-scale links in a krill centered food web. *Philos. Trans. R. Soc. B* 362, 113–148. doi: 10.1098/rstb.2006.1957

Myers, R. A., and Pepin, P. (1990). The robustness of lognormal-based estimators of abundance. *Biometrics* 46, 1185–1192. doi: 10.2307/2532460

Nicol, S. (2006). Krill, currents, and sea ice: *Euphausia superba* and its changing environment. *BioScience* 56 (2), 111–120. doi: 10.1641/0006-3568(2006)056[0111:KCASIE]2.0.CO;2

Niklitschek, E. J., and Skaret, G. (2016). Distribution, density and relative abundance of Antarctic krill estimated by maximum likelihood geostatistics on acoustic data collected during commercial fishing operations. *Fish. Res.* 178, 114–121. doi: 10.1016/j.fishres.2015.09.017

Pennington, M. (1983). Efficient estimators of abundance, for fish and plankton surveys. *Biometrics* 39(1), 281–286.

Pennington, M. (1986). Some statistical techniques for estimating abundance indices from trawl surveys. *Fish. Bull.* 84, 519–525.

Pennington, M. (1991). Comments on the robustness of lognormal-based abundance estimators. *Biometrics* 47, 1623.

Pennington, M. (1996). Estimating the mean and variance from highly skewed marine data. *Fish. Bull.* 94, 498–505.

Pennington, M., and Strømme, T. (1998). Surveys as a research tool for managing dynamic stocks. *Fish. Res.* 37 (1-3), 97–106. doi: 10.1016/S0165-7836(98)00129-5

Piñones, A., Hofmann, E. E., Daly, K. L., Dinniman, M. S., and Klinck, J. M. (2013). Modeling the remote and local connectivity of Antarctic krill populations along the western Antarctic peninsula. *Mar. Ecol. Prog. Ser.* 481, 69–92. doi: 10.3354/meps10256

Piñones, A., Hofmann, E. E., Dinniman, M. S., and Klinck, J. M. (2011). Lagrangian Simulation of transport pathways and residence times along the western Antarctic peninsula. *Deep-Sea Res. Part II: Topical Stud. Oceanogr.* 58 (13-16), 1524–1539. doi: 10.1016/j.dsr2.2010.07.001

Reiss, C. S., Cossio, A. M., Loeb, V., Demer, D. A., et al (2008). Variations in the biomass of Antarctic krill (Euphausia superba) around the south Shetland islands 1996-2006. *ICES J. Mar. Sci.* 65 (4), 497–508. doi: 10.1093/icesjms/fsn033

SC-CAMLR-XXX (2011). *Report of the thirty-eighth meeting of scientific committee* (Hobart, Australia: CCAMLR).

SC-CAMLR-XXXVIII (2019). *Report of the thirty-eighth meeting of scientific committee* (Hobart, Australia: CCAMLR).

SG-ASAM-2017 (2017). *Report of the meeting of the subgroup on acoustic survey and analysis methods*. In: Working Group meeting held in Qingdao, China (Hobart, Australia: CCAMLR).

SG-ASAM-2018 (2018). *Report of the meeting of the subgroup on acoustic survey and analysis methods*. In: Working Group meeting held in Punta Arenas, Chile (Hobart, Australia: CCAMLR).

SG-ASAM-2019 (2019). *Report of the meeting of the subgroup on acoustic survey and analysis methods*. In: Working Group meeting held in Bergen, Norway (Hobart, Australia: CCAMLR).

Smith, S. J. (1981). A comparison of estimators of location for skewed populations, with applications to groundfish trawl surveys. *Can. Special Publ. Fish. Aquat. Sci.* 58, 154–163.

Smith, S. J. (1988). Evaluating the efficiency of the Δ-distribution mean estimator. *Biometrics* 44 (2), 485–493. doi: 10.2307/2531861

Smith, S. J. (1996). Analysis of data from bottom trawl surveys. *NAFO Sci. Council Stud.* 28, 25–53. doi: 10.1016/S0967-0653(97)85798-5

Thorpe, S. E., Murphy, E. J., and Watkins, J. L. (2007). Circumpolar connections between Antarctic krill (*Euphausia superba dana*) populations: investigating the roles of ocean and ice transport. *Deep-Sea Res. Part I* 54, 792–810. doi: 10.1016/j.dsr.2007.01.008

Trathan, P. N., and Hill, S. L. (2016). *The importance of krill predation in the southern ocean. in: The biology and ecology of Antarctic krill, euphausia superba Dana 1850*. Ed. V. Siegel (Dordrecht, The Netherlands: Springer), pp 321–pp 350.

Trathan, P. N., Warwick-Evans, V., Young, E. F., Friedlaender, A., Kim, J. H., and Kokubun, N. (2022). The ecosystem approach to management of the Antarctic krill fishery - the "devils are in the detail" at small spatial and temporal scales. *J. Mar. Syst.* 225, 103598. doi: 10.1016/j.jmarsys.2021.103598

Wang, X. L., Skaret, G., and Godø, O. R. (2017a). Processing of acoustic recordings from krill fishing vessels collected during fishing operations and surveying. In: Working Paper submitted to the CCAMLR Working Group on Acoustic Survey and Analysis Methods (SG-ASAM-2017/03). (Hobart, Australia: CCAMLR). Available from the CCAMLR Secretariat or the authors.

Wang, X. L., Skaret, G., Godø, O. R., and Zhao, X. Y. (2017b). Dynamics of Antarctic krill in the bransfield strait during austral summer and autumn investigated using acoustic data from a fishing vessel. In: Working Paper submitted to the CCAMLR Working Group on Ecosystem Monitoring and management (WG-EMM-2017/40) (Hobart, Australia: CCAMLR). Available from the CCAMLR Secretariat or the authors.

Wang, X. L., Zhang, J. C., and Zhao, X. Y. (2016). A post-processing method to remove interference noise from acoustic data collected from Antarctic krill fishing vessels. *CCAMLR Sci.* 23, 17–30.

Wang, X. L., Zhao, Y. X., Fan, G. Z., Ying, Y. P., Zhao, X. Y., and Zhang, J. C. (2021). Acoustic biomass estimates of Antarctic krill in subarea 48.1 to facilitate the development of the new management approach for the krill fishery. In: Working Paper submitted to the SC-CAMLR (SC-CAMLR-2021/13). CCAMLR, Hobart, Australia. Available from the CCAMLR Secretariat or the authors.

Wang, X. L., Zhao, X. Y., Zou, B., Fan, G. Z., Yu, X. T., Zhu, J. C., et al. (2019). Implementation and preliminary results from the synoptic krill survey in Area 48, 2019 conducted by the Chinese krill fishing vessel Fu Rong Hai. In: Working Paper submitted to the CCAMLR Working Group on Ecosystem Monitoring and management (WG-EMM-2019/43). CCAMLR: Hobart, Australia. Available from the CCAMLR Secretariat or the authors.

Warwick-Evans, V. A., Santora, J., Waggitt, J. J., and Trathan, P. N. (2021). Multi-scale assessment of distribution and density of procellariiform seabirds within the Northern Antarctic Peninsula marine ecosystem. *ICES Journal of Marine Science*. doi: 10.1093/icesjms/fsab020

Watkins, J. L., Hewitt, R., Naganobu, M., and Sushin, V.. (2004). The CCAMLR 2000 survey: a multinational, multi-ship biological oceanography survey of the Atlantic sector of the southern ocean. *Deep Sea Res. Part II Topical Stud. Oceanogr.* 51, 1205–1213. doi: 10.1016/S0967-0645(04)00075-X

Watkins, J. L., Reid, K., Ramm, D., Zhao, X. Y., Cox, M., Skaret, G., et al. (2016). The use of fishing vessels to provide acoustic data on the distribution and abundance of Antarctic krill and other pelagic species. *Fish. Res.* 178, , 93–,100. doi: 10.1016/j.fishres.2015.07.013

WG-EMM-2019 (2019). *Report of the Meeting of the Working Group on Ecosystem Monitoring and Management*. In: Working Group meeting held in Concarneau, France (Hobart, Australia: CCAMLR).

Ying, Y. P., Wang, X. L., Zhu, J. C., and Zhao, X. Y. (2017). *Krill CPUE standardisation and comparison with acoustic data based on data collected from Chinese fishing vessels in subarea 48.1*. In: Working Paper submitted to the CCAMLR Working Group on Ecosystem Monitoring and management (WG-EMM-2017/41) (Hobart, Australia: CCAMLR).

Ying, Y. P., Zhao, X. Y., Fan, G. Z., and Wang, X. L. (2021). The various spatial scales available for consideration and the distribution of the krill fishery in Subarea 48.1. In: Working Paper submitted to the CCAMLR Working Group on Acoustic Survey and Analysis Methods (WG-ASAM-2021/09). CCAMLR, Hobart, Australia. Available from the CCAMLR Secretariat or the authors.

Yuan, X. W., Jiang, Y. Z., and Cheng, J. H. (2011). Estimating the average stock density with dominating large catches based on Δ–distribution model. *Prog. Fish.*

*Sci.* 32 (1), 1–7 (in Chinese, with English abstract). doi: 10.3969/j.issn.1000-7075.2011.01.001

Yuan, X. W., Yan, L. P., Liu, Z. L., and Cheng, J. H. (2014). A performance comparison of stock density estimation of *Larimichthys polyactis* in the East China Sea using different models based on bottom trawl survey. *South China Fish. Sci.* 10 (6), 20–26 (in Chinese, with English abstract). doi: 10.3969/j.issn.2095-0780.2014.06.003

Zhao, L., Chen, J. X., Xu, M. Q., and Li, M. (2010). Bootstrap method and its application in biology. *J. Zool.* 29 (4), 638–641 (in Chinese, with English abstract). doi: CNKI:SUN:SCDW.0.2010-04-045

Zhao, X. Y., Wang, X. L., Ying, Y. P., Fan, G. Z., Xu, Q. C., Gao, D. Q., et al. (2021). The potential impact of krill fishery concentration needs to be assessed against the highly patchy and dynamic nature of krill distribution. In: Working Paper submitted to the CCAMLR Working Group on Fish Stock Assessment (WG-FSA-2021/56). Hobart, Australia: CCAMLR. Available from the CCAMLR Secretariat or the authors.

Zhao, Y. X., Wang, X. L., Zhao, X. Y., Ying, Y. P., and Zhang, J. C. (2021). Monthly variation of Antarctic krill biomass in a main fishing ground in the Bransfield strait based on fishing vessel acoustic data collected during routine fishing operations. In: Working Paper submitted to the CCAMLR Working Group on Acoustic Survey and Analysis Methods (WG-ASAM-2021/10). Hobart, Australia: CCAMLR. Available from the CCAMLR Secretariat or the authors.

Zhao, X. Y., Zuo, T., Leng, K. L., and Tang, Q. S. (2016). Engineering science and technology challenges in the Antarctic krill fishery. *Chinese Journal of Engineering Science*. 18, 2, 85–90 (in Chinese, with English abstract). doi: 10.15302/J-SSCAE-2016.02.010

frontiers | Frontiers in Marine Science

TYPE Brief Research Report
PUBLISHED 04 October 2022
DOI 10.3389/fmars.2022.971441



OPEN ACCESS

EDITED BY
Wei Liu,
Qilu University of Technology (Shandong Academy of Sciences), China

REVIEWED BY
Tonmoy Ghosh,
Indian Institute of Technology Indore, India
Muhammad Shafiq,
Shantou University, China

*CORRESPONDENCE
Weijie Wang
weijiewang@ncst.edu.cn
Lei Zhao
zhaol@tib.cas.cn
Fangjian Chen
chen_fj@tib.cas.cn

†These authors have contributed equally to this work

SPECIALTY SECTION
This article was submitted to Marine Fisheries, Aquaculture and Living Resources, a section of the journal Frontiers in Marine Science

RECEIVED 17 June 2022
ACCEPTED 21 September 2022
PUBLISHED 04 October 2022

CITATION
Guo Z, Hou Y, Liu Z, Ma Y, Han T, Hao N, Yao Y, Lan C, Ge T, Safavi M, Wang W, Zhao L and Chen F (2022) Combination of bicarbonate and low temperature stress induces the biosynthesis of both arachidonic and docosahexaenoic acids in alkaliphilic microalgae *Dunaliella salina* HTBS. *Front. Mar. Sci.* 9:971441. doi: 10.3389/fmars.2022.971441



# Combination of bicarbonate and low temperature stress induces the biosynthesis of both arachidonic and docosahexaenoic acids in alkaliphilic microalgae *Dunaliella salina* HTBS

Zhile Guo[1,2†], Yuyong Hou[2,3†], Zhiyong Liu[2,3], Yanbo Ma[1,2], Tong Han[2], Nahui Hao[2], Yuanjiang Yao[1,2], Chunxuan Lan[1,2], Tongling Ge[2,3], Maliheh Safavi[4], Weijie Wang[1*], Lei Zhao[2,3*] and Fangjian Chen[2,3*]

[1]College of Life Science, North China University of Science and Technology, Tangshan, China, [2]Key Laboratory of Systems Microbial Biotechnology, Tianjin Institute of Industrial Biotechnology, Chinese Academy of Sciences, Tianjin, China, [3]National Center of Technology Innovation for Synthetic Biology, Tianjin, China, [4]Department of Biotechnology, Iranian Research Organization for Science and Technology, Tehran, Iran

High bicarbonate levels and low temperature may have an impact on microalgae cultivation. However, changes in cellular composition in response to the combination of the above stresses are still poorly understood. In this study, the combined effects of bicarbonate and low temperature on biochemical changes in alkaliphilic microalgae *Dunaliella salina* HTBS were investigated. Comparing to the control condition of 25°C without bicarbonate, the cell density was increased from 0.69 to 1.18 in the treatment condition of 0.15 M bicarbonate and low temperature (16 °C) while the lipid\protein \carbohydrate contents were increased from 34.71% to 43.94%, 22.44% to 26.03%, 22.62% to 29.18%, respectively. Meanwhile, the PUFAs, arachidonic acid (AA) and docosahexaenoic acid (DHA) contents reached to 3.52% and 4.73% with the combination of low temperature and bicarbonate, respectively, whereas they were not detected when the cells were treated with single condition. Moreover, both the chlorophyll and carotenoid contents were also detected with increased profiles in the combined treatments. As a result, the maximum photochemical efficiency but not reduced non-photochemical quenching was strengthened, which enhanced the photosynthetic performance. Additionally, our results indicated that *D. salina* HTBS could acclimate to the combined stress by up-regulating the activity of SOD\CAT and reducing MDA content. These findings demonstrated that the addition of a certain bicarbonate under low temperature could effectively enhance the

biomass production and accumulation of AA and DHA, which would benefit the development of the microalgae industry in value-added products.

KEYWORDS

*Dunaliella salina* HTBS, bicarbonate, low temperature, arachidonic acid, docosahexaenoic acid

## Introduction

Microalgae, as photosynthetic organisms, are utilized as potential candidates for carbon sequestration and valuable compounds production with a higher growth rate and efficiency in $CO_2$ fixation than terrestrial plants (Chaunhan et al., 2022; Jakhwal et al., 2022). Among the great diversity of metabolites in microalgal cells, polyunsaturated fatty acids (PUFAs), such as arachidonic acid (AA) and docosahexaenoic acid (DHA), have been widely used as the key ingredients for nutrient supplements and pharmaceutical industrial products. Although both AA and DHA are reported to be accumulated in microalgae under certain conditions, their biosynthesis could be greatly affected by culture medium modifications, such as nutrients supplementation, limitation, and abiotic condition changes (Almutairi, 2020).

Biosynthesis of AA and DHA is closely related to carbon metabolism and temperature changes. Studies have shown that the PUFAs are increased from 32.3% to 37.9% in *Pavlova lutheri* with the addition of bicarbonate from 2 mM to 18 mM in the medium, which are also the case with both biomass and lipid contents (Guihéneuf and Stengel, 2013). The biosynthesis of both lipid and AA is active in *Parietochloris Incisa* under high C/N conditions (Khozin-Goldberg et al., 2002). Interestingly, bicarbonate is convenient to transport and cost effective when compared with $CO_2$, it can be considered as an excellent carbon resource for microalgae cultivation with high carbon utilization. Therefore, bicarbonate supplementation has been regarded as an effective way for the enhancement of secondary metabolites biosynthesis and growth acceleration. In contrast, PUFAs were detected with reduced content under high carbon conditions (Morales et al., 2021), and both the PUFAs biosynthesis and cell growth varied depending on the bicarbonate concentration and microalgae strain (Nunez et al., 2016). When added with bicarbonate, a large amount of cations are accumulated in both the microalgae cells and medium, which may inhibit cell division, resulting in cell death (Chen et al., 2009; Chi et al., 2014; Srinivasan et al., 2015; Ratomski et al., 2021). Due to the lack of strains tolerant to high-concentration cations, the effects of high bicarbonate on facilitating PUFAs biosynthesis in microalgae have been rarely reported.

Temperature is the other key factor which affects the biosynthesis of both AA and DHA. Low temperatures ranging from 10 °C to 25 °C trigger the PUFAs metabolic pathway, which leads to a 120% increase in PUFAs content (Jakhwal et al., 2022), and the accumulated PUFAs improve the cell membrane fluidity, which reduces the damage to cells caused by low temperatures (Lu et al., 2017). The PUFAs content increased to 35.23% when the temperature was decreased from 45 °C to 25 °C in *Galdieria* sp (Lu et al., 2021). Similarly, the positive effects of low temperature on PUFAs biosynthesis were also observed in the cultivation of *Nannochloropsis, Isochrysis, Rhodomonas*, and *Dixioniella grisea* (Aussant et al., 2018; Lu et al., 2021). However, microalgal growth is inhibited when PUFAs accumulate under low temperature conditions. Therefore, the strains with high bicarbonate and low-temperature tolerance are urgently needed to solve the previously mentioned problems.

In our previous study, *Dunaliella salina* strain HTBS, with a high tolerance to bicarbonate, was reported to be able to grow well under 70 g/L bicarbonate and low temperature. Nevertheless, the combined effects of bicarbonate supplementation and low temperature on the biochemical composition of HTBS changes are still unclear. Therefore, the objective of this study was to investigate the role of the combination of high bicarbonate and low temperature in physiological and biochemical changes in HTBS. Changes of cell density, pigments, lipid, carbohydrate, and protein contents, particularly the high value products AA and DHA content were initially monitored. Then, stress biomarkers like antioxidative enzyme superoxide dismutase (SOD), catalase (CAT) and malondialdehyde (MDA), along with Ci and nitrogen consumption curve were evaluated to elucidate the physiological mechanism of HTBS in response to the combined stress as well as to study their effects on PUFAs. These results will provide valuable information to produce PUFAs using microalgae and will benefit industrial development.

## Materials and methods

### Strain and cultivation conditions

*Dunaliella salina* strain HTBS with high tolerance to $HCO_3^-$ and low temperature was obtained and cultured to an early stationary phase, then centrifuged and washed twice with sterile seawater for inoculation based on our previous study (Hou et al.,

2016). For evaluating the effects of different bicarbonate contents at low temperature on physiological and biochemical changes in HTBS, the cells were inoculated in the modified f/2 medium (750 mg/L $NaNO_3$) under a light intensity of 80 μmol $m^{-2}$ $s^{-1}$ containing various bicarbonate concentrations ranging from 0 M to 0.6 M at 16°C.

## Analytical methods

During the cultivation, the cell growth was evaluated by measuring the optical density (OD) at 680 nm using a spectrometer. The algae suspension was centrifuged to harvest the cell pellets at 8,000 rpm for 5 min, the pellets were freeze dried using a vacuum freeze-drying machine. About 50 mg of cells were resuspended with 4 mL of chloroform and 2 mL of methanol, then incubated at 30°C for 16 h for lipid extraction. Then the mixture was centrifuged at 5,000 rpm for 10 min after adding another 2 mL of methanol and 3.6 mL of $ddH_2O$. Subsequently, the organic phase was transferred to a pre-weighed glass tube and dried with $N_2$ protection under 65 °C. The lipid was dissolved in 2.5 mL of 2% (v/v) $H_2SO_4$-methanol solution and heated at 85°C for 2.5 h. The fatty acid methyl ester (FAME) was obtained with 1 mL of n-hexane and 1 mL of saturated sodium chloride solution addition. FAME analysis was carried out using GC (GC2010, Shimadzu; SP-2560, 100m×0.25mm×0.2μm, Supelco, USA) (Zhang et al., 2020a).

The cell pellets were also used for other metabolites analysis. For pigment measurement, the cells at $8^{th}$ day were mixed with 80% (v/v) acetone and ethanol solution and incubated in the dark at 4°C for 60 min, then centrifuged at 7,500 rpm for 5 min to obtain the supernatant for chlorophyll and carotenoid content detection with ultraviolet spectrophotometer (Thermo Scientific, USA). 0.5 M NaOH was used to extract the protein by boiling for 10 min, then the supernatant after centrifugation was measured using the Bradford assay (Chen et al., 2012). For carbohydrate analysis, the cell pellets were re-suspended in 4 mL of $ddH_2O$ and transferred to a tube with 1 mL of 5% (w/v) phenol solution and 5 mL of HCl. The tube was incubated at 25°C for 10 min, then at 30°C for 20 min, and $OD_{483}$ was then measured (Liang et al., 2020). For fluorescence parameters measurement, 3 mL of algal suspension were adapted for 15 min in dark place then measured by Palm Water Chlorophyll Fluorometer (Aquapen-C AP-C 100, Photonic System Instrument, Czech Republic) (Zhang et al., 2020b).

To investigate the effect of the antioxidase system in cells, the harvested cells were broken using an Ultrasonic Cell Disruption System (Nanjing XinChen JY96-II, Nainjing, China) at 4°C for 15 min (3 s on and 3 s off). Then the supernatant obtained by centrifugation (12,000 rpm at 4°C for 10 min) was assayed according to Solarbio BC0170, BC0200 and BC0020 for SOD, CAT and MDA, respectively. (Zhang et al., 2020b).

The supernatant was detected by inorganic carbon content analyzer (MULTI N/C 2100 N5 221/I). For nitrogen concentration determination, the obtained supernatant was mixed with 20 μM HCl and 0.08% sulfamic acid according to Liu's report (Liu et al., 2013).

## Statistical analysis

All the experiments in this study were conducted in triplicate. Data is represented as the mean value with standard deviation (error bars). SPSS Statistics software program was used for one-way ANOVA at the significance level of 0.05 to calculate the salient difference between treatments.

# Results and discussion

## Effects of different combinations of temperature and bicarbonate content on growth and major metabolites accumulation in HTBS

Growth of the strain HTBS with high tolerance to low temperature and high bicarbonate content was evaluated under the combination of these above conditions. As shown in Figure 1A, the growth was inhibited slightly when cells were cultured at 16°C. However, cell density increased significantly with the addition of bicarbonate (0-0.15), then decreased when the bicarbonate content exceeded 0.15 M. The $OD_{680}$ reached to 1.18 under the condition of 0.15 M bicarbonate on day 7 when cultured at 16°C, which was 60.9% and 69.6% higher than cells under 25°C and 16°C without bicarbonate treatment, respectively. These results suggest that temperature and bicarbonate may affect the growth rate in microalgae cultivation. Previous study indicated the underlying mechanism that low temperature can inhibit the metabolic activity and result in the rigidification of the bilayer lipid membrane, which consequently affects the nutrient permeability and utilization (Chua et al., 2020). Furthermore, low temperature decreases the intracellular enzyme activity, which results in low cell density (Yang et al., 2019). Meanwhile, the addition of bicarbonate brings a high concentration of $Na^+$, 0.2 M of which can inhibit many algal strains (Srinivasan et al., 2015). Therefore, it seems as if the growth might be inhibited significantly by the combination of high $HCO_3^-$ and low temperature. Interestingly, the strain HTBS exhibited good bicarbonate-tolerance ability under low temperature condition in this study. The results suggested that the addition of bicarbonate was beneficial for algal strains to overcome the bottleneck caused by low temperature.

Bicarbonate and temperature conditions can also affect the biosynthesis of cellular components. As shown in Figure 1B, the lipid content of the group with 16°C and 0 M bicarbonate was 1.7% higher than treatment with 25°C and 0 M bicarbonate

(control), then increased from 36.41% to 43.94% when the bicarbonate supplement increased from 0 M to 0.15 M under 16°C. Carbohydrate as the other carbon storage material of HTBS increased from 24.67% to 29.18% (Figure 1C), which was consistent with previous results that carbon sources are positively related to carbohydrate content (Xu et al., 2017). Similar results were also obtained for protein content analysis (19.66% to 26.03%) (Figure 1D). With the addition of bicarbonate, the increased C/N ratio results in more lipid and carbohydrate biosynthesis for carbon storage with the excess energy (Peng et al., 2019; Singh et al., 2022; Xie et al., 2022). Although the lipid accumulation and protein biosynthesis present competitive relationships with each other, the increased profile of both lipid and protein content were observed in this study, possibly owing to the modified nitrogen content (750 mg/L), which was 10-fold higher than f/2 medium and promotes more intracellular conversion to protein (Vishwakarma et al., 2019). Hence, we speculate that the combination of stress could be used as an effective method for regulating the biosynthesis of main intracellular metabolites in HTBS.

## Effects of different combinations of temperature and bicarbonate content on fatty acid components changes in HTBS

The effects of different bicarbonate contents on the profile of fatty acids were investigated at 25°C and 16°C at 8 days after inoculation (Table 1). The results showed that C16:0 was the main saturated fatty acids in various conditions. C16:0 decreased slightly from 31.5% to 28.5% when cells were transferred from 25°C to 16°C without the addition of bicarbonate, whereas the unsaturated fatty acids, C18:1n9c significantly increased from 5.9% to 9.1% with an increment of 54.2%. A similar trend was observed at 25°C with 0.15 M bicarbonate addition. In contrast, the highly valued components C20:4 (AA) and C22:6 (DHA) were not found neither in both treatments at 25°C nor in treatment at low temperature without bicarbonate. Previous studies have emphasized the important effect of bicarbonate and low temperature on microalgae metabolites production (Chua et al., 2020). Lower temperature affects lipid composition, which is important to maintain membrane fluidity, and brings in an increase in the content of unsaturated fatty acids (Gao et al.,

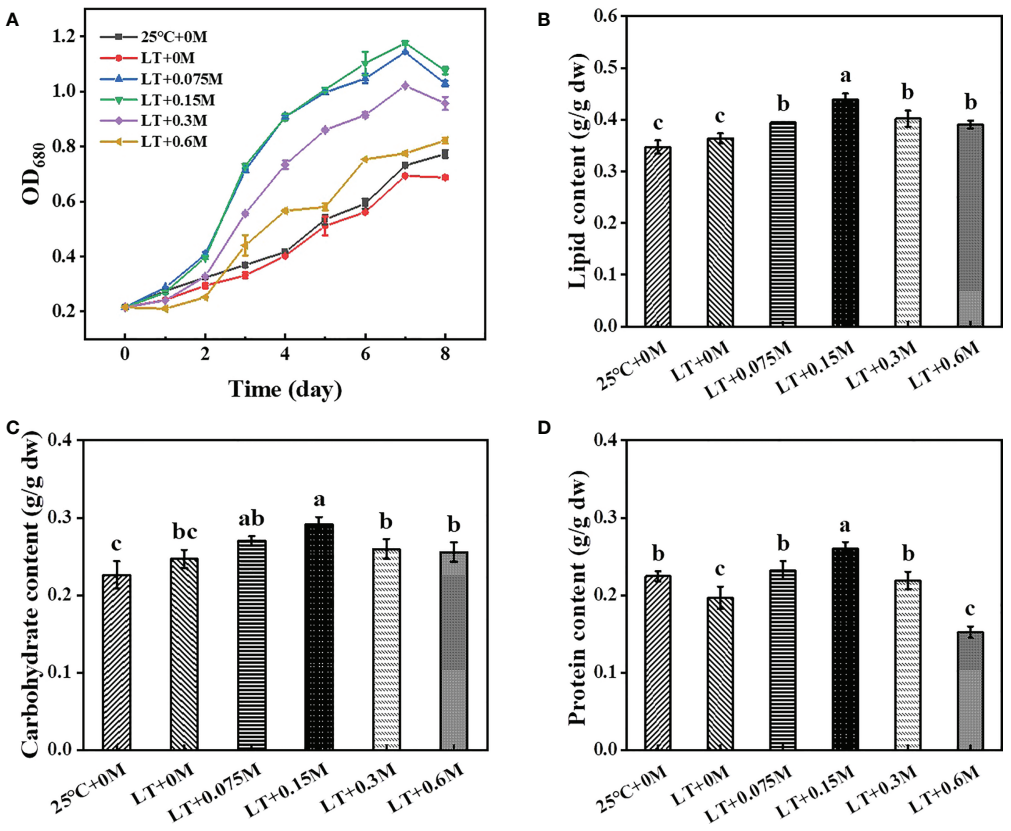


FIGURE 1
Effects of different combinations of bicarbonate and temperature on growth **(A)** and major metabolites (**B**, lipid; **C**, carbohydrate; **D**, protein) accumulation in HTBS.

TABLE 1 Fatty acids profile of HTBS cells under various conditions.

| Fatty acids(% in TFA) | 25 °C | | 16 °C | | | | |
|---|---|---|---|---|---|---|---|
| | 0 M[1] | 0.15 M[1] | 0 M[2] | 0.075 M[2] | 0.15 M[2] | 0.3 M[2] | 0.6 M[2] |
| C14:0 | 1.9 ± 0.1 | 1.3 ± 0.1 | 2.0 ± 0.2 | 1.3 ± 0.0 | 1.3 ± 0.0 | 1.0 ± 0.2 | 1.7 ± 0.2 |
| C16:0 | 31.6 ± 0.9 | 30.5 ± 0.6 | 28.5 ± 1.2 | 30.7 ± 0.9 | 30.8 ± 0.7 | 33.3 ± 1.4 | 29.2 ± 1.1 |
| C16:1 | 1.1 ± 0.2 | 1.1 ± 0.1 | 1.7 ± 0.3 | 1.0 ± 0.0 | 1.3 ± 0.1 | 0.6 ± 0.0 | 0.9 ± 0.0 |
| C18:0 | 6.6 ± 0.4 | 7.5 ± 0.9 | 6.8 ± 1.2 | 7.7 ± 0.1 | 8.4 ± 0.7 | 11.6 ± 0.3 | 7.4 ± 0.9 |
| C18:1n9c | 5.9 ± 0.5 | 8.1 ± 0.3 | 9.1 ± 1.1 | 9.2 ± 0.2 | 10.6 ± 1.3 | 10.1 ± 0.1 | 10.2 ± 0.8 |
| C18:2n6t | 11.8 ± 1.0 | 10.2 ± 1.0 | 11.9 ± 0.3 | 8.2 ± 0.1 | 8.3 ± 0.8 | 7.2 ± 0.5 | 8.4 ± 0.8 |
| C18:2n6c | 4.9 ± 1.6 | 6.8 ± 0.6 | 5.6 ± 0.2 | 11.2 ± 0.3 | 9.1 ± 0.5 | 6.2 ± 0.2 | 7.9 ± 0.0 |
| C18:3n6 | 1.7 ± 0.0 | 1.3 ± 0.1 | 1.6 ± 0.8 | 1.3 ± 0.0 | 1.4 ± 0.1 | 0.8 ± 0.1 | 1.1 ± 0.1 |
| C18:3n3 | 34.5 ± 1.2 | 33.2 ± 1.6 | 32.9 ± 2.2 | 27.2 ± 1.5 | 25.7 ± 1.0 | 21.0 ± 0.4 | 26.5 ± 0.5 |
| C20:4 (AA) | – | – | – | 0.4 ± 0.1 | 1.1 ± 0.2 | 3.5 ± 0.5 | 2.0 ± 0.4 |
| C22:6 (DHA) | – | – | – | 1.8 ± 0.2 | 2.1 ± 0.4 | 4.7 ± 0.3 | 4.6 ± 0.1 |

Data represent mean ± SD of three replicates. TFA, total fatty acids. "-" represents that the fatty acid was not detected. "[1]" represents the results in 25°C, "[2]" represents the results in 16°C.

2018). The strain HTBS appears to be incapable of biosynthesizing AA and DHA under either low temperature or high bicarbonate conditions. Interestingly, the combination resulted in AA and DHA accumulation. Moreover, the profiles of the two fatty acids varied in different bicarbonate content treatments at 16°C. AA concentration increased from 0.38% to 3.52% with the content of bicarbonate increased from 0.075 M to 0.3 M, then decreased to 2.0% when bicarbonate reached to 0.6 M. Similarly, the relative percentages of DHA were 1.8%, 2.1%, 4.7% and 4.6% for 0.075 M, 0.15 M, 0.3 M and 0.6 M bicarbonate under 16°C, respectively. The highest AA and DHA concentrations in total fatty acids were found in 0.3 M bicarbonate condition, which accounted for 8.2% of the total fatty acids. In contrast, the PUFA (EPA, C20:5) of *Nannochloropsis oculata* was observed in normal culture condition and increased obviously in the group at 15°C (Willette et al., 2018; Chua et al., 2020). Another *D. salina* strain was reported to produce AA and DHA at 25°C, and the content of AA and DHA increased slightly with carbon stress (Almutairi, 2020). By contrast, AA and DHA were undetectable in *D. salina* Y6 under various conditions, such as high-light, nitrogen-depleted and high-salt conditions. In general, microalgae cells accumulate more PUFAs to increase membrane fluidity to counteract the negative effect caused by lower temperatures (Lu et al., 2017). Nevertheless, with the good ability of tolerance to cold treatment, the membrane fluidity of HTBS is activated as the cells grow well at 16°C and 4°C, thus the PUFAs such as AA and DHA are unnecessary to be synthesized (Hou et al., 2016; Wu et al., 2020). Then, more carbon resource is provided with the supplement of bicarbonate, which might be used for secondary metabolites conversion (Chua et al., 2020; Wu et al., 2021). In addition, bicarbonate may induce ROS production, which could be counteracted by increasing PUFA synthesis (Xie et al., 2021; Ju et al., 2022; Vinuganesh et al., 2022). As a result, AA and DHA are accumulated with the combinatorial stresses.

## Effects of different combinations on photosynthetic performance and carbon and nitrogen removal rate of HTBS

To illustrate the potential reason for the effects of various bicarbonate contents with low temperature on growth and metabolite biosynthesis, the photosynthetic performance and carbon\nitrogen utilization rate were investigated (Figure 2). The maximum photochemical efficiency (Fv/Fm) was reduced by 19.35% compared to the control culture at 25 °C due to the low temperature and lack of bicarbonate supply. The addition of bicarbonate alleviated low temperature-induced photosynthesis impairment, as Fv/Fm increased by 54.67%, 34.22%, 14.67% and 12% at 0.075 M, 0.15 M, 0.3 M and 0.6 M bicarbonate, respectively, which was consistent with the previous study (Sun et al., 2020). Similarly, microalgae cells with an increased bicarbonate conditions showed a gradually significant rise in Fv/Fm, which suggested an increase in photosynthetic carbon fixation and metabolic activity (Singh et al., 2022). With the sustained addition of bicarbonate, the salinity increases to suppress of photosynthetic activity (Salbitani et al., 2020). Luckily, the extracellular carbon anhydrases in HTBS are sufficient to provide enough Ci for the growth under high bicarbonate levels (Hou et al., 2016). Then the carboxylation reaction catalyzed by Rubisco in the dark reaction could be enhanced, which resulted in ATP and NADPH consumption. Hence, Fv/Fm was increased to promote electron transfer to generate more energy for carbon fixation, which resulted in a higher carbon removal rate (Figure 2C) and higher biomass (Figure 1) (Xie et al., 2022). The increased non-photochemical quenching (NPQ) means that the cells are suffering from environmental stress (Xue et al., 2022). Therefore, the reductions of NPQ at 0.075 M and 0.15M bicarbonate groups suggest that a certain bicarbonate content can help to relieve the

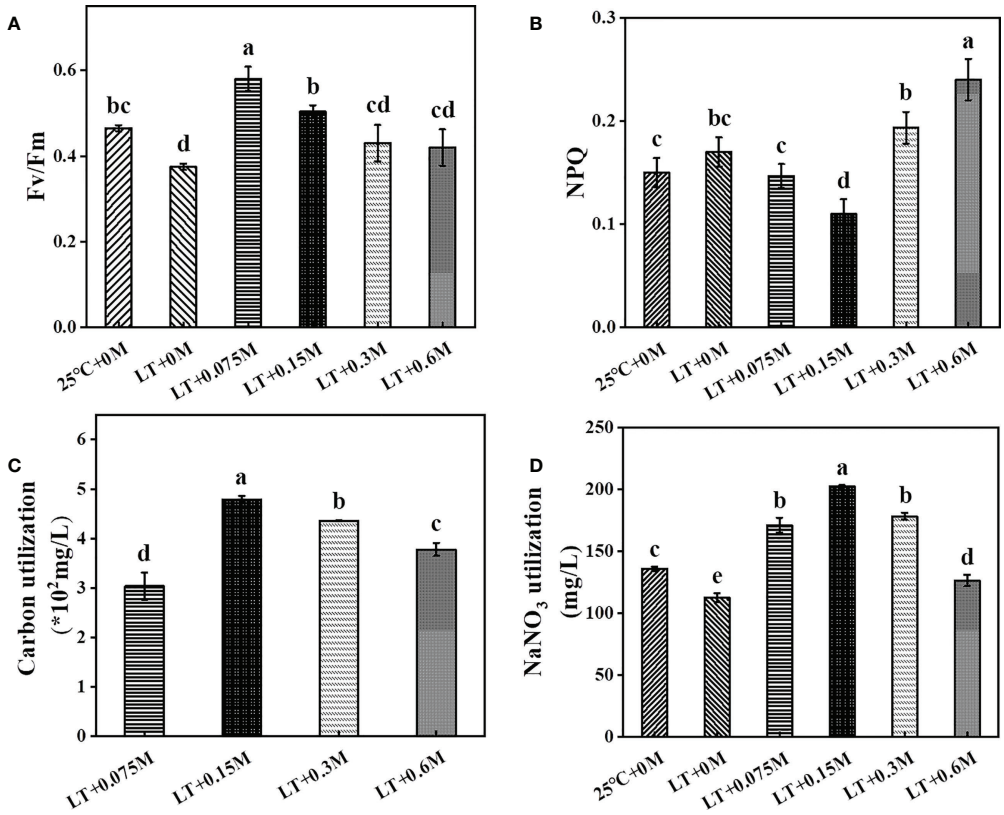


FIGURE 2
Effects of various combinations on HTBS photosynthetic performance [**(A)**, Fv/Fm; **(B)**, NPQ] and nutrient removal rate [**(C)**, carbon; **(D)**, nitrogen]. Data were mean ± SD of three replicates.

stress caused by low temperature, which is consistent with the report that a high concentration of $CO_2$ declines NPQ to benefit carbon and nitrogen sequestration, resulting in more metabolite synthesis (Singh et al., 2022). As a consequence, the carbon and nitrogen removal rates of the combined groups were significantly increased compared to low temperature treatment without bicarbonate supply. The visible nutrient utilization might be attributed to the increased Fv/Fm and decreased NPQ. Overall, these results indicated that HTBS with the combination of optimum bicarbonate concentration and low temperature showed good photosynthetic performance, which resulted in a significant increase in cell proliferation.

## Pigment changes in HTBS in response to different combined stresses

As shown in Figure S1, low temperature without bicarbonate affected chlorophyll (Chl) biosynthesis slightly. However, the additional bicarbonate showed a dose-dependent effect. Chl was gradually increased by 9.67%, 27.43% and 43.58% with the added bicarbonate content increasing from 0.075 M to 0.3 M, while the extremely high content of bicarbonate (0.6 M) inhibited Chl biosynthesis. It means that a certain bicarbonate content accelerates Chl synthesis to maintain photosynthetic activity and alleviate the stress caused by low temperature (Xie et al., 2022). Meanwhile, carotenoids, another important pigment for light harvest and energy transfer, were affected by the combination of low temperature and bicarbonate. The carotenoid contents of the combined stress groups increased compared with the low temperature without bicarbonate, which indicated that more energy is required for carbon utilization under high carbon resources in HTBS (Ding et al., 2017).

## The effects of the combined stresses on oxidation resistance parameter

To respond to the stress-induced ROS, the antioxidant system is activated to protect cells from oxidative damage (Rezayian et al., 2019). Superoxide dismutase (SOD) and catalase (CAT) were up-regulated to scavenge superoxide radicals and hydrogen peroxide at low temperature. In this study, SOD and CAT decreased under low temperature

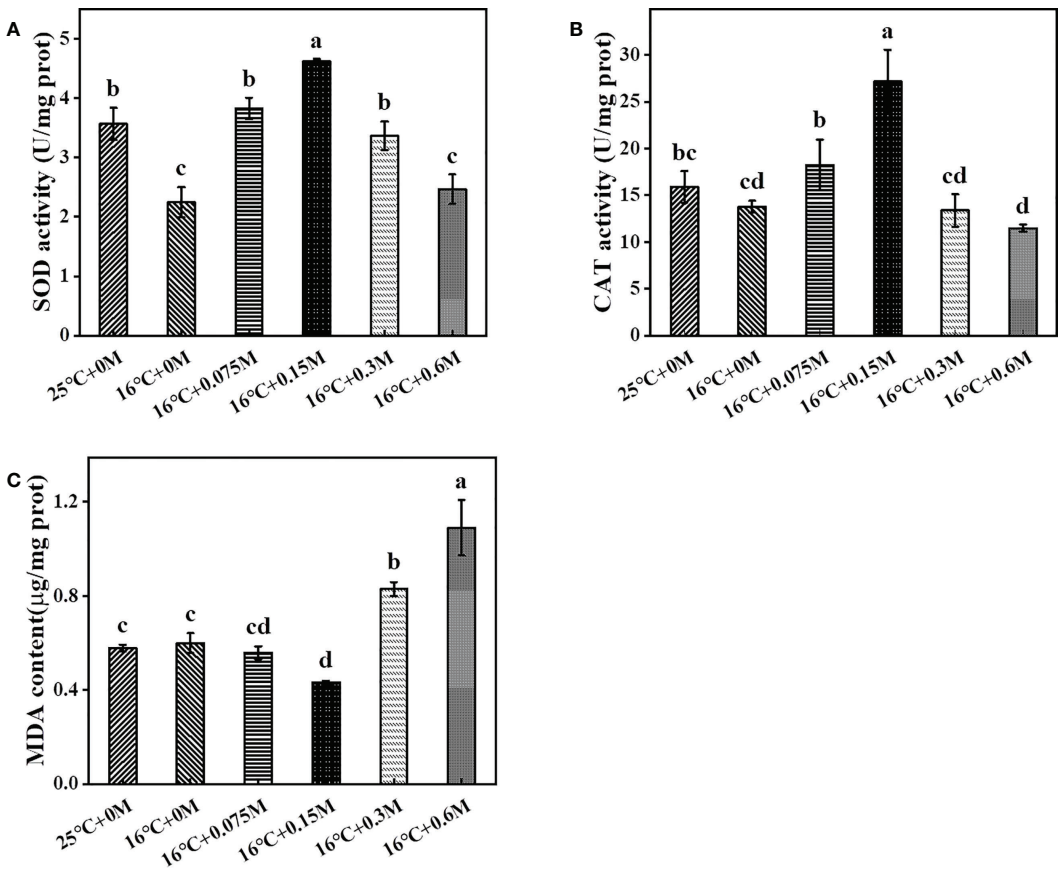


FIGURE 3
Changes of SOD **(A)**, CAT **(B)** activities and MDA **(C)** content in HTBS cells grown under different stresses.

without bicarbonate, probably due to the good low-temperature tolerance of HTBS (Hou et al., 2016). SOD activity increased and reached its maximum at the 0.15 M bicarbonate group, which was 89% higher than that in the group without carbon supply, followed by a decrease in activity (Figure 3A). The increased SOD activity resulted in $H_2O_2$ accumulation, which could be converted to $H_2O$ by CAT. CAT activity was closely associated with SOD activity (Figure 3B). On the other hand, MDA, the biomarker for evaluating oxidative damage, was also assessed. With the addition of bicarbonate at 16 °C, MDA decreased slightly and then significantly increased (Figure 3C). These results suggested that HTBS adapted to the environment by regulating specific enzymes in response to the combined stresses (Srinivasan et al., 2018).

## Conclusions

In this study, the effects of a combination of low temperature and bicarbonate on physiological and biochemical changes in HTBS were investigated. Compared to single stress (low temperature or bicarbonate), the content of pigment and, Fv/Fm was increased while NPQ was decreased under the combination of low temperature and bicarbonate stress. All of the above changes benefited carbon and nitrogen absorption and utilization, which resulted in an increase in cell growth, lipid, protein and carbohydrate with combined conditions. Moreover, AA and DHA reached 3.52% and 4.73%, respectively, whereas they were not detected with single treatment. The present study demonstrates that supplementing bicarbonate under low temperature could effectively enhance the biomass production and accumulation of AA and DHA in *D. salina* HTBS, which benefits the development of the microalgae industry in value-added products.

## Data availability statement

The original contributions presented in the study are included in the article/Supplementary Material. Further inquiries can be directed to the corresponding authors.

## Author contributions

WW, ZL, CF and HY conceived the ideas and the experimental design. GZ, LZ, GT and MY collected the data. HT, HN, YY and LC analyzed the data. HY, GZ and GT drafted the manuscript. MS, WW, ZL and CF reviewed and edited the manuscript. All authors contributed to the article and approved the submitted version.

## Funding

This work was supported by the National Key R&D Program of China (2019YFA0904600; 2018YFE0107200), the Science and Technology Partnership Program, Ministry of Science and Technology of China (KY202001017), the Tianjin Synthetic Biotechnology Innovation Capacity Improvement Project (TSBICIP-IJCP-001; TSBICIP-CXRC-027), and the TIB-VIB Joint Center of Synthetic Biology (TSBICIP-IJCP-002).

## Conflict of interest

The authors declare that the research was conducted in the absence of any commercial or financial relationships that could be construed as a potential conflict of interest.

## Publisher's note

All claims expressed in this article are solely those of the authors and do not necessarily represent those of their affiliated organizations, or those of the publisher, the editors and the reviewers. Any product that may be evaluated in this article, or claim that may be made by its manufacturer, is not guaranteed or endorsed by the publisher.

## Supplementary material

The Supplementary Material for this article can be found online at: https://www.frontiersin.org/articles/10.3389/fmars.2022.971441/full#supplementary-material

## References

Almutairi, A. W. (2020). Effects of nitrogen and phosphorus limitations on fatty acid methyl esters and fuel properties of *Dunaliella salina*. *Environ. Sci. pollut. Res.* 27 (26), 32296–32303. doi: 10.1007/s11356-020-08531-8

Aussant, J., Guihéneuf, F., and Stengel, D. (2018). Impact of temperature on fatty acid composition and nutritional value in eight species of microalgae. *Appl. Microbiol. Biotechnol.* 102 (12), 5279–5297. doi: 10.1007/s00253-018-9001-x

Chauhan, D., Sahoo, L., and Mohanty, K. (2022). Maximize microalgal carbon dioxide utilization and lipid productivity by using toxic flue gas compounds as nutrient source. *Bioresour. Technol.* 348, 126784. doi: 10.1016/j.biortech.2022.126784

Chen, H., and Jiang, J. (2009). Osmotic responses of *Dunaliella* to the changes of salinity. *J. Cell Physiol.* 219 (2), 251–258. doi: 10.1002/jcp.21715

Chen, F., Liu, Z., Li, D., Liu, C., Zheng, P., and Chen, S. (2012). Using ammonia for algae harvesting and as nutrient in subsequent cultures. *Bioresour. Technol.* 121, 298–303. doi: 10.1016/j.biortech.2012.06.076

Chi, Z., Elloy, F., Xie, Y., Hu, Y., and Chen, S. (2014). Selection of microalgae and cyanobacteria strains for bicarbonate-based integrated carbon capture and algae production system. *Appl. Biochem. Biotechnol.* 172, 447–457. doi: 10.1007/s12010-013-0515-5

Chua, E. T., Dal'Molin, C., Thomas-Hall, S., Netzel, M. E., Netzel, G., and Schenk, P. M. (2020). Cold and dark treatments induce omega-3 fatty acid and carotenoid production in *Nannochloropsis oceanica*. *Algal Res.* 51, 102059. doi: 10.1016/j.algal.2020.102059

Ding, Y., Li, X., Li, Z., Wang, Z., Li, Z., Geng, Y., et al. (2017). Ammonium bicarbonate supplementation as carbon source in alkaliphilic *Spirulina* mass culture. *Aquac. Res.* 48 (9), 4886–4896. doi: 10.1111/are.13308

Gao, G., Clare, .A S., Chatzidimitriou, E., Rose, C., and Caldwell, G. S. (2018). Effects of ocean warming and acidification, combined with nutrient enrichment, on chemical composition and functional properties of *Ulva rigida*. *Food Chem.* 258, 71–78. doi: 10.1016/j.foodchem.2018.03.040

Guihéneuf, F., and Stengel, D. B. (2013). LC-PUFA-enriched oil production by microalgae: accumulation of lipid and triacylglycerols containing n-3 LC-PUFA is triggered by nitrogen limitation and inorganic carbon availability in the marine haptophyte *Pavlova lutheri*. *Mar. Drugs* 11, 4246–4266. doi: 10.3390/md11114246

Hou, Y., Liu, Z., Zhao, Y., Chen, S., Zheng, Y., and Chen, F. (2016). CAH1 and CAH2 as key enzymes required for high bicarbonate tolerance of a novel microalga *Dunaliella salina* HTBS. *Enzyme. Microb. Tech.* 87-88, 17–23. doi: 10.1016/j.enzmictec.2016.02.010

Jakhwal, P., Biswas, J. K., Tiwari, A., Kwon, E. E., and Bhatnagar, A. (2022). Genetic and non-genetic tailoring of microalgae for the enhanced production of eicosapentaenoic acid (EPA) and docosahexaenoic acid (DHA) - a review. *Bioresour. Technol.* 344 (Pt B), 126250. doi: 10.1016/j.biortech.2021.126250

Ju, Z., Feng, T., Feng, J., Lv, J., Xie, S., and Liu, Q. (2022). Physiological response of an oil-producing microalgal strain to salinity and light stress. *Foods.* 11 (2), 11020215. doi: 10.3390/foods11020215

Khozin-Goldberg, I., Bigogno, C., Shrestha, P., and Cohen, Z. (2002). Nitrogen starvation induces the accumulation of arachidonic acid in the freshwater green alga *parietochloris incisa* (*trebuxiophyceae*). *J. Phycol.* 38, 991–994. doi: 10.1046/j.1529-8817.2002.01160.x

Liang, C., Yang, X., Wang, L., Fan, X., Zhang, X., Xu, D., et al. (2020). Different physiological and molecular responses of the green algae *Chlorella variabilis* to long-term and short-term elevated $CO_2$.J. *Appl. Phycol.* 32 (2), 951–966. doi: 10.1007/s10811-019-01943-1

Liu, Z., Liu, C., Hou, Y., Chen, S., Xiao, D., Zhang, J., et al. (2013). Isolation and characterization of a marine microalga for biofuel production with astaxanthin as a co-product. *Energies.* 6 (6), 2759–2772. doi: 10.3390/en6062759

Lu, Q., Li, J., Wang, J., Li, K., Li, J. J., Han, P., et al. (2017). Exploration of a mechanism for the production of highly unsaturated fatty acids in scenedesmus sp. at low temperature grown on oil crop residue based medium. *Bioresour. Technol.* 244 (Pt 1), 542–551. doi: 10.1016/j.biortech.2017.08.005

Lu, Q., Li, H., Xiao, Y., and Liu, H. (2021). A state-of-the-art review on the synthetic mechanisms, production technologies, and practical application of polyunsaturated fatty acids from microalgae. *Algal Res.* 55, 102281. doi: 10.1016/j.algal.2021.102281

Morales, M., Aflalo, C., and Bernard, O. (2021). Microalgal lipids: A review of lipids potential and quantification for 95 phytoplankton species. *Biomass. Bioenerg.* 150, 106108. doi: 10.1016/j.biombioe.2021.106108

Nunez, M., and Quigg, A. (2016). "Changes in growth and composition of the marine microalgae *Phaeodactylum tricornutum* and *Nannochloropsis salina* in response to changing sodium bicarbonate concentrations." appl. *Phycol.* 28 (4), 2123–2138. doi: 10.1007/s10811-015-0746-7

Peng, Y. Y., Gao, F., Hang, W., Yang, H., Jin, W., and Li, C. (2019). Effects of organic matters in domestic wastewater on lipid/carbohydrate production and nutrient removal of *Chlorella vulgaris* cultivated under mixotrophic growth conditions. *J. Chem. Technol. Biot.* 94 (11), 3578–3584. doi: 10.1002/jctb.6161

Ratomski, P., Hawrot-Paw, M., and Koniuszy, A. (2021). Utilisation of $CO_2$ from sodium bicarbonate to produce *Chlorella vulgaris* biomass in tubular

photobioreactors for biofuel purposes. *Sustainability* 13 (16), 9118. doi: 10.3390/su13169118

Rezayian, M., Niknam, V., and Ebrahimzadeh, H. (2019). Oxidative damage and antioxidative system in algae. *Toxicol. Rep*. 6, 1309–1313. doi: 10.1016/j.toxrep.2019.10.001

Salbitani, G., Bolinesi, F., Affuso, M., Carraturo, F., Mangoniand, O., and O.Carfagna, S. (2020). Rapid and positive effect of bicarbonate addition on growth and photosynthetic efficiency of the green microalgae *Chlorella sorokiniana* (*Chlorophyta, trebouxiophyceae*). *Appl. Sci.* 10 (13), 4515. doi: 10.3390/app10134515

Singh, R. P., Yadav, P., Kumar, A., Hashem, A., Al-Arjani, A. F., Allah, E. F. A, et al. (2022). Physiological and biochemical responses of bicarbonate supplementation on biomass and lipid content of green algae scenedesmus sp. BHU1 isolated from wastewater for renewable biofuel feedstock. *Front. Microbiol.* 13, 839800. doi: 10.3389/fmicb.2022.839800

Srinivasan, R., Kumar, V. A., Kumar, D., Ramesh, N., Babu, S., Gothandam, K. M., et al. (2015). Effect of dissolved inorganic carbon on beta-carotene and fatty acid production in dunaliella sp. appl. biochem. *Biotechnol.* 175 (6), 2895–2906. doi: 10.1007/s12010-014-1461-6

Srinivasan, R., Mageswari, A., Subramanian, P., Suganthi, C., Chaitanyakumar, A., Aswini, V., et al. (2018). Bicarbonate supplementation enhances growth and biochemical composition of *Dunaliella salina* V-101 by reducing oxidative stress induced during macronutrient deficit conditions. *Sci. Rep.* 8 (1), 6972. doi: 10.1038/s41598-018-25417-5

Sun, H., Ren, Y., Mao, X., Li, X., Zhang, H., Lao, Y., et al. (2020). Harnessing C/N balance of *Chromochloris zofingiensis* to overcome the potential conflict in microalgal production. *Commun. Biol.* 3 (1), 186. doi: 10.1038/s42003-020-0900-x

Vishwakarma, J., Parmar, V., and Vavilala, S. L. (2019). Nitrate stress-induced bioactive sulfated polysaccharides from *Chlamydomonas reinhardtii. Biomed. Res. J.* 6 (1), 7–16. doi: 10.4103/BMRJ.BMRJ_8_19

Vinuganesh, A., Kumar, A., Prakash, S., Alotaibi, M., Saleh, A., Mohammed, A., et al. (2022). Influence of seawater acidification on biochemical composition and oxidative status of green algae *Ulva compressa. Sci. Total. Environ.* 806 (Pt 1), 150445. doi: 10.1016/j.scitotenv.2021.150445

Willette, S., Gill, S. S., Dungan, B., Schaubb, T. M., Jarvisb, J. M., Hilairea, R. S., et al. (2018). Alterations in lipidome and metabolome profiles of *Nannochloropsis salina* in response to reduced culture temperature during sinusoidal temperature and light. *Algal Res.* 32, 79–92. doi: 10.1016/j.algal.2018.03.001

Wu, M., Zhu, R., Lu, J., Lei, A., Zhu, H., Hu, Z., et al. (2020). Effects of different abiotic stresses on carotenoid and fatty acid metabolism in the green microalga *Dunaliella salina* Y6. *Ann. Microbiol.* 70, 48. doi: 10.1186/s13213-020-01588-3

Wu, M., Gao, G., Jian, W., and Xu, J. (2021). High $CO_2$ increases lipid and polyunsaturated fatty acid productivity of the marine diatom *Skeletonema costatum* in a two-stage model. *J. Appl. Phycol.* 34 (1), 43–50. doi: 10.1007/s10811-021-02619-5

Xie, G., Ding, K., Liu, W., Zheng, Z., Liu, Y., and Wang, Y. (2021). Characteristics of lipid biosynthesis in *Chlorella pyrenoidosa* as subjected to nutrient deficiency stress. *Phycologia*. 60 (4), 384–393. doi: 10.1080/00318884.2021.1948751

Xie, S., Lin, F., Zhao, X., and Gao, G. (2022). Enhanced lipid productivity coupled with carbon and nitrogen removal of the diatom *Skeletonema costatum* cultured in the high $CO_2$ level. *Algal. Res.* 61, 102589. doi: 10.1016/j.algal.2021.102589

Xue, S., Zang, Y., Chen, J., Shang, S., and Tang, X. (2022). Effects of enhanced UV-b radiation on photosynthetic performance and non-photochemical quenching process of intertidal red macroalgae *Neoporphyra haitanensis. Environ. Exp. Bot.* 199, 104888. doi: 10.1016/j.envexpbot.2022.104888

Xu, Z., Gao, G., Xu, J., and Wu, H. (2017). Physiological response of a golden tide alga (*Sargassum muticum*) to the interaction of ocean acidification and phosphorus enrichment. *Biogeosciences* 14 (3), 671–681. doi: 10.5194/bg-14-671-2017

Yang, J., Yu, D., Ma, Y., Yin, Y., and Shen, S. (2019). Antioxidative defense response of *Ulva prolifera* under high or low-temperature stimulus. *Algal Res.* 44, 101703. doi: 10.1016/j.algal.2019.101703

Zhang, S., Hou, Y., Liu, Z., Ji, X., Wu, D., Wang, W., et al. (2020a). Electro-fenton based technique to enhance cell harvest and lipid etraction from microalgae. *Energies* 13 (15), 3813. doi: 10.3390/en13153813

Zhang, C., Li, R., Zhu, Q., Hang, W., Zhang, H., Cui, H., et al. (2020b). Antioxidant enzymes and the mitochondrial alternative oxidase pathway play important roles in chilling tolerance of *Haematococcus pluvialis* at the green motile stage. *Algal Res.* 50, 102003. doi: 10.1016/j.algal.2020.102003

frontiers | Frontiers in Marine Science

TYPE Original Research
PUBLISHED 21 November 2022
DOI 10.3389/fmars.2022.1057201



OPEN ACCESS

EDITED BY
Liandong Zhu,
Wuhan University, China

REVIEWED BY
Hongli Cui,
Shanxi Agricultural University, China
Ravi Raghavbhai Sonani,
Jagiellonian University, Poland

*CORRESPONDENCE
Jianke Huang
jkhuang@hhu.edu.cn
Ai-Hua Zhang
ahz@hhu.edu.cn

SPECIALTY SECTION
This article was submitted to Marine Fisheries, Aquaculture and Living Resources, a section of the journal Frontiers in Marine Science

RECEIVED 29 September 2022
ACCEPTED 31 October 2022
PUBLISHED 21 November 2022

CITATION
Yao T, Huang J, Su B, Wei L, Zhang A-H, Zhang D-F, Zhou Y and Ma G (2022) Enhanced phycocyanin production of *Arthrospira maxima* by addition of mineral elements and polypeptides using response surface methodology.
*Front. Mar. Sci.* 9:1057201.
doi: 10.3389/fmars.2022.1057201



# Enhanced phycocyanin production of *Arthrospira maxima* by addition of mineral elements and polypeptides using response surface methodology

Ting Yao[1], Jianke Huang[1,2]*, Bocheng Su[1], Liang Wei[1], Ai-Hua Zhang[1]*, Dao-Feng Zhang[1], Yongsheng Zhou[3] and Guangyuan Ma[3]

[1]Jiangsu Province Engineering Research Center for Marine Bio-resources Sustainable Utilization, College of Oceanography, Hohai University, Nanjing, Jiangsu, China, [2]Nantong institute of ocean and offshore engineering, Hohai University, Nantong, Jiangsu, China, [3]Jiangsu Innovation Center of Marine Bioresources, Jiangsu Coast Development Group Co., Ltd, Nanjing, Jiangsu, China

**Introduction:** As a pigment protein, phycocyanin has been widely used in the fields of food, nutraceutical and biotechnology due to its excellent biological activities of antioxidant. So far, *Arthrospira* has been generally considered as a great species for phycocyanin production.

**Methods:** In this study, independent and interactive effect of three factors, NaCl, Bainengsi (BS) and Bainengtai (BT) on microalgae growth and phycocyanin production were explored by response surface methodology (RSM). Using Box-Behnken design (BBD) method, the well-fitting quadratic models were established based on experimental results.

**Results:** Moreover, the maximum phycocyanin concentration reached 704.66 mg $L^{-1}$ at the optimal condition (185 mM NaCl, 200 mg $L^{-1}$ BS, and 20 mg $L^{-1}$ BT), while the maximum phycocyanin content of 19.03% was obtained at another optimal condition (136 mM NaCl, 200 mg $L^{-1}$ BS, and 50 mg $L^{-1}$ BT). Compared to control, the concentration and content of phycocyanin were increased by 22.98% and 16.73%, respectively.

**Discussion:** Overall, this study demonstrated that addition of exogenous substances (BS, BT) into culture medium optimized by RSM was an effective approach to increase phycocyanin production, which paved a potential way to realizing high efficient production of algal biomass and bioactive substances.

KEYWORDS

***Arthrospira maxima*, phycocyanin, response surface methodology, mineral elements complexes, polypeptides, medium optimization**

# 1 Introduction

Microalgae have been extensively considered as renewable and sustainable resources for the production of various bioactive substances, such as phycobiliproteins (Manirafasha et al., 2016), carotenoids (Novoveská et al., 2019), polyunsaturated fatty acids (Lu et al., 2021), and polysaccharide (Sathasivam et al., 2019). Phycobiliprotein is a kind of pigment protein that widely exists in cyanobacteria, rhodophyta, cryptophyta, and glaucophyta (Lawrenz et al., 2011; Yu et al., 2017). In cyanobacteria, phycobiliprotein can account for 40% of the total soluble protein (Pandey et al., 2013). Generally, there are four types of phycobiliprotein, namely phycoerythrin, phycocyanin, phycoerythrocyanin, and allophycocyanin (Pagels et al., 2019). Phycocyanin shows great antioxidant and radical scavenging activity (Fratelli et al., 2021; Li, 2022). Besides, phycocyanin has other biological activities, like anti-inflammatory, anti-cancer, anti-diabetes, neuroprotective and hepatoprotective effects (Romay et al., 2003; Jiang et al., 2017; Prabakaran et al., 2020). Thereby, phycocyanin nowadays is widely used in food, nutraceutical, cosmetics, and pharmaceutical industries (Manirafasha et al., 2016; Khazi et al., 2020). Presently, the commercial price of phycocyanin varies enormously depending on its purity. It was reported that the price of food-grade phycoerythrin was approximately \$130 $g^{-1}$ (Hsieh-Lo et al., 2019). Moreover, the market demands for phycoerythrin continuously increased in the past few years due to its natural and functional properties. Specifically, the global market size of phycocyanin was valued at \$155.3 million in 2020 and it is estimated to reach \$409.8 million by 2030 (Thevarajah et al., 2022).

*Arthrospira*, commonly known as *Spirulina*, is a multicellular and filamentous cyanobacteria (Soni et al., 2017). It is generally rich in protein, carbohydrates, phycocyanin, fatty acids, and chlorophyll (Anvar and Nowruzi, 2021). *Arthrospira* is well considered as an excellent source of the production of phycocyanin (CPC) (Nethravathy et al., 2019; Silva et al., 2020). To date, numerous studies have been conducted to improve the phycocyanin productivity and content of *Arthrospira*. The main strategies includes culture medium improvement, exogenous substances addition (Manirafasha et al., 2018), environmental condition optimization (Bachchhav et al., 2016), and changing of culture mode (Chen et al., 2006). The optimization of culture medium is always a basic work to enhance microalgal growth and phycocyanin production. Nitrogen is one of the primary nutrient requirements for algal cell growth. With the nitrogen ($NaNO_3$) concentration in the medium increased from 0.63 to 2.5 g $L^{-1}$, the biomass concentration of *Arthrospira* highly increased from 0.83 to 1.04 g $L^{-1}$ (Can et al., 2017). In addition to nitrogen concentration, microalgae growth and phycocyanin production are also affected by type of nitrogen source. Mousavi et al. (2022) found that *Arthrospira* cultured in the medium containing $(NH_4)_2SO_4$ produced the largest amount of phycocyanin (118 mg $L^{-1}$) while the medium with $KNO_3$ as the nitrogen source resulted in the highest biomass output (1.18 g $L^{-1}$). In addition, salinity of culture medium significantly influences algal cell growth and phycocyanin accumulation. The Zarrouk medium with 0.1 M NaCl considerably raised the biomass productivity from 139.5 mg $L^{-1}$ $d^{-1}$ at the normal condition (0.02 M NaCl) to 221.33 mg $L^{-1}$ $d^{-1}$, and the total phycobiliprotein content increased from 11.08% to 15.63% (Abd El-Baky and El-Baroty, 2012). However, the impact of salinity on cell growth and phycobiliprotein production is highly related to NaCl concentration. The tremendously high NaCl concentration would result in very low biomass and phycobiliprotein productivity (Chen et al., 2016).

Besides, the addition of exogenous substances is also an efficient approach to promote the biomass and phycocyanin accumulation. The supplements of mineral elements, organic acids, and vitamins in culture medium have been reported to enhance biomass and phycocyanin production (Jung et al., 2014; Bachchhav et al., 2016; Mogany et al., 2018). Stepwise addition of selenium (Se) during the exponential growth phase of *Arthrospira. platensis* grown mixotrophically increased the phycocyanin production by 21.2% compared to control (Chen et al., 2006). The metabolic stress conditions induced by nutrient enrichment through additionally adding sodium glutamate and succinic acid strongly boosted the biomass production and phycocyanin concentration of *Arthrospira platensis* (Bachchhav et al., 2016). Hence, the addition of suitable substance in culture medium at an appropriate range is critical to efficient production of phycocyanin.

Response surface methodology (RSM) is a set of mathematical and statistical techniques that are based on fitting a polynomial equation to experimental data (Bezerra et al., 2008). Currently, the RSM has been used to optimize the culture process of microalgae. To maximize the biomass production of *Chlorella* sp. as biofuel production stock, the optimal concentration of nitrogen and glycerol (0.114 g $L^{-1}$ and 2.70 g $L^{-1}$) were determined by the RSM, and the highest biomass reached 2.41 g $L^{-1}$ at this condition (Skorupskaite et al., 2015). Verma et al. (2020) performed the culture experiments to improved medium using the RSM, and obtained the highest biomass productivity of 0.86 g $L^{-1}$ $d^{-1}$ at the optimal conditions. Undoubtedly, RSM is an efficient and effective means to optimize the culture medium.

There are commercial products of mineral element complexes and peptide complexes, commonly called Bainengsi (BS) and Bainengtai (BT), respectively, in China. BS contains many mineral elements including Si, Mo, Se, Ni, Bo, K and so on. BT is composed of enzymatic hydrolysates of high-quality proteins sourced from plants. BS and BT have been used in agriculture and feed industries to enhance the plant and animal growth. In the present study, we consider BS and BT as the additional supplements for *Arthrospira maxima* culture. The main aim of the research is to evaluate the independent and

interaction effect of three factors (BS, BT, and NaCl concentrations) on biomass and phycocyanin production of *Arthrospira maxima*, and to determine the optimal addition amounts of these substances using RSM to maximize the productivity and content of phycocyanin.

# 2 Materials and methods

## 2.1 Microalgae strain

*Arthrospira maxima* (FACHB-438) was obtained from the Freshwater Algae Culture Collection at the Institute of Hydrobiology (FACHB), China. For stock culture preparation, the microalgal cells were cultivated in Zarrouk medium (Zarrouk, 1996) at 31°C and light intensity of 80 μ mol $m^{-2}$ $s^{-1}$.

## 2.2 Exogenous substances

Two types of exogenous substances (BS and BT) were added into culture medium to explore their impacts on the growth and phycocyanin production of Arthrospira maxima. BS and BT were purchased from Jiangsu Rishengchang Biotechnology Company, China. BS is the mineral element complexes and composed of various inorganic microelements. Based on element analysis *via* the method of inductively coupled plasma optical emission spectrometer (ICP-OES), the contents of Na, K, Cl, Fe, Mn, Mg, Mo, Ba, S, B, Al, Ti, Zn, Rb, Ni and Ir were 34.24, 13.35, 7.36, 1.37, 0.84, 0.44, 0.23, 0.21, 0.15, 0.12, 0.11, 0.09, 0.06, 0.04, 0.03 and 0.01 mg $kg^{-1}$, respectively. BT is a mixture of amino acids, polypeptide and proteins, and generally recognized as polypeptides complexes. According to the formula provided by the company, it contains 5.1% amino acids (<180 Da), 34.2% small peptides (180~6000 Da), 31.6% polypeptide (6000~30000 Da) and 29.1% proteins (>30000 Da), respectively. The major types of amino acids were arginine, phenylalanine, valine, lysine, leucine, isoleucine, threonine and methionine. The commercial prices of BS and BT are \$4.83 $kg^{-1}$ and \$4.14 $kg^{-1}$, respectively.

## 2.3 Experiments design

RSM using the Box-Behnken Design (BBD) method was employed to optimize the culture medium with the supplement of BS and BT. The effects of three independent variables (concentrations of NaCl, BS and BT) at different ranges on biomass concentration and phycocyanin production were assessed. For this, a three-factor three-level experimental design was employed (Table 1). Ranges of variables were chosen based on our preliminary studies. According to single-factor experiments, the three factors had a positive effect on biomass and phycocyanin accumulation at low concentration, and showed an inhibitory effect at high concentration. The optimal concentration of each factor was selected as the central point of the BBD. The quantitative relationship between dependent [$Y_1$: biomass concentration, $Y_2$: phycocyanin concentration ($CPC_{conc}$) and $Y_3$: phycocyanin content ($CPC_{cont}$)] and independent variables (A: NaCl, B: BS and C: BT) was determined. The experimental design, mathematical model and statistical analysis were carried out using Design-Export software (13.0.1.0).

TABLE 1 Independent variables (NaCl, BS and BT concentration) and their levels used in the Box-Behnken design.

| Factors | Units | Coded symbols | Range of variables (Levels) | | |
|---|---|---|---|---|---|
| | | | -1 | 0 | 1 |
| NaCl | mM | A | 10 | 115 | 220 |
| BS | mg $L^{-1}$ | B | 200 | 300 | 400 |
| BT | mg $L^{-1}$ | C | 20 | 50 | 80 |

According to BBD, the total experiments included 17 groups (Table 2). The medium of each experimental group differed by varying addition amounts of NaCl, BS, and BT into Zarrouk medium. All media were autoclaved at 121°C for 20 min after the initial pH was adjusted to 9.5 with 1 M NaOH. Microalgae cultivated at logarithmic growth phase were inoculated into 250 mL flasks with 100 mL culture medium at 10% (v/v) inoculation rate after the medium cooled to room temperature. *Arthrospira maxima* were cultivated at 31°C in shake flasks with rotation rate of 120 rpm, and illuminated by 6 light tubes at light intensity of 144 μ mol $m^{-2}$ $s^{-1}$ for 16 days. Then, microalgae cells were harvested by filtration to measure the biomass concentration, $CPC_{conc}$ and $\mathbf{CPC_{cont}}$. Each experiment was conducted in triplicate. Taking the maximum value of $CPC_{conc}$ and $\mathbf{CPC_{cont}}$ as targets, respectively, validation experiments were conducted based on the optimal conditions predicted by the model.

## 2.4 Analytical methods

### 2.4.1 Biomass concentration and productivity

Biomass concentration was determined by dry weight method. In brief, algal cells were harvested using 500 mesh screens, then washed with deionized water 2 times, and transferred to a pre-dried weighing disc, followed by oven drying at 75°C until constant weight. The biomass concentration (X) and productivity ($P_{biomass}$) (Skorupskaite et al., 2015) were calculated using the following equations:

$$X(g\,L^{-1}) = \frac{m_1 - m_0}{V_{cul}} \quad (1)$$

where $m_1$ represents the weight (g) of dried weighing disc containing the sample, and $m_0$ (g) represents the weight of pre-dried empty weighing disc. $V_{cul}$ (L) is the sampling volume.

TABLE 2 Experimental data and predicted value based on established models of $CPC_{conc}$ and $CPC_{cont}$.

| Std | Run | Variables | | | | | | Responses | | | | | |
|---|---|---|---|---|---|---|---|---|---|---|---|---|---|
| | | A: NaCl | | B: BS | | C: BT | | $CPC_{conc}$ | | | $CPC_{cont}$ | | |
| | | mM | | mg $L^{-1}$ | | mg $L^{-1}$ | | mg $L^{-1}$ | | | % | | |
| | | Actual | Coded | Actual | Coded | Actual | Coded | Actual | Predicted | Residual | Actual | Predicted | Residual |
| 1 | 16 | 10 | -1 | 200 | -1 | 50 | -1 | 528.22 | 527.94 | 0.28 | 17.60 | 17.44 | 0.16 |
| 2 | 3 | 220 | 1 | 200 | 1 | 50 | -1 | 646.22 | 646.62 | -0.40 | 18.08 | 18.09 | -0.01 |
| 3 | 2 | 10 | -1 | 400 | -1 | 50 | 1 | 588.98 | 588.58 | 0.40 | 17.47 | 17.46 | 0.01 |
| 4 | 12 | 220 | 1 | 400 | 1 | 50 | 1 | 550.09 | 550.37 | -0.28 | 16.93 | 17.09 | -0.16 |
| 5 | 7 | 10 | -1 | 300 | -1 | 20 | 0 | 564.06 | 556.32 | 7.74 | 16.93 | 17.05 | -0.12 |
| 6 | 10 | 220 | 1 | 300 | 1 | 20 | 0 | 631.03 | 622.6 | 8.43 | 16.61 | 16.56 | 0.05 |
| 7 | 14 | 10 | -1 | 300 | -1 | 80 | 0 | 491.91 | 500.34 | -8.43 | 16.08 | 16.13 | -0.05 |
| 8 | 9 | 220 | 1 | 300 | 1 | 80 | 0 | 506.79 | 514.53 | -7.74 | 17.02 | 16.9 | 0.12 |
| 9 | 11 | 115 | 0 | 200 | 0 | 20 | -1 | 677.91 | 685.94 | -8.03 | 17.86 | 17.9 | -0.04 |
| 10 | 4 | 115 | 0 | 400 | 0 | 20 | 1 | 639.75 | 647.89 | -8.14 | 17.68 | 17.57 | 0.10 |
| 11 | 6 | 115 | 0 | 200 | 0 | 80 | -1 | 591.82 | 583.68 | 8.14 | 17.67 | 17.77 | -0.10 |
| 12 | 8 | 115 | 0 | 400 | 0 | 80 | 1 | 594.14 | 586.11 | 8.03 | 17.14 | 17.11 | 0.04 |
| 13 | 13 | 115 | 0 | 300 | 0 | 50 | 0 | 605.94 | 609.17 | -3.24 | 17.87 | 18.25 | -0.38 |
| 14 | 17 | 115 | 0 | 300 | 0 | 50 | 0 | 620.54 | 609.17 | 11.37 | 18.48 | 18.25 | 0.23 |
| 15 | 15 | 115 | 0 | 300 | 0 | 50 | 0 | 602.18 | 609.17 | -6.99 | 18.08 | 18.25 | -0.16 |
| 16 | 5 | 115 | 0 | 300 | 0 | 50 | 0 | 615.48 | 609.17 | 6.31 | 18.35 | 18.25 | 0.10 |
| 17 | 1 | 115 | 0 | 300 | 0 | 50 | 0 | 601.73 | 609.17 | -7.45 | 18.45 | 18.25 | 0.20 |

$$P_{biomass}\ (g\ L^{-1}\ d^{-1}) = \frac{X_1 - X_0}{t_1 - t_0} \quad (2)$$

where $X_1$ and $X_0$ represent the biomass concentration (g $L^{-1}$) on days $t_1$ and $t_0$, respectively.

### 2.4.2 Determination of phycocyanin

Phycocyanin was extracted from *Arthrospira maxima* by using modified wet extraction method (Khazi et al., 2018). Specifically, 5 mL culture was filtered with 500 mesh screens to obtain wet biomass. It was washed by deionized water, re-suspended in 20 mL of 100 mM sodium phosphate buffer (pH 7), and subjected a freeze of -20°C for 12h. Thereafter, the sample was centrifuged at 8000×g for 10 min and the blue supernatant was collected. The $CPC_{conc}$ in the supernatant was determined by measuring the absorbance at 620 and 652 nm using ultraviolet-visible spectrophotometer (UV-5200) (Mogany et al., 2018; Novoveská et al., 2019). The concentration and the content of CPC were calculated as follows:

$$CPC_{conc}\ (mg\ L^{-1}) = \frac{(A_{620nm} - 0.474 \times A_{652nm}) \times 1000 \times V_{extr}}{5.34 \times V_{cul}} \quad (3)$$

Where $CPC_{conc}$ was the concentration of CPC in the solution of microalgae, $A_{620}$ and $A_{652}$ were optical density of extracting solution at 620 and 652 nm, respectively. $V_{extr}$ (L) and $V_{cul}$ (L) were the volume of extracting solution and culture sample, respectively.

$$CPC_{cont}\ (\%) = \frac{CPC_{conc}}{10X} \quad (4)$$

where $CPC_{conc}$ was the concentration of CPC (mg $L^{-1}$) obtained from Eq. (3), and X was the biomass concentration (g $L^{-1}$) obtained from Eq. (1).

The gross volumetric productivity of CPC was calculated using Eq. (5).

$$P_{CPC}(mg\ L^{-1} d^{-1}) = \frac{CPC_{conc\_end}}{t} \quad (5)$$

where $CPC_{conc\_end}$ was the final CPC concentration (mg $L^{-1}$), and t was the total duration of the cultivation (d).

## 2.5 Statistical analysis

After performing all experiments, the quadratic second-order equation with interaction terms was used to model the relationship between dependent and independent variables:

$$y_i = \beta_0 + \sum_{i=1}^{n} b_i x_i + \sum_{i=2}^{n} b_{ii} x_i^2 + \sum_{i=1}^{n-1} \sum_{j=i+1}^{n} b_{ij} x_i x_j \quad (6)$$

where $y_i$, and $\beta_0$ represent response variable and interception coefficient, respectively, and $b_i$, $b_{ii}$, and $b_{ij}$ are regression

coefficients, n is the number of studied variables, $x_i$ and $x_j$ represent independent variables.

The statistical differences among the experiments were assessed by the analysis of variance (ANOVA) *via* the Design-Export software (13.0.1.0). The main effects and interaction effects of each factor were analyzed. All analyses are significant at $p<0.05$.

# 3 Results

## 3.1 Model fitting and statistical analysis

In order to achieve the maximal biomass concentration and phycocyanin accumulation, the relationship between the three independent and dependent variables was analyzed. The response surface models were identified for the coded factors and the quadratic second-order equations with interaction terms were used for data fitting. The final model equations and the variance analysis for the responses were shown in Table 3. The significance of the models was specified by low p-values ($p<0.05$) (Nemanja et al., 2019). The p-values of the fitting models of biomass concentration, phycocyanin concentration and content were 0.0007,<0.0001 and 0.001, respectively, indicating that all generated models were significant. Meanwhile, the high values of $R^2$ (>0.9481) represented that all models were well fitting. For each model, the adequate precision was more than 4, which was desirable for good discrimination and indicated an adequate signal for the models to be used to navigate design space. Moreover, the low variation coefficients (1.33 to 2.28%) and the insignificant lack of fit ($p>0.05$) implied a high experimental reliability and a good correlation between the responses and the independent variables.

## 3.2 Microalgal growth

The biomass concentration and productivity of *Arthrospira maxima* under various cultivation conditions were summarized in Table 4. Compared with the control, the growth performance of most experimental groups decreased after adding three exogenous substances synchronously. There were only four treatments (run 3, 4, 10 and 11) in which the biomass concentrations and productivities were higher than that of the control. Among them, the run 10 showed the best microalgae growth, attaining the highest biomass concentration of 3.8 g $L^{-1}$ and productivity of 0.22 g $L^{-1}$ $d^{-1}$. The common feature of these four treatments was the addition of middle-high concentration of NaCl (115 and 220 mM) and low-middle concentration of BT (20 and 50 mg $L^{-1}$). Moreover, the perturbation plot revealed that the biomass was sensitive to NaCl and BT (Figure 1A). Hence, it can be speculated that adding a relative high concentration of NaCl and a small amount of BT can help to increase the biomass concentration. 3D response surfaces and contour plots showed more details about the relationships between the three variables and responses (Figure 2). The effect of exogenous substances at different concentration levels on the biomass concentration was shown in Figures 2A–C. The curvatures indicated that there was a strong interactive effect between the NaCl and BS concentration, as well as the NaCl and BT concentration with the low p-values of 0.0026 and 0.090, respectively (Table S1). Overall, the biomass concentration first increased and then declined with the increase of NaCl concentration at the fixed concentration of BT (50 mg $L^{-1}$). However, the point of trend change depended on the BS concentration. For the combined impact of NaCl and BT, the maximal biomass concentration was achieved at the high NaCl and low BT concentration. The interaction between BS and BT was not significant for the growth of *Arthrospira maxima* ($p>0.05$, Table S1).

## 3.3 Phycocyanin concentration

Likewise, the relationships between the phycocyanin concentration and three independent variables were analyzed. The ANOVA results of the model showed that the single factors (A, C), interaction terms (AB, AC), and secondary terms ($A^2$, $B^2$) had significant effects on phycocyanin concentration and the p-values of these factors were all less than 0.05 (Table S2). The phycocyanin concentration was more sensitive to NaCl concentration than BS and BT concentrations (Figure 1B),

TABLE 3 Analysis of variance for the response surface models.

| Source | Modified Equations with Significant Terms | p-value | $R^2$ | Adj.$R^2$ | SD | Lack of Fit |
|---|---|---|---|---|---|---|
| Biomass concentration | $4.26877+0.011369A-0.006224B-0.021286C-0.000017AB-0.000044AC+0.000025BC-0.000014A^2+0.000012B^2+0.000119C^2$ | 0.0007 | 0.9539 | 0.8947 | 0.0769 | 0.08 |
| $CPC_{conc}$ | $706.87395+2.64811A-1.22795B-1.17036C-0.003735AB-0.004133AC+0.003373BC-0.00491A^2+0.002333B^2-0.007333C^2$ | <0.0001 | 0.9797 | 0.9536 | 10.74 | 0.20 |
| $CPC_{cont}$ | $16.26259+0.020213A-0.004221B+0.076443C-0.000024AB+0.0001AC-0.000028BC-0.000075A^2+0.000009915B^2-0.000844C^2$ | 0.001 | 0.9481 | 0.8813 | 0.2338 | 0.69 |

Biomass concentration; $CPC_{conc}$, phycocyanin concentration; $CPC_{cont}$, phycocyanin content; A, NaCl concentration; B, $CPC_{conc}$; C, $CPC_{cont}$; $R^2$, determination coefficient; Adj.$R^2$, adjusted $R^2$; SD, standard deviation; CV, coefficient of variation.

TABLE 4 Comparison of biomass concentration and productivity among the different treatments.

| Medium types | Treatment | Addition ratio of exogenous substances | | | Biomass concentration ($g\ L^{-1}$) | Biomass productivity ($g\ L^{-1}\ d^{-1}$) |
|---|---|---|---|---|---|---|
| | | NaCl(mM) | BS ($mg\ L^{-1}$) | BT ($mg\ L^{-1}$) | | |
| Control medium | Run 0 | 0 | 0 | 0 | 3.52 | 0.20 |
| Experimental medium | Run 1 | 115 | 300 | 50 | 3.26 | 0.19 |
| | Run 2 | 10 | 400 | 50 | 3.38 | 0.20 |
| | Run 3 | 220 | 200 | 50 | 3.58 | 0.21 |
| | Run 4 | 115 | 400 | 20 | 3.62 | 0.21 |
| | Run 5 | 115 | 300 | 50 | 3.35 | 0.19 |
| | Run 6 | 115 | 200 | 80 | 3.35 | 0.19 |
| | Run 7 | 10 | 300 | 20 | 3.33 | 0.19 |
| | Run 8 | 115 | 400 | 80 | 3.47 | 0.20 |
| | Run 9 | 220 | 300 | 80 | 2.98 | 0.17 |
| | Run 10 | 220 | 300 | 20 | 3.80 | 0.22 |
| | Run 11 | 115 | 200 | 20 | 3.80 | 0.22 |
| | Run 12 | 220 | 400 | 50 | 3.25 | 0.19 |
| | Run 13 | 115 | 300 | 50 | 3.39 | 0.20 |
| | Run 14 | 10 | 300 | 80 | 3.06 | 0.18 |
| | Run 15 | 115 | 300 | 50 | 3.33 | 0.19 |
| | Run 16 | 10 | 200 | 50 | 3.00 | 0.17 |
| | Run 17 | 115 | 300 | 50 | 3.36 | 0.19 |

which was confirmed by the linear model coefficients (Table 3). The interactive effect of NaCl and BS concentration was similar to that on biomass concentration (Figures 2A, D). Specifically, the effect of NaCl concentration on $CPC_{conc}$ was dependent on the BS concentration. The high $CPC_{conc}$ were obtained at the extreme low BS concentration (200 $mg\ L^{-1}$) and NaCl concentration ranged from 125-220 mM (Figure 2E). The interactive effect of NaCl and BT concentration was significant but not strong. The $CPC_{conc}$ increased first and then decreased with the increase of NaCl concentration. The high concentration of BT reduced the $CPC_{conc}$. A combination of a high concentration of NaCl (100-200 mM) and a low concentration of BT (20-25 $mg\ L^{-1}$) was beneficial to the CPC accumulation. The interaction between BS and BT is not significant ($p>0.05$, Table S2). Both low concentrations of BT and BS is beneficial to CPC synthesis.

## 3.4 Phycocyanian content

It was observed that a trend of first dramatically increasing and then decreasing phycocyanin content as the NaCl

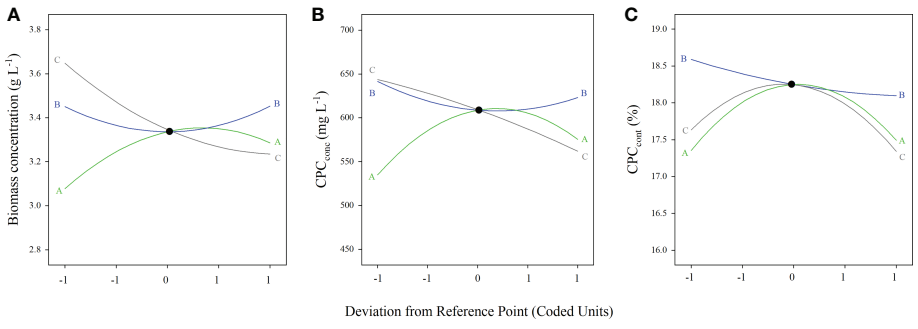


FIGURE 1
Perturbation plots of the dependent variables. **(A)** biomass concentration, **(B)** $CPC_{conc}$, and **(C)** $CPC_{cont}$. **(A)** NaCl concentration; **(B)** BS concentration; **(C)** BT concentration.

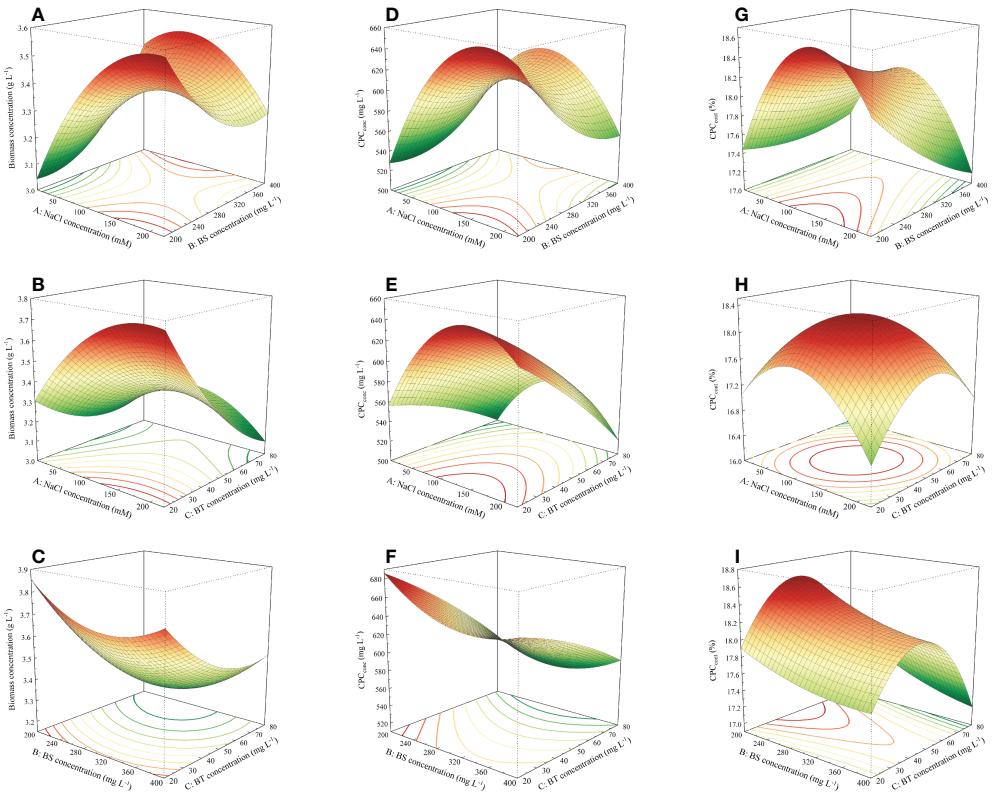


FIGURE 2
Response surface plots visualizing the interactive effects among the NaCl, BS and BT concentration for responses. **(A–C)** biomass concentration, **(D–F)** $CPC_{conc}$, and **(G–I)** $CPC_{cont}$.

concentration increased from 50 mM to 220 mM (Figure 2G). The maximum $CPC_{conc}$ was found when the NaCl concentration ranged from 100 to 180 mM. The variation in BT concentration, however, had slight impact on the content of phycocyanin when the NaCl concentration was ranged from about 10-40 mM. The perturbation plot demonstrated that the $CPC_{cont}$ was sensitive to NaCl and BT concentrations (Figure 1C), and their interaction was significant ($p<0.05$, Table S3). 3D model presented that $CPC_{cont}$ was low at the extreme concentrations of NaCl and BT. When the concentration of NaCl or BT is constant, the $CPC_{cont}$ significantly increased first and then declined sharply with the increase of another factor. The sensitivity of $CPC_{cont}$ to BT was also reflected in the interaction between BS and BT (Figure 2I). As the increase of BT concentration from 20 to 80 mg $L^{-1}$, the $CPC_{cont}$ increased first and then decreased, and the optimum concentration of BT was about 50 mg $L^{-1}$. With the variation in BS concentration, the $CPC_{cont}$ did not change obviously, indicating that the $CPC_{cont}$ was not sensitive to BS, which was consistent with the results shown in the perturbation plots (Figure 1C).

## 3.5 Optimization and experimental validation

The comparison between the actual experimental and the predicted data using the quadratic regression model was shown in Figure 3. The strong linear relationship indicated that there was a good agreement between the predicted and experimental results, demonstrating this model can be used in prediction and optimization. According to the model predication, the maximum $CPC_{conc}$ was achieved when the concentrations of NaCl, BS and BT were 185 mM, 200 mg $L^{-1}$ and 20 mg $L^{-1}$, respectively. However, it should be noted that the $CPC_{cont}$ was not maximum at this condition. The optimal condition estimated for obtaining the maximum $CPC_{cont}$ were 136 mM NaCl, 200 mg $L^{-1}$of BS and 50 mg $L^{-1}$ of BT. Subsequently, the validation experiments were performed at the optimal conditions. The experimental results ($CPC_{conc}$ of 704.66 mg $L^{-1}$, $CPC_{cont}$ of 19.03%) were very close to the predicted data ($CPC_{conc}$ of 710.13 mg $L^{-1}$, $CPC_{cont}$ of 18.63%) at the respective optimal condition (Figure 4).

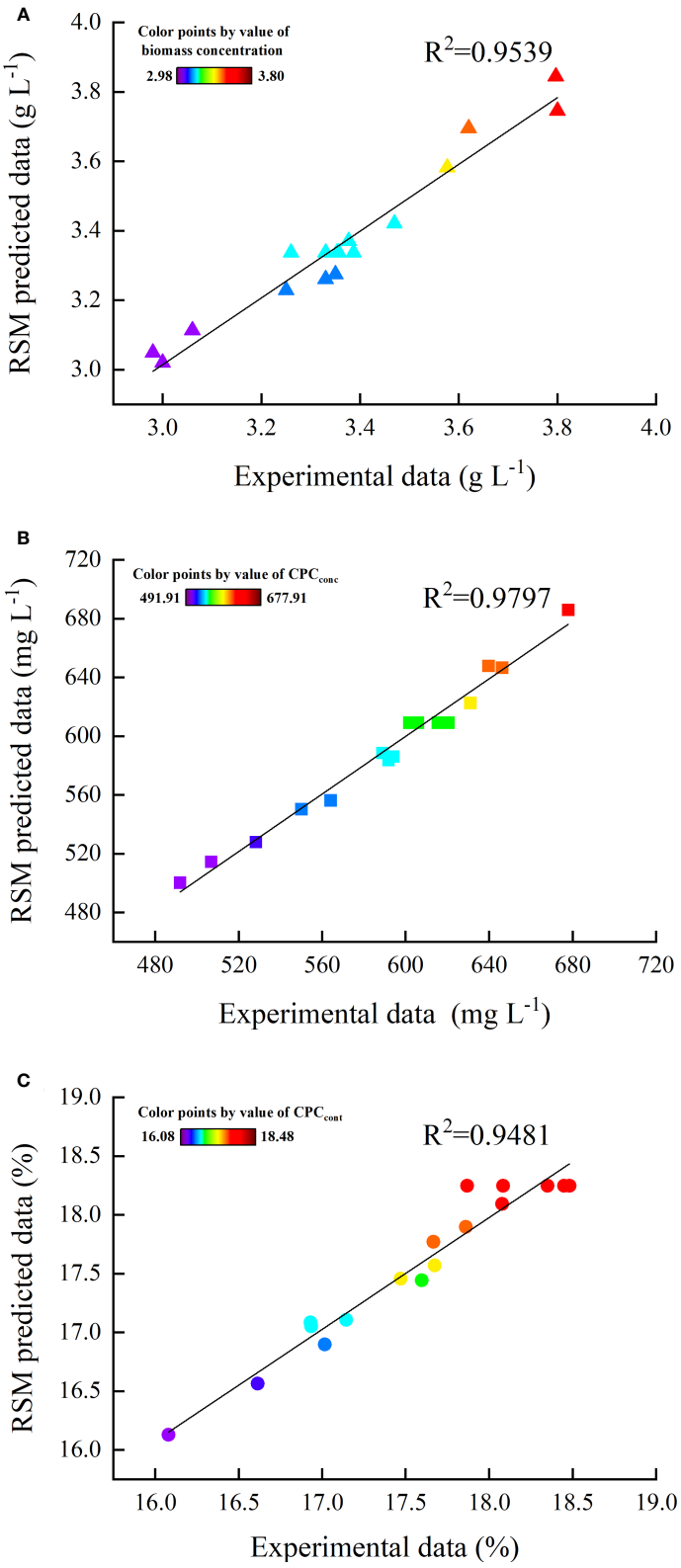


FIGURE 3
Comparison between experimental and predicted values of **(A)** biomass concentration, **(B)** $CPC_{conc}$, and **(C)** $CPC_{cont}$.

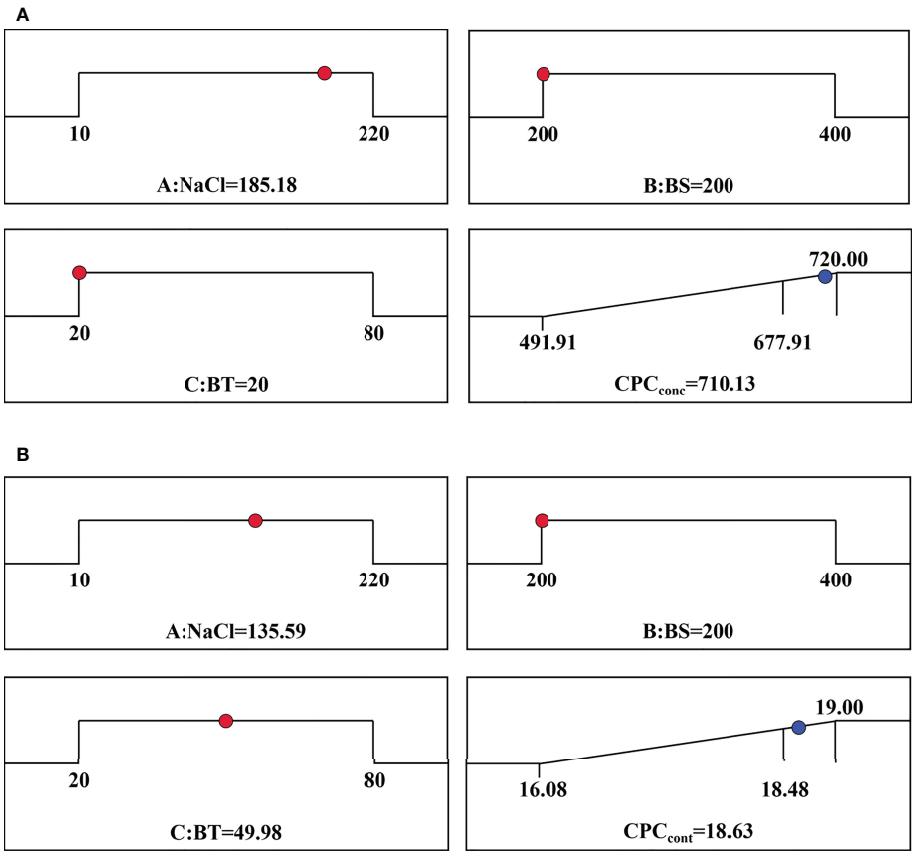


FIGURE 4
Optimal conditions predicted by the models for **(A)** $CPC_{conc}$ and **(B)** $CPC_{cont}$.

## 4 Discussion

Three factors (NaCl, BS, and BT) were chosen in this study to evaluate their impacts on the growth and phycocyanin production of *Arthrospira maxima*. The RSM model of algal biomass revealed that two of the factors, NaCl and BT, had a more substantial impact in comparison with BS concentration. The results of microalgae growth indicated that higher NaCl concentrations (100-220 mM) were advantageous for microalgae growth, which was basically consistent with previous studies (Abd El-Baky and El-Baroty, 2012). They reported that the medium containing 100 mM of NaCl can dramatically increase the growth of *Arthrospira maxima* as compared to control (20 mM NaCl), and the corresponding specific growth rate increased from 0.089 to 0.097 $d^{-1}$. Nevertheless, cell proliferation of *Arthrospira platensis* was sharply slowed down when the concentration of NaCl raised above 500 mM because of more severe detrimental effect of salt stress (Chen and Tang, 2012). The content of chlorophyll and carotenoid in algal cell was also decreased, which consequentially resulted in declining of photosynthetic rate. The culture experiment results demonstrated that the addition of BT into medium was beneficial to microalgae growth. BT can be considered as nitrogen source as the primary component of BT is polypeptide. Nitrogen source is essential for cell growth and involved in the synthesis of amino acids, purines, pyrimidines, and other compounds used in cellular metabolism (Li et al., 2018). Hence, the increase of nitrogen concentration in a certain range can efficiently encourage the growth of microalgae (Mousavi et al., 2022). As the nitrogen concentration ($NaNO_3$) increased from 0.625 to 2.5 g $L^{-1}$, the biomass of *Arthrospira platensis* enhanced by 1.25 times at the culture temperature of 35°C (Can et al., 2017). In addition to nitrogen concentration, the type of nitrogen source was also highly affected the microalgae growth. Costa et al. (2001) observed that the optimal order of the nitrogen type for the growth of *Arthrospira platensis* was sodium nitrate, ammonium nitrate, acid ammonium phosphate, urea, ammonium sulphate, and ammonium chloride, at the same concentration of 10 mM. Interestingly, this order greatly changed when the nitrogen source concentration increased up to 30 and 50 mM, indicating the effect of nitrogen source on microalgae growth

depended on its concentration. Besides, exogenous addition of organic nitrogen source into culture medium is a effective approach to enhance microalgae growth. Shanthi et al. (2018) found that the biomass productivity of *Arthrospira platensis* increased to 175, 153 and 144 mg $L^{-1}$ $d^{-1}$ by addition of L-Arginine, L-Asparagine and L-Glutamine, respectively. These growth rates were significantly higher than 114 mg $L^{-1}$ $d^{-1}$ obtained in the control group. And, these findings also confirmed that the type of nitrogen source (structure of amino acids) influenced the microalgae growth. Manirafasha et al. (2018) examined the effect of various concentration of sodium glutamate additionally added into Zarrouk medium on the growth of *Arthrospira platensis*, and found that the biomass concentration at 4 mM concentration of sodium glutamate reached 2.54 g $L^{-1}$ that is much higher than ~1.4 g $L^{-1}$ obtained in the control. In the present study, overall, algal biomass was gradually increased as the BT concentration increased, which is probably due to the beneficial impact of multiple amino acids degraded from polypeptide. In contrast, there was a little influence of BS on microalgae growth ($p>0.05$), which was possibly attributed to the sufficient minerals already existed in the Zarrouk medium. Further increased in minerals concentration did not allow the increase of microalgae growth.

NaCl had a huge impact on phycocyanin accumulation, as seen by the 3D surface plots and contour plots (Figures 2D–F). The phycocyanin concentration peaked when the NaCl concentration was 136 mM. Enhanced production of phycocyanin by NaCl is mostly related to the growth performance of microalgae and the reflection of phycocyanin synthesis metabolism to salt stress. On one hand, the increase in phycocyanin concentration caused by the ongoing accumulation of biomass in the region of 100-200 mM NaCl concentration. On the other hand, the phycocyanin concentration was associated with intracellular phycocyanin content. The increase of phycocyanin content can facilitate the production of phycocyanin. Phycocyanin can be generated in greater numbers like some antioxidant enzyme to resist damage from reactive oxygen radicals caused by environmental stresses (Singh et al., 2018; Gauthier et al., 2020). But an excessive concentration of NaCl will inhibit the synthesis of phycocyanin. Electron transport is hampered by extreme salt stress, which could halt the photosystem II activity and cause the amount of phycocyanin to decrease (Kirst, 1990).

However, the adaptability and domestication of *Arthrospira* can be used to overcome the challenge of high concentrations of NaCl impeding microalgae growth and phycocyanin. (Tredici et al., 1986; Hagemann, 2011). Liu et al. (2016) domesticated two strains of *Arthrospira platensis* (SP843 and SP972) using 200-800 mM of NaCl, and observed that they grew well in the medium containing 200 and 400 mM of NaCl, respectively. Meanwhile, the concentrations of phycocyanin increased by 180% and 157%, respectively, in comparison to the control. After salt acclimation, *Arthrospira* has a better capacity to produce phycocyanin at high salt concentration. Thereby, *Arthrospira* can be domesticated to increase its tolerance to salt stress, which can help *Arthrospira* culture in locations where excessive salinity makes it difficult.

As a nitrogen source, BT was conducive to the microalgae growth and phycocyanin production. In addition to affecting the growth of *Arthrospira*, the nitrogen source also affected the synthesis of phycocyanin. Nitrogen deficiency will limit the production of proteins associated with photosynthetic activity such as phycocyanin (Li et al., 2018). Thus, the increase of nitrogen concentration will improve the production of phycocyanin. The types of nitrogen sources also had an impact on phycocyanin accumulation. Gladfelter et al. (2022) discovered that compared to nitrate, the reduced nitrogen forms (ammonium/ammonia and urea) can much more promote algae growth and phycocyanin accumulation. In addition, in a research on improving the sources of nitrogen in the culture medium, the phycocyanin content was increased by 23% after optimizing the medium that included soda ash production wastes, $NaNO_3$, KCl and $KH_2PO_4$ (Xie and Wang, 2017).

In this work, the addition of BS into the medium did not exert a obvious positive effect to the phycocyanin production. This result slightly differed from the findings of the other previous study. Mostly researches showed that the addition of mineral components can promote the phycocyanin accumulation. Compared to the control (Zarrouk medium), phycocyanin concentration increased by 1.6 times when the modified Zarrouk medium containing more $Ca^{2+}$ from oyster shell and soil extract was used (Jung et al., 2014). A low concentration (<0.3 μg $mL^{-1}$) of Ni increased the content of phycocyanin in Microcystis aeruginosa (Liu et al., 2005). It was reported that the dual effects of Se on promoting growth at low concentrations while also being toxic at high concentrations to *Arthrospira* (Chen et al., 2007). The addition of Se increased the phycocyanin concentration of *Arthrospira maxima* from 226 to 274 mg $L^{-1}$ which was 21.2% higher than that in the control group (Chen et al., 2006). Most studies on the influence of mineral elements on phycocyanin presently focused on a single factor, such as Ni, Ca and Fe (Sloth et al., 2006; Velu et al., 2019; Rawat et al., 2022; Yang et al., 2022), and showed a good effect on phycocyanin. *Arthrospira* requires a small number of mineral components to grow. It is possibly that the conventional Zarrouk medium has enough minerals, to support the cell growth and phycocyanin production. Thus, the extra-addition of BS, a complex of different mineral elements, cannot generate significant positive impact, even showed inhibitory effect on phycocyanin production at a high concentration because of the resulted toxic of some metal elements.

In order to optimize the *Arthrospira* medium, we established the predicted models of algal biomass and phycocyanin production using response surface method. The maximum concentration (704.66 mg $L^{-1}$) and content (19.03%) of phycocyanin were successfully achieved using the ideal conditions predicted by this model. These values were 22.98% and 16.73% higher than those of the control group.

At present, there have been many studies on improving the production of phycocyanin, and the corresponding results are summarized in Table 5. It can be seen that the phycocyanin concentration varied greatly, which ranged from 100-1500 mg $L^{-1}$, with most of it concentrated in the range of 200-500 mg $L^{-1}$. Also, phycocyanin content had a large range that from ~5% to ~20%. This great variation in concentration and content of CPC was probably caused by the different culture condition employed in the different literature, such as algal strains, culture medium, reactor type, culture mode, temperature and light intensity. In the current study, the maximum $CPC_{conc}$ and $CPC_{cont}$ reached 704.66 mg $L^{-1}$ and 19.03%, respectively, and these values were comparable to or even higher than the most results obtained in the previous studies. It is noteworthy, in the study conducted by Chaiklahan et al. (2022), that the phycocyanin content reached 19.88% that is slightly higher than our result (19.03%), whereas the phycocyanin productivity (123.66 mg $L^{-1}$ $d^{-1}$) is much greater than 44.04 mg $L^{-1}$ $d^{-1}$ achieved by our study. The main reason was that they used the semi-continuous culture mode, in which the regular addition of fresh medium greatly ensured the nutrients required for the growth of microalgae, achieving a high biomass productivity (0.62 g $L^{-1}$ $d^{-1}$) and consequent high phycocyanin productivity. In contrast, the batch mode was employed in the present study and the resulted biomass productivity was only 0.23 g $L^{-1}$ $d^{-1}$. Surprisingly, the extreme high level of phycocyanin concentrations (>1000 mg $L^{-1}$) was attained by Zeng et al. (2012) and Xie et al. (2015). In the former study, the intermittent supply of $CO_2$ provided sufficient carbon source to microalgae growth, thus achieving a very high biomass concentration (7.26 g $L^{-1}$). Xie et al. (2015) employed a feed-batch mode which is more efficient in terms of biomass accumulation compared to the batch mode, leading to a high biomass concentration (6.78 g $L^{-1}$) and consequent high phycocyanin concentration (1034.8 mg $L^{-1}$).

It should be noted that the conecntration of NaCl in the culture medium was increased and additional BS and BT were added after optimizaiton, which will increase the produce cost. Thereby, we briefly conducted a economic analysis as it is very important and essential. At the optimal condition achieving the maxiumum phycocyanin concentration, the phycocyanin production will additionally increase 0.13 g $L^{-1}$ compared to the control. However, the extra additon of these substances in 1 L culture medium brought extra cost (~$0.03) that was calculated through multipling the additional quantities of subtansces (NaCl, BS and BT) by their commerical prices. In terms of the market price of food-grade phycocyanin ($0.5 $g^{-1}$) (Güroy et al., 2017), the extra production of phycocyanin per liter (0.13 g) valued approximately $0.07, which exceeded the input cost ($0.03). Therefore, it would be cost-effective and economically feasible for the phycocyanin production after optimizaiton.

Overall, a high level of phycocyanin production was achieved by optimization of culture medium added by BT and BS based on RSM. However, this study used the mode of batch

TABLE 5 Summary of algal growth and phycocyanin production of *Arthrospira* reported in the literature and this study.

| Number | Species | Special culture condition | Culture mode | Biomass concentration (g $L^{-1}$) | Biomass productivity (g $L^{-1}$ $d^{-1}$) | CPC concentration (mg $L^{-1}$) | CPC content (%) | Phycocyanin productivity (mg $L^{-1}$ $d^{-1}$) | Reference |
|---|---|---|---|---|---|---|---|---|---|
| 1 | *Arthrospira platensis* | $(NH_4)_2SO_4$ as nitrogen source | batch | 1.04 | 0.07* | NA | 11.3% | NA | Mousavi et al., 2022 |
| 2 | *Arthrospira platensis* | addition of sodium glutamate | batch | 8.00 | 1.14* | 452.32* | 5.65% | 64.62* | Manirafasha et al., 2018 |
| 3 | *Arthrospira platensis* | addition of succinic acid | batch | 5.57 | 0.80* | 288.86* | 5.18% | 41.27* | |
| 4 | *Arthrospira platensis* | addition of NaAC | batch | 1.65 | NA | 226.05* | 13.7% | NA | Chen et al., 2006 |
| 5 | *Arthrospira platensis* | cultivation using blue light | batch | 0.97* | 0.19* | 128.63 | 13.2% | 25.73* | Chini Zittelli et al., 2022 |
| 6 | *Arthrospira platensis* | intermittent $CO_2$ supply | batch | 7.26* | 0.40* | 1220 | 16.8% | 67.8 | Zeng et al., 2012 |
| 7 | *Arthrospira platensis* | synergistic effects of light intensity, photoperiod and cell density | semi-continuous | NA | 0.62 | NA | 19.88% | 123.66 | Chaiklahan et al., 2022 |
| 8 | *Arthrospira platensis* | optimization of light intensity and initial biomass concentration | feed-batch | 6.78 | 0.588 | 1034.8 | 16.1% | 94.8 | Xie et al., 2015 |
| 9 | *Arthrospira maxima* | NaCl stress and addition of BS and BT | batch | 3.63 | 0.23 | 704.66 | 19.03% | 44.04 | This study |

*It indicated that the values were calculated based on the relative data reported in the articles.
NA, the data is unavailable.

culture. Moreover, during the process, there was no additional carbon (such as $CO_2$) supplied into the medium. Therefore, more work could be performed in the next step to further increase the phycocyanin productivity by using feed-batch or semi-continuous mode, as well as providing additional carbon source based on the optimized medium.

## 5 Conclusions

In this study, the forecasting models has been established based on RSM, aiming to optimize culture conditions to enhance algal biomass and phycocyanin accumulation. According to the models, it was observed that NaCl was the most important factor to the responses. Meanwhile, the interactive effect of NaCl and BT had the greatest effect on phycocyanin production. The maximum values of phycocyanin concentration and content (704.66 mg $L^{-1}$ and 19.03%) were reached at the respective optimal conditions determined by the models. Hence, BS and BT can be potentially considered as the great exogenous additives to promote *Arthrospira maxima* growth and phycocyanin synthesis. In the next step, semi-continuous or feed-batch mode as well as the supply of $CO_2$ can be used to further increase the productivity of algal biomass and phycocyanin.

## Data availability statement

The original contributions presented in the study are included in the article/Supplementary Material. Further inquiries can be directed to the corresponding authors.

## Author contributions

TY: conceptualization, methodology, data curation, formal analysis, visualization, and writing-original draft. JH: conceptualization, methodology, data curation, formal analysis, investigation, supervision and writing-review and editing, funding acquisition. BS: investigation, data curation, formal analysis. LW: methodology, data curation, formal analysis. A-HZ: conceptualization, writing-review and editing, funding acquisition. D-FZ: funding acquisition, project administration. YZ: project administration, resources. GM: project administration, resources. All authors contributed to the article and approved the submitted version.

## Funding

The study was supported by Nantong social livelihood science and technology plan (MS12021024), and National Natural Science Foundation of China (32273157).

## Conflict of interest

YZ and GM were employed by Jiangsu Coast Development Group Co., Ltd.

The remaining authors declare that the research was conducted in the absence of any commercial or financial relationships that could be construed as a potential conflict of interest.

## Publisher's note



## Supplementary material

The Supplementary Material for this article can be found online at: https://www.frontiersin.org/articles/10.3389/fmars.2022.1057201/full#supplementary-material

## References

Abd El-Baky, H. H., and El-Baroty, G. S. (2012). Characterization and bioactivity of phycocyanin isolated from spirulina maxima grown under salt stress. *Food Funct.* 3 (4), 381–388. doi: 10.1039/c2fo10194g

Anvar, A. A., and Nowruzi, B. (2021). Bioactive properties of spirulina: A review. *Microbial Bioactives* 4 (1), 134–142. doi: 10.25163/microbbioacts.412117B0719110521

Bachchhav, M. B., Kulkarni, M. V., and Ingale, A. G. (2016). Enhanced phycocyanin production from spirulina platensis using light emitting diode. *J. Institution Engineers (India): Ser. E* 98 (1), 41–45. doi: 10.1007/s40034-016-0090-8

Bezerra, M. A., Santelli, R. E., Oliveira, E. P., Villar, L. S., and Escaleira, L. A. (2008). Response surface methodology (RSM) as a tool for optimization in analytical chemistry. *Talanta* 76 (5), 965–977. doi: 10.1016/j.talanta.2008.05.019

Can, S. S., Koru, E., and Cirik, S. (2017). Effect of temperature and nitrogen concentration on the growth and lipid content of spirulina platensis and biodiesel production. *Aquaculture Int.* 25 (4), 1485–1493. doi: 10.1007/s10499-017-0121-6

Chaiklahan, R., Chirasuwan, N., Srinorasing, T., Attasat, S., Nopharatana, A., and Bunnag, B. (2022). Enhanced biomass and phycocyanin production of arthrospira (Spirulina) platensis by a cultivation management strategy: Light intensity and cell concentration. *Bioresour Technol.* 343, 126077. doi: 10.1016/j.biortech.2021.126077

Chen, C. Y., Kao, P. C., Tan, C. H., Show, P. L., Cheah, W. Y., Lee, W. L., et al. (2016). Using an innovative pH-stat CO2 feeding strategy to enhance cell growth and c-phycocyanin production from spirulina platensis. *Biochem. Eng. J.* 112, 78–85. doi: 10.1016/j.bej.2016.04.009

Chen, M., and Tang, Y. L. (2012). Investigation on the detrimental effects of salt stress on photosynthesis of spirulina platensis. *Agric. Sci. & Technol.* 8), 1625–1627 +1770. doi: 10.16175/j.cnki.1009-4229.2012.08.042

Chen, S. J., Yang, F., Zheng, W. J., Bai, Y., Huang, Z., and Zhou, Y. H. (2007). Effects of selenium stress on antioxidase system of spirulina platensis. *Acta Hydrobiologica Sin.* 5), 706–711. doi: 10.1016/S1872-2032(08)60016-5

Chen, T. F., Zheng, W. J., Yang, F., Bai, Y., and Wong, Y. S. (2006). Mixotrophic culture of high selenium-enriched spirulina platensis on acetate and the enhanced production of photosynthetic pigments. *Enzyme Microbial Technol.* 39 (1), 103–107. doi: 10.1016/j.enzmictec.2005.10.001

Chini, Z. G., Mugnai, G., Milia, M., Cicchi, B., Silva, B. A.M., Angioni, A., et al (2022). Effects of blue, orange and white lights on growth, chlorophyll fluorescence, and phycocyanin production of Arthrospira platensis cultures. *Algal Res* 61, 102583. doi: 10.1016/j.algal.2021.102583

Costa, J. A. V., Cozza, K. L., Oliveira, L., and Magagnin, G. (2001). Different nitrogen sources and growth responses of spirulina platensis in microenvironments. *World J. Microbiol. Biotechnol.* 17 (5), 439–442. doi: 10.1023/a:1011925022941

Fratelli, C., Burck, M., Amarant, M. C. A., and Braga, A. R. C. (2021). Antioxidant potential of nature's "something blue": Something new in the marriage of biological activity and extraction methods applied to c-phycocyanin. *Trends Food Sci. Technol.* 107, 309–323. doi: 10.1016/j.tifs.2020.10.043

Gauthier, M. R., Senhorinho, G. N. A., and Scott, J. A. (2020). Microalgae under environmental stress as a source of antioxidants. *Algal Res.* 52, 102104. doi: 10.1016/j.algal.2020.102104

Gladfelter, M. F., Buley, R. P., Belfiore, A. P., Fernandez-Figueroa, E. G., Gerovac, B. L., Baker, N. D., et al. (2022). Dissolved nitrogen form mediates phycocyanin content in cyanobacteria. *Freshw. Biol.* 67 (6), 954–964. doi: 10.1111/fwb.13892

Güroy, B., Karadal, O., Mantoğlu, S., and Cebeci, O. I. (2017). Effects of different drying methods on c-phycocyanin content of spirulina platensis powder. *Ege J. Fisheries Aquat. Sci.* 34 (2), 129–132. doi: 10.12714/egejfas.2017.34.2.02

Hagemann, M. (2011). Molecular biology of cyanobacterial salt acclimation. *FEMS Microbiol. Rev.* 35 (1), 87–123. doi: 10.1111/j.1574-6976.2010.00234.x

Hsieh-Lo, M., Castillo, G., Ochoa-Becerra, M. A., and Mojica, L. (2019). Phycocyanin and phycoerythrin: Strategies to improve production yield and chemical stability. *Algal Res.* 42, 101600. doi: 10.1016/j.algal.2019.101600

Jiang, L. Q., Wang, Y. J., Yin, Q. F., Liu, G. X., Liu, H. H., Huang, Y. J., et al. (2017). Phycocyanin: A potential drug for cancer treatment. *J. Cancer* 8 (17), 3416–3429. doi: 10.7150/jca.21058

Jung, J. Y., Kim, S., Lee, H., Kim, K., Kim, W., Park, M. S., et al. (2014). Use of extracts from oyster shell and soil for cultivation of spirulina maxima. *Bioprocess Biosyst. Eng.* 37 (12), 2395–2400. doi: 10.1007/s00449-014-1216-3

Khazi, M. I., Demirel, Z., and Conk Dalay, M. (2018). Enhancement of biomass and phycocyanin content of spirulina platensis. *Front. bioscience (Elite edition)* 10 (2), 276–286. doi: 10.2741/e822

Khazi, M. I., Demirel, Z., Liaqat, F., and Dalay, M. C. (2020). Analytical grade purification of phycocyanin from cyanobacteria. *Methods Mol. Biol. (Clifton N.J.)* 1980, 173–179. doi: 10.1007/7651_2018_202

Kirst, G. O. (1990). Salinity tolerance of eukaryotic marine algae. *Annu. Rev. Plant Biol.* 41 (21), 53. doi: 10.1146/annurev.pp.41.060190.000321

Lawrenz, E., Fedewa, E. J., and Richardson, T. L. (2011). Extraction protocols for the quantification of phycobilins in aqueous phytoplankton extracts. *J. Appl. Phycology* 23 (5), 865–871. doi: 10.1007/s10811-010-9600-0

Li, Y. (2022). The bioactivities of phycocyanobilin from spirulina. *J. Immunol. Res.* 2022, 4008991. doi: 10.1155/2022/4008991

Li, X., Li, W., Zhai, J., and Wei, H. (2018). Effect of nitrogen limitation on biochemical composition and photosynthetic performance for fed-batch mixotrophic cultivation of microalga spirulina platensis. *Bioresour Technol.* 263, 555–561. doi: 10.1016/j.biortech.2018.05.046

Liu, J., Chang, X. X., Huang, L. J., and Ma, Z. G. (2005). Effects of Ni on the growth, absorption spectrum and phycobiliprotein content of microcystis aeruginosa. *J. Yunnan Univ. (Natural Science)* 27 (4), 365–368. doi: 10.3321/j

Liu, C., Li, L. J., Wu, C. Y., Guo, K. N., and Li, J. H. (2016). Growth and antioxidant production of spirulina in different NaCl concentrations. *Biotechnol. Lett.* 38 (7), 1089–1096. doi: 10.1007/s10529-016-2087-2

Lu, Q., Li, H. K., Xiao, Y., and Liu, H. (2021). A state-of-the-art review on the synthetic mechanisms, production technologies, and practical application of polyunsaturated fatty acids from microalgae. *Algal Research-Biomass Biofuels Bioproducts* 55. doi: 10.1016/j.algal.2021.102281

Manirafasha, E., Murwanashyaka, T., Ndikubwimana, T., Rashid Ahmed, N., Liu, J., Lu, Y., et al. (2018). Enhancement of cell growth and phycocyanin production in arthrospira (Spirulina) platensis by metabolic stress and nitrate fed-batch. *Bioresour Technol.* 255, 293–301. doi: 10.1016/j.biortech.2017.12.068

Manirafasha, E., Ndikubwimana, T., Zeng, X. H., Lu, Y. H., and Jing, K. J. (2016). Phycobiliprotein: Potential microalgae derived pharmaceutical and biological reagent. *Biochem. Eng. J.* 109, 282–296. doi: 10.1016/j.bej.2016.01.025

Mogany, T., Kumari, S., Swalaha, F. M., and Bux, F. (2018). Extraction and characterisation of analytical grade c-phycocyanin from euhalothece sp. *J. Appl. Phycology* 31 (3), 1661–1674. doi: 10.1007/s10811-018-1661-5

Mousavi, M., Mehrzad, J., Najafi, M. F., Zhiani, R., and Shamsian, S.A.I A. (2022). Nitrate and ammonia: two key nitrogen sources for biomass and phycocyanin production by arthrospira (Spirulina) platensis. *J. Appl. Phycology*. 5, 2271–2281. doi: 10.1007/s10811-021-02664-0

Nemanja, T., Nemanja, B., Dušan, R., Aleksandar, T., Zoran, Z., Aleksandar, F., et al. (2019). Defatted wheat germ as source of polyphenols–optimization of microwave-assisted extraction by RSM and ANN approach. *Chem. Eng. Process. - Process Intensification* 143, 107634. doi: 10.1016/j.cep.2019.107634

Nethravathy,, Mehar, J. G., Mudliar, S. N., and Shekh, A. Y. (2019). Recent advances in microalgal bioactives for food, feed, and healthcare products: Commercial potential, market space, and sustainability. *Compr. Rev. Food Sci. Food Saf.* 18 (6), 1882–1897. doi: 10.1111/1541-4337.12500

Novoveská, L., Ross, M. E., Stanley, M. S., Pradelles, R., Wasiolek, V., and Sassi, J. F. (2019). Microalgal carotenoids: A review of production, current markets, regulations, and future direction. *Mar. Drugs* 17 (11), 640–661. doi: 10.3390/md17110640

Pagels, F., Guedes, A. C., Amaro, H. M., Kijjoa, A., and Vasconcelos, V. (2019). Phycobiliproteins from cyanobacteria: Chemistry and biotechnological applications. *Biotechnol. Adv.* 37 (3), 422–443. doi: 10.1016/j.biotechadv.2019.02.010

Pandey, V. D., Pandey, A., and Sharma, V. (2013). Biotechnological applications of cyanobacterial phycobiliproteins. *int.j.curr.microbiol.app.sci.* 2, 89–97.

Prabakaran, G., Sampathkumar, P., Kavisri, M., and Moovendhan, M. (2020). Extraction and characterization of phycocyanin from spirulina platensis and evaluation of its anticancer, antidiabetic and antiinflammatory effect. *Int. J. Biol. Macromol* 153, 256–263. doi: 10.1016/j.ijbiomac.2020.03.009

Rawat, D., Sharma, U., Poria, P., Finlan, A., Parker, B., Sharma, R. S., et al. (2022). Iron-dependent mutualism between chlorella sorokiniana and ralstonia pickettii forms the basis for a sustainable bioremediation system. *ISME Commun.* 2 (1), 83–96. doi: 10.1038/s43705-022-00161-0

Romay, C., Gonzalez, R., Ledon, N., Remirez, D., and Rimbau, V. (2003). C-phycocyanin: A biliprotein with antioxidant, anti-inflammatory and neuroprotective effects. *Curr. Protein Pept. Sci.* 4 (3), 207–216. doi: 10.2174/1389203033487216

Sathasivam, R., Radhakrishnan, R., Hashem, A., and Abd Allah, E. F. (2019). Microalgae metabolites: A rich source for food and medicine. *Saudi J. Biol. Sci.* 26 (4), 709–722. doi: 10.1016/j.sjbs.2017.11.003

Shanthi, G., Premalatha, M., and Anantharaman, N. (2018). Effects of l-amino acids as organic nitrogen source on the growth rate, biochemical composition and polyphenol content of spirulina platensis. *Algal Res.* 35, 471–478. doi: 10.1016/j.algal.2018.09.014

Silva, S. C., Ferreira, I. C. F. R., Dias, M. M., and Barreiro, M. F. (2020). Microalgae-derived pigments: A 10-year bibliometric review and industry and market trend analysis. *Molecules* 25 (15), 3406–3428. doi: 10.3390/molecules25153406

Singh, R., Upadhyay, A. K., Chandra, P., and Singh, D. P. (2018). Sodium chloride incites reactive oxygen species in green algae chlorococcum humicola and chlorella vulgaris: Implication on lipid synthesis, mineral nutrients and antioxidant system. *Bioresour Technol.* 270, 489–497. doi: 10.1016/j.biortech.2018.09.065

Skorupskaite, V., Makareviciene, V., and Levisauskas, D. (2015). Optimization of mixotrophic cultivation of microalgae chlorella sp for biofuel production using response surface methodology. *Algal Research-Biomass Biofuels Bioproducts* 7, 45–50. doi: 10.1016/j.algal.2014.12.001

Sloth, J. K., Wiebe, M. G., and Eriksen, N. T. (2006). Accumulation of phycocyanin in heterotrophic and mixotrophic cultures of the acidophilic red

alga galdieria sulphuraria. *Enzyme Microbial Technol.* 38 (1-2), 168–175. doi: 10.1016/j.enzmictec.2005.05.010

Soni, R. A., Sudhakar, K., and Rana, R. S. (2017). Spirulina – from growth to nutritional product: A review. *Trends Food Sci. Technol.* 69, 157–171. doi: 10.1016/j.tifs.2017.09.010

Thevarajah, B., Nishshanka, G. K. S. H., Premaratne, M., Nimarshana, P. H. V., Nagarajan, D., Chang, J. S., et al. (2022). Large-Scale production of spirulina-based proteins and c-phycocyanin: A biorefinery approach. *Biochem. Eng. J.* 185, 108541. doi: 10.1016/j.bej.2022.108541

Tredici, M. R., Papuzzo, T., and Tomaselli, L. (1986). Outdoor mass culture ofSpirulina maximain sea-water. *Appl Microbiol Biot.* 24, 1, 47–50. doi: 10.1007/BF00266284

Velu, C., Cires, S., Brinkman, D. L., and Heimann, K. (2019). Effect of CO2 and metal-rich waste water on bioproduct potential of the diazotrophic freshwater cyanobacterium, tolypothrix sp. *Heliyon* 5 (4), e01549. doi: 10.1016/j.heliyon.2019.e01549

Verma, R., Kumari, K. V. L. K., Srivastava, A., and Kumar, A. (2020). Photoautotrophic, mixotrophic, and heterotrophic culture media optimization for enhanced microalgae production. *J. Environ. Chem. Eng.* 8 (5), 104199. doi: 10.1016/j.jece.2020.104149

Xie, Y., Jin, Y., Zeng, X., Chen, J., Lu, Y., and Jing, K. (2015). Fed-batch strategy for enhancing cell growth and c-phycocyanin production of arthrospira (Spirulina) platensis under phototrophic cultivation. *Bioresour Technol.* 180, 281–287. doi: 10.1016/j.biortech.2014.12.073

Xie, L. D., and Wang, S. Y. (2017). Optimization of *Spirulina* media by response surface methodology. *Acta Agriculturae Zhejiangensis* 29 (2), 307–314. doi: 10.3969/j.issn.1004-1524.2017.02.18

Yang, J., Li, W., Xing, C., Xing, G., Guo, Y., and Yuan, H. (2022). Ca(2+) participates in the regulation of microalgae triacylglycerol metabolism under heat stress. *Environ. Res.* 208, 112696. doi: 10.1016/j.envres.2022.112696

Yu, P., Wu, Y. T., Wang, G. W., Jia, T. M., and Zhang, Y. S. (2017). Purification and bioactivities of phycocyanin. *Crit. Rev. Food Sci. Nutr.* 57 (18), 3840–3849. doi: 10.1080/10408398.2016.1167668

Zarrouk, C. (1996). Contribution to the study of a cyanophyceae: Influence of various physical and chemical factors on the growth and photosynthesis of Spirulina maxima. PhD Thesis, University of Paris, Paris.

Zeng, X. H., Danquah, M. K., Zhang, S. D., Zhang, X., Wu, M. Y., Chen, X. D., et al. (2012). Autotrophic cultivation of spirulina platensis for CO2 fixation and phycocyanin production. *Chem. Eng. J.* 183, 192–197. doi: 10.1016/j.cej.2011.12.062

frontiers | Frontiers in Marine Science

TYPE Original Research
PUBLISHED 18 January 2023
DOI 10.3389/fmars.2023.1095411



OPEN ACCESS

EDITED BY
Wei Liu,
Qilu University of Technology (Shandong Academy of Sciences), China

REVIEWED BY
Chongliang Zhang,
Ocean University of China, China
Siquan Tian,
Shanghai Ocean University, China

*CORRESPONDENCE
Zuozhi Chen
chenzuozhi@scsfri.ac.cn

SPECIALTY SECTION
This article was submitted to Marine Fisheries, Aquaculture and Living Resources, a section of the journal Frontiers in Marine Science

RECEIVED 11 November 2022
ACCEPTED 05 January 2023
PUBLISHED 18 January 2023

CITATION
Zhang K, Zhang J, Zhang P, Su L, Hong X, Qiu Y and Chen Z (2023) This is what we know: Assessing the stock status of the data-poor skipjack tuna (*Katsuwonus pelamis*) fishery in the South China Sea. *Front. Mar. Sci.* 10:1095411. doi: 10.3389/fmars.2023.1095411



# This is what we know: Assessing the stock status of the data-poor skipjack tuna (*Katsuwonus pelamis*) fishery in the South China Sea

Kui Zhang[1,2], Jun Zhang[1,2], Peng Zhang[1,2], Li Su[1,2], Xiaofan Hong[1], Yongsong Qiu[1,2] and Zuozhi Chen[1,2]*

[1]South China Sea Fisheries Research Institute, Chinese Academy of Fishery Sciences, Guangzhou, China, [2]Key Laboratory for Sustainable Utilization of Open-sea Fishery, Ministry of Agriculture and Rural Affairs, Guangzhou, China

Skipjack tuna (*Katsuwonus pelamis*) is a highly migratory species of significant value in global marine fisheries. The South China Sea (SCS) is the largest marginal sea in the northwestern Pacific Ocean, and many tuna and tuna-like species occur within it. Although a recent Western and Central Pacific Fisheries Commission report identified skipjack tuna in the western and central Pacific to be sustainably fished, the exploitation status of skipjack tuna in the SCS is still unclear, due to limited data. We apply two data-poor methods, length-based Bayesian biomass estimation (LBB) and length-based spawning potential ratio (LBSPR), to assess the status of skipjack tuna stock in the SCS. We use electronic length frequency analysis to estimate von Bertalanffy growth parameters (asymptotic length $L_{inf}$ and growth coefficient $K$) to serve as priors for LBB and LBSPR estimation. Estimates are calculated for SCS skipjack tuna $L_{inf}$ (68.3 cm), $K$ (0.325 year$^{-1}$), natural mortality (0.49 year$^{-1}$) and mean fork length at 50% sexual maturity (36.7 cm). LBB analysis reveals the estimated relative stock size (0.29) indicates that the SCS skipjack tuna stock maybe heavily overfished. LBSPR analysis reveals the estimated spawning potential ratio for this fishery to be 3%, which is significantly below the limit reference point of 20%. Accordingly, for the SCS skipjack tuna stock we identify a need to reduce fishing mortality by controlling fishing effort and increasing catchable size.

KEYWORDS

**tuna fishery, western and central Pacific, data-poor fisheries, length-based methods, overfished**

## Introduction

The highly migratory skipjack tuna (*Katsuwonus pelamis*) occurs widely throughout tropical, subtropical and temperate oceans. This species ranks third in catch tonnage ($2.8 \times 10^6$ t in 2020; FAO, 2022) in global marine fisheries (behind Anchoveta *Engraulis ringens*, and Alaska pollock *Gadus chalcogrammus*)—a position it has held for 11 consecutive years. The largest skipjack tuna fishery is in the Western and Central Pacific Ocean (WCPO), with catches contributing to 62% of global catch in 2020 (Hare et al., 2021). The Western and Central Pacific Fisheries Commission (WCPFC), responsible for managing tuna species, recently reported this fishery was in a sustainable condition in the whole WCPO (Hare et al., 2021). However, the spawning potential of skipjack tuna in region 5 (of the eight skipjack tuna stock assessment regions) (Figure 1) was considered to have decreased in recent years. A recent assessment report also stated the concern of the unquantified (and probably heavy) fishing pressure on juvenile skipjack tuna in this region (Prince et al., 2022). Limited data for region 5 meant that the exploitation status of skipjack tuna was unclear in some sea areas, such as the South China Sea (SCS). Although the SCS belongs to region 5 of the WCPO, there is no effective multilateral fisheries management mechanism while there are increasing fishing efforts from many surrounding countries. Despite its regional significance, knowledge of the SCS's fisheries and stock status remains scarce, the initial assessments of commercial species appear to be particularly significant.

Overfishing is one of the most intractable challenges facing marine ecosystems. The Food and Agricultural Organization of the United Nations (FAO) suggest that the percentage of fishery stocks exploited at unsustainable levels had increased from 10% to 35.4% since the 1970s (FAO, 2022). Stock assessment is becoming increasingly necessary to implement effective fishery management and sustainability. Nevertheless, only one fifth of the global landings comes from assessed species, and less than one eighth of the world's fisheries are sufficiently well managed or have detailed stock assessments for management purposes (Costello et al., 2012; FAO, 2022; Kindong et al., 2022). The severity of this problem is increasingly recognized, and various types of data-poor stock assessment methods have been put forward over the past 20 years as part of a solution (Zhang et al., 2021a; Liao et al., 2022). Among these methods, length-based assessment models are widely used because length-frequency data are rather cost-effective and easy to collect (Quinn and Deriso, 1999; Hordyk et al., 2015; Hordyk et al., 2016; Mildenberger et al., 2017; Froese et al., 2018; Chong et al., 2020).

In this study, we apply length-based spawning potential ratio (LBSPR) and length-based Bayesian biomass estimation (LBB) models to assess the status of skipjack tuna stocks in the SCS. We calculate the prior information required for these models, asymptotic length ($L_{inf}$) and growth coefficient ($K$), by electronic length frequency analysis (ELEFAN). Results are important for more informed and effective management of this fishery resource, and to ensure its sustainable exploitation in an otherwise data-poor environment.

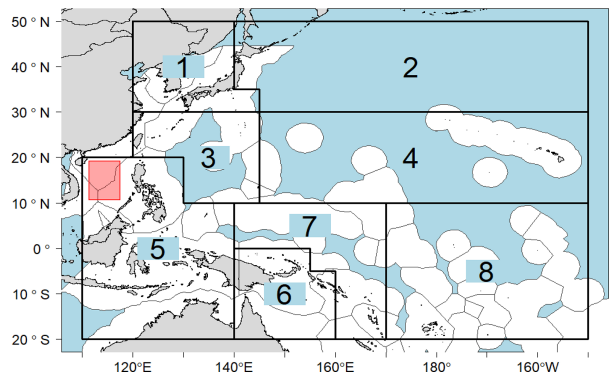


FIGURE 1
Eight (1–8) WCPO skipjack tuna stock assessment regions (sourced WCPFC, available online at https://www.wcpfc.int/doc/03/skipjack-tuna ). The red rectangle represents the South China Sea skipjack tuna sampling area.

## Materials and methods

### Data collection

Skipjack tuna in the SCS were mainly caught by the Philippines, Vietnam, China, Malaysia and Indonesia. The main fishing gears were purse seine, handline, light falling-net, troll, hook and line (Prince et al., 2022). Skipjack tuna in the SCS (Figure 1) were collected using a light falling-net (290-m circumference, 85-m stretched length, 22-mm cod-end mesh, and 52-mm net mouth mesh) in series of scientific surveys conducted by South China Sea Fisheries Research Institute, Chinese Academy of Fishery Sciences, from 2014–2019. The surveys covered four seasons. The light falling-net is a relatively new type of fishing gear which first appeared in the SCS in the early 1990s, and widely used in deep waters of the SCS in recent years. In this fishery, lamps function as fish-aggregating devices. Two rows of lamps (n = 230, 1 kw/lamp) are arranged along the sides of a vessel to attract fish (Zhang et al., 2021b). The main fishing targets are cephalopods, phototrophic species, and the pelagic fish species (e.g., skipjack tuna) which feed on them (Wang et al., 2021; Zhang et al., 2021b).

All species caught in the net during surveys were sampled, identified, and counted. Biological data for main commercial species, e.g., skipjack tuna, were collected. When fewer than 50 individuals were caught in a trap, all individuals were measured; otherwise, 50 individuals were randomly sampled for measurement. For each skipjack tuna, fork length (nearest mm) and body weight (nearest g) were measured. The maturity was macroscopically determined based on gonad development; specimens were attributed to one of six stages. We regard individuals with stage IV–VI gonads to be sexually mature, and those of stage I–III to be immature (Li et al., 2011).

### Data analysis

The length–weight relationship is described by the power function:

$$W = aL^b$$

where $W$ is the body weight (g) of an individual fish, $L$ represents its fork length (cm), $a$ is a scaling coefficient, and $b$ is an allometric growth parameter. The difference in length–weight relationship parameters between males and females was tested by one-way analysis of variance (ANOVA).

Length-frequency data were grouped into monthly catches, assuming that samples represented the monthly length distribution of the overall catch (Kindong et al., 2022). We used ELEFAN in the "TropFishR" package (Mildenberger et al., 2017) to estimate the asymptotic length ($L_{inf}$) and growth coefficient ($K$) of skipjack tuna. Growth is described by the von Bertalanffy growth function:

$$L_t = L_{inf}(1 - e^{-K(t-t_0)})$$

where $L_t$ represents mean length (cm) at age $t$, $L_{inf}$ is the asymptotic length, $K$ is the growth coefficient, and $t_0$ is the theoretical age when $L_t = 0$.

The parameter $t_0$ was estimated using the empirical equation (Pauly, 1983):

$$\log_{10}(-t_0) = -0.3922 - 0.275\log_{10}L_{inf} - 1.038\log_{10}K$$

The growth performance index ($\Phi$) was eatimated from the following equation (Pauly and Munro, 1984):

$$\Phi = \log_{10}K + 2\log_{10}L_{inf}$$

Natural mortality ($M$) was estimated using six empirical methods:

$$M1 = \frac{3K}{e^{(0.38\times A_{max}\times K)-1}}$$

Alverson and Carney (1975)

$$M2 = e^{-0.0152+0.6543\times\ln(K)-0.279\times\ln(L_{inf})+0.4634\times\ln(T)}$$

Pauly (1980)

$$M3 = e^{1.46-1.01\times\ln(A_{max})}$$

Hoenig (1983)

$$M4 = e^{1.44-0.98\times\ln(A_{max})}$$

Hewitt and Hoenig (2005)

$$M5 = 4.899 \times A_{max}^{-0.916}$$

Then et al. (2015)

$$M6 = 4.118 \times K^{0.73} \times L_{inf}^{-0.33}$$

Then et al. (2015)

where $A_{max}$ is the maximum reported age (12) for skipjack tuna (Froese and Pauly, 2022), and $T$ is the mean environmental temperature (°C), which we assume to be 27°C (Yu et al., 2019). We average the $M1$–$M6$ estimates to obtain a true value for skipjack tuna.

Mean fork length at 50% sexual maturity ($L_{50}$) was calculated based on relationships between the arcsin square-root (ASR) transformative percentage $P_i$ of mature individuals in each 20-mm fork length interval and the midpoint value of the standard-length interval ($X_i$), as per the following equation (Chen and Paloheimo, 1994):

$$\mathrm{ASR}(P_i) = \frac{\mathrm{ASR}(G)}{1 + \exp[-\delta(X_i - L_{50})]} + \varepsilon_i$$

where $G$ is the maximum attainable proportion of mature fish ($G = 1$ in this study), $\delta$ is the instantaneous rate of maturation, and $\varepsilon_i$ is the error. The mean fork length at 95% sexual maturity ($L_{95}$) was estimated by $1.1 \times L_{50}$ (Prince et al., 2015).

## LBB method

LBB is a recently developed method used to assess the exploitation status of data-poor fisheries based on length-frequency data (for single or multiple years). It uses a Bayesian Monte Carlo Markov Chain (MCMC) to calculate mortality parameters and the relative stock size. The principle of LBB method is that the absolute values of biomass and age can be replaced by their relative values (Froese et al., 2018). LBB is appropriate to use for species that can grow continuously through their life (Pons et al., 2020). This method can estimate asymptotic length ($L_{inf}$), length of 50% of individuals captured by a gear ($L_c$), relative natural mortality ($M/K$), fishing mortality relative to natural mortality ($F/M$), the exploited biomass relative to the unexploited biomass ($B/B_0$), and the relative stock size ($B/B_{MSY}$) for a target species (where MSY is the maximum sustainable yield). Although the LBB method only requires length-frequency data, the priors of $M/K$, $L_{inf}$, and $L_{50}$ can also be included to obtain more accurate results (Table 1). We use the priors of $M/K$, $L_{inf}$, and $L_{50}$ estimated using aforementioned approaches, including "TropFishR," empirical formulas for $M$, and the ASR method.

We determined the exploitation status of the skipjack tuna fishery based on estimates of $B/B_{MSY}$. We regard a stock to be healthy if $B/B_{MSY} > 1$; slightly overexploited where $0.8 < B/B_{MSY} \leq 1$; overfished where $0.8 \leq B/B_{MSY} \leq 0.5$; heavily overfished where $0.2 < B/B_{MSY} \leq 0.5$, and collapsed when $B/B_{MSY} \leq 0.2$ (Palomares et al., 2018). Stocks are also considered to suffer from 'growth overfishing' (when fish are harvested at an average size that is smaller than the size that would produce the maximum yield per recruit) if the estimated $L_c/L_{c\_opt} < 1$ (Zhang et al., 2021a), where $L_{c\_opt}$ represents the length at first capture that maximizes the catch and biomass. More details of LBB

TABLE 1 Summary of data requirements for LBB and LBSPR methods (red boxes represent required data; green boxes represent optional data).

| Parameters | Estimates | LBSPR | LBB |
|---|---|---|---|
| Length-frequency data | / | | |
| Asymptotic length ($L_{inf}$) | 68.3 cm | | |
| Growth coefficient ($K$) | 0.325 year$^{-1}$ | | |
| Natural mortality ($M$) | 0.49 year$^{-1}$ | | |
| $M/K$ | 1.51 | | |
| Mean fork length at 50% sexual maturity ($L_{50}$) | 36.7 cm | | |
| Mean fork length at 95% sexual maturity ($L_{95}$) | 40.4 cm | | |
| Coefficient of variation of $L_{inf}$ | 0.1 | | |
| Length–weight relationship parameter ($a$) | 0.0057 | | |
| Length–weight relationship parameter ($b$) | 3.3304 | | |

method are presented in Froese et al. (2018). All LBB analyses were performed using an R code (LBB_33a. R), downloaded from http://oceanrep.geomar.de/44832/(access date: 5 September 2022) following user guidelines.

## LBSPR method

The spawning potential ratio (SPR) is a well-known biological reference point that can be used to inform fisheries management decisions for data-limited fisheries (Hordyk et al., 2015). It can be interpreted as the proportion of the unfished spawning potential remaining under fishing pressure (Walters and Martell, 2004). We use the LBSPR method to estimate the SPR of skipjack tuna in the SCS. This method has been widely used in stock assessments for data-poor fisheries (Prince et al., 2015; Prince et al., 2020; Han et al., 2021; Alam et al., 2022); Kindong et al., 2022, and it has proven to be a consistent and accurate model (Chong et al., 2020; Pons et al., 2020). LBSPR assumes that SPR of an exploited fish stock is a function of relative fishing mortality ($F/M$) and two life-history ratios ($M/K$ and $L_{50}/L_{inf}$). In addition to target species length-frequency data, other parameters needed in the estimation (Table 1) include the $M/K$ ratio, $L_{inf}$, variability of length-at-age (default value 10%), and $L_{50}$ and $L_{95}$ (Prince et al., 2015). We estimate these parameters using aforementioned approaches, including "TropFishR," empirical formulas for $M$, and the ASR method. To analyze the uncertainty of nature mortality on LBSPR method, $M1$–$M6$ estimates were also used to run LBSPR and check the results.

In the LBSPR model, mean fork length at 50% and 95% selectivity ($SL_{50}$ and $SL_{95}$), and relative fishing mortality ($F/M$) are estimated using the maximum likelihood method. The LBSPR model applies maximum likelihood estimation to evaluate the selectivity ogive, which is expected to be a logistic curve described by the selection parameters ($SL_{50}$ and $SL_{95}$), and $F/M$, which are then utilized to estimate the SPR (Prince et al., 2015; Hordyk et al., 2016). Note that SPR estimates of 20% represent a limit reference point; SPR estimates< 20% suggest a level likely to reduce recruitment and a stock verging on collapse; and SPR estimates range 0.35–0.4 are generally associated with a stock at MSY levels (Hordyk et al., 2015; Prince et al., 2015; Kindong et al., 2022). All LBSPR analyses were performed using R code, available at https://cran.r-project.org/web/packages/LBSPR (access date: 11 September 2022).

# Results

## Parameter estimation

A total of 2033 skipjack tuna individuals of 8.3–52.9-cm fork length and 10–3250-g body weight were collected between 2014 and 2019. The length-frequency distribution was unimodal, with 58.1% of individuals ranging 21–30-cm fork length. There was no significant difference in parameters ($a$ and $b$) in length–weight relationships (Figure 2) between males and females ($F$= 0.32, $p > 0.05$; $F = 0.71$, $p > 0.05$). Length–weight relationships are estimated as:

$$\text{Male}: \ W = 0.0058L^{3.3267} \ \ (r^2 = 0.972, \ n = 239, \ p < 0.001)$$

$$\text{Female}: \ W = 0.0055L^{3.3428} \ \ (r^2 = 0.974, \ n = 204, \ p < 0.001)$$

$$\text{All}: \ W = 0.0057L^{3.3304} \ \ (r^2 = 0.988, \ n = 2033, \ p < 0.001)$$

Estimated von Bertalanffy growth parameters using the ELEFAN method and Pauly's empirical equation are 68.3 cm for $L_{inf}$, 0.325 year$^{-1}$ for $K$, and −0.41 for $t_0$. These results indicate that skipjack tuna attains a maximum fork length of 68.3 cm with a relatively low growth rate. The estimated growth performance index ($\Phi$) is 3.18 with a high goodness of fit value ($R_n$) of 0.515. The von Bertalanffy growth function is described by:

$$L_t = 68.3 \times (1 - e^{-0.325(t+0.41)})$$

Estimated natural mortalities ($M$) of skipjack tuna using empirical formulas $M1$–$M6$ are 0.60, 0.67, 0.35, 0.37, 0.50, and 0.45, respectively. We use the mean value (0.49) and set the prior $M/K$ for LBB and LBSPR to 1.51 (= 0.49/0.325) (Table 1).

Based on an ASR logistic curve fitted by nonlinear regression (Figure 3), the estimated mean fork length at 50% sexual maturity ($L_{50}$) of skipjack tuna is 36.7 cm, with 95% confidence interval (CI) 32.1–41.0 cm. The estimated mean fork length at 95% sexual maturity ($L_{95}$) is 1.1 × $L_{50}$ = 40.4 cm.

## LBB assessment results

According to LBB outputs (Figure 4), the estimated $L_{inf}$ is 68.7 cm (95% CI = 67.6–69.7 cm) and $M/K$ is 1.59 (95% CI = 1.45–1.72). The estimated relative stock size $B/B_{MSY}$ is 0.29 (95% CI = 0.232–0.352), and the estimated $L_c/L_{c\_opt}$ is 0.53, which indicates that the current SCS skipjack tuna stock is heavily overfished ($0.2< B/B_{MSY} \leq 0.5$) and experiencing growth overfishing ($L_c/L_{c\_opt}< 1$). Meanwhile, the estimated $F/M$ is 2.28 (95% CI = 1.94–2.68), indicating that fishing mortality is twice as high as natural mortality. Therefore, the exploitation rate $E$ can be calculated by $F/(F+M)$ = 0.695, which also indicates an overfished stock status. The estimated length at first capture that maximizes the catch and biomass $L_{c\_opt}$ is 40.0 cm, but only 5.2% of all individuals exceeded this length. Therefore, the optimum skipjack tuna catchable size should be increased.

## LBSPR assessment results

According to LBSPR outputs (Figure 5A–D), the mean $F/M$ estimate is 3.1, and the exploitation rate $E$ (0.756) is higher than the LBB estimate of 0.695. The ogive curve for selectivity and maturity (Figure 5B) reveals the length at maturity to be higher than the length at first capture. The estimated fork length at 50% and 95% selectivity ($SL_{50}$ and $SL_{95}$) are 20.0 and 27.6 cm, respectively (Figure 5C). Assuming that our length- frequency data are in a steady-state (Hordyk et al., 2015), the estimated SPR for the current SCS skipjack tuna stock is at 3%, which is significantly below the limit reference point of 20%. The length composition which should be targeted to maintain the threshold level (SPR = 0.2) against the current observed length-frequency data is shown in Figure 5D. The

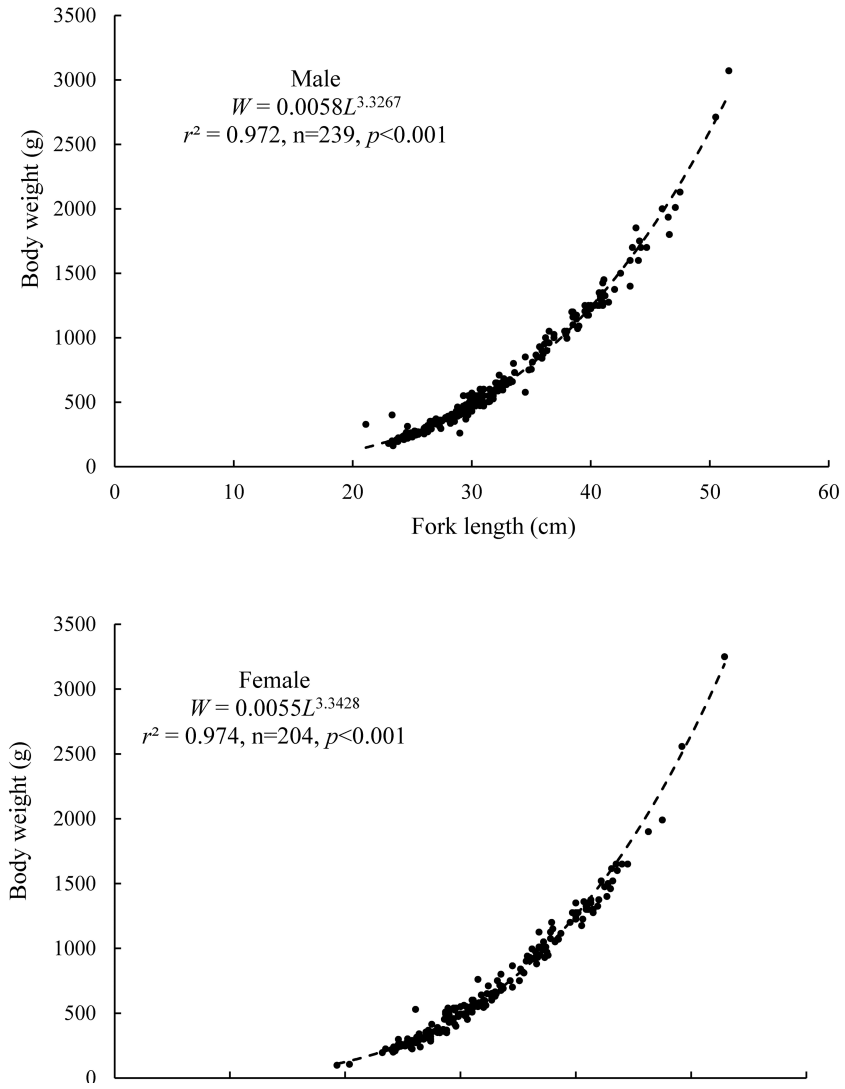


FIGURE 2
Male (upper) and female (lower) skipjack tuna length–weight relationships in the South China Sea.

uncertainty of nature mortality has effected the SPR values, and were 0.04, 0.05, 0.01, 0.01, 0.03 and 0.02, respectively, using *M*1–*M*6 estimates. The size of fish currently targeted by this fishery is significantly lower than would be expected, indicating that most caught fish are juveniles. Therefore, this fishery is overfished and the catchable size of skipjack tuna should be increased.

## Discussion

This study attempted to apply two length-based methods (LBB and LBSPR) on stock assessment for the data-poor skipjack tuna stock in the SCS. Results show a precarious situation for this fishery, with a current relative stock size $B/B_{MSY}$ of 0.29 and SPR of 3%. Although the WCPFC announced in a recent report that this fishery was sustainable in the WCPO (Hare et al., 2021), both LBB and LBSPR length-based methods suggest that it might be heavily overfished in the SCS. A recent assessment (Prince et al., 2022) also used LBSPR to evaluate skipjack tuna fishery in the SCS. Our study differed from this assessment by the following two points. Firstly, two length-based methods (LBB and LBSPR) were applied in our study and the results of LBB and LBSPR corroborated each other. Prince et al. (2022) used only LBSPR but length data from many fisheries and different countries. Secondly, we estimated the growth, mortality and maturity parameters directly from our existing data collected in the SCS while Prince et al. (2022) used previous and similar estimates (e.g., $L_{50}$ = 40.9 cm, $L_{95}$ = 45.0 cm). Actually, our estimates showed skipjack tuna in the SCS matured earlier ($L_{50}$ = 36.7 cm), and population parameters might be different with other regions (Table 1). Therefore, prior information used in LBSPR seemed more precise in our study. Our analyses contribute significantly to understanding the status of skipjack tuna stocks throughout the entire WCPO region.

The SCS occupies a central position in the Indo-West Pacific region, and is the third largest marginal sea in the world (Li et al., 2019). Fish diversity and fisheries resources within it are extremely rich (Zhang et al., 2021a), there are limited data available for many of its fisheries (Zhang et al., 2017). Shallow water (< 200 m) fisheries

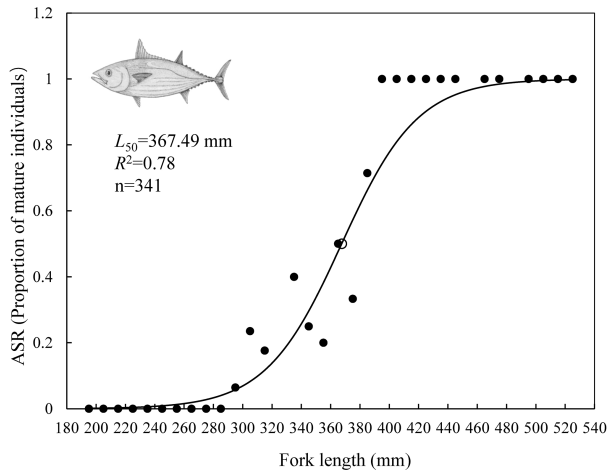


FIGURE 3
Proportions of mature skipjack tuna and logistic curves fitted using the ASR model. Solid points represent observed data, and the circle represents the estimated mean fork length at 50% sexual maturity ($L_{50}$).

provide effective prior information for this method (Zhang et al., 2021a; Liao et al., 2022). Therefore, we used ELEFAN in the "TropFishR" package to calculate priors of important growth parameters ($L_{inf}$, $K$) for skipjack tuna before LBB and LBSPR estimation. Our results differ from previous estimates of von Bertalanffy growth parameters for skipjack tuna in the Pacific and Atlantic oceans (Table 2). The estimated $L_{inf}$ in the SCS is smaller than elsewhere. The estimated $K$ is greater than values for the Atlantic Ocean, and about average for Pacific Ocean values. The growth performance index ($\Phi$) ranged 3.02–3.58 in all results, and our result ($\Phi$ = 3.18) is consistent with them. The "TropFishR" package allows users to visualize fitted scores across a range of $L_{inf}$-$K$ combinations in response surface analysis (RSA). This visualization of $R_n$ scores across discrete combinations of both variables may also aid in narrowing possible variable ranges in subsequent, more refined searches (Mildenberger et al., 2017). While our $R_n$ score (0.515) is higher than that reported in other recent studies (Alam et al., 2022; Kindong et al., 2022), the parameters estimated by "TropFishR" match those of other studies (Table 2). Therefore, the priors that we used in LBB and LBSPR are sound and informative.

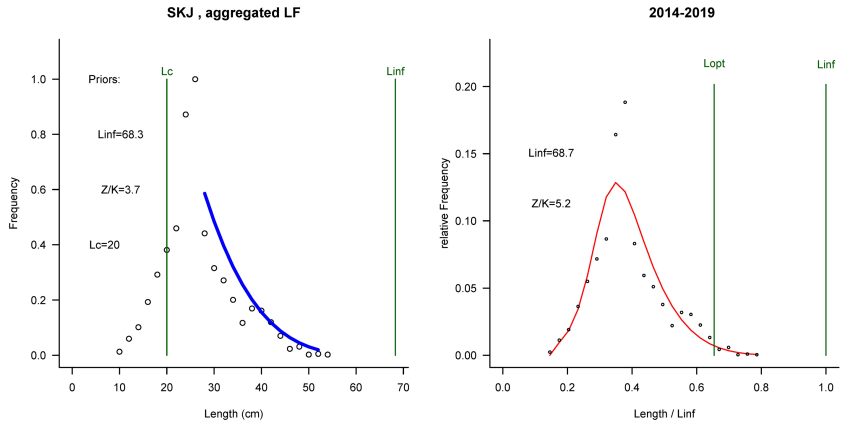


FIGURE 4
Length-based Bayesian biomass estimates for skipjack tuna in the South China Sea. Left: fits of the model to length data; right: predictions of the LBB analysis. $L_{inf}$, asymptotic length; $L_c$, length of 50% individuals captured by the gear; $L_{opt}$, length where the maximum biomass of the unexploited stock is obtained.

resources in the northern SCS had been overfished in the 1990s (Zhang et al., 2017; Zhang et al., 2021a). The main commercial fish species in deeper SCS waters are tuna and tuna-like species, e.g., yellowfin tuna (*Thunnus albacares*), bigeye tuna (*Thunnus obesus*), skipjack tuna, bullet tuna (*Auxis rochei*), frigate tuna (*Auxis thazard*), and Carangidae species (Wang et al., 2021; Zhang et al., 2021b). The status of most of these fish stocks has not been assessed because of data limitations. For data-poor fisheries, three methods (length-, catch-, and abundance-based) are usually used to calculate biological reference points within the context of MSY (Liao et al., 2022). Because accurate catch statistics in the SCS are not available, and there is a lack of time-series survey abundance data, catch- and abundance-based methods cannot be applied to assess the status of the skipjack tuna fishery in this region. Accordingly, we applied two length-based models on the SCS skipjack tuna assessment.

Previous sensitivity analysis have demonstrated the results of LBB to be sensitive to $L_{inf}$ settings, and that the ELEFAN method can

Results of the two models suggest that the SCS skipjack tuna fishery might be overfished. However, the evaluation processes and the reference points obtained from LBB and LBSPR differ. LBB works for species that grow throughout their lives, and estimates asymptotic length, length at first capture, relative natural mortality, and relative fishing mortality using MCMC analysis. Standard fisheries equations can then be used to approximate the current exploited biomass relative to the unexploited biomass (Froese et al., 2018). The relative stock size ($B/B_{MSY}$) is a useful biological reference point and management limit that is commonly used in tuna fishery management (ICCAT, 2013; Hare et al., 2021; Liao et al., 2022). The estimated $B/B_{MSY}$ (0.29) of the SCS skipjack tuna fishery is quite low for the WCPO (Hare et al., 2021). Hordyk et al. (2019) indicated that the LBB analysis did not correct for pile-up effects and may result in a biased estimate of fishing mortality $F$ and $M/K$. Zhang et al. (2021a) also suggested using other methods in conjunction with LBB if decisions regarding actual fisheries had to be made. Therefore, we

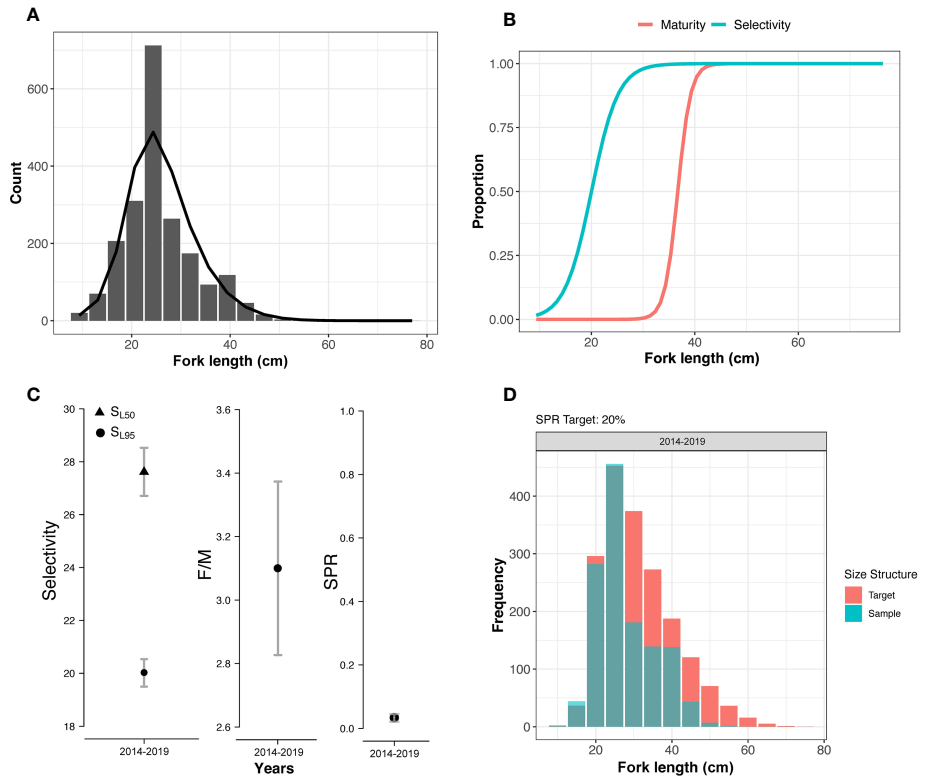


FIGURE 5
LB-SPR model outputs for South China Sea skipjack tuna. **(A)** length-frequency distribution (pillars), and predicted fished size composition (black line); **(B)** maturity and selectivity curves from the fitted LBSPR model when $L_{50}$ = 36.7 cm and $L_{95}$ = 40.4 cm; **(C)** shows the distribution of mean selectivity parameters ($SL_{50}$ and $SL_{95}$), fishing mortality to natural mortality ($F/M$), and spawning potential ratio; **(D)** observed length-frequency data against an expected size composition at a target SPR = 0.2.

TABLE 2 Growth parameters and growth performance index of skipjack tuna stocks.

| Location | Period | von Bertalanffy growth parameters | | Growth performance index ($\Phi$) | Method | Reference |
|---|---|---|---|---|---|---|
| | | $L_{inf}$ (cm) | $K$ (year$^{-1}$) | | | |
| South China Sea | 2010s | 68.3 | 0.325 | 3.18 | Length-frequency | This study |
| Western and central Pacific | 2000s | 70.6 | 0.64 | 3.50 | Dorsal Spine | Wang et al., 2010 |
| Western Pacific | 2000s | 93.6 | 0.43 | 3.58 | Otolith | Tanabe et al., 2003 |
| Western and central Pacific | 2000s | 77.4 | 0.176 | 3.02 | Otolith | Ku et al., 2015 |
| Banda Sea | 2010s | 70.1 | 0.26 | 3.11 | Length-frequency | Tadjuddah et al., 2017 |
| Southwestern Atlantic | 2000s | 92.4 | 0.161 | 3.14 | Dorsal Spine | Garbin and Castello, 2014 |
| Southwestern Atlantic | 2010s | 90.1 | 0.24 | 3.29 | Length-frequency | Soares et al., 2019 |
| Western Atlantic | 2010s | 122.5 | 0.12 | 3.26 | Dorsal Spine | Cunha-Neto et al., 2022 |

also applied another length-based method (LBSPR) to assess fishery stocks. The LBSPR method assumes that length-at-age is normally distributed with a constant coefficient of variation (CV), and assesses stock status by comparing the spawning potential as measured through length composition data to that expected in an unfished stock (Hordyk et al., 2015; Hordyk et al., 2016). The SPR obtained by LBSPR is a well-established biological reference point, and a powerful tool to help assess the impact of present-day fishing pressure on a stock's reproductive potential. The estimated SPR (0.03) of the SCS skipjack tuna fishery is the lowest throughout the WCPO (Hare et al., 2021). Therefore, we conclude that fishing mortality must be reduced by controlling fishing effort, and that the skipjack tuna catchable size

must be increased in the SCS. We also emphasize collaboration mechanism should be established by the main fishing countries for management and sustainability of skipjack tuna fishery in the SCS.

There are some limitations in this study. The two methods assume that the length composition of the catch data is representative of the exploited population, and LBSPR assumes that selectivity is well represented by a logistic curve. However, the estimated $L_{inf}$ in the SCS is the lowest thus-far reported (Table 2). This may be because the predominant size-class of skipjack tuna elsewhere ranges 40–60 cm (Garbin and Castello, 2014; Hare et al., 2021), while those from the SCS are smaller (20–40 cm). Possible explanations for this include density-dependent effects, the influence of environmental factors (e.g., higher water temperature), and fishing-induced evolution (Zhang et al., 2020). But most likely, skipjack tuna caught in unassociated (free-swimming) schools are larger than those taken in schools associated with fish aggregating devices such as light falling-net (Hare et al., 2021). Meanwhile, we found skipjack tuna in the SCS matured earlier ($L_{50}$ = 36.7 cm), which indicated the body size might be smaller than those of other regions. Therefore, the sampling representativeness and smaller body size in the SCS should be explored in further studies.

## Data availability statement

The raw data supporting the conclusions of this article will be made available by the authors, without undue reservation.

## Ethics statement

The animal study was reviewed and approved by South China Sea Fisheries Research Institute Animal Welfare Committee.

## Author contributions

KZ conceived the study and wrote the first draft. JZ and PZ provided the original length data. LS, and XH performed the data analyses and prepared the graphs. YQ, and ZC revised the manuscript. All authors contributed to the article and approved the submitted version.

## Funding

This work was supported by the Key Research and Development Project of Guangdong Province (2020B1111030001), the Central Public-Interest Scientific Institution Basal Research Fund, CAFS (2020TD05), and the Central Public Interest Scientific Institution Basal Research Fund, South China Sea Fisheries Research Institute, CAFS (2021SD01).

## Conflict of interest

The authors declare that the research was conducted in the absence of any commercial or financial relationships that could be construed as a potential conflict of interest.

## Publisher's note

All claims expressed in this article are solely those of the authors and do not necessarily represent those of their affiliated organizations, or those of the publisher, the editors and the reviewers. Any product that may be evaluated in this article, or claim that may be made by its manufacturer, is not guaranteed or endorsed by the publisher.

## References

Alam, M. S., Liu, Q., Schneider, P., Mozumder, M. M. H., Chowdhury, M. Z. R., Uddin, M. M., et al. (2022). Length-based stock assessment for the data-poor bombay duck fishery from the northern bay of Bengal coast, Bangladesh. *J. Mar. Sci. Eng.* 10, 213. doi: 10.3390/jmse10020213

Alverson, D. L., and Carney, M. J. (1975). A graphic review of the growth and decay of population cohorts. *ICES J. Mar. Sci.* 36, 133–143. doi: 10.1093/icesjms/36.2.133

Chen, Y., and Paloheimo, J. E. (1994). Estimating fish length and age at 50% maturity using a logistic type model. *Aquat. Sci.* 56, 206–219. doi: 10.1007/BF00879965

Chong, L., Mildenberger, T. K., Rudd, M. B., Taylor, M. H., Cope, J. M., Branch, T. A., et al. (2020). Performance evaluation of data-limited, length-based stock assessment methods. *ICES. J. Mar. Sci.* 77, 97–108. doi: 10.1093/icesjms/fsz212

Costello, C., Ovando, D., Hilborn, R., Gaines, S. D., Deschenes, O., and Lester, S. E. (2012). Status and solutions for the world's unassessed fisheries. *Science* 338, 517–520. doi: 10.1126/science.1223389

Cunha-Neto, M. A., Hazin, H. G., and Silva, G. B. (2022). Age and growth of skipjack tuna (*Katsuwonus pelamis*) in the western equatorial Atlantic based on dorsal spines analysis. *Bol. Inst. Pesca* 48, e686. doi: 10.20950/1678-2305/bip.2022.48.e686

FAO (2022). "The state of world fisheries and aquaculture 2022," in *Towards blue transformation* (Rome: FAO).

Froese, R., and Pauly, D. (2022) *FishBase. world wide web electronic publication*. Available at: www.fishbase.org (Accessed 19 October 2022).

Froese, R., Winker, H., Coro, G., Demirel, N., Tsikliras, A. C., Dimarchopoulou, D., et al. (2018). A new approach for estimating stock status from length frequency data. *ICES J. Mar. Sci.* 75, 2004–2015. doi: 10.1093/icesjms/fsy078

Garbin, T., and Castello, J. P. (2014). Anges in population structure and growth of skipjack tuna, *Katsuwonus pelamis* during 30 years of exploitation in the southwestern Atlantic. *Lat. Am. J. Aquat. Res.* 42, 434–446. doi: 10.3856/vol42-issue3-fulltext-13

Han, Q., Shan, X., Jin, X., Gorfine, H., Yang, T., and Su, C. (2021). Data-limited stock assessment for fish species devoid of catch statistics: case studies for *Pampus argenteus* and *Setipinna taty* in the Bohai and Yellow Seas. *Front. Mar. Sci.* 8,766499. doi: 10.3389/fmars.2021.766499

Hare, S. R., Williams, P. G., Castillo, J. C., Hamer, P. A., Hampton, W. J., Scott, R. D., et al. (2021). "The western and central Pacific tuna fishery: 2020 overview and status of stocks," in *Tuna fisheries assessment report no. 21* (Noumea, New Caledonia: Pacific Community), 53.

Hewitt, D.A., and Hoenig, J.M. (2005). Comparison of two approaches for estimating natural mortality based on longevity. *Fish. Bull.* 103, 433-437.

Hoenig, J. M. (1983). Empirical use of longevity data to estimate mortality rates. *Fish. Bull.* 82, 898–903.

Hordyk, A., Ono, K., Prince, J. D., and Walters, C. J. (2016). A simple length-structured model based on life history ratios and incorporating size-dependent selectivity: application to spawning potential ratios for data-poor stocks. *Can. J. Fish. Aquat. Sci.* 13, 1–13. doi: 10.1139/cjfas-2015-0422

Hordyk, A., Ono, K., Valencia, S., Loneragan, N., and Prince, J. (2015). A novel length-based empirical estimation method of spawning potential ratio (SPR), and tests of its performance, for small-scale, data-poor fisheries. *ICES J. Mar. Sci.* 72, 217–231. doi: 10.1093/icesjms/fsu004

Hordyk, A. R., Prince, J. D., Carruthers, T. R., and Walters, C. J. (2019). Comment on "A new approach for estimating stock status from length frequency data" by froese et al., (2018). *ICES J. Mar. Sci.* 76, 457–460. doi: 10.1093/icesjms/fsy168

ICCAT (2013). *Report of the 2013 ICCAT north and south Atlantic albacore data preparatory meeting* (Madrid, Spain: The International Commission for the Conservation of Atlantic Tunas), 68.

Kindong, R., Sarr, O., Wu, F., and Tian, S. (2022). Length-based assessment methods for the conservation of a pelagic shark, *Carcharhinus falciformis* from the tropical Pacific Ocean. *Fishes* 7, 184. doi: 10.3390/fishes7040184

Ku, J. E., Lee, S., Kim, J.-K., Park, H. W., Lee, M. K., Kim, Z. G., et al. (2015). Age and growth of the skipjack tuna *Katsuwonus pelamis* in the western and central Pacific Ocean. *Kor. J. Fish. Aquat. Sci.* 48, 377–385. doi: 10.5657/KFAS.2015.0377

Liao, B., Xu, Y., Sun, M., Zhang, K., and Liu, Q. (2022). Performance comparison of three data-poor methods with various types of data on assessing southern Atlantic albacore fishery. *Front. Mar. Sci.* 9, 825461. doi: 10.3389/fmars.2022.825461

Li, Z., Shan, X., Jin, X., and Dai, F. (2011). Long-term variations in body length and age at maturity of the small yellow croaker (*Larimichthys polyactis* bleeker 1877) in the Bohai Sea and the Yellow Sea, China. *Fish. Res.* 110, 67–74. doi: 10.1016/j.fishres.2011.03.013

Li, Y., Wang, C., Zou, X., Feng, Z., Yao, Y., Wang, T., et al. (2019). Occurrence of polycyclic aromatic hydrocarbons (PAHs) in coral reef fish from the South China Sea. *Mar. pollut. Bull.* 139, 339–345. doi: 10.1016/j.marpolbul.2019.01.001

Mildenberger, T. K., Taylor, M. H., and Wolff, M. (2017). TropFishR: An r package for fisheries analysis with length-frequency data. *Meth. Ecol. Evol.* 8, 1520–1527. doi: 10.1111/2041-210X.12791

Palomares, M. L. D., Froese, R., Derrick, B., Nöel, S.-L., Tsui, G., Woroniak, J., et al. (2018). *A preliminary global assessment of the status of exploited marine fish and invertebrate populations* (Washington, DC, USA: OCEANA).

Pauly, D. (1980). On the interrelationships between natural mortality, growth parameters, and mean environmental temperature in 175 fish stocks. *ICES J. Mar. Sci.* 39, 175–192. doi: 10.1093/icesjms/39.2.175

Pauly, D. (1983). *Some simple methods for the assessment of tropical fish stocks* (Rome, Italy: FAO), 234.

Pauly, D., and Munro, J. L. (1984). Once more on the composition of growth in fish and invertebrates. *Fishbyte* 2, 1–21.

Pons, M., Cope, J. M., and Kell, L. T. (2020). Comparing performance of catch-based and length-based stock assessment methods in data-limited fisheries. *Can. J. Fish. Aquat. Sci.* 77, 1026–1037. doi: 10.1139/cjfas-2019-0276

Prince, J., Creech, S., Madduppa, H., and Hordyk, A. (2020). Length-based assessment of spawning potential ratio in data-poor fisheries for blue swimming crab (*Portunus* spp.) in Sri Lanka and Indonesia: Implications for sustainable management. *Reg. Stud. Mar. Sci.* 36, 101309. doi: 10.1016/j.rsma.2020.101309

Prince, J., Victor, S., Kloulchad, V., and Hordyk, A. (2015). Length based SPR assessment of eleven Indo-Pacific coral reef fish populations in Palau. *Fish. Res.* 171, 42–58. doi: 10.1016/j.fishres.2015.06.008

Prince, J., Wang, X., Lin, K., Suryanti, A., Jamon, S., Santos, M. D., et al. (2022) *The CFRA: A joint assessment of South China Sea skipjack tuna stocks*. Available at: http://www.scspi.org/en/yjbg/cfra-joint-assessment-south-china-sea-skipjack-tuna-stocks (Accessed 16 December 2022).

Quinn, T. J. I. I., and Deriso, R. B. (1999). *Quantitative fish dynamics* (Oxford, UK: Oxford University Press).

Soares, B. J., Monteiro-Neto, C., Costa, M. R., Martins, R. R. M., Vieira, F. C. S., Andrade-Tubino, M. F., et al. (2019). Size structure, reproduction, and growth of skipjack tuna (*Katsuwonus pelamis*) caught by the pole-and-line fleet in the southwest Atlantic. *Fish. Res.* 212, 136–145. doi: 10.1016/j.fishres.2018.12.011

Tadjuddah, M., Anadi, L., Mustafa, A., Arami, H., Abdullah, K. S., et al. (2017). Growth pattern and size structure of skipjack tuna caught in Banda Sea, Indonesia. *AACL Bioflux.* 10, 227–233.

Tanabe, T., Kayama, S., and Ogura, M. (2003). "Precise age determination of young to adult skipjack tuna (*Katsuwonus pelamis*) with validation of otolith daily increment," in *Proceedings of the 16th Meeting of the Standing Commitee on Tuna and Billfish*, (Mooloolaba, Aus).

Then, A. Y., Hoenig, J. M., Hall, N. G., Hewitt, D. A., and Jardim, H. E. E. (2015). Evaluating the predictive performance of empirical estimators of natural mortality rate using information on over 200 fish species. *ICES J. Mar. Sci.* 72, 82–92. doi: 10.1093/icesjms/fsu136

Walters, C. J., and Martell, S. J. D. (2004). *Fisheries ecology and management* (Princeton, USA: Princeton University Press).

Wang, X. F., Xu, L. X., Zhu, G. P., and Wang, C. L. (2010). Age identification and growth characteristics of *Katsuwonus pelamis* in western and central Pacific Ocean. *Chin. J. Appl. Ecol.* 21, 756–762.

Wang, T., Zhang, P., Li, J., Zhang, J., Xie, B., Yan, L., et al. (2021). Distribution of skipjack tuna (*Katsuwonus pelamis*) associated with a light falling-net in the South China Sea. *J. Fish. Sci. China* 28, 79–89. doi: Doi: 10.3724/SP.J.1118.2021.20104

Yu, Y., Zhang, H., Jin, J., and Wang, Y. (2019). Trends of sea surface temperature and sea surface temperature fronts in the South China Sea during 2003–2017. *Acta Oceanol. Sin.* 38, 106–115. doi: 10.1007/s13131-019-1416-4

Zhang, K., Guo, J. Z., Xu, Y. W., Jiang, Y., Fan, J. T., Xu, S. N., et al. (2020). Long-term variations in fish community structure under multiple stressors in a semi-closed marine ecosystem in the South China Sea. *Sci. Total Environ.* 745, 140892. doi: 10.1016/j.scitotenv.2020.140892

Zhang, K., Liao, B., Xu, Y., Zhang, J., Sun, M., Qiu, Y., et al. (2017). Assessment for allowable catch of fishery resources in the South China Sea based on the statistical data. *Haiyang Xuebao* 39, 25–33. doi: 10.3969/j.issn.0253-4193.2017.08.003

Zhang, K., Li, J., Hou, G., Huang, Z., Shi, D., Chen, Z., et al. (2021a). Length-based assessment of fish stocks in a data-poor, jointly exploited (China and Vietnam) fishing ground, northern South China Sea. *Front. Mar. Sci.* 8, 718052. doi: 10.3389/fmars.2021.718052

Zhang, J., Zhang, K., Chen, Z., Dong, J., and Qiu, Y. (2021b). Hydroacoustic studies on *Katsuwonus pelamis* and juvenile *Thunnus albacares* associated with light fish-aggregating devices in the South China Sea. *Fish. Res.* 233, 105765. doi: 10.1016/j.fishres.2020.105765

frontiers | Frontiers in Marine Science

TYPE Original Research
PUBLISHED 06 March 2023
DOI 10.3389/fmars.2023.1100949



OPEN ACCESS

EDITED BY
Wei Liu,
Qilu University of Technology (Shandong Academy of Sciences), China

REVIEWED BY
Victor Hugo Valiati,
University of the Rio dos Sinos Valley, Brazil
Khaled Mohammed-Geba,
University of Maryland, College Park, United States

*CORRESPONDENCE
Xidong Mu
muxd@prfri.ac.cn

SPECIALTY SECTION
This article was submitted to Marine Fisheries, Aquaculture and Living Resources, a section of the journal Frontiers in Marine Science

RECEIVED 17 November 2022
ACCEPTED 21 February 2023
PUBLISHED 06 March 2023

CITATION
Yang Y, Wang Y, Wu Y, Liu Y, Liu C, Jiang Z and Mu X (2023) Population genetics of zig-zag eel (*Mastacembelus armatus*) uncover gene flow between an isolated island and the mainland China. *Front. Mar. Sci.* 10:1100949. doi: 10.3389/fmars.2023.1100949



# Population genetics of zig-zag eel (*Mastacembelus armatus*) uncover gene flow between an isolated island and the mainland China

Yexin Yang[1,2], Yuanyuan Wang[1], Yuli Wu[3], Yi Liu[1], Chao Liu[1], Zhiyong Jiang[3] and Xidong Mu[1]*

[1]Key Laboratory of Prevention and Control for Aquatic Invasive Alien Species, Ministry of Agriculture and Rural Affairs, Guangdong Modern Recreational Fisheries Engineering Technology Center, Pearl River Fisheries Research Institute, Chinese Academy of Fishery Sciences, Guangzhou, China, [2]Key Laboratory of Aquatic Animal Immune Technology of Guangdong Province, Pearl River Fisheries Research Institute, Chinese Academy of Fishery Sciences, Guangzhou, China, [3]Department of Fisheries, Agro-Tech Extension Center of Guangdong Province, Guangzhou, China

**Introduction:** *Mastacembelus armatus* is a commercially valuable fish, normally distributed in southern China and Southeast Asia. The natural population size of M. armatus is shrinking in recent years because of overfishing and habitat loss. In order to clarify the genetic diversity and differentiation of *M. armatus* populations, we collected 114 samples from eight populations in southern China and Vietnam and analyzed their population structure using nuclear ribosomal DNA sequences, the concatenated 18S and ITS2 regions.

**Methods:** Genomic DNA from the fin clip was extracted and sequenced on an Illumina novaseq 6000 (Illumina, USA) high-throughput sequencing platform in accordance with the manufacturer's instructions. After assembly and annotation, haplotype diversity, TCS network analysis, AMOVA analysis, population pairwise genetic distances, and UPGMA tree construction were conducted based on the concatenated sequences of 18S and ITS2.

**Results and discussion:** In total, eleven nrDNA haplotypes were detected based on the concatenated sequences of 18S and ITS2. Amongst, three haplotypes were the main haplotypes, as representatives of three corresponding Clusters. There were two major Clusters in China, however, the Cluster in Vietnam was significantly divergent from the other two in China, likely due to the lack of river connection between China and Vietnam. Interestingly, based on low FST value, we found that gene flow occurred between the isolated island, Hainan Province, and the mainland China of Guangxi Province, probably as a result of exposed continental shelf connected them during glacial periods. In general, combing our data and literature data, genetic diversity and differentiation of *M. armatus* populations are relatively high regardless of spatial scale, although their natural population size is declining. This suggests that it is not too late to adopt measures to protect M. armatus, which benefits not only species itself but also the whole ecosystem.

KEYWORDS

**genetic diversity, populations, *mastacembelus armatus*, southern China, Vietnam**

# Introduction

*Mastacembelus armatus*, the common name is zig-zag eel or tire-track spiny eel, is an economically important fish, belonging to the Order Symbranchiformes (Family: Mastacembelidae; Genus: *Mastacembelus*). Among the four species of the genus, *M. armatus* is the largest (Serajuddin and Pathak, 2012). It is widely distributed in southern China, mainly in Yangtze River and Pearl River (Xue et al., 2020), and Southeast Asia, such as India, Thailand, Nepal, Vietnam, Sri Lanka, and Pakistan (Hossain et al., 2015; Gupta and Banerjee, 2016; Han et al., 2019). Usually, it inhabits rivers, streams, ponds, beels and inundated fields (Hossain et al., 2015; Gupta and Banerjee, 2016). *M. armatus* is a carnivorous fish, it prefers to feed on crustacean and insect larvae when young while the adults devour small fish and tadpoles (Hossain et al., 2015). *M. armatus* is in high demand on the market as it attracts consumers with its delicious taste, no intermuscular spines and high nutritional value (Gupta and Banerjee, 2016; Li et al., 2016; Xue et al., 2020). Besides, the appealing color pattern of *M. armatus* makes it a popular aquarium fish as well (Gupta and Banerjee, 2016).

However, due to overfishing and habitat loss, the wild population size of *M. armatus* gradually declines year by year (Hossain et al., 2012; Rahman et al., 2016; Xue, 2018). *M. armatus* is designated as an endangered species in Bangladesh (IUCN Bangladesh, 2000) and has been classified as least concern by the International Union for Conservation of Nature (IUCN) (IUCN, 2019). In addition, large-scale artificial breeding has not been achieved for *M. armatus* (Jiang, 2018). Therefore, it is urgently needed to clarify the present condition of natural populations of *M. armatus*, particularly their genetic diversity and structure, thus providing basis for their biological conservation. As a native species in China, *M. armatus* is assigned as a key protected wild aquatic animal by Fujian, Guangdong, and Hunan provinces, and moreover, a national germplasm resource reserve of *M. armatus* has been established in Fujian Province (Jiang, 2018). Furthermore, aquaculture of *M. armatus* has intensified in several provinces of China, greatly facilitating its artificial breeding (Han et al., 2017; Han et al., 2019).

So far, a lot of studies have been conducted on *M. armatus*, such as studies at individual level on their morphology (Shu et al., 2017; Zhou et al., 2019), nutritional composition (Wu et al., 2010; Fan et al., 2018), metal bioaccumulation (Javed and Usmani, 2016; Pandey et al., 2017), karyotype (Oliveira et al., 1997);, taxonomy (Jiang, 2018; Duong et al., 2020), reproduction (Serajuddin and Pathak, 2012), histopathology (Dhole et al., 2011), sex-specific markers (Xue et al., 2020; Xue et al., 2021b), artificial breeding (Lin et al., 2016; Xue, 2018), Toll-Like Receptors (TLR) (Han et al., 2017; Han et al., 2019), mitochondrial genome sequencing (Li et al., 2016; Han et al., 2018), whole genome sequences at the chromosomal scale (Xue et al., 2021a), as well as population studies (Wang et al., 2012; Zou, 2013; Chen, 2014; Yang et al., 2016; Lin, 2017; Jiang, 2018; Thapliyal et al., 2020; Gao et al., 2022). Among the above listed population studies, some used mitochondrial DNA markers, such as COI (Chen, 2014; Jiang, 2018; Gao et al., 2022), Cytb (Wang et al., 2012; Thapliyal et al., 2020; Gao et al., 2022) and D-loop (Chen, 2014), and others employed nuclear makers, like SSR (Zou, 2013; Yang et al., 2016; Lin, 2017) and exon-primed intron-crossing markers (EPICs) (Jiang, 2018). These studies, however, are all from Chinese populations, except one study from India (Thapliyal et al., 2020). Population data from Southeast Asia is very scarce. Therefore, we expanded our sampling area from China to Vietnam to fill our knowledge gap. Additionally, mitochondrial markers were mostly used in *M. armatus* population studies, only few nuclear markers like SSR and EPICs, while no reports were based on nuclear ribosomal DNA (nrDNA) markers to reveal their genetic diversity (Wang et al., 2012; Zou, 2013; Chen, 2014; Yang et al., 2016; Lin, 2017; Jiang, 2018; Gao et al., 2022). It is well known that nrDNA markers have been successfully employed in various fish population research (Mladineo et al., 2013; Garcia et al., 2015; Ağdamar and Tarkan, 2019), such as 18S, ITS1, ITS2 and 28S, due to their high evolutionary rates (Presa et al., 2002). Therefore, in this study, we employed the concatenated 18S and ITS2 sequences to assess levels of genetic diversity and differentiation of *M. armatus* populations from China and Vietnam at different spatial scale.

# Materials and methods

## Sampling

*M. armatus* from seven regions in southern China and one region in Vietnam were sampled in 2021. Sample sets collected from a single region were considered a population. In China, we collected *M. armatus* from four Provinces. Two populations were sampled from Guangdong Province, three populations from Guangxi Province, one population from Jiangxi Province and one population from Hainan Province (Table 1, Figure 1). What should be noted is that Hainan Province is located in an independent island, spatially separated with the mainland China by Qiongzhou Strait. Additionally, Guangxi Province is geographically adjacent with Vietnam. The Vietnam samples were collected from Guangzhou Lanhai Marine Technology Co., Ltd, Guangzhou city, Guangdong Province, China (latitude: 23.21° N, longitude: 113.47°E). More specifically, we collected 12 and 16 samples in GDHY and GDQY regions from Guangdong Province, respectively; 18, 18, 15 samples in GXBS, GXLZ and GXYL regions from Guangxi Province, respectively; 7 samples in HNHK region from Hainan Province, 13 samples in JXGZ region from Jiangxi Province, 15 samples in YN region from Vietnam. A total of 114 samples from eight populations were collected in this study (Table 1).

## DNA extraction and sequencing

A 30-40 mg fin clip was collected and preserved in 95% ethanol at -20°C for later genomic sequencing. Both DNA sequencing and assembly were performed by Science Corporation of Gene (SCGene) Co., Ltd, Guangzhou city, Guangdong Province, China. Total genomic DNA was extracted with a Tissue DNA Kit (OMEGA E.Z.N.A) following the manufacturer's protocol. The quality and quantity of genomic DNAs were determined by 0.8% agarose gel

TABLE 1 Summary of samples and genetic diversity of *Mastacembelus armatus* (N: number of samples; $N_h$: number of nrDNA haplotypes; hd: haplotype diversity; π: nucleotide diversity; F/M: ratio of the number of females to males).

| Country | Province | Region | N | Sex ratio (F/M) | $N_h$ | Haplotypes | hd ± S.D | π ± S.D |
|---|---|---|---|---|---|---|---|---|
| China | Guangdong | GDHY | 12 | 2/10 (0.20) | 2 | H1(10),H4(2) | 0.303± 0.147 | 0.00025 ± 0.00012 |
| | | GDQY | 16 | 9/7 (1.29) | 3 | H1(14),H6(1),H7(1) | 0.242± 0.135 | 0.00010 ± 0.00006 |
| | | Total | 28 | 11/17 (0.65) | 4 | H1(24),H4(2),H6(1),H7(1) | 0.267± 0.107 | 0.00017 ± 0.00008 |
| | Guangxi | GXBS | 18 | 8/10 (0.8) | 2 | H1(17),H5(1) | 0.111± 0.096 | 0.00005 ± 0.00004 |
| | | GXLZ | 18 | 10/8 (0.8) | 1 | H1(18) | 0 | 0 |
| | | GXYL | 15 | 7/8 (0.88) | 2 | H2(14),H8(1) | 0.133± 0.105 | 0.00006 ± 0.00005 |
| | | Total | 51 | 25/26 (0.96) | 4 | H1(35),H2(14),H5(1),H8(1) | 0.462± 0.060 | 0.00071 ± 0.00009 |
| | Hainan | HNHK | 7 | 3/4 (0.75) | 2 | H2(6),H9(1) | 0.286± 0.157 | 0.00012 ± 0.00011 |
| | Jiangxi | JXGZ | 13 | 5/8 (0.63) | 1 | H1(13) | 0 | 0 |
| | Total (China) | | 99 | 8/12 (0.67) | 8 | H1(72),H2(20),H4(2),H5(1),H6(1),H7(1),H8(1),H9(1) | 0.434± 0.052 | 0.00064 ± 0.00008 |
| Vietnam | YN | | 15 | 8/7 (1.14) | 3 | H3(13),H10(1),H11(1) | 0.257± 0.142 | 0.00011 ± 0.00006 |
| Overall (China and Vietnam) | | | 114 | 52:62 (0.84) | 11 | H1(72),H2(20),H3(13),H4(2),H5(1),H6(1),H7(1),H8(1),H9(1), H10(1),H11(1) | 0.561± 0.047 | 0.00199 ± 0.00028 |

electrophoresis and NanoDrop 2000 spectrometer (Thermo Scientific, Waltham, MA, USA). High-quality genomic DNAs were used to construct a paired-end sequencing library with an insert size of 450 bp. The library was then sequenced on an Illumina novaseq 6000 (Illumina, USA) high-throughput sequencing platform in accordance with the manufacturer's instructions.

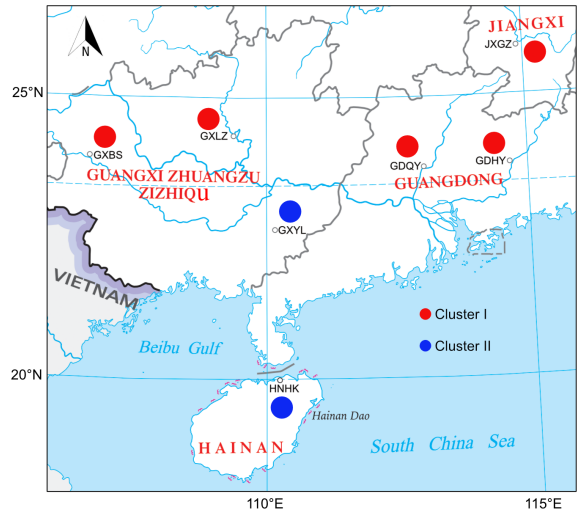


FIGURE 1
Distribution of sampling sites of *Mastacembelus armatus* populations in China. Region abbreviations follow those in Table 1. Pie charts represent the Cluster frequency of nrDNA haplotypes belong to in each region; the colour of each Cluster is consistent with Figures 2, 3.

## Sequence assembly

Adaptors and low-quality reads were filtered using Trimmomatic v0.39 (Bolger et al., 2014), resulting the raw reads, which number were between 3,876,630 and 51,352,359. Paired-end reads of 2 × 150 bp were generated, and the quality threshold was set to Q20. Qualified reads were then compared by BWA (Li and Durbin, 2009) employing setting of 0 match and 0 gap. Afterwards, the obtained reads were assembled using SOAPdenovo (Luo et al., 2012). To verify the correctness of the assembly, assembled whole nrDNA sequences were amplified and sequenced by Sanger sequencing. The annotation of assembled nrDNAs was performed using blastn in NCBI with closely related and well-annotated sequences, manually verified afterwards. Finally, respective region sequences were generated, including 18S, ITS1, 5.8S, ITS2 and 28S.

## Data analysis

Standard diversity indices, including number of haplotypes ($N_h$), haplotype diversity (hd) and nucleotide diversity (π), were calculated using DnaSP v 5.10 (Librado and Rozas, 2009). A TCS network was

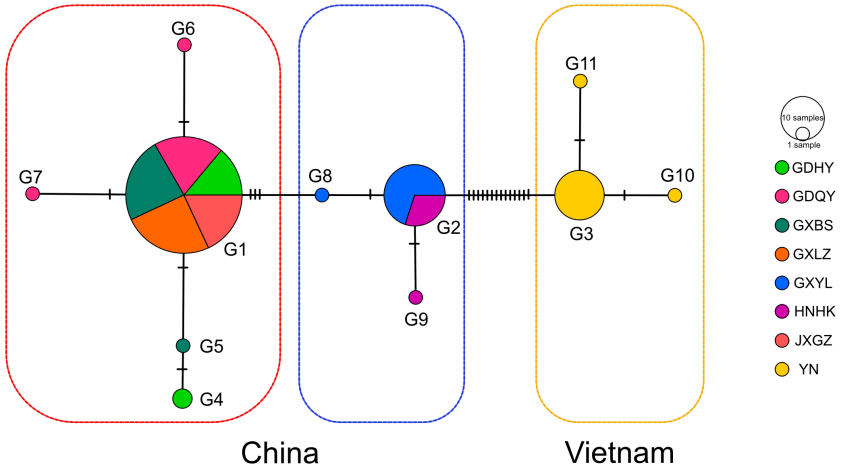


FIGURE 2
TCS network based on the concatenated sequences of 18S and ITS2 of *Mastacembelus armatus*. Each tick represents a mutational step. nrDNA haplotypes are named as in Table 1. Circle size is proportional to the haplotype frequency.

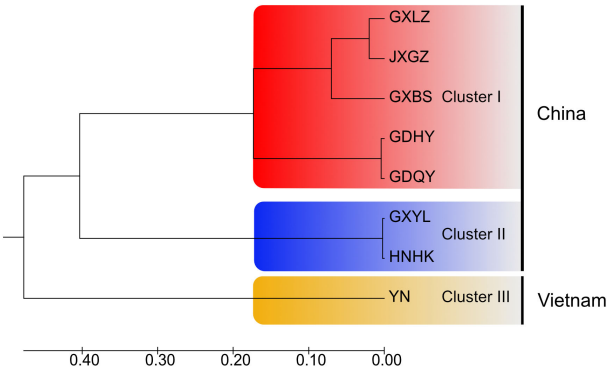


FIGURE 3
UPGMA dendrogram of eight populations of *Mastacembelus armatus* based on pairwise genetic distances between populations.

constructed with PopArt (Clement et al., 2002; Leigh and Bryant, 2015) to investigate genealogical relationships among populations inferred from the concatenated sequences of 18S and ITS2. Hierarchical analysis of molecular variance (AMOVA) was performed to detect genetic variations within and among different regions using Arlequin v 3.5 (AMOVA; Excoffier and Lischer, 2010), with statistical significance determined by 1,000 permutations. To quantify the genetic dissimilarity between populations, population pairwise genetic distances ($F_{ST}$) were also calculated by Arlequin v 3.5 (Excoffier and Lischer, 2010). The genetic distance among different populations was used to construct the UPGMA tree in MEGA X (Kumar et al., 2018).

# Results

## Characteristics of nrDNA

Variations of the length of either whole nrDNA sequences or respective region sequences were slight, see details in Table 2. To be specific, the length of 18S and 5.8S of all individuals were all the same, with 1,840 bp and 154 bp, respectively. Especially, all sequences of 5.8S were completely identical. In addition, there was also very little variation in the length of 28S, with only a 2 bp difference in length. In the 28S alignment of all individuals, 30 variable sites were found, accounting for 0.85%, compared with 3 in 18S (0.16%), 20 in ITS2 (3.37%) and 66 in ITS1 (5.77%). It is worth to note that although the proportion of variable sites in the 28S alignment was low, the majority of variable sites, 21 out of 30, were singletons variable sites. Clearly, ITS1 and ITS2 were regions with greater variability. Furthermore, we found that many indels occurred in the alignment of ITS1, for example, the longest indel was 14 bp in length, located at 1020 nt - 1043 nt. The GC content of whole nrDNA in all populations was similar, between 62.5% and 62.7%, showing a high GC content.

More than 5% indels and 5.77% variable sites occurred in the alignment of ITS1, directly affecting the accuracy of subsequent analyses. Additionally, in the alignment of 28S, too many singletons variable sites were detected, which is also thought to negatively impact the molecular analyses, such as phylogenetic analysis and population genetics (Dress et al., 2008; Steenwyk et al., 2020). Besides, the 5.8S sequences of all individuals were the same, we thus decided to use the concatenated sequence of 18S and ITS2 for all later analyses.

## Genetic diversity

Eleven nrDNA haplotypes were identified from the concatenated sequences of 18S and ITS2, consistently inferred from DnaSP results and TCS network (Table 1, Figure 2). The overall genetic diversity was relatively high (0.561 ± 0.047) while nucleotide diversity was low (0.00199 ± 0.00028) (Table 1). The highest haplotype diversity was found in GDHY region in China, followed by HNHK, YN, and GDQY region. Most regions harbored more than one haplotype, except GXLZ and JXGZ region. In a word, we found eight haplotypes in China and three haplotypes in

TABLE 2 The length and GC content of whole nrDNA and respective region of *Mastacembelus armatus* from eight populations.

| Country | Province | Region | Length (bp) | | | | | | Overall GC content |
|---|---|---|---|---|---|---|---|---|---|
| | | | 18S | ITS1 | 5.8S | ITS2 | 28S | Overall | |
| China | Guangdong | GDHY | 1840 | 1080-1087 | 154 | 580-585 | 3518 | 7176-7183 | 62.6-62.7% |
| | | GDQY | 1840 | 1080-1088 | 154 | 584-585 | 3518 | 7176-7185 | 62.6-62.7% |
| | Guangxi | GXBS | 1840 | 1080-1088 | 154 | 583-586 | 3518 | 7176-7186 | 62.6-62.7% |
| | | GXLZ | 1840 | 1084-1090 | 154 | 584-586 | 3518 | 7178-7187 | 62.6-62.7% |
| | | GXYL | 1840 | 1077-1086 | 154 | 581-586 | 3518 | 7173-7181 | 62.5-62.6% |
| | Hainan | HNHK | 1840 | 1077-1084 | 154 | 581-584 | 3518-3520 | 7173-7178 | 62.5-62.6% |
| | Jiangxi | JXGZ | 1840 | 1087-1095 | 154 | 584-586 | 3518 | 7184-7192 | 62.70% |
| Vietnam | YN | | 1840 | 1074-1088 | 154 | 581-585 | 3518-3520 | 7171-7184 | 62.6-62.7% |
| Total | | | 1840 | 1074-1095 | 154 | 580-586 | 3518-3520 | 7171-7192 | 62.5-62.7% |

Vietnam (Table 1, Figure 2), and H1, H2 and H3 were the main haplotypes, making three different Clusters (Figure 2). Amongst, H1 and H2 were the main haplotypes found in China and H3 in Vietnam. Moreover, in China, the genetic diversity of *M. armatus* in Guangxi province was the highest (0.462 ± 0.060), consisting of two main haplotypes H1 and H2, while only H1 was detected in Jiangxi Province, predominant H1 in Guangdong Province, and predominant H2 in Hainan Province.

Overall, more males were found in our study. In Vietnam, the number of females exceeded males, compared to Chinese populations with dominant males.

## Population structure

In general, AMOVA analyses presented that there was high genetic differentiation in overall populations of *M. armatus* (ΦST = 0.882, $p < 0.001$), and the largest level of genetic differentiation was found among populations (88.19%) (Table 3). The similar pattern was shown at the province level (ΦST = 0.796, $p < 0.001$) and at the country level (ΦST = 0.886, $p < 0.001$) as well (Table 3).

Pairwise $F_{ST}$ comparisons revealed that most populations were significantly differentiated (Table 4). Particularly, pronounced differences among different provinces were found in a range of $F_{ST}$ between 0.210 and 0.970, all being statistically significant (Table 5), in agreement with AMOVA result that most variations were from among provinces (79.59%) at the province level (Table 3). In addition, the UPGMA tree demonstrated that all populations were divided into three groups (Figure 3). Cluster I consisted of all populations from Jiangxi and Guangdong Province and two of three populations of Guangxi Province (GXLZ and GXBS). While the other population of Guangxi Province (GXYL) was clustered with the population from Hainan Province, forming Cluster II, consistent with the low $F_{ST}$ value between them, only 0.004. The Vietnam population was a single group, Cluster III. Overall, Cluster I and Cluster II were grouped together, making the Chinese Cluster. Furthermore, the genetic differentiation of Clusters between China and Vietnam was also distinctive, characterized with different nrDNA haplotypes (Table 1, Figure 2) and distinct phylogenetic Clusters (Figure 3), as well as shown in the AMOVA analysis, with 88.59% variances from among countries (Table 3).

TABLE 3 Analysis of molecular variance (AMOVA) of *Mastacembelus armatus* populations at different spatial scale.

| Pattern | Source of variation | d.f. | Variance components | Percentage variation | Fixation indices | Significance |
|---|---|---|---|---|---|---|
| country level | among countries | 1 | 15.036 Va | 88.59 | $\Phi_{ST} = 0.886$ | $p < 0.001$ |
| | within countries | 112 | 1.937 Vb | 11.41 | | |
| | total | 113 | 16.973 | | | |
| Province level | among provinces | 4 | 5.581Va | 79.59 | $\Phi_{ST} = 0.796$ | $p < 0.001$ |
| | within provinces | 109 | 1.432 Vb | 20.41 | | |
| | total | 113 | 7.013 | | | |
| Overall | among populations | 7 | 5.353 Va | 88.19 | $\Phi_{ST} = 0.882$ | $p < 0.001$ |
| | within populations | 106 | 0.717Vb | 11.81 | | |
| | total | 113 | 6.07 | | | |

# Discussion

## Genetic diversity and population structure

Previous population studies (Wang et al., 2012; Zou, 2013; Chen, 2014; Yang et al., 2016; Lin, 2017; Jiang, 2018; Gao et al., 2022) all showed high genetic diversity of *M. armatus* populations in China, but the haplotype diversity in our result (hd=0.434) is lower than that in other population studies, for example, Wang et al. (2012), Jiang (Jiang, 2018) and Gao et al. (2022) reported the haplotype diversity in China was 0.965, 0.768 and 0.895, respectively. This may be due to different markers employed and the small sample size in our study compared to other studies. Additionally, the overall genetic diversity of *M. armatus* populations in this study was over 0.5, showing a relative high diversity (Grant and Bowen, 1998). In general, combing our data and literature data, the genetic diversity of *M. armatus* maintains at a relatively high level, although the size of natural population is declining as reported (Hossain et al., 2012; Rahman et al., 2016; Xue, 2018). Furthermore, genetic differentiation between most populations is pronounced, regardless of spatial scale. Guangxi Province harbored the highest genetic diversity. Amongst, GXLZ population and GXBS population were grouped together, in agreement with low $F_{ST}$ value between them. GXYL population, nevertheless, was in a distinct cluster, either shown in TCS network or UPGMA tree. This suggests not only high genetic diversity but also high genetic differentiation among Guangxi Province populations. Surprisingly, GXYL population was clustered together with HNHK population. Further, the low $F_{ST}$ value between Hainan Province and the mainland means that gene flow occurred between them, despite the fact that Hainan Province is an isolated island and separated from the mainland by sea waters. In contrast, most Chinese population studies revealed that the population from Hainan Province was genetically partitioned with the mainland populations (Yang et al., 2016; Lin, 2017; Jiang, 2018). Gene flow between the population of Hainan Province and the mainland, revealed by nuclear makers in our study, is congruent with the latest research of Gao et al. (2022) discovered by mitochondrial markers. This gene flow is probably as a consequence of geological changes during glacial periods, when the exposed continental shelf connected Hainan and the mainland China (Sun et al., 2000; Voris, 2000). However, Guangxi Province and Vietnam possess completely different nrDNA haplotypes, despite their proximity. This is mainly because that there are no rivers connecting Guangxi Province and Vietnam.

## Sex ratio

It is well known that the population size is closely related with sex ratio, and an unbalanced sex ratio may significantly reduce the effective size of populations (Dubreuil et al., 2010). We checked the sex of each individual after sampling, and we found that all sampling sites in China are male dominated, except GDQY. However, Vietnam is female dominated. In fact, the sex ratio of *M. armatus* in the nature is on debate. One research reported female dominance trend (Panikkar et al., 2013), while the other one showed an equal proportion of male and female (Serajuddin and Pathak, 2012). We need more natural population data to clarify the sex ratio of *M. armatus* in the future, in order to provide more references for the further biological conservation. In addition, we discovered that the sex ratio of *M. armatus* is very unbalanced during the artificial breeding process, characterized with significant female dominance. For example, the proportion of females can reach 86.33% in the report of Xue et al. (2021b). This suggests that there are differences and difficulties in sexual differentiation of *M. armatus*, which may also occur in nature. At present, although some

TABLE 4 Pairwise estimates of genetic differentiation ($F_{ST}$) of *Mastacembelus armatus* between different populations (**$p$<0.05).

| Populations | GDHY | GDQY | GXBS | GXLZ | GXYL | HNHK | JXGZ |
|---|---|---|---|---|---|---|---|
| GDQY | 0.079 | | | | | | |
| GXBS | 0.411** | 0.479** | | | | | |
| GXLZ | 0.225** | 0.185** | 0.176** | | | | |
| GXYL | 0.722** | 0.790** | 0.777** | 0.780** | | | |
| HNHK | 0.775** | 0.870** | 0.856** | 0.859** | 0.004 | | |
| JXGZ | 0.351** | 0.427** | 0.104** | 0.040 | 0.772** | 0.865** | |
| YN | 0.950** | 0.971** | 0.966** | 0.968** | 0.919** | 0.938** | 0.970** |

TABLE 5 Pairwise estimates of genetic differentiation ($F_{ST}$) of *Mastacembelus armatus* between different provinces (**$p$<0.05).

| Province | Guangdong | Guangxi | Hainan | Jiangxi |
|---|---|---|---|---|
| Guangxi | 0.210** | | | |
| Hainan | 0.840** | 0.476** | | |
| Jiangxi | 0.326** | 0.110** | 0.865** | |
| YN | 0.961** | 0.881** | 0.938** | 0.970** |

studies have been done on the sex differentiation of *M. armatus*, most focus on the development of sex markers (Xue et al., 2020; Xue et al., 2021b) and Y chromosome differential (Xue et al., 2021a). The underlying sex determination mechanisms are still unclear, which also make challenges to investigate the sex ratio of *M. armatus*.

### Biological conservation

The biological conservation of species heavily depends on their genetic diversity. Understanding intraspecific genetic diversity and differentiation can help us take scientific and effective measures to protect threatened or endangered animals. Combing the results of our study with other previous studies, we found that the present genetic diversity of *M. armatus* populations is not low, indicating that it is not too late to take action to protect them, so that their genetic diversity can remain high. For example, precisely constructing more reserves for *M. armatus* based on the distribution of different genotypes/haplotypes, strengthening the investigation and protection of *M. armatus* in the isolated island, Hainan Province, which may provide crucial clues for their expansion, and exploring artificial breeding techniques to better conserve the germplasm resource.

## Conclusion

In conclusion, we researched the genetic diversity and population structure of *M. armatus* in China and Vietnam, based on nuclear ribosomal DNA markers. The genetic diversity and differentiation of *M. armatus* populations were at a relatively high level according to the data from this study and previous studies. Three Clusters were classified according to the genetic distance between each population, characterized with two Clusters in China and a distinct Cluster in Vietnam. In particular, we found that gene flow occurred between an isolated island and the mainland China based on the low $F_{ST}$ value between them.

## Data availability statement

The original contributions presented in the study are publicly available. This data can be found here: NCBI, OP847241 - OP847354.

## Ethics statement

The study was approved by the Laboratory Animal Ethics Committee of Pearl River Fisheries Research Institute, CAFS (number: LAEC-PRFRI-20201219).

## Author contributions

Conceptualization: XM. Resources: YY, YWa, YWu, YL, CL, ZJ. Methodology: XM, YY. Investigation: YY, YWa, YWu, YL, CL, ZJ. Analysis: YY, YWa, XM. Writing – original draft: YY and YWa wrote the manuscript. Writing – review and editing: all authors. Funding acquisition: XM and YWu. All authors contributed to the article and approved the submitted version.

## Funding

This study was supported by the Rural Revitalization Strategy Special Provincial Organization and Implementation Project Funds (2022RS-2-1), Guangdong Provincial Special Fund for Modern Agriculture Industry Technology Innovation Team (2022KJ150), China-ASEAN Maritime Cooperation Fund (CAMC-2018F), and National Freshwater Genetic Resource Center (FGRC18537).

## Conflict of interest

The authors declare that the research was conducted in the absence of any commercial or financial relationships that could be construed as a potential conflict of interest.

## Publisher's note



## References

Ağdamar, S., and Tarkan, A. S. (2019). High genetic diversity in an invasive freshwater fish species, *Carassius gibelio*, suggests establishment success at the frontier between native and invasive ranges. *Zoologischer Anzeiger* 283, 192–200. doi: 10.1016/j.jcz.2019.10.002

Bolger, A. M., Lohse, M., and Usadel, B. (2014). Trimmomatic: a flexible trimmer for illumina sequence data. *Bioinformatics* 30 (15), 2114–2120. doi: 10.1093/bioinformatics/btu170

Chen, T. T. (2014). Population differentiation and phylogeography of *Mastacembelus armatus* in southern China based on COI and d-loop (Master dissertation, south China normal university, China).

Clement, M., Snell, Q., Walke, P., Posada, D., and Crandall, K. (2002). TCS: estimating gene genealogies. In *Proceedings of the 16th International Parallel and Distributed Processing Symposium, International* (IEEE Computer Society) 3, 184.

Dhole, J., Tambe, D., and Chavan, R. (2011). Histopathological study of *Mastacembelus armatus* (Leceped, 1800) infected with tapeworm from osmanabad district (MS) India. *Recent Research in Science and Technology* 3, 3.

Dress, A. W., Flamm, C., Fritzsch, G., Grünewald, S., Kruspe, M., Prohaska, S. J., et al. (2008). Noisy: identification of problematic columns in multiple sequence alignments. *Algorithms Mol. Biol.* 3 (1), 1–10. doi: 10.1186/1748-7188-3-7

Dubreuil, M., Riba, M., González-Martínez, S. C., Vendramin, G. G., Sebastiani, F., and Mayol, M. (2010). Genetic effects of chronic habitat fragmentation revisited: strong genetic structure in a temperate tree, *Taxus baccata* (Taxaceae), with great dispersal capability. *Am. J. Bot.* 97 (2), 303–310. doi: 10.3732/ajb.0900148

Duong, T. Y., Tran, L. V. D., Nguyen, N. T. T., Jamaluddin, J. A. F., and Azizah, M. N. S. (2020). Unravelling taxonomic ambiguity of the *Mastacembelidae* in the Mekong

delta (Vietnam) through DNA barcoding and morphological approaches. *Tropical Zoology* 33 (2).

Excoffier, L., and Lischer, H. E. (2010). Arlequin suite ver 3.5: a new series of programs to perform population genetics analyses under Linux and windows. *Mol. Ecol. Resour.* 10 (3), 564–567. doi: 10.1111/j.1755-0998.2010.02847.x

Fan, H. P., Qiu, M. L., Zhong, Q. F., Xue, L. Z., and Qin, Z. Q. (2018). Comparison of nutritional component of wild and cultured *Mastacembelus armatus* in different growth stages. *J. Anhui Agric. Sci.* 46 (8), 92–96.

Gao, S., Li, Y. F., li, J., and Chen, W. T. (2022). Genetic structure and demographic history of *Mastacembelus armatus* in southern China. *South China Fisheries Sci.* 19, 1–8. doi: 10.12131/20220200

Garcia, G., Pereyra, S., Gutierrez, V., Oviedo, S., Miller, P., and Domingo, A. (2015). Population structure of *Squatina guggenheim* (Squatiniformes, squatinidae) from the south-western Atlantic ocean. *J. Fish Biol.* 86 (1), 186–202. doi: 10.1111/jfb.12560

Grant, W. A. S., and Bowen, B. W. (1998). Shallow population histories in deep evolutionary lineages of marine fishes: insights from sardines and anchovies and lessons for conservation. *J. Heredity* 89 (5), 415–426. doi: 10.1093/jhered/89.5.415

Gupta, S., and Banerjee, S. (2016). Food, feeding habit and reproductive biology of tire-track spiny eel (*Mastacembelus armatus*): A review. *J. Aquaculture Res. Dev.* 7 (5), 429. doi: 10.4172/2155-9546.1000429

Han, C., Li, Q., Lin, J., Zhang, Z., and Huang, J. (2018). Characterization of complete mitochondrial genomes of *Mastacembelus erythrotaenia* and *Mastacembelus armatus* (Synbranchiformes: Mastacembelidae) and phylogenetic studies of *Mastacembelidae*. *Conserv. Genet. Resour.* 10 (3), 295–299. doi: 10.1007/s12686-017-0807-0

Han, C., Li, Q., Liu, J., Hao, Z., Huang, J., and Zhang, Y. (2019). Characterization, evolution, and expression analysis of TLR7 gene subfamily members in *Mastacembelus armatus* (Synbranchiformes: *Mastacembelidae*). *Dev. Comp. Immunol.* 95, 77–88. doi: 10.1016/j.dci.2019.02.002

Han, C., Li, Q., Zhang, Z., and Huang, J. (2017). Characterization, expression, and evolutionary analysis of new TLR3 and TLR5M genes cloned from the spiny eel *Mastacembelus armatus*. *Dev. Comp. Immunol.* 77, 174–187. doi: 10.1016/j.dci.2017.08.007

Hossain, M. Y., Hossen, M. A., Yahya, K., Ahmed, Z. F., Sarder, M. R. I. , Islam, M. A., et al. (2015). Threatened fishes of the world: *Mastacembelus armatus* (Lacepede 1800) (Synbranchiformes: *Mastacembelidae*). *Croatian J. Fisheries* 73 (3), 137–139. doi: 10.14798/73.3.820

Hossain, M. Y., Rahman, M. M., Jewel, M. A. S., Ahmed, Z. F., Ahamed, F., Fulanda, B., et al. (2012). Conditions-and form-factor of the five threatened fishes from the jamuna (Brahmaputra river distributary) river, northern Bangladesh. *Sains Malaysiana* 41 (6), 671–678.

IUCN (2019). *IUCN red list of threatened species. Version 2019*, (IUCN Red List of Threatened Species)3.

IUCN Bangladesh. (2000). *Red book of threatened fishes of Bangladesh* (Bangladesh: IUCN Bangladesh, Dhaka) 116.

Javed, M., and Usmani, N. (2016). Accumulation of heavy metals and human health risk assessment *via* the consumption of freshwater fish *Mastacembelus armatus* inhabiting, thermal power plant effluent loaded canal. *SpringerPlus* 5 (1), 1–8. doi: 10.1186/s40064-016-2471-3

Jiang, X. L. (2018). Genetic diversity and phylogeography of different populations of *Mastacembelus armatus* in southern China and its adjacent areas (Master dissertation, guangzhou university, China).

Kumar, S., Stecher, G., Li, M., Knyaz, C., and Tamura, K. (2018). MEGA X: molecular evolutionary genetics analysis across computing platforms. *Mol. Biol. Evol.* 35 (6), 1547. doi: 10.1093/molbev/msy096

Leigh, J. W., and Bryant, D. (2015). POPART: Full-feature software for haplotype network construction. *Methods Ecol. Evolution.* 6 (9), 1110–1116. doi: 10.1111/2041-210X.12410

Li, H., and Durbin, R. (2009). Fast and accurate short read alignment with burrows–wheeler transform. *Bioinformatics* 25 (14), 1754–1760. doi: 10.1093/bioinformatics/btp324

Li, Q., Xu, R., Shu, H., Chen, Q., and Huang, J. (2016). The complete mitochondrial genome of the zig-zag eel *Mastacembelus armatus* (Teleostei, *Mastacembelidae*). *Mitochondrial DNA Part A* 27 (1), 330–331. doi: 10.3109/19401736.2014.892102

Librado, P., and Rozas, J. (2009). DnaSP v5: a software for comprehensive analysis of DNA polymorphism data. *Bioinformatics* 25 (11), 1451–1452. doi: 10.1093/bioinformatics/btp187

Lin, T. T. (2017). Isolation of microsatellite markers and population genetic diversity analysis in *Mastacembelus armatus* (Master dissertation, guangzhou university, China).

Lin, W. Q., Liao, X. P., Chen, T., Xu, Z. S., Liang, W. L., and Su, Y. L. (2016). Research on artificial propagation techniques for *Mastacembelus armatus*. *Ocean and Fishery* 7, 50–53.

Luo, R., Liu, B., Xie, Y., Li, Z., Huang, W., Yuan, J., et al. (2012). SOAPdenovo2: an empirically improved memory-efficient short-read *de novo* assembler. *Gigascience* 1 (1), 2047–217X. doi: 10.1186/2047-217X-1-18

Mladineo, I., Šegvić-Bubić, T., Stanić, R., and Desdevises, Y. (2013). Morphological plasticity and phylogeny in a monogenean parasite transferring between wild and reared fish populations. *PloS One* 8 (4), e62011. doi: 10.1371/journal.pone.0062011

Oliveira, C., Torres, R. A., Favorito, S., and Foresti, F. (1997). Cytogenetic studies of *Mastacembelus armatus* (Pisces, *Mastacembelidae*). *Cytobios* 83-89.

Pandey, M., Pandey, A. K., Mishra, A., and Tripathi, B. D. (2017). Assessment of metal bioaccumulation in *Mastacembelus armatus* (eel) and exposure evaluation in human. *Environ. Nanotechnology Monit. Manage.* 7, 103–109. doi: 10.1016/j.enmm.2017.02.002

Panikkar, P., Khan, M. F., Sharma, A. P., Jha, B. C., and Vijaykumar, M. E. (2013). Index of relative importance of diet components in *Mastacembelus armatus* (Lacepède 1800) from karapuzha reservoir, wayanad, kerala, India. *Indian J. Fisheries* 60 (1), 37–40.

Presa, P., Pardo, B. G., Martínez, P., and Bernatchez, L. (2002). Phylogeographic congruence between mtDNA and rDNA ITS markers in brown trout. *Mol. Biol. Evol.* 19, 2161–2175. doi: 10.1093/oxfordjournals.molbev.a004041

Rahman, M. M., Ali, M. R., Sarder, M. R. I., Mollah, M. F. A., and Khan, N. S. (2016). Development of sperm cryopreservation protocol of endangered spiny eel, *Mastacembelus armatus* (Lacepede 1800) for ex-situ conservation. *Cryobiology* 73 (3), 316–323. doi: 10.1016/j.cryobiol.2016.10.004

Serajuddin, M., and Pathak, B. C. (2012). Study of reproductive traits of spiny eel, *Mastacembelus armatus* (Mastacembeliforms) from kalinadi-a tributary of the gangesriver basin, India. *Res. J. Biol.* 2 (05), 145–150.

Shu, H., Jiang, X. L., Yang, H. Q., Lin, T. T., Zhou, H. Q., Zhang, M. Q., et al. (2017). Analysis of morphological variations among seven wild populations of *Mastacembelus armatus* in south China area. *J. Guangzhou Univ. (Natural Sci. Edition)* 16 (3), 8–14.

Steenwyk, J. L., Buida, T. J.III, Li, Y., Shen, X. X., and Rokas, A. (2020). ClipKIT: A multiple sequence alignment trimming software for accurate phylogenomic inference. *PloS Biol.* 18 (12), e3001007. doi: 10.1371/journal.pbio.3001007

Sun, X., Li, X., Luo, Y., and Chen, X. (2000). The vegetation and climate at the last glaciation on the emerged continental shelf of the south China Sea. *Palaeogeography Palaeoclimatology Palaeoecol.* 160 (3-4), 301–316. doi: 10.1016/S0031-0182(00)00078-X

Thapliyal, M., Sati, B. K., and Thapliyal, A. (2020). Assessing impact of dams on genetic diversity of native fish *Mastacembelus armatus* in river yamuna using mitochondrial DNA cytochrome-b sequences as a molecular marker. *Environ. Conserv. J.* 21 (1&2), 39–47. doi: 10.36953/ECJ.2020.211205

Voris, H. K. (2000). Maps of pleistocene sea levels in southeast Asia: shorelines, river systems and time durations. *J. Biogeography* 27 (5), 1153–1167. doi: 10.1046/j.1365-2699.2000.00489.x

Wang, F., Huang, X. L., La, D., and Zhao, J. (2012). Research on population genetics and phylogeography of mastacembelus armatus populations in south China area. In *Proceedings of the 2012 Symposium of the Ichthyology Branch of the Chinese Society of Zoology, Lanzhou, Chinese Society for Oceanology and Limnology, Chinese Ichthyological Society*, 23.

Wu, Y., Liang, Z. Q., Li, C. W., Liu, L., Chen, X. Y., and Liu, Q. M. (2010). Analysis and evaluation of nutritional components in the muscle of two kinds of *Mastacembelus*. *Acta Nutrimenta Sin.* 32 (5), 499–502. doi: 10.13325/j.cnki.acta.nutr.sin.2010.05.012

Xue, L. (2018). Effects of exogenous hormone, temperature and parental weight on artificial induced spawning and incubation of *Mastacembelue armatus*. *Acta Hydrobiologica Sin.* 42 (2), 333–341. doi: 10.7541/2018.042

Xue, L., Gao, Y., Wu, M., Tian, T., Fan, H., Huang, Y., et al. (2021a). Telomere-to-telomere assembly of a fish y chromosome reveals the origin of a young sex chromosome pair. *Genome Biol.* 22 (1), 1–20. doi: 10.1186/s13059-021-02430-y

Xue, L. Z., Guo, X. F., Zhou, Y. L., Wang, Z. W., Fan, H. P., Li, D. P., et al. (2020). Screening and characterization of sex-specific markers by 2b-RAD sequencing in zig-zag eel (*Mastacembelus armatus*) with implication of XY sex determination system. *Aquaculture* 528, 735550. doi: 10.1016/j.aquaculture.2020.735550

Xue, L., Jia, D., Xu, L., Huang, Z., Fan, H., Chen, B., et al. (2021b). Bulk and single-cell RNA-seq reveal the sexually dimorphic expression pattern of dmrtb1 in zig-zag eel (*Mastacembelus armatus*). *Aquaculture* 545, 737194. doi: 10.1016/j.aquaculture.2021.737194

Yang, H. Q., Li, Q., Shu, H., Yue, L., Lin, T. T., and Liu., Y. B. (2016). Genetic diversity of *Mastacembelus armatus* in southern China and surrounding areas based on ISSR analysis. *Acta Hydrobiologica Sin.* 40 (1), 63–70. doi: 10.7541/2016.9

Zhou, H. Q., Li, F., Shu, H., Zhong, D. M., He, P. Y., Huang, X. Q., et al. (2019). Analysis on morphological indexes and discrimination of Male and female *Mastacembelus armatus*. *J. Guangdong Ocean Univ.* 39 (1), 1–6. doi: 10.3969/j.issn.1673-9159.2019.01.001

Zou, Y. (2013). Development of microsatellite markers and genetic variations of *Mastacembelus armatus* (Master dissertation, south China normal university, China).

# Frontiers in Marine Science

**Explores ocean-based solutions for emerging global challenges**

The third most-cited marine and freshwater biology journal, advancing our understanding of marine systems and addressing global challenges including overfishing, pollution, and climate change.

---

## Discover the latest Research Topics

See more →

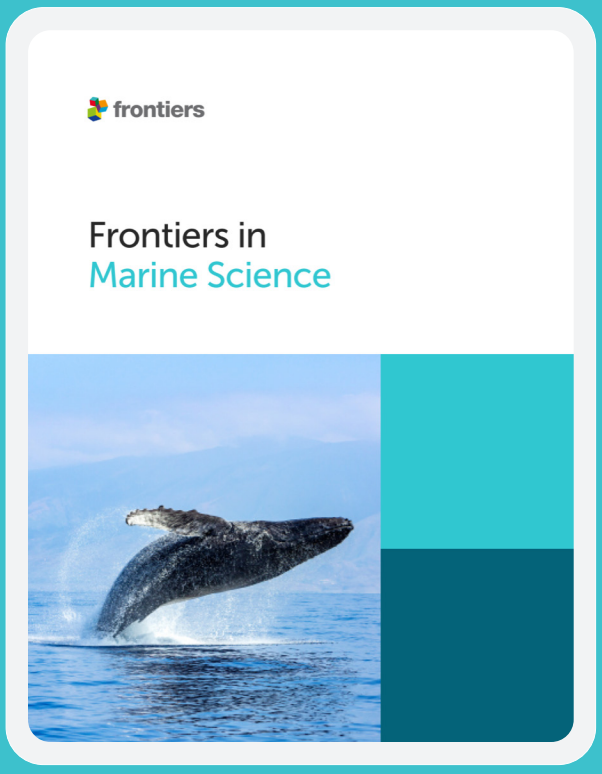


**Frontiers**

Avenue du Tribunal-Fédéral 34
1005 Lausanne, Switzerland
frontiersin.org

**Contact us**

+41 (0)21 510 17 00
frontiersin.org/about/contact